uOttawa

L'Université canadienne
Canada's university

FACULTÉ DES ÉTUDES SUPÉRIEURES ET POSTOCTORALES

uOttawa

L'Université canadienne
Canada's university

FACULTY OF GRADUATE AND POSDOCTORAL STUDIES

Larisa Mikelsons

AUTEUR DE LA THÈSE / AUTHOR OF THESIS

Ph.D. (Chemistry)

GRADE / DEGREE

Department of Chemistry

FACULTÉ, ÉCOLE, DÉPARTEMENT / FACULTY, SCHOOL, DEPARTMENT

Experimental and Computational Studies of the Interactions of Cyanine Dyes with DNA

TITRE DE LA THÈSE / TITLE OF THESIS

J.C. Scaiano

DIRECTEUR (DIRECTRICE) DE LA THÈSE / THESIS SUPERVISOR

CO-DIRECTEUR (CO-DIRECTRICE) DE LA THÈSE / THESIS CO-SUPERVISOR

EXAMINATEURS (EXAMINATRICES) DE LA THÈSE / THESIS EXAMINERS

Bruce Armitage

Maria DeRosa

Robert Ben

Natalie Goto

Gary W. Slater

Le Doyen de la Faculté des études supérieures et postdoctorales / Dean of the Faculty of Graduate and Postdoctoral Studies

# Experimental and Computational Studies of the Interactions of Cyanine Dyes with DNA

**Larisa Mikelsons**

Thesis submitted to the
Faculty of Graduate and Postdoctoral Studies
in partial fulfillment of the requirements for the degree of
Doctor of Philosophy
in the Ottawa-Carleton Chemistry Institute
Department of Chemistry, University of Ottawa


Université d'Ottawa · University of Ottawa

| Candidate | Supervisor |
| --- | --- |
| Larisa Mikelsons | Professor J. C. Scaiano |

*Your file Votre référence*
*ISBN: 978-0-494-49381-6*
*Our file Notre référence*
*ISBN: 978-0-494-49381-6*

To my mom, for giving me so much

# Abstract

This thesis focuses on understanding the interactions of cyanine dyes with DNA, through the use of both experimental and computational techniques. Although cyanine dyes are widely used as nucleic acids stains in fluorescence applications, the nature of the association process is not always clear. The cyanine dye PicoGreen® (PG) has proven to be extremely useful in monitoring DNA damage but its structure is proprietary, making it impossible to understand its specific interactions with DNA. However, its structure is known to resemble that of another cyanine dye, thiazole orange (TO). We anticipated that the N-propyl pyridinium derivative of TO (PTO) would also intercalate in DNA and that its extra positive charge, relative to TO, would aid in the association. Our studies have focused on the associations of PG, TO and PTO with DNA.

Chapter 3 deals with the association of the dyes with single-stranded DNA homopolymers. The combination of spectroscopic techniques and molecular dynamics (MD) calculations provides a unique understanding of the associations of TO and PTO with single-stranded DNA homopolymers. There is highly specific binding of TO and PTO to poly(dG) and poly(dA), while poly(dC) and poly(dT) bind the dyes very weakly and appear to promote dye aggregation. Due to its proprietary structure, PG could not be studied computationally. However, the experimental spectral results suggest that PG associates differently with single-stranded DNA than do TO and PTO.

There are two major findings in Chapter 4. Firstly, the dyes associate strongly with double-stranded DNA, as demonstrated by the experimental spectral results and the MD calculations. Experimental evidence supports not only monomeric dye intercalation in DNA, but also dimeric dye intercalation. The results of the MD simulations suggest that TO and PTO bind to DNA without sequence specificity. The second major finding was that a new type of stable dye/DNA complex is formed when single strands of poly(dA) and poly(dT) are hybridized in

the presence of PG or PTO, which cannot be obtained by addition of the dye to poly(dA)•poly(dT). For all three dyes, complete DNA renaturation did not occur during thermal cycling of dye/double-stranded calf thymus DNA. These results suggest that intercalating cyanine dyes can interfere with DNA hybridization to double-stranded DNA.

Chapter 5 is concerned with a more practical aspect of the association of cyanine dyes with DNA: using thiazole orange to report UVC-induced DNA damage. A variety of spectroscopic techniques, as well as agarose gel electrophoresis, were examined for their ability to detect UVC-induced DNA damage. The most sensitive methodology of all of those tested was fluorescence spectroscopy using TO. All of the spectroscopic techniques involving TO suggest that TO intercalation is susceptible to UVC-induced DNA damage. The computational studies suggest that the presence of cyclobutadipyrimidines, and not 8-oxo-2'-deoxyguanosine, is a factor in the experimentally observed reduction in dye intercalation. These studies have been a proof-of-concept, to demonstrate the usefulness of this fluorescence technique in detecting high levels of DNA damage, comparable to those used in food irradiation.

# Acknowledgements

When I began a co-op work term in the Scaiano lab, I pictured it as an opportunity to return to Ottawa from Waterloo and to do some interesting chemistry, but I never had graduate studies on my mind. As I completed my undergraduate degree and visited various universities to learn about their graduate programs, I realized that the chemistry I loved the most was photochemistry, and the best place to do it was in the Scaiano laboratory. As Elda once said, "You've got to get them hooked when they're young." My decision was also helped by knowing the type of person Tito is. Speaking with other students in the chemistry department, I've come to realize that Tito is a one-of-a-kind supervisor, who only wants the best for his students. Tito's passion for photochemistry is contagious, and I admire the hours he spends at home doing work, which he considers "fun". I am extremely grateful to Tito for turning me on to photochemistry, and for giving me the opportunity to work in his lab. I'm also grateful to Elda for being so kind and for making me feel welcome in the group. You are both such generous, incredibly kind people.

I also owe a big thank you to Colleen Trevithick-Sutton for all of her help in making this thesis what it is. I'm very grateful for your prompt and insightful comments. I was also very happy to collaborate with you on the DNA project. At the beginning of my thesis I was the only person working on the DNA project and it was quite lonely, so it was very nice to have you around to discuss ideas and to work together. I've realized that you're an all-around generous person: I couldn't believe it when you offered to lend me your suit when I get a job interview.

I must also thank all of the past and present group members of the Scaiano lab for making this a wonderful experience. Claude Schweitzer got me started on the DNA project, and Alexis Aspée was very patient when teaching me how to use the picosecond laser system. Even though I would joke around with Claudio Carra about his age, he was extremely helpful in teaching me how to use AMBER. I have to thank Marius Ivan for being a great deskmate and for making life interesting: I will

always remember your prank phone calls. I have to thank Marie Laferrière for being my ally in the male-dominated office, and for her friendship; as you and I have both written our theses I've greatly missed our daily conversations. Kathy-Sarah Focsaneanu and I have gone through both good times and stressful (school-related) ones, and I'm glad we made it through together! It was wonderful going to the ESP conference in Aix-les-Bains with Belinda Heyne: I couldn't have asked for a better companion! All of the post-docs in our group have always been very eager to help and offer advice: thank you Carlos Sanrame, Matt Lukeman, Carolina Aliaga, Vincent Maurel, and Chad Beddie. Life outside of the lab has been fun, thanks to Mathieu Frenette, Mark Perry, Kathy McGilvray, Jessie Blake and Paul Billone.

I was lucky to supervise two undergraduate students: Marija Antonic and Vasilisa Filippenko. Marija, it was so nice to see your eagerness, and your willingness to learn. Vasilisa, your biochemistry knowledge was greater than mine and it was wonderful to learn from you.

I have to thank Gino Cuglietta for helping me maintain the picosecond laser system, and for his help in the design of the Couette cell. Your knowledge was invaluable, and your approachable personality made it possible to ask "dumb" questions. Tito's secretaries, Anita Bowman and Betty Yakimenko, greatly simplified life at Ottawa U – thank you!

I'd like to acknowledge the financial support I've received from the Government of Ontario and the University of Ottawa.

I'd also like to thank all of my friends, not only for their friendship, but also for their support and understanding while I've been writing this thesis. I can't mention everyone but I would like to thank two very special people. Erin, we've been friends since we were 10 years old and I know we'll be friends for the rest of our lives. Angela, I can't imagine doing my undergrad without you: you made classes and labs fun, life outside of school great, and you're a wonderful friend.

I want to thank my family for their encouragement over the years. You've always encouraged me to do the best I could, and have been so proud of my accomplishments. Amanda, growing up we didn't get along so well but there's no

one else I'd want as my sister. Veci and Vectetis, you're wonderful role models and I hope that I can be as happy and successful as you are. Aunt Linda and Uncle Ralph, you've always been so good to me and treated me like your own daughter. I also have to thank Kevin, Gabi and Colin, and all of your extended family, for treating me like family since the day we first met – it means so much to me!

Jason, I don't think I could have done this as successfully without you. Whenever I was feeling stressed, your mere presence would relax me. In these past few months all I've done is write, write, write...and I am so grateful that you took over the wedding planning, especially since I know you weren't very eager to do it. I'm glad that this chapter of our lives is over, and we can now move on to even better things!

Mom, I never would have gotten to this point without you. I know you've made a lot of sacrifices for me over the years, and I'll always be grateful. Thank you for giving me so much!

# Table of Contents

# List of Figures

# List of Schemes

# List of Tables

# List of Abbreviations

| | |
|---|---|
| **µM** | micromolar |
| **6-4PP** | pyrimidine (6-4) pyrimidone photoproduct |
| **8-oxo-dG** | 8-oxo-2'-deoxyguanosine |
| **A** | adenine |
| **Å** | Angstrom |
| **AC** | alternating current |
| **AMBER** | Assisted Model Building with Energy Refinement |
| **atm** | atmosphere |
| **C** | cytosine |
| **CD** | circular dichroism |
| **CHARMM** | Chemistry at HARvard Macromolecular Mechanics |
| **CMC** | critical micelle concentration |
| **COSY** | correlation spectroscopy |
| **CPDs** | cyclobutadipyrimidines |
| **CPU** | central processing unit |
| **CT** | calf thymus |
| **CW** | continuous wave |
| **d/b** | dye to base pair |
| **DAPI** | 4'-6-diamidino-2-phenylindole |
| **DC** | direct current |
| **DMSO** | dimethyl sulfoxide |
| **DNA** | deoxyribonucleic acid |
| **dsDNA** | double-stranded DNA |
| **EB** | ethidium bromide |
| **EDTA** | ethylenediaminetetraacetic acid |
| **EPL** | elliptically polarized light |
| **FRET** | fluorescence resonance energy transfer |
| **fs** | femtosecond |
| **fwhm** | full width at half maximum |
| **G** | guanine |
| **Gy** | Gray |
| **h** | hour |
| **HPLC** | high performance liquid chromatography |
| **ICD** | induced circular dichroism |
| **K** | kelvin |
| **kbp** | kilo base pairs |
| **kcal** | kilocalorie |
| **kJ** | kilojoule |
| **LCPL** | left-circularly polarized light |
| **LD** | linear dichroism |
| **$LD^r$** | reduced linear dichroism |
| **M** | molar |
| **m** | meter |
| **MD** | molecular dynamics |
| **mdeg** | millidegree |
| **min** | minute |
| **mJ** | millijoule |

| | |
|---|---|
| **mM** | millimolar |
| **MM** | molecular mechanics |
| **mm** | millimeter |
| **MS** | mass spectrometry |
| **ms** | millisecond |
| **NHE** | normal hydrogen electrode |
| **nm** | nanometer |
| **NMR** | nuclear magnetic resonance |
| **NOE** | nuclear Overhauser effect |
| **NOESY** | nuclear Overhauser effect spectroscopy |
| **ns** | nanosecond |
| **°C** | degrees Celsius |
| **PCR** | polymerase chain reaction |
| **PES** | potential energy surface |
| **PG** | PicoGreen® |
| **PMT** | photomultiplier tube |
| **poly(dA)** | polydeoxyadenylate |
| **poly(dC)** | polydeoxycytidylate |
| **poly(dG)** | polydeoxyguanylate |
| **poly(dT)** | polydeoxythymidylate |
| **poly(rA)** | polyadenylic acid |
| **poly(rC)** | polycytidylic acid |
| **poly(rU)** | polyuridylic acid |
| **ps** | picosecond |
| **PTO** | N-propyl pyridinium derivative of thiazole orange |
| **RCPL** | right-circularly polarized light |
| **RNA** | ribonucleic acid |
| **rpm** | revolutions per minute |
| **RT** | room temperature |
| **s** | second |
| **$S_0$** | ground state |
| **$S_1$** | lowest-energy singlet state |
| **SDS** | sodium dodecyl sulfate |
| **$S_n$** | upper excited singlet state |
| **ssDNA** | single-stranded DNA |
| **T** | thymine |
| **$T_1$** | lowest-energy triplet state |
| **TAE** | Tris-Acetate-EDTA |
| **TIFF** | Tagged Image File Format |
| **TO** | thiazole orange |
| **TOTO** | homodimer of thiazole orange |
| **TRF** | time-resolved fluorescence |
| **Tris** | 2-amino-2-hydroxymethyl-1,3-propanediol |
| **UV** | ultraviolet |
| **UVA** | ultraviolet-A |
| **UVB** | ultraviolet-B |
| **UVC** | ultraviolet-C |
| **V** | volt |
| **W** | Watt |
| **YAG** | yttrium-aluminium-garnet |
| **YO** | oxazole yellow |
| **YOYO** | homodimer of oxazole yellow |

# 1. Introduction

## 1.1. Objectives

Although cyanine dyes are frequently used as sensors for DNA and its structural changes, their associations with DNA are not always well understood. One of the primary objectives in this thesis was to better understand the mechanisms of association of cyanine dyes with both single- and double-stranded DNA. Spectroscopic techniques provide valuable information regarding dye/DNA complexes, but combining these with molecular dynamics simulations can provide a more complete description of the association process. Thus experimental and computational techniques were used in this thesis to gain an understanding of the fundamental associations of cyanine dyes with DNA.

The comet assay (discussed in further detail in Section 1.8) is commonly used to measure DNA damage, but it has major disadvantages, including subjectivity due to operator judgment. We chose to study DNA damage with more objective measurement strategies. Previous work in our laboratory demonstrated that fluorescence lifetimes of intercalated dyes (objective measurements), particularly the cyanine dye PicoGreen® (PG), can be used to distinguish single- from double-stranded DNA, and ultimately to monitor DNA damage.[1,2] However, this technique has its best sensitivity in the 1-100 Gray (Gy) range. The Gray is a unit of absorbed dose corresponding to the absorption of one Joule of radiation in one kilogram of material. The doses used in health sciences are relatively low. For example, an average chest X-ray delivers a dose of approximately 0.001 Gy. On the other hand, the doses used in food irradiation are relatively high. Certain foods are irradiated in order to disinfect them and to extend their shelf life,[3] and during this process they receive doses between 0.5 and 10 kGy. Altering the DNA unwinding conditions in the above-mentioned PG technique can change its sensitivity, making it amenable to food authenticity applications. The current limitations of this technique relate to the high cost of the instrumentation and the high level of operator expertise required.

In the course of our studies on the fundamental associations of cyanine dyes with DNA, we discovered that one of these dyes, thiazole orange, is particularly useful in reporting high levels of DNA damage. The ability of thiazole orange to intercalate in damaged DNA is compromised, resulting in a decrease in its fluorescence emission intensity relative to that in pristine DNA. As these are steady-state fluorescence measurements, they can be performed easily and relatively quickly. Although practical applications of our technique would only occur in the future, this novel technique provides a fast screening method to identify (but not characterize) damage to DNA, which is geared towards high levels of damage, such as those that may result during radiation treatment of food products.

## 1.2. Deoxyribonucleic Acid Structure

The accurate translation of genetic information into necessary proteins, gene expression, etc., is essential to the survival of all organisms. Since deoxyribonucleic acid (DNA) is the chemical entity that stores and transmits genetic information, it plays a central role in the survival of all organisms. The genetic information is coded by the bases in DNA, which are adenine (A), cytosine (C), guanine (G) and thymine (T). The structures of the DNA bases are shown in Figure 1.1. Adenine and guanine are purines, while cytosine and thymine are pyrimidines. The Watson-Crick base pairs are A•T and G•C.

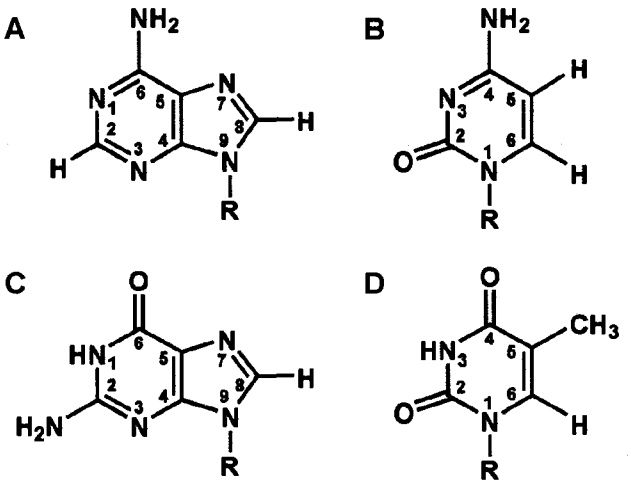


**Figure 1.1: Structures of the DNA bases: (A) adenine, (B) cytosine, (C) guanine, and (D) thymine.[4]**

The bases are attached to 2'-deoxyribose sugars: the pyrimidines are linked at N1 while the purines are linked at N9. A base and a sugar are referred to as a nucleoside, which is shown in Figure 1.2A. Connecting the sugars by making phosphate esters at the 3'- and 5'-OH groups creates nucleotides (see Figure 1.2B,C).

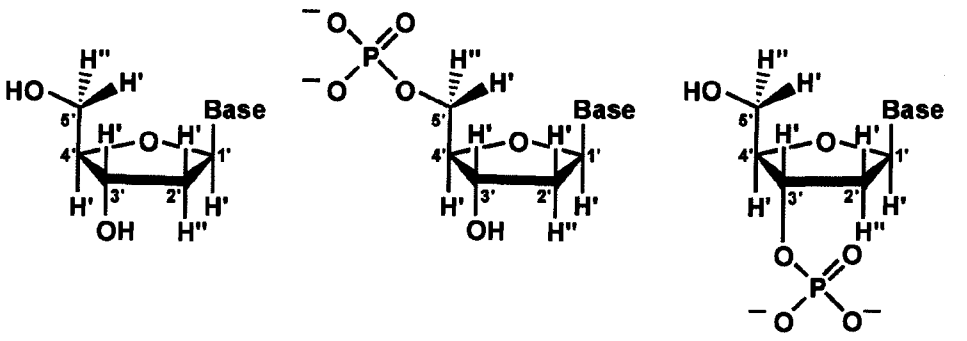


**A) Deoxynucleoside** **B) 5'-deoxynucleotide** **C) 3'-deoxynucleotide**

**Figure 1.2: Structures of a deoxynucleoside, a 5'-deoxynucleotide and a 3'-deoxynucleotide. Adapted from Cantor and Schimmel.[4]**

Double-stranded DNA consists of two complementary strands of nucleotides that are antiparallel, i.e. one strand runs in the 5' to 3' direction while the other strand runs in the 3' to 5' direction. The helical structure of double-stranded B-form DNA, which is believed to represent the conformation of most cellular DNA,[5] is illustrated in Figure 1.3A. Molecular dynamics simulations can be used to study the behaviour of DNA. The structure shown in Figure 1.3B, generated using the AMBER 8 package (see Chapter 2), represents double-stranded B-form DNA.

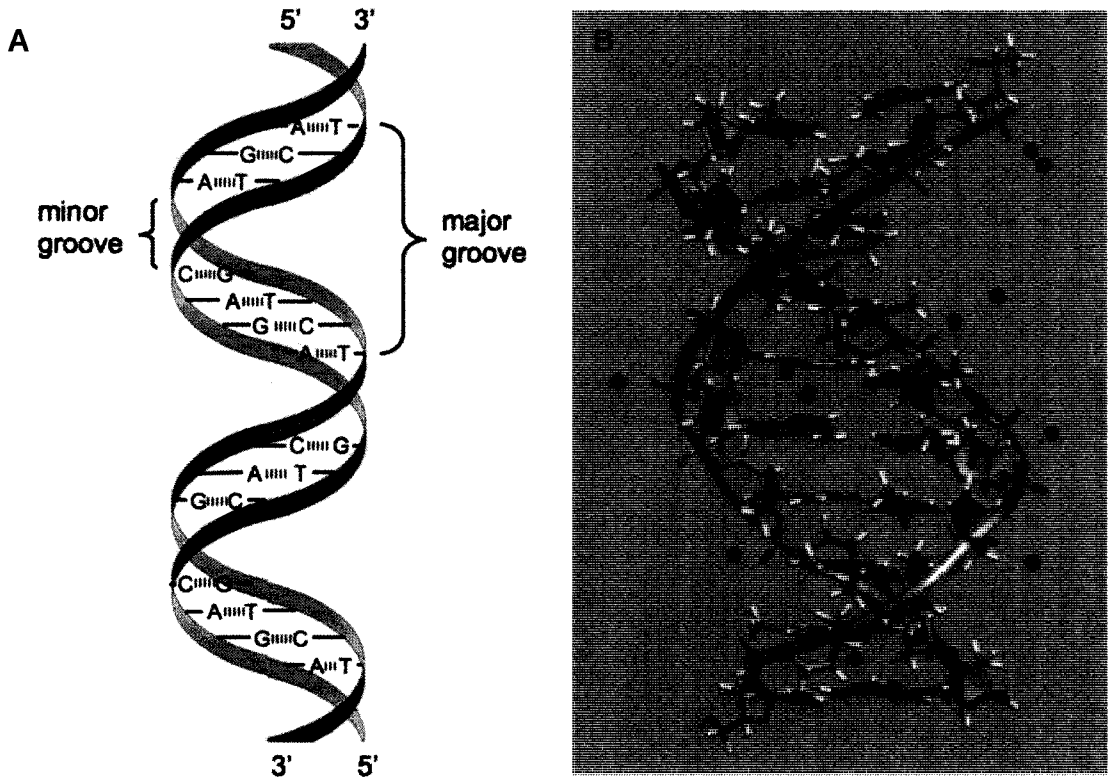


**Figure 1.3: (A) A schematic representation of the B-DNA double helix, adapted from Bates and Maxwell.[5] (B) $(dA)_{10}$•$(dT)_{10}$ oligomer (including blue dots that are the $Na^+$ counterions) that was generated using the AMBER 8 package.**

## 1.3. Binding Modes of Small Molecules to DNA

The non-covalent associations of small molecules with DNA can be categorized into three classes: (i) electrostatic binders, (ii) intercalators, and (iii) groove binders,[6] and class (iii) can be further separated into major and minor groove binders. In general, electrostatic interactions are weak and non-specific, and major groove binding is a rare occurrence for small molecules, making intercalation and minor groove binding the two most common binding modes.[7] Examples of typical intercalators and minor groove binders can be seen in Figure 1.4.

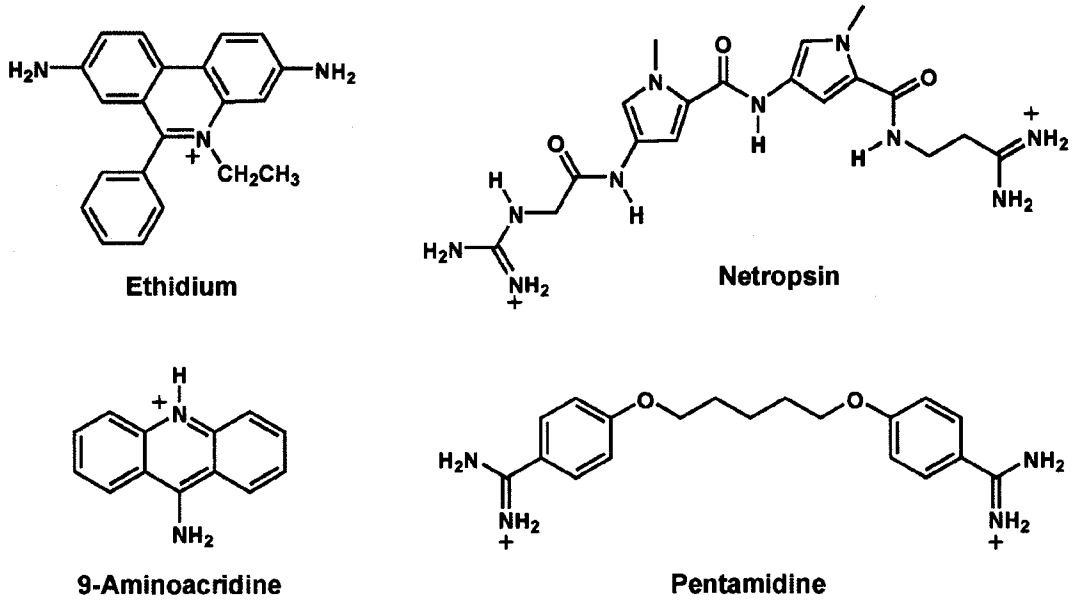


**Figure 1.4: Examples of well-known DNA (left) intercalators and (right) minor groove binders, after Armitage.[7]**

Although intercalation necessitates unwinding of the DNA helix and changes to the π-stacking of the base pairs to accommodate the intercalator, these energetic penalties are compensated by van der Waals, hydrophobic, and electrostatic forces

in the newly formed complex.[6] Intercalation typically occurs for planar polyaromatic molecules that have a sufficiently large surface area, i.e. a minimum of two fused ring systems, and appropriate steric properties.[8]

As with intercalation, minor groove binding is driven by van der Waals, hydrophobic, and electrostatic forces, in addition to hydrogen bonding.[6] Minor groove binders are typically either curved or have some flexibility, allowing the molecule to follow the helical curvature of the minor groove without significantly distorting the DNA stucture.[7]

## 1.4. The Quest for a Dye that can Selectively Detect dsDNA

Previous work in our laboratory[9] assessed the ability of nine different DNA-associating dyes to distinguish between single- (ss) and double-stranded (ds) DNA, because the ratio of ss- to dsDNA is an established measure of DNA damage.[2,10] The dyes that were studied were benzimide or indole-derived dyes (Hoechst 33342 [bisbenzimide trihydrochloride], Hoechst 33258 [bisbenzimide] and 4'-6-diamidino-2-phenylindole [DAPI]), phenanthridinium dyes (ethidium bromide and propidium iodide hydrate), and cyanine dyes (PicoGreen, SYBR Gold, SYBR Green I and YOYO-1 iodide), whose structures are shown in Figure 1.5.

The phenanthridinium dyes had similar fluorescence lifetimes in both ss- and dsDNA, making discrimination between the two forms impossible. The benzimide/indole dyes exhibited multiexponential fluorescence decays, which would require a cumbersome (and error-prone) analysis to determine the relative proportions of ss- and dsDNA. With the exception of YOYO-1, the cyanine dyes decayed monoexponentially and biexponentially when complexed with dsDNA and ssDNA, respectively, and of the three dyes PicoGreen (PG) was selected as the best candidate for discriminating between ss- and dsDNA. In samples containing both ss- and dsDNA, the PG decay is a six-variable function that can be reduced to a single parameter, making it possible to determine the ratio of ss- to dsDNA and hence DNA damage.[1,2]

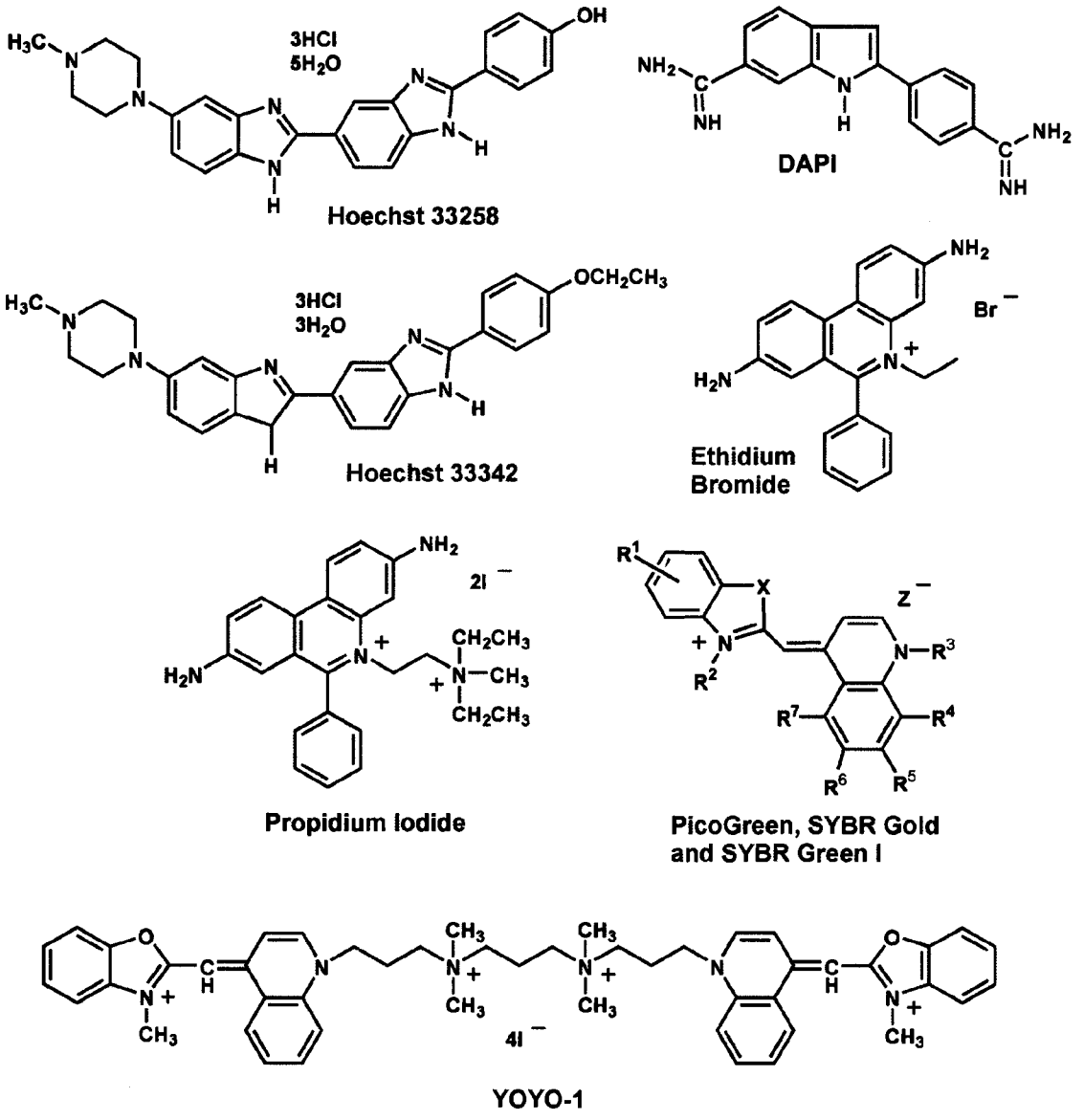


**Figure 1.5: Structures of the dyes that were studied by Cosa *et al.*[9] In the case of PicoGreen and SYBR Gold, X is either S or O. Many different substituents ($R^n$) can be found on the conjugated rings. The counterion $Z^-$ is chloride, iodide, perchlorate, and/or various sulfonates.[11,12]**

The property that makes cyanine dyes such good sensors is that they experience structural mobility restrictions upon interacting with DNA, which is

discussed in detail in Section 1.5. In addition to being able to undergo forced planarity upon intercalation, another criterion in selecting a DNA sensor is that it possesses at least one positive charge, which increases its water solubility and its attraction to the negatively charged DNA.

One limitation of using PG as a DNA damage sensor is that fluorescence lifetime measurements are obtained with an expensive picosecond laser system that requires a high level of operator expertise. Initially, other cyanine dyes (shown in Figure 1.6) were examined in the hope that they would exhibit longer fluorescence lifetimes when complexed with DNA, allowing measurements to be performed on the much simpler nanosecond laser systems. Unfortunately, this was not the case but other interesting observations (for example the effect of the dye on DNA strand hybridization, discussed in Chapter 4) led us to study their fundamental interactions with DNA.

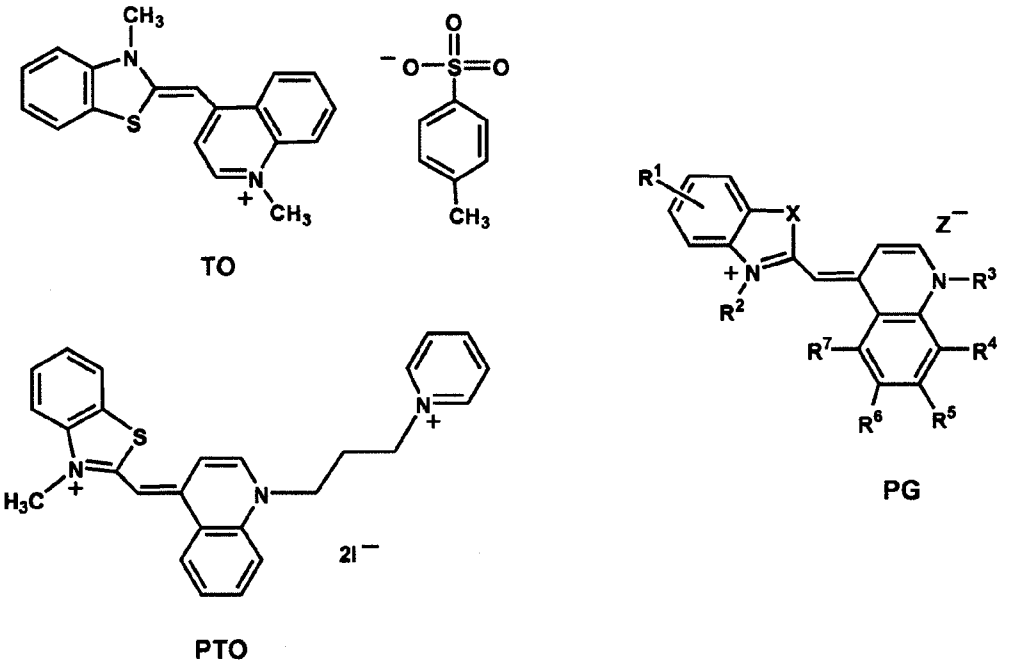


**Figure 1.6: Structures of the cyanine dyes under study in this thesis. Top left: thiazole orange (TO); bottom left: N-propyl pyridinium derivative of TO (PTO); right: PicoGreen (PG). In the case of PG, X is either S or O. Many different substituents ($R^n$) can be found on the conjugated rings. The counterion $Z^-$ is chloride, iodide, perchlorate, and/or various sulfonates.[11,12]**

## 1.5. Cyanine Dyes and their Associations with DNA

Cyanine dyes have the general formula

$R_2N[CH=CH]_nCH=N^+R_2 \leftrightarrow R_2N^+=CH[CH=CH]_nNR_2$

where *n* is a small number, and frequently the nitrogen and a portion of the conjugated chain comprise a heterocyclic system,[13] as seen in Figure 1.7. The absorption and emission maxima of cyanine dyes can be tuned in the visible and near-infrared regions by changing the heterocycle and the length of the methine bridge.[14] Cyanine dyes have been used in photography since 1856, and they also have applications in photonic technologies, as photosensitizers in photodynamic therapy, and as fluorescent labels and probes in biological systems.[15] These dyes are generally non-fluorescent in solution and undergo dramatic increases in fluorescence upon binding to nucleic acids, making them particularly useful nucleic acid stains.

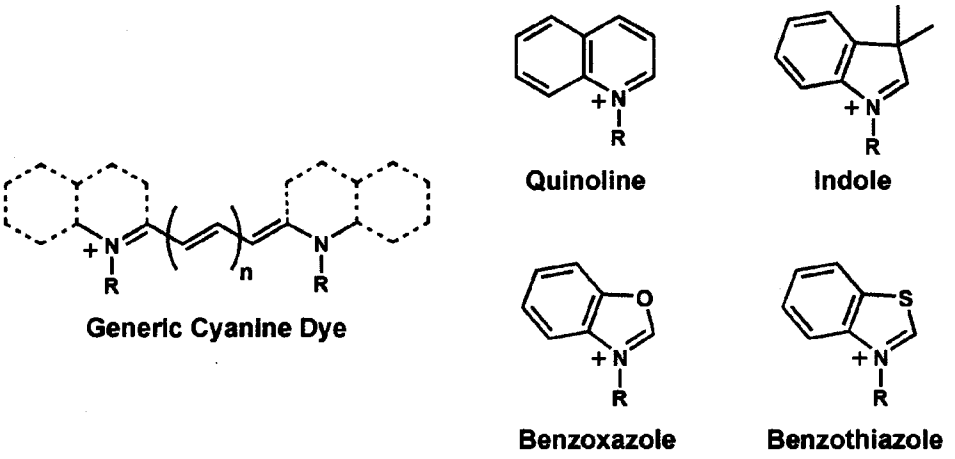


**Figure 1.7: Generic structure and examples of the most common heterocyclic components found in cyanine dyes, after Hannah and Armitage.[14]**

Absorption of a photon causes a molecule to enter an upper excited singlet state ($S_n$), where it will generally undergo rapid non-radiative processes (vibrational relaxation and internal conversion) to populate the lowest singlet excited state ($S_1$),

as illustrated in Figure 1.8. To dissipate its excess energy and return to the ground state, the singlet excited state can either release the energy radiatively in the process known as fluorescence, or else release the energy non-radiatively, i.e. as heat. Another option is to undergo intersystem crossing, which requires a change in multiplicity, to an excited triplet state, generally the lowest triplet excited state ($T_1$). Subsequent decay to the ground state occurs via phosphorescence (a radiative process involving flipping of electron spins) or intersystem crossing.

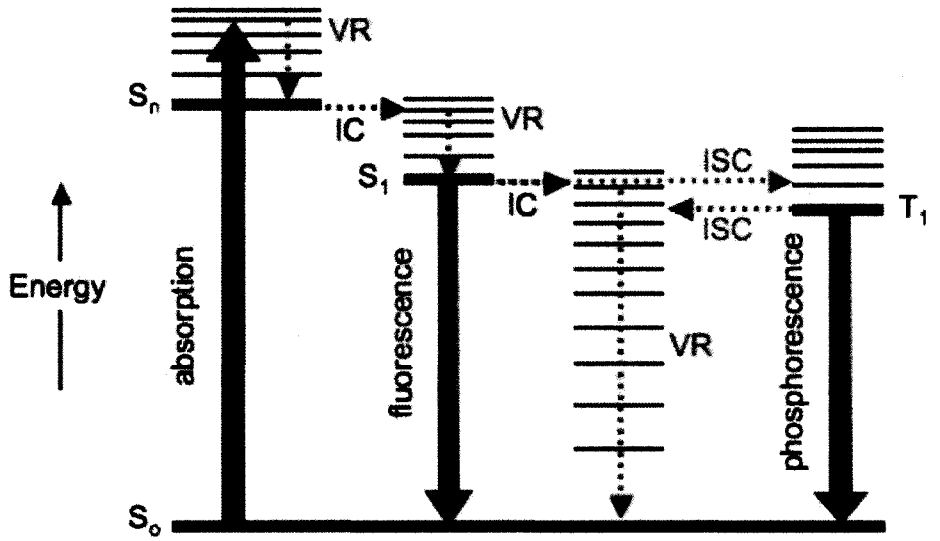


**Figure 1.8: A typical Jablonski diagram. $S_0$: ground state, $S_1$: lowest singlet excited state, $S_n$: upper singlet excited state, $T_1$: lowest triplet excited state, VR: vibrational relaxation, IC: internal conversion, ISC: intersystem crossing. Full arrows represent radiative transitions while dashed arrows represent non-radiative transitions. Adapted from Gilbert and Baggott.[16]**

It is believed that cyanine dyes undergo rapid deactivation from the singlet excited state by rotation around the internuclear double bond joining the two ring systems.[17-21] Upon absorption of a photon, the *trans*-singlet excited state ($S_1$) proceeds to a twisted excited state ($TS_1$), as illustrated in Figure 1.9. The twisted excited state can undergo internal conversion to the twisted ground state ($TS_0$),

where it can relax back to the *trans*-ground state ($S_0$) or to the *cis*-ground state ($PS_0$). It has been shown by Ruillière that deactivation occurs principally through the twisted excited state rather than directly through internal conversion between $S_1$ and $S_0$, and that most of the molecules populating $TS_1$ return to $S_0$ rather than going to $PS_0$.[21] This non-radiative energy releasing mechanism dramatically reduces fluorescence. However, if a dye is intercalated in DNA the base pairs hinder the rotation that would convert it to the twisted excited state, forcing it to dissipate its energy predominantly through fluorescence. This rationale has been used to explain the fluorescence enhancement of cyanine dyes upon binding to nucleic acids.[17,22,23] An increase in fluorescence can also occur when a dye binds in the minor groove of DNA, due to restricted internal rotation.[7]

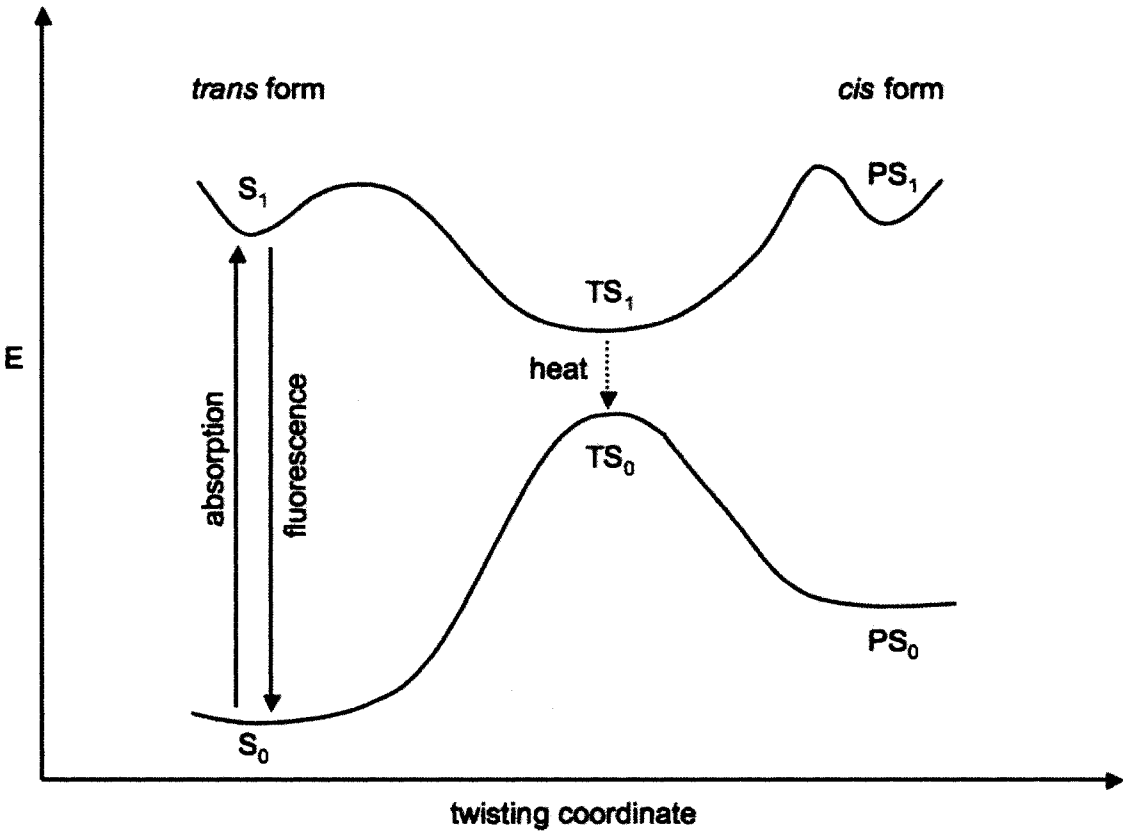


**Figure 1.9: Diagram illustrating cyanine dye photoisomerization where the energy (E) is a function of twisting coordinate. $S_0$: *trans*-ground state, $S_1$: *trans*-singlet excited state, $PS_0$: photoisomer ground state, $PS_1$: photoisomer singlet excited state, $TS_0$: twisted ground state, $TS_1$: twisted singlet excited state. Adapted from Rullière.[21]**

## 1.6. Modeling the Associations of Cyanine Dyes with DNA

Computational methods are extremely valuable in understanding the interactions of small molecules with DNA. When modeling the associations of cyanine dyes with DNA, a (relatively) large number of atoms are required. There is not only the dye and the DNA, but also the counterions and water molecules. Luckily, only a few thousand water molecules are required for the simulations (rather than Avogadro's number for bulk water) because of the use of periodic boundary conditions. The details of the molecular dynamics simulations will be discussed in Chapter 2. Nevertheless, there are still too many atoms for *ab initio* calculations to be feasible. Instead, *ab initio* calculations are used to generate the ground state geometry of the dye. This geometry is used with a molecular modeling package, in our case AMBER 8,[24] that generates the DNA structure and allows one to position the dye in the proximity of the DNA, and to add counterions and water molecules. Molecular mechanics are used for calculations on the entire system (dye, DNA, counterions and water), providing good results in a reasonable amount of time. DNA containing the standard bases can be generated using the NUCGEN utility embedded in AMBER, however it is possible to create strands containing DNA lesions with the appropriate library files.

## 1.7. UV-Induced DNA Damage

Ultraviolet radiation is harmful to all organisms, and the resulting DNA damage can lead to mutagenesis, carcinogenesis, and premature ageing. Even though most of the extraterrestrial ultraviolet light is absorbed by stratospheric ozone, small amounts of ultraviolet-B (UVB) radiation reach the Earth's surface. Absorption of this UVB light by cellular DNA is mainly responsible for the deleterious effects of solar radiation on living organisms.[25]

The purines and pyrimidines absorb ultraviolet-C light (200-280 nm) strongly so this radiation source has been employed in numerous studies on DNA damage due to the efficient photochemical reactions in DNA.[26-43] Although ultraviolet-C (UVC) radiation does not reach the Earth, in the laboratory it forms the DNA photoproducts that also result from atmosphere-penetrating UVB radiation, thus it can be used to mimic the DNA photoproducts formed from sunlight.

The major DNA photoproducts upon exposure to UVB light (280-315 nm) are cyclobutadipyrimidines (CPDs) and pyrimidine (6-4) pyrimidone adducts (6-4PPs), occurring with a ratio around 3:1 CPD:6-4PP in cellular DNA.[26] CPDs are created between adjacent pyrimidine bases by a [2+2] cycloaddition of the C5-C6 double bonds (Scheme 1.1). Although several diastereomers can theoretically be formed, only *syn* isomers will be produced in DNA because of steric constraints. Of the two *syn* isomers, the dominant diastereomer is the *cis-syn* form.[31]

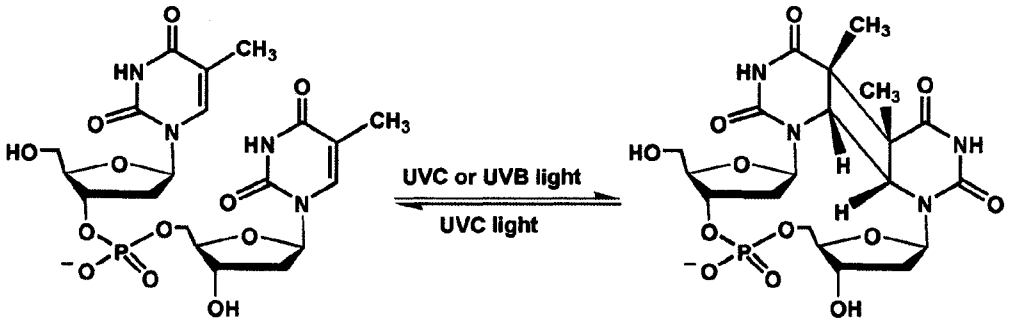


**Scheme 1.1: Formation of a *cis-syn* cyclobutane thymine dimer, adapted from Douki *et al.*[31]**

A [2+2] cycloaddition of the C5-C6 double bond of the 5'-end pyrimidine and either the C4 carbonyl group of the 3'-end thymine or the 4-imino function of the 3'-end cytosine forms an unstable oxetane or azetidine, respectively. The spontaneous rearrangement of the oxetane or azetidine creates the pyrimidine (6-4) pyrimidone adduct. 6-4PPs are formed at 5'-T-C-3', 5'-C-C-3' and 5'-T-T-3' sites, but not at 5'-C-T-3'.[25] The 6-4PPs are easily converted to their Dewar valence isomers by wavelengths of light greater than 280 nm.[44,45] The formation and photoisomerization of the TT (6-4) photoproduct is illustrated in Scheme 1.2. CPDs are not alkali-labile (they are repaired by enzymes) while 6-4PPs are alkali-labile lesions.[28]

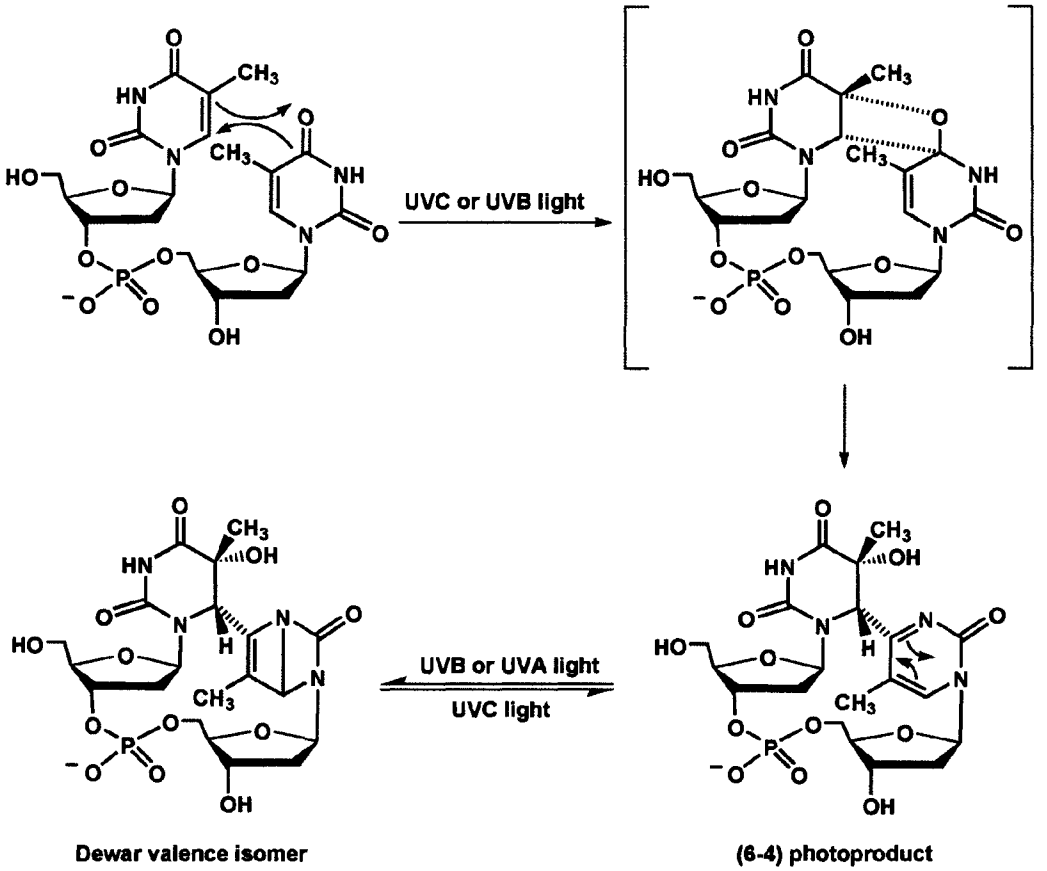


**Scheme 1.2: The formation and photoisomerization of the TT (6-4) photoproduct, adapted from Taylor.[46]**

5'-TT-3' and 5'-TC-3' sites in cellular DNA are one order of magnitude more photoreactive than 5'-CT-3' and 5'-CC-3' sites.[26] Although 5'-CC-3' sites are less photoreactive than 5'-TT-3' and 5'-TC-3' sites, 5'-CC-3' sites are where mutations occur (CC→TT), providing a signature of exposure to UV light.[47,48]

While the majority of UVB-induced DNA damage occurs at dipyrimidine sites, the purines are also photoreactive. One category of purine photoproducts involves adenine: two adjacent adenines can dimerize or one adenine residue can undergo an addition to an adjacent thymine to form the photoproducts shown in Figure 1.10. Even though the quantum yields of formation of these photoproducts are very low,[49,50] they may have a biological effect given that the A-T adduct is mutagenic.[51]

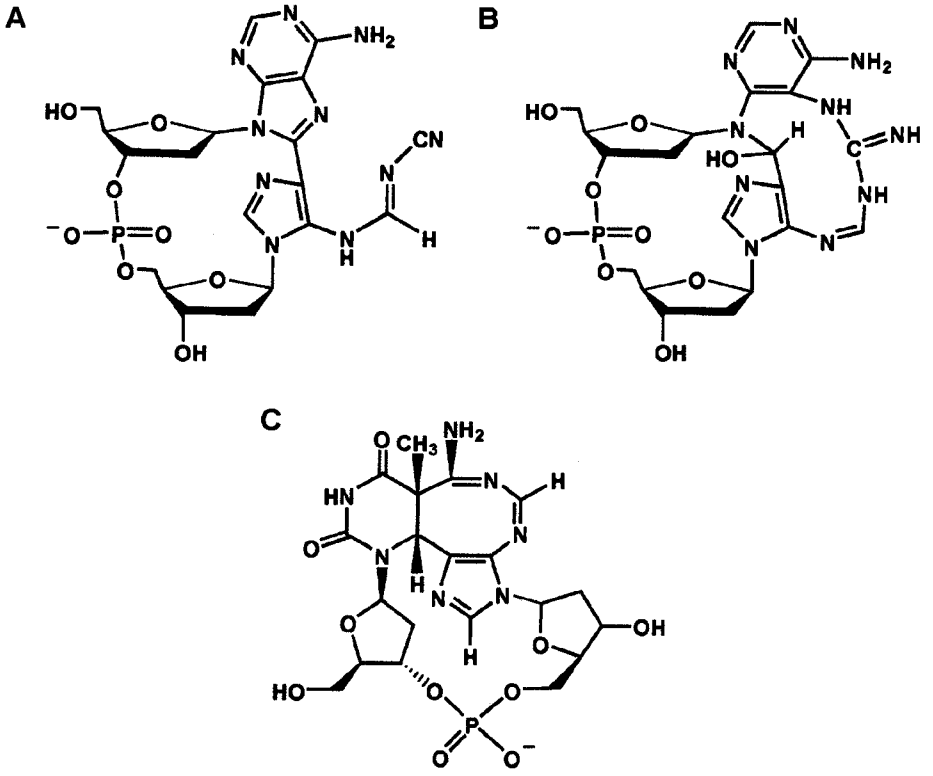


**Figure 1.10: Structures of adenine-containing photoproducts: (A) and (B) adenine dimers[52] and (C) a thymine-adenine adduct.[53]**

Another purine photoproduct is 8-oxo-2'-deoxyguanosine (8-oxo-dG), which can be generated by all forms of ultraviolet light.[54] There are at least four different pathways by which 8-oxo-dG can be created, as seen in Scheme 1.3, the main one being the one-electron oxidation pathway. Nevertheless, 8-oxo-dG is a minor photoproduct of UVB exposure.[26]

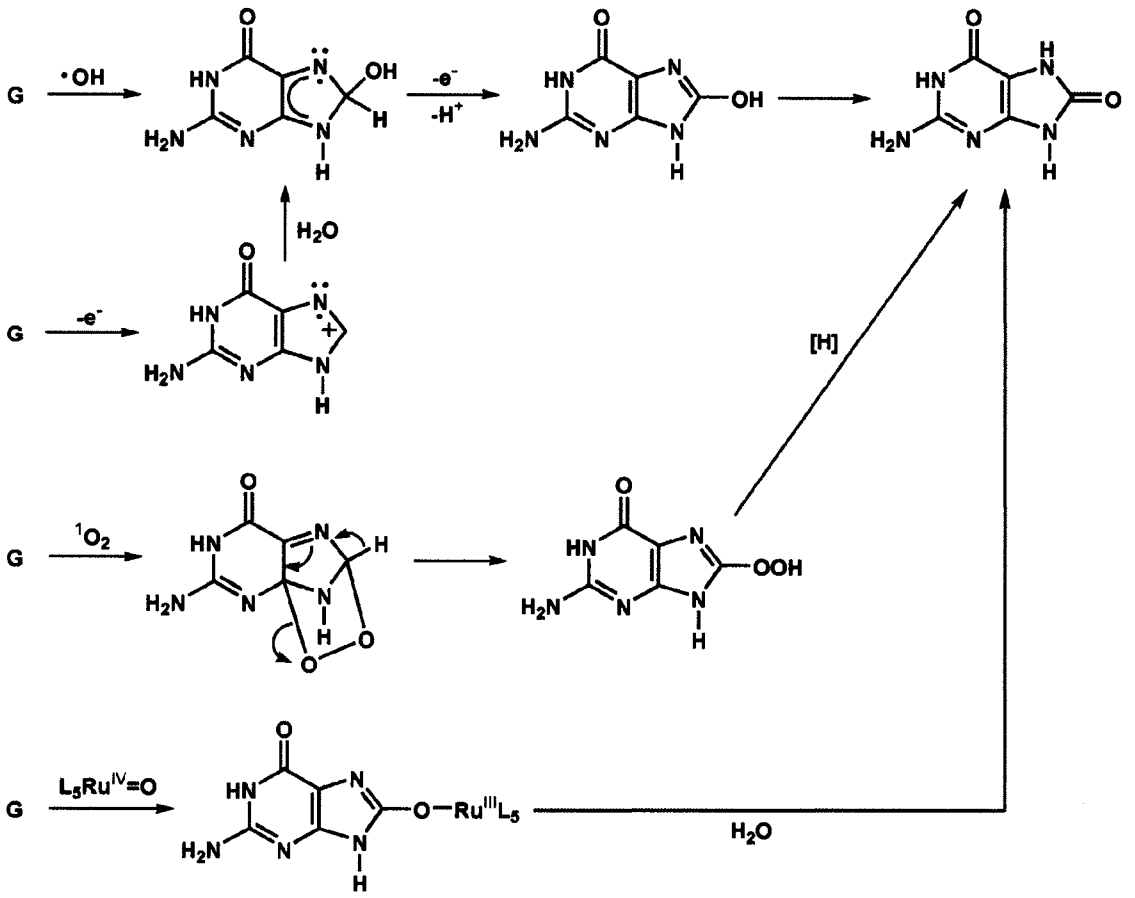


**Scheme 1.3: Guanine (G) reactions leading to 8-oxo-2'-deoxyguanosine, after Burrows and Muller.[28]**

Although native DNA does not absorb ultraviolet-A (UVA) light (315-400 nm), UVA light can initiate secondary photoreactions of previously formed DNA photoproducts or be responsible for photosensitized DNA damage by endogenous or exogenous sensitizers. Once excited, the sensitizer can undergo one of two competing processes: the Type I and Type II reactions, illustrated in Scheme 1.4. The excited sensitizer can react with a substrate (in this case DNA) or the solvent (Type I reaction), or with oxygen (Type II reaction). The Type I reaction involves hydrogen atom or electron transfer, producing radicals or radical ions. The majority of Type II reactions involve energy transfer from the sensitizer to molecular oxygen,

producing singlet oxygen. The other Type II reactions involve electron transfer from the sensitizer to oxygen, generating the oxidized sensitizer and the superoxide ion. It has been shown that exposure of cellular DNA to UVA light produces 8-oxo-dG as the major photoproduct, along with a few oxidized pyrimidine bases.[26]

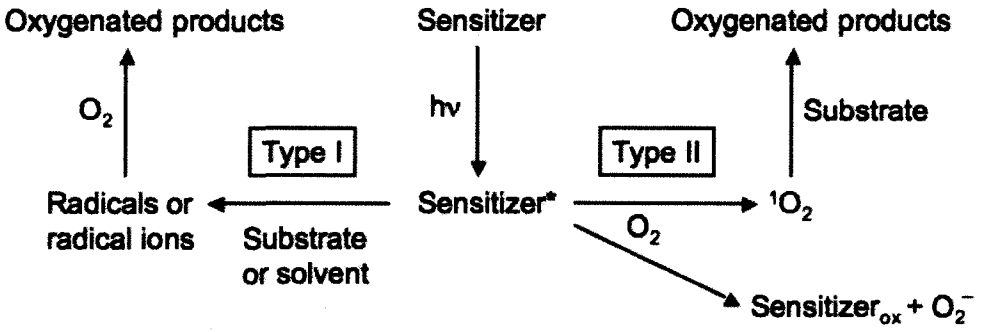


**Scheme 1.4: Type I and Type II photosensitized oxidation reactions, after Foote.[55]**

## 1.8. Detecting UV-induced DNA Damage

DNA damage via base modification will generally not lead to direct strand scission: a second step, such as heat, alkali, or enzymatic treatment, is necessary for cleavage.[28] Unmodified bases will be unaffected by the treatment while damaged bases will undergo strand scission. The modified bases are removed by glycosidic bond hydrolysis or nucleophilic displacement, and subsequent phosphate elimination results in cleavage (Scheme 1.5). Since the 4'-H is acidic, the fragment can undergo another elimination reaction.

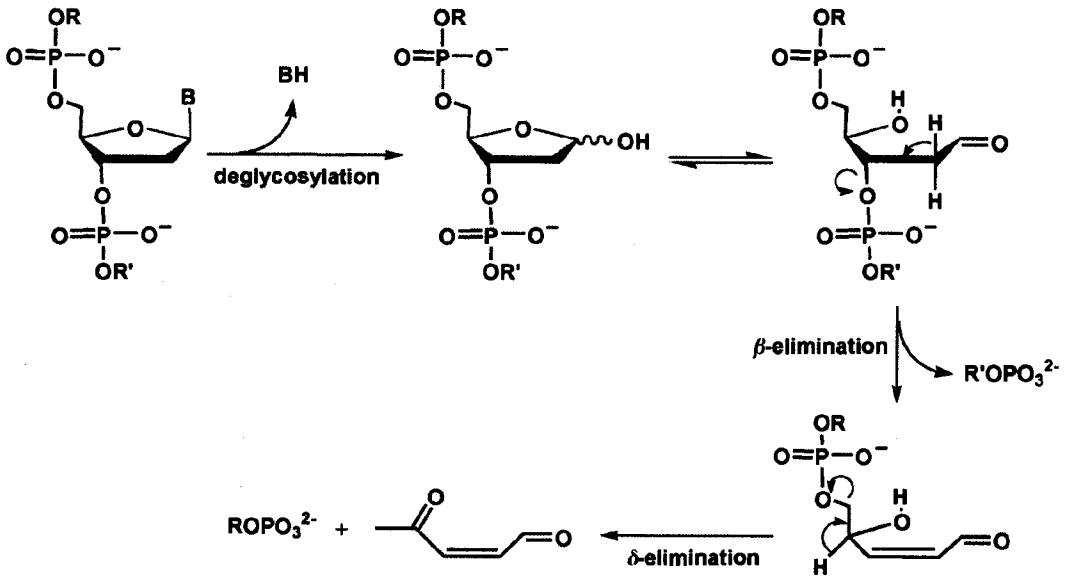


**Scheme 1.5: Mechanism of β-elimination and δ-elimination after formation of an abasic site, after Burrows and Muller.[28]**

Nucleic acid fragments can be studied using agarose or polyacrylamide gel electrophoresis. The fragments are generally labeled with fluorescent stains, one of the most popular being ethidium bromide, and their migration distances are compared with those of known DNA length standards, called DNA ladders, to estimate the size of the fragments in one's sample. As the size of the fragment decreases, its mobility through the gel increases. However, this technique does not

provide information on the preferred cleavage sites. This can be accomplished using end-labeling where one end of a strand is labeled with a radioactive or chemiluminescent tag, and this tagged nucleic acid is used to create a sequencing ladder via chemical or enzymatic methods.[56] The migration pattern of the damaged DNA is compared with that of the sequencing ladder. If there are no preferred cleavage sites then there will be a variety of bands of equal intensity, as illustrated in Figure 1.11A. However, if cleavage is specific then only some of the bands will be present, as illustrated in Figure 1.11B, and the cleavage sites can be identified.

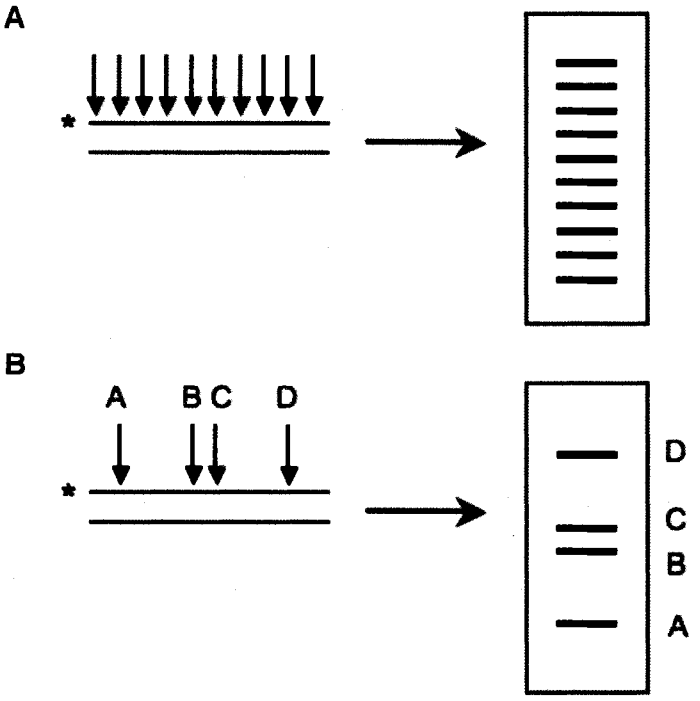


**Figure 1.11: Illustration demonstrating how the sequence selectivity for cleavage is visualized by polyacrylamide gel electrophoresis/autoradiography.[56] The asterisk (*) denotes a radioactive end label on one strand of the duplex. (A) The photocleaver exhibits no sequence selectivity, leading to a "ladder" of cleavage bands after electrophoresis and radiography. (B) The photocleaver exhibits a high level of sequence selectivity, leading to only a few, discrete cleavage bands on the film.**

Gel electrophoresis can also be used to measure DNA damage in individual cells, a technique that is referred to as the comet assay.[57] The cells (a minimum of approximately one thousand) are embedded in an agarose gel on a microscope slide and lysed. The DNA is then electrophoresed at a set voltage and stained with a fluorescent DNA-binding dye. Individual cells are visualized under a fluorescence microscope, where the DNA appears much like a comet. The comet tail, representing damaged DNA, migrates farther than the comet head, which corresponds to intact DNA. The "tail moment", defined as the product of DNA content in the tail and the mean migration distance in the tail, is the best descriptor of cellular DNA damage.[58] However, it is a subjective measurement affected by operator judgment. Although the comet assay is widely used, it suffers from a lack of standardization thus the descriptors of DNA damage vary with electrophoresis conditions and equipment, the DNA stain, camera sensitivity, and the image analysis software.[59] Initial efforts have been made by Tice *et al.*[60] to standardize the protocols and the analysis.

Two techniques were developed in the Scaiano laboratory that provide objective measurements of DNA damage. The first technique quantifies the ratio of single- to double-stranded DNA by measuring the lifetime of an intercalated fluorescent dye, providing a direct determination of DNA damage.[1,2] The dye employed in these studies was the cyanine dye PicoGreen that, as discussed in Section 1.5, decays in water almost exclusively by radiationless transitions around its central methine bridge. This decay pathway is suppressed during intercalation, forcing the dye to dissipate its energy predominantly via fluorescence emission. The more restrictive environment in double-stranded DNA hinders dye rotation, extending the excited dye lifetime relative to that in single-stranded DNA. However, the limitations of this technique are the high cost of the instrumentation and the high level of operator expertise required. The second technique provides a rapid, relatively cheap alternative that makes use of steady-state fluorescence measurements. Single- to double-stranded DNA ratios are quantified through simultaneous measurements of steady-state fluorescence from PicoGreen and

ethidium bromide.[61] The same principle is applied where free dye is negligibly fluorescent while intercalated dye is strongly fluorescent. The only restriction with this technique is that the DNA concentration must be accurately known.

To determine sites of DNA damage, one can isolate and study individual nucleosides. The DNA is hydrolyzed or enzymatically degraded down to nucleotides, which are converted to nucleosides via alkaline phosphatase. The DNA lesions can be separated using chromatographic techniques, for example high performance liquid chromatography (HPLC) with electrochemical detection[62,63] or HPLC-MS/MS.[64] Although a nucleoside and its corresponding modified nucleoside may have similar retention times in HPLC, electrochemical detection enables them to be distinguished as long as their redox potentials differ. In general, base modification also leads to sugar degradation, as seen in Scheme 1.5. Mass spectrometry can frequently be used to detect the DNA fragments and to determine their origin, i.e. whether or not the fragment was derived from H-abstraction at a certain position on the sugar. The detection of unmodified bases suggests that the damage resulted in sugar degradation rather than base modification, especially if the quantum yield for base release is approximately equal to the quantum yield for strand cleavage.[56]

## 1.9. Overview

As the storage and transmission vehicle of genetic information, DNA is extremely important to the survival of all organisms. Understanding the interactions of small molecules with DNA is of fundamental interest as well as having practical applications, such as drug design or monitoring DNA damage. In this chapter, the structure of DNA was briefly discussed, as well as the various binding modes of small molecules to DNA, with an emphasis on intercalation and minor groove binding. Previous work in our laboratory involved the study of nine different DNA dyes to establish which one could selectively detect double-stranded DNA. The cyanine dyes were found to be the best suited for this task, owing to the forced planarity that they undergo upon binding to DNA. These findings were what prompted the study of the dyes in this thesis. Originally we began investigating the association of these dyes with double-stranded DNA, but quickly realized that a thorough knowledge of their association with single-stranded DNA was needed before making any interpretations. As the ultimate goal of our work is to use these dyes to detect DNA damage, this chapter also reviewed the various DNA lesions that are formed upon ultraviolet exposure (mainly UVB- and UVC-induced DNA photoproducts).

In Chapters 3 and 4, the interactions of the cyanine dyes (TO, PTO and PG) with single-stranded and double-stranded DNA are examined, using both spectroscopic and computational methods. In Chapter 4, a new type of stable dye/DNA complex is formed when single-strands of poly(dA) and poly(dT) are hybridized in the presence of PG or PTO, which cannot be obtained by the addition of the dye to poly(dA)•poly(dT). In Chapter 5, various methodologies for identifying UVC-induced DNA damage are examined and the most sensitive is found to be fluorescence spectroscopy using TO.

## 1.10. References


1. Cosa, G.; Focsaneanu, K.-S.; McLean, J. R. N.; Scaiano, J. C., Direct determination of single-to-double stranded DNA ratio in solution applying time-resolved fluorescence measurements of dye-DNA complexes. *Chem. Commun.* **2000,** 8, 689-690.

2. Cosa, G.; Vinette, A. L.; McLean, J. R. N.; Scaiano, J. C., Novel DNA damage detection technique applying time-resolved fluorescence measurements. *Anal. Chem.* **2002,** 74, (24), 6163-6169.

3. Mikelsons, L.; Scaiano, J. C., Will my strawberries glow in the dark? *Canadian Chemical News, October issue* **2004**, 18-19.

4. Cantor, C. R.; Schimmel, P. R., Structures of nucleic acids. In *Biophysical Chemistry Part I: The conformation of biological macromolecules*, W.H. Freeman and Company: San Francisco, 1980; Vol. 1, pp 155-205.

5. Bates, A. D.; Maxwell, A., *DNA Topology.* Oxford University Press: New York, 2005; p 198.

6. Tidwell, R. R.; Boykin, D. W., Dicationic DNA minor groove binders as antimicrobial agents. In *Small Molecule DNA and RNA Binders: From Synthesis to Nucleic Acid Complexes*, Demeunynck, M.; Bailly, C.; Wilson, D. W., Eds. Wiley-VCH: Weinheim, 2003; Vol. 2, pp 414-460.

7. Armitage, B. A., Cyanine dye-DNA interactions: intercalation, groove binding, and aggregation. *Top. Curr. Chem.* **2005,** 253, 55-76.

8. Denny, W. A., Acridine-4-carboxamides and the concept of minimal DNA intercalators. In *Small Molecule DNA and RNA Binders: From Synthesis to Nucleic Acid Complexes*, Demeunynck, M.; Bailly, C.; Wilson, D. W., Eds. Wiley-VCH: Weinheim, 2003; Vol. 2, pp 482-502.

9. Cosa, G.; Focsaneanu, K.-S.; McLean, J. R. N.; McNamee, J. P.; Scaiano, J. C., Photophysical properties of fluorescent DNA-dyes bound to single- and double-stranded DNA in aqueous buffered solution. *Photochem. Photobiol.* **2001,** 73, (6), 585-599.

10. Affentranger, M. I.; Burkart, W., Resolution of DNA damage at the single-cell level shows largely different actions of X-rays and bleomycin. *J. Histochem. Cytochem.* **1995,** 43, (2), 229-235.

11. Yue, S. T.; Singer, V. L.; Roth, B. L.; Mozer, T. J.; Millard, P. J.; Jones, L. J.; Jin, X.; Haugland, R. P.; Poot, M. "Substituted unsymmetrical cyanine dyes with selected permeability", World Intellectual Property Organization, WO 96/13552. 1996.

12. Haugland, R. P.; Yue, S. T.; Millard, P. J.; Roth, B. L. "Cyclic-substituted unsymmetrical cyanine dyes", United States Patent Office, US5436134. 1995.

13. *IUPAC Compendium of Chemical Terminology.* 2nd ed.; 1997.

14. Hannah, K. C.; Armitage, B., DNA-templated assembly of helical cyanine dye aggregates: a supramolecular chain polymerization. *Acc. Chem. Res.* **2004,** 37, (11), 845-853.

15. Mishra, A.; Behera, R. K.; Behera, P. K.; Mishra, B. K.; Behera, G. B., Cyanines during the 1990s: a review. *Chem. Rev.* **2000,** 100, (6), 1973-2011.

16. Gilbert, A.; Baggott, J., *Essentials of Molecular Photochemistry.* Blackwell Scientific Publications: Oxford, 1991.

17. Carlsson, C.; Larsson, A.; Jonsson, M.; Albinsson, B.; Nordén, B., Optical and photophysical properties of the oxazole yellow DNA probes YO and YOYO. *J. Phys. Chem.* **1994,** 98, (40), 10313-10321.

18. Paerschke, H.; Süsse, K.-E.; Welsch, D.-G., Investigation of vibronic energy relaxation of polymethin cyanine dyes by picosecond spectroscopy. *Chem. Phys. Lett.* **1979,** 66, (2), 376-380.

19. Sundström, V.; Gillbro, T., Viscosity dependent radiationless relaxation rate of cyanine dyes. A picosecond laser spectroscopy study. *Chem. Phys.* **1981,** 61, 257-269.

20. Ponterini, G.; Momicchioli, F., Trans-cis photoisomerization mechanism of carbocyanines: experimental check of theoretical models. *Chem. Phys.* **1991,** 151, 111-126.

21. Rullière, C., Laser action and photoisomerisation of 3,3'-diethyl oxadicarbocyanine iodide (DODCI): influence of temperature and concentration. *Chem. Phys. Lett.* **1976,** 43, (2), 303-308.

22. Lee, L. G.; Chen, C.-H.; Chiu, L. A., Thiazole orange: a new dye for reticulocyte analysis. *Cytometry* **1986,** 7, 508-517.

23. Spielmann, H. P.; Wemmer, D. E.; Jacobsen, J. P., Solution structure of a DNA complex with the fluorescent bis-intercalator TOTO determined by NMR spectroscopy. *Biochemistry* **1995,** 34, (27), 8542-8553.

24. Case, D. A.; Darden, T. A.; Cheatham III, T. E.; Simmerling, C. L.; Wang, J.; Duke, R. E.; Luo, R.; Merz, K. M.; Wang, B.; Pearlman, D. A.; Crowley, M.; Brozell, S.; Tsui, V.; Gohlke, H.; Mongan, J.; Hornak, V.; Cui, G.; Beroza, P.; Schafmeister, C.; Caldwell, J. W.; Ross, W. S.; Kollman, P. A. *AMBER 8*, University of California, San Francisco, 2004.

25. Sinha, R. P.; Häder, D.-P., UV-induced DNA damage and repair: a review. *Photochem. Photobiol. Sci.* **2002,** 1, (4), 225-236.

26. Ravanat, J.-L.; Douki, T.; Cadet, J., Direct and indirect effects of UV irradiation on DNA and its components. *J. Photochem. Photobiol. B.* **2001,** 63, 88-102.

27. Bogdanov, K. V.; Chukhlovin, A. B.; Zaritskey, A. Y.; Frolova, O. L.; Afanasiev, B. V., Ultraviolet irradiation induces multiple DNA double-strand breaks and apoptosis in normal granulocytes and chronic myeloid leukaemia blasts. *Brit. J. Haematology* **1997,** 98, (4), 869-872.

28. Burrows, C. J.; Muller, J. G., Oxidative nucleobase modifications leading to strand scission. *Chem. Rev.* **1998,** 98, (3), 1109-1151.

29. Cavalieri, L. F.; Bendich, A., The ultraviolet absorption spectra of pyrimidines and purines. *J. Am. Chem. Soc.* **1950,** 72, (6), 2587-2594.

30. Choy, C. K. M.; Benzie, I. F. F.; Cho, P., UV-mediated DNA strand breaks in corneal epithelial cells assessed using the comet assay procedure. *Photochem. Photobiol.* **2005,** 81, (3), 493-497.

31. Douki, T.; Court, M.; Sauvaigo, S.; Odin, F.; Cadet, J., Formation of the main UV-induced thymine dimeric lesions within isolated and cellular DNA as measured by high performance liquid chromatography-tandem mass spectrometry. *J. Biol. Chem.* **2000,** 275, (16), 11678-11685.

32. Douki, T.; Perdiz, D.; Gróf, P.; Kuluncsics, Z.; Moustacchi, E.; Cadet, J.; Sage, E., Oxidation of guanine in cellular DNA by solar UV radiation: biological role. *Photochem. Photobiol.* **1999,** 70, (2), 184-190.

33. Hall, A.; Ballantyne, J., Characterization of UVC-induced DNA damage in bloodstains: forensic implications. *Anal. Bioanal. Chem.* **2004,** 380, 72-83.

34. Mφller, P.; Wallin, H.; Dybdahl, M.; Frentz, G.; Nexφ, B., Psoriasis patients with basal cell carcinoma have more repair-mediated DNA strand breaks after UVC damage in lymphocytes than psoriasis patients without basal cell carcinoma. *Cancer Lett.* **2000,** 151, (2), 187-192.

35. Madigan, J. P.; Chotkowski, H. L.; Glaser, R. L., DNA double-strand break-induced phosphorylation of *Drosophila* histone variant H2Av helps prevent radiation-induced apoptosis. *Nucleic Acids Res.* **2002,** 30, (17), 3698-3705.

36. Munch-Petersen, B., Thymidine in the micromolar range promotes rejoining of UVC-induced DNA strand breaks and prevents azidothymidine from inhibiting the rejoining in quiescent human lymphocytes. *Mutat. Res.* **1997,** 383, (2), 143-153.

37. Peak, J. G.; Peak, M. J., Ultraviolet light induces double-strand breaks in DNA of cultured human P3 cells as measured by neutral filter elution. *Photochem. Photobiol.* **1990,** 52, (2), 387-392.

38. Smith, C. A.; Taylor, J.-S., Preparation and characterization of a set of deoxyoligonucleotide 49-mers containing site-specific cis-syn, trans-syn-I, (6-4), and Dewar photoproducts of thymidylyl(3'-5') thymidine. *J. Biol. Chem.* **1993,** 268, (15), 11143-11151.

39. Wei, H.; Cai, Q.; Rahn, R.; Zhang, X., Singlet oxygen involvement in ultraviolet (254 nm) radiation-induced formation of 8-hydroxy-deoxyguanosine in DNA. *Free Rad. Biol. Med.* **1997,** 23, (1), 148-154.

40. Wei, Z.; Lifen, J.; Jiliang, H.; Jianlin, L.; Baohong, W.; Hongping, D., Detecting DNA repair capacity of peripheral lymphocytes from cancer patients with UVC challenge test and bleomycin challenge test. *Mutagenesis* **2005,** 20, (4), 271-277.

41. Zhang, X.; Rosenstein, B. S.; Wang, Y.; Lebwohl, M.; Wei, H., Identification of possible reactive oxygen species involved in ultraviolet radiation-induced oxidative DNA damage. *Free Radic. Biol. Med.* **1997,** 23, (7), 980-985.

42. Zhang, X. S.; Rosenstein, B. S.; Wang, Y.; Lebwohl, M.; Mitchell, D. M.; Wei, H. C., Induction of 8-oxo-7,8-dihydro-2'-deoxyguanosine by ultraviolet radiation in calf thymus DNA and HeLa cells. *Photochem. Photobiol.* **1997,** 65, (1), 119-124.

43. Zheng, W.; He, J. L.; Jin, L. F.; Lou, J. L.; Wang, B. H., Assessment of human DNA repair (NER) capacity with DNA repair rate (DRR) by comet assay. *Biomed. Environ. Sci.* **2005,** 18, (2), 117-123.

44. Taylor, J.-S.; Cohrs, M. P., DNA, light, and Dewar pyrimidones: the structure and biological significance of TpT3. *J. Am. Chem. Soc.* **1987,** 109, (9), 2834-2835.

45. Taylor, J.-S.; Lu, H.; Kotyk, J. J., Quantitative conversion of the (6-4) photoproduct of TpdC to its Dewar valence isomer upon exposure to simulated sunlight. *Photochem. Photobiol.* **1990,** 51, (2), 161-167.

46. Taylor, J.-S., Unraveling the molecular pathway from sunlight to skin cancer. *Acc. Chem. Res.* **1994,** 27, (3), 76-82.

47. Dumaz, N.; Drougard, C.; Sarasin, A.; Daya-Grosjean, L., Specific UV-induced mutation spectrum in the p53 gene of skin tumors from DNA-repair-deficient xeroderma pigmentosum patients. *Proc. Natl. Acad. Sci. U.S.A.* **1993,** 90, 10529-10533.

48. Nakazawa, H.; English, D.; Randell, P. L.; Nakazawa, K.; Martel, N.; Armstrong, B. K.; Yamasaki, H., UV and skin cancer: Specific p53 gene mutation in normal skin as a biologically relevant exposure measurement. *Proc. Natl. Acad. Sci. U.S.A.* **1994,** 91, (1), 360-364.

49. Sharma, N. D.; Davies, R. J. H., Extent of formation of a dimeric adenine photoproduct in polynucleotides and DNA. *J. Photochem. Photobiol. B: Biol.* **1989,** 3, 247-258.

50. Bowden, G. M.; Davies, R. J. H., A sequence-specific alkali-labile photolesion mapping to adenine in single-stranded DNA. *Photochem. Photobiol.* **1997,** 66, 413-417.

51. Zhao, X.; Taylor, J.-S., Mutation spectra of TA*, the major photoproduct of thymidylyl-(3'-5')-deoxyadenosine, in *Escherichia coli* under SOS conditions. *Nucleic Acids Res.* **1996,** 24, (8), 1561-1565.

52. Kumar, S.; Joshi, P. C.; Sharma, N. D.; Bose, S. N.; Davies, R. J. H.; Takeda, N.; McCloskey, J.A., Adenine photodimerization in deoxyadenylate sequences: elucidation of the mechanism through structural studies of a major d(ApA) photoproduct. *Nucleic Acids Res.* **1991,** 19, (11), 2841-2847.

53. Zhao, X.; Nadji, S.; Kao, J. L.-F.; Taylor, J.-S., The structure of d(TpA)*, the major photoproduct of thymidylyl-(3'-5')-deoxyadenosine. *Nucleic Acids Res.* **1996,** 24, (8), 1554-1560.

54. Zhang, X.; Rosenstein, B. S.; Wang, Y.; Lebwohl, M.; Mitchell, D. M.; Wei, H., Induction of 8-hydroxy-2'-deoxyguanosine by ultraviolet radiation in calf thymus DNA and HeLa cells. *Photochem. Photobiol.* **1997,** 65, 119-124.

55. Foote, C. S., Definition of Type I and Type II photosensitized oxidation. *Photochem. Photobiol.* **1991,** 54, (5), 659.

56. Armitage, B., Photocleavage of nucleic acids. *Chem. Rev.* **1998,** 98, (3), 1171-1200.

57. Olive, P. L., Cell proliferation as a requirement for development of the contact effect in Chinese hamster V79 spheroids. *Radiat. Res.* **1989,** 117, (1), 79-92.

58. Olive, P. L.; Banáth, J. P.; Durand, R. E., Heterogeneity in radiation-induced DNA damage and repair in tumor and normal cells measured using the "comet" assay. *Radiat. Res.* **1990,** 122, (1), 86-94.

59. Olive, P. L., DNA damage and repair in individual cells: applications of the comet assay in radiobiology. *Int. J. Radiat. Biol.* **1999,** 75, (4), 395-405.

60. Tice, R. R.; Agurell, E.; Anderson, D.; Burlinson, B.; Hartmann, A.; Kobayashi, H.; Miyamae, Y.; Rojas, E.; Ryu, J.-C.; Sasaki, Y. F., Single cell gel/comet assay: guidelines for *in vitro* and *in vivo* genetic toxicology testing. *Environ. Mol. Mutagen.* **2000,** 35, (3), 206-221.

61. Beach, L.; Schweitzer, C.; Scaiano, J. C., Direct determination of single-to-double stranded DNA ratio in solution using steady-state fluorescence measurements. *Org. Biomol. Chem.* **2003,** 1, (3), 450-451.

62. Floyd, R. A.; Watson, J. J.; Wong, P. K.; Altmiller, D. H.; Rickard, R. C., Hydroxyl free radical adduct of deoxyguanosine: sensitive detection and mechanisms of formation. *Free Radic. Res. Commun.* **1986,** 1, (3), 163-172.

63. Kaur, H.; Halliwell, B., Measurement of oxidized and methylated DNA bases by HPLC with electrochemical detection. *Biochem. J.* **1996,** 318, 21-23.

64. Ravanat, J.-L.; Duretz, B.; Guiller, A.; Douki, T.; Cadet, J., Isotope dilution high-performance liquid chromatography-electrospray tandem mass spectrometry assay for the measurement of 8-oxo-7,8-dihydro-2'-deoxyguanosine in biological samples. *J. Chromatogr. B* **1998,** 715, 349-356.

# 2. Spectroscopic Techniques and Molecular Dynamics Simulations

## 2.1. Introduction

This chapter discusses the various spectroscopic techniques that are employed in this thesis to study the interactions of cyanine dyes with DNA. Since most readers are already familiar with the principles of absorption spectroscopy and steady-state fluorescence spectroscopy, and the associated instrumentation, these techniques will not be covered; specific instruments are discussed in the Materials and Methods section of each chapter. Instead, emphasis will be placed on circular dichroism and linear dichroism spectroscopies, time-resolved fluorescence spectroscopy, and molecular dynamics simulations, all of which are available at the University of Ottawa. Examples involving the association of cyanine dyes with DNA will be shown whenever possible. Circular dichroism and linear dichroism spectroscopies are particularly useful for confirming and characterizing the association of a molecule with DNA. When the molecule does not exhibit a signal of its own, but shows an induced signal upon binding to DNA, then these techniques can be used as a diagnostic for molecule/DNA association. Time-resolved fluorescence spectroscopy reports on the environment of the molecule, and molecular modeling provides insight into the association of small molecules with DNA. We have found that the calculations are an extremely useful complement to the spectroscopic techniques in the study of dye/DNA complexes.

## 2.2. Spectroscopic Techniques Employing Polarized Light

In this section, two techniques employing polarized light are discussed, which are used to study chiral molecules (circular dichroism spectroscopy) and oriented molecules (linear dichroism spectroscopy). Circular dichroism (CD) spectroscopy utilizes circularly polarized light where the electric field vector has constant magnitude but traces out a helix as it propagates (see Figure 2.1A). Linear dichroism spectroscopy makes use of linearly polarized light where the magnitude of the electric field oscillates but the propagation direction remains in one plane (see Figure 2.1B). Linearly polarized light is made up of two circularly polarized components that have equal intensity.

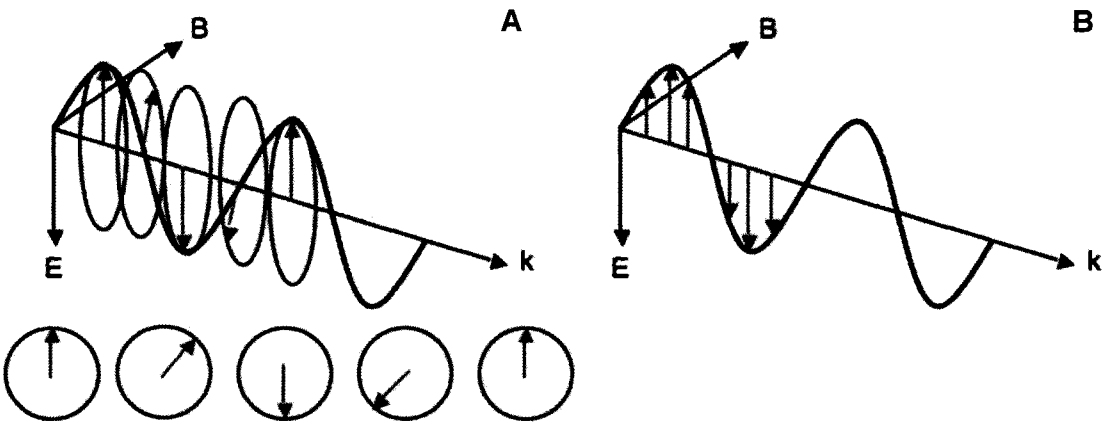


**Figure 2.1: (A) Circularly and (B) linearly polarized electromagnetic radiation. B: magnetic field, E: electric field, k: direction of propagation. Red arrows indicate the direction of E. Adapted from Rodger and Nordén.[1]**

### 2.2.1. Circular Dichroism Spectroscopy

When a sample absorbs unpolarized light, the absorbance ($A$) is defined by Equation 2-1.

**Equation 2-1**

$$A = \log_{10}\left(\frac{I_0}{I}\right)$$

where $I_0$ and $I$ are the intensities of incident and transmitted light, respectively. The Beer-Lambert law (Equation 2-2) relates the absorbance of a sample with its concentration ($c$).

**Equation 2-2** $$A = \varepsilon c l$$

where $\varepsilon$ is the molar extinction coefficient and $l$ is the optical path length.

Circular dichroism ($CD$) is defined as the difference in absorption of left- and right-circularly polarized light (Equation 2-3).

**Equation 2-3** $$CD \equiv A_L - A_R = \Delta A$$

Equation 2-4 gives the equivalent relationship of Equation 2-2 for circular dichroism.

**Equation 2-4** $$\Delta A = (\Delta\varepsilon) c l$$

where $\Delta A$ is the difference between the absorbance of the two types of circularly polarized light while $\Delta\varepsilon$ is molar circular dichroism (the difference between the extinction coefficients for the two types of circularly polarized light).

Even though modern commercial spectropolarimeters measure $\Delta A$, for historical reasons measurements are reported in ellipticity, which is an alternative measure of CD. When plane polarized light passes through a substance that exhibits CD, its two circular components are absorbed to different extents and the transmitted light is elliptically polarized, as illustrated in Figure 2.2. This concept was the basis for the original method of measuring CD.

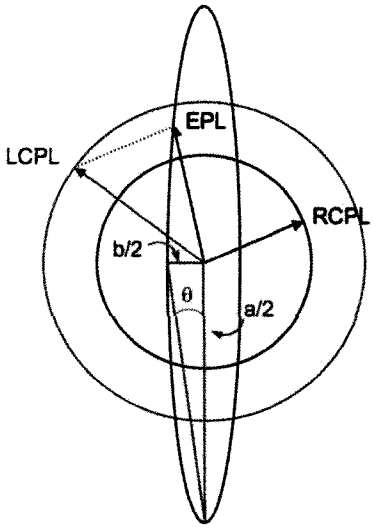


**Figure 2.2: Elliptically polarized light (EPL), formed by left- and right-circularly polarized light (LCPL and RCPL, respectively) of unequal intensities. The ellipticity is the angle θ, the tangent of which is the ratio of the minor axis (b) to the major axis (a) of the ellipse. Adapted from Woody.[2]**

The ellipticity is the angle θ, the tangent of which is the ratio of the minor to the major axis of the ellipse. In general this angle is very small, thus tan θ can be approximated as θ in radians (Equation 2-5).

**Equation 2-5**

$$\theta(rad) \approx \tan\theta = \frac{|E_L| - |E_R|}{|E_L| + |E_R|}$$

where $E_L$ and $E_R$ are the electric field vectors of the left- and right-circularly polarized light, respectively. The intensity of light is proportional to the square of the electric field vector thus Equation 2-5 can be written as Equation 2-6.

**Equation 2-6**

$$\theta(rad) = \frac{|I_L^{1/2}| - |I_R^{1/2}|}{|I_L^{1/2}| + |I_R^{1/2}|}$$

Putting Equation 2-1 in natural logarithm form gives Equation 2-7.

**Equation 2-7**

$$I = I_0 \exp(-A\ln(10))$$

Substituting Equation 2-7 into Equation 2-6 gives Equation 2-8.

**Equation 2-8**

$$\theta(rad) = \frac{\exp(-A_L/2) - \exp(-A_R/2)}{\exp(-A_L/2) + \exp(-A_R/2)}$$

Expanding the exponentials in Equation 2-8, neglecting terms of the order of $\Delta A$ in comparison with unity (since $\Delta A$ <<1), and converting from radians to degrees gives Equation 2-9.

**Equation 2-9**

$$\theta(\text{deg}) = \Delta A\left(\frac{\ln(10)}{4}\right)\left(\frac{180}{\pi}\right) = 32.982\Delta A = 32.982(CD)$$

Equation 2-9 demonstrates that ellipticity, θ, is directly proportional to CD. Circular dichroism spectra are usually recorded in millidegrees (mdeg) versus wavelength, and the ellipticity can easily be converted to CD, as seen in Equation 2-10.

**Equation 2-10**

$$CD = \frac{\theta(\text{mdeg})}{32{,}982}$$

Only molecules with an electric dipole transition moment and a magnetic dipole transition moment have observable circular dichroism. Consequently, a molecule must possess either an inherently asymmetric chromophore or a symmetric chromophore in an asymmetric environment. DNA is a molecule that possesses both types of chromophores. The DNA bases have a plane of symmetry, hence they do not have any intrinsic optical activity. The 2'-deoxyribose sugars in DNA are asymmetric and induce CD in the bases. The sugar transitions are usually weak, resulting primarily from $\sigma \rightarrow \sigma^*$ transitions in saturated groups containing C-C, C-O, C-H, and O-H bonds. The phosphate groups in DNA absorb below 170 nm so their transitions will not be observed in CD spectra recorded on traditional spectropolarimeters. The intense bands seen in the CD spectra of DNA are the result of strong base-to-base interactions, specifically $\pi \rightarrow \pi^*$ transitions. The $n \rightarrow \pi^*$ transitions are usually weak and as a result are hidden under the stronger

$\pi \rightarrow \pi^*$ transitions. The electronic transition moment directions of the DNA bases are illustrated in Figure 2.3.

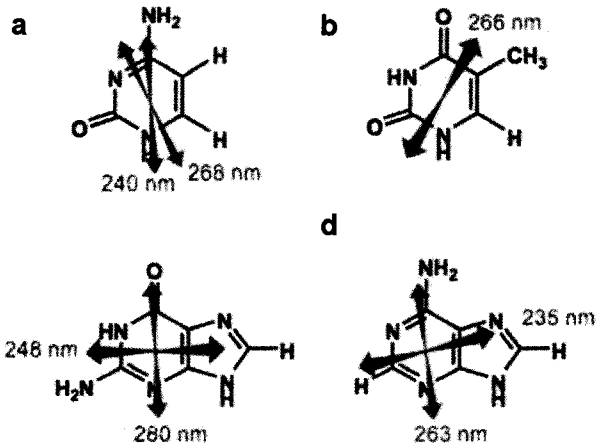


**Figure 2.3: Electronic transition moment directions of (a) cytosine, (b) thymine, (c) guanine, and (d) adenine.[3]**

When achiral molecules associate with chiral DNA they can acquire an induced CD (ICD) signal in their electronic transitions. There are two possible causes for this ICD. The first is that the DNA has structurally perturbed the achiral molecule, rendering it chiral. The second is that the transitions in the achiral molecule have coupled with those in the DNA, giving them a helical element. The observation of ICD confirms that there is an association, making CD a useful technique for studying the interactions of achiral molecules and DNA. An example is shown in Figure 2.4. The N-propyl pyridinium derivative of thiazole orange (PTO) is achiral thus it has no intrinsic CD. Upon complexation with DNA (in this example single-stranded poly(dG)) PTO shows ICD in the wavelength region where it absorbs.

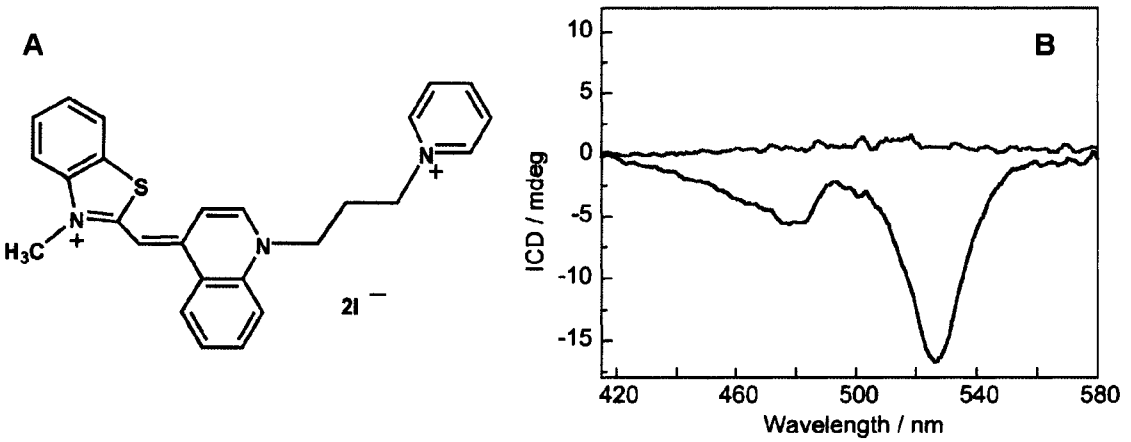


**Figure 2.4: (A) Structure of PTO. (B) PTO in buffer (purple) does not exhibit induced circular dichroism, while PTO in the presence of poly(dG) (blue) does. Adapted from Mikelsons *et al.*[4] (see also Chapter 3).**

### 2.2.1.1. Optical System for Spectropolarimetry

A typical optical system for spectropolarimetry is illustrated in Figure 2.5, where the light source is a xenon lamp. The $M_1$ mirror converges the emitted light into the $S_1$ entrance slit, which is the beginning of a double monochromator. The components between the $S_1$ entrance slit and the $S_2$ intermediate slit comprise the first monochromator, while the second monochromator is made up of the optical system between the $S_2$ intermediate slit and the $S_3$ exit slit. Since circular dichroism involves extremely small changes in absorbance, the ability of a double monochromator to reduce stray light is vital for CD measurements.

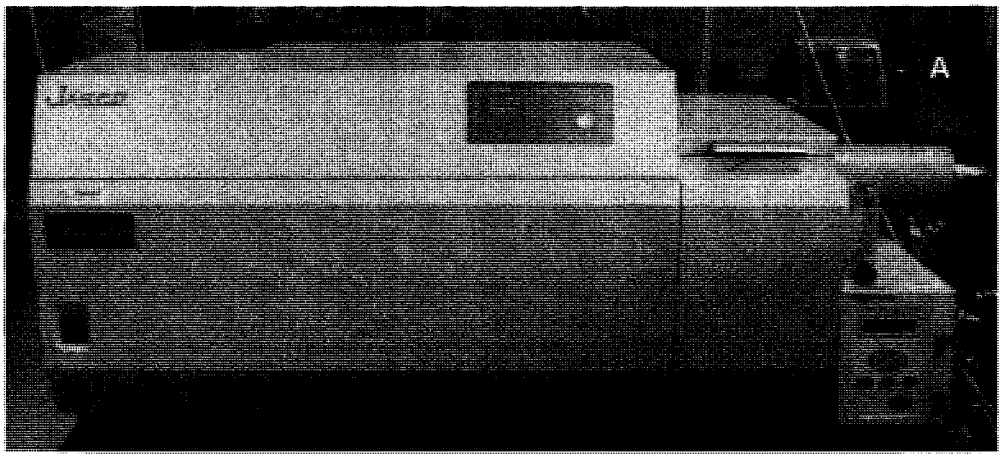


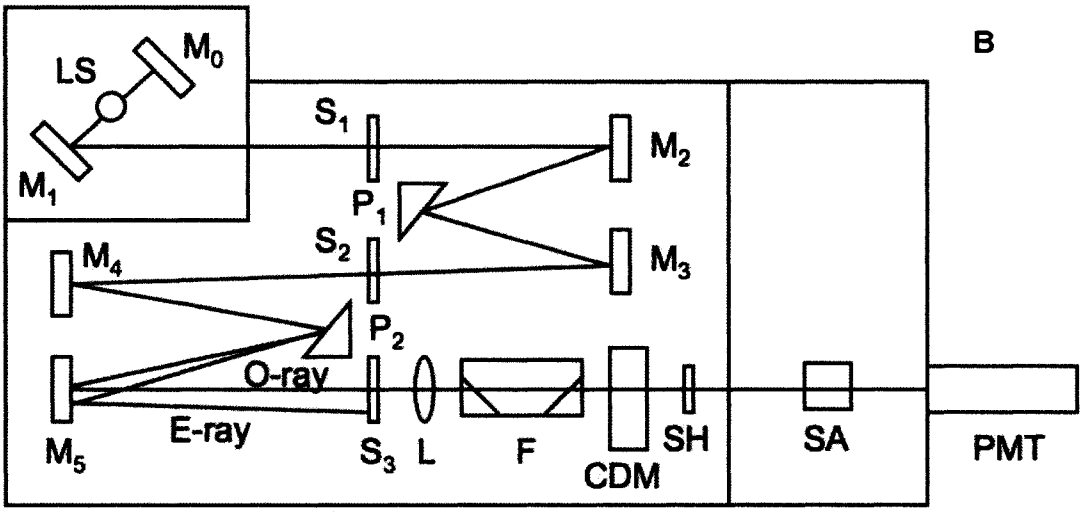


**Figure 2.5: (A) Picture of our JASCO J-810 spectropolarimeter. (B) Schematic diagram of the optical system of a typical spectropolarimeter, shown here for the JASCO J-810 spectropolarimeter. LS: light source, $M_{0-5}$: mirror, $S_{1-3}$: slit, $P_1$: first prism (horizontal optical axis), $P_2$: second prism (vertical optical axis), O-ray: ordinary ray, E-ray: extraordinary ray, L: lens, F: filter, CDM: modulator, SH: shutter, SA: sample, PMT: photomultiplier tube.[5]**

The light that exits the double monochromator is linearly polarized via crystal prisms ($P_1$ and $P_2$) that have different axial orientations. When the linearly polarized light passes through the modulator, it is changed into left- and right-

circularly polarized light. This is accomplished via the Piezo effect, where the modulator subjects quartz to mechanical stress, producing circular polarization in the crystal. The light exiting the modulator alternates between left- and right-circularly polarized light at the modulation frequency. The circularly polarized light passes through the sample and the transmitted light hits the photomultiplier tube (PMT), which produces a current. A lock-in amplifier detects this current, consisting of a small alternating current (AC) and a larger direct current (DC). The ratio of the AC and DC currents is directly proportional to the circular dichroism. The DC component, which depends on the total absorption of light by the sample, is kept constant by adjusting the high voltage applied to the PMT. Consequently, the circular dichroism is directly proportional to the AC component and thus the gain of the amplifier. The lock-in amplifier determines the phase of the AC component and thus the sign of the CD.

### 2.2.2. Linear Dichroism Spectroscopy

Linear dichroism (LD) is defined as the differential absorption of linearly polarized light (Equation 2-11).

**Equation 2-11** $$LD \equiv A_{\parallel} - A_{\perp}$$

In Equation 2-11, $A_{\parallel}$ and $A_{\perp}$ are the absorbances of light that is linearly polarized parallel and perpendicular, respectively, to an orientation axis. Thus linear dichroism is observed for systems that are either intrinsically oriented or are oriented using a molecular alignment technique. To measure LD, either the sample or the polarization of the light must be rotated 90°. Most current circular dichroism spectropolarimeters, such as the one shown in Figure 2.5, can also perform LD measurements. This is accomplished by increasing the voltage (by a factor of 2) across the quarter-wave photoelastic modulator, converting it to a half wave plate with alternating horizontal and vertical polarizations.

If the polarization (the direction of the electric transition moment) of the examined transition is perfectly parallel to the orientation direction, then Equation 2-11 follows the relationship in Equation 2-12.

**Equation 2-12** $$LD \equiv A_{\parallel} - A_{\perp} = A_{\parallel} > 0$$

On the other hand, if the polarization is perfectly perpendicular to the orientation direction, then Equation 2-13 will hold.

**Equation 2-13** $$LD \equiv A_{\parallel} - A_{\perp} = -A_{\perp} < 0$$

For all polarizations between perfectly parallel and perfectly perpendicular (to the orientation direction), the LD will be between the values in Equation 2-12 and Equation 2-13. Consequently, if the molecular orientation (relative to the orientation axis) is known then LD provides information on the polarization of the transition, and the converse is also true.

One of the primary uses of LD is to confirm that a drug is bound to DNA. If there is no interaction between the drug and the DNA, then the LD spectra of the combined drug/DNA solution will be no different than separate DNA or drug solutions. Upon binding of the drug to the DNA, the drug becomes oriented and exhibits LD in its absorption region,[6] which is analogous to drug induced circular dichroism. DNA exhibits negative LD, due to the more or less perpendicular orientation of its bases relative to the helical axis (which is parallel to the orientation axis). If a drug is intercalated between the DNA bases, i.e. the drug is perpendicular to the helical axis, then it too will show a negative LD in its absorption region.[7] An example involving PTO is shown in Figure 2.6. In the absence of DNA, PTO (whose structure is shown in Figure 2.4A) does not exhibit LD. Upon binding to double-stranded calf thymus DNA, PTO shows a negative LD signal in its absorption region, indicating dye intercalation.

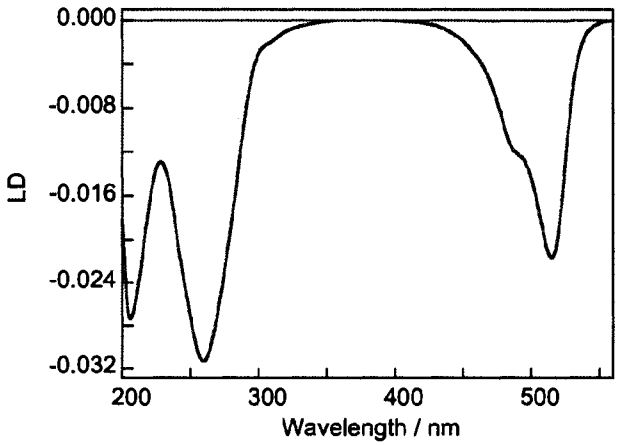


**Figure 2.6: PTO in buffer (purple) does not exhibit linear dichroism, while PTO in the presence of double-stranded calf thymus DNA (red) does. For more details, see Chapter 4.**

On the other hand, if the drug is bound in the grooves of the DNA then its LD will be positive. However, the width of the major groove is approximately twice that of the minor groove, so drugs bound in the major groove may be able to adopt a variety of orientations; thus it would appear as though their overall orientation was random and there would be negligible LD.[8]

The reduced linear dichroism ($LD^r$), defined in Equation 2-14, is the LD divided by the isotropic absorbance ($A_{iso}$).

**Equation 2-14** $$LD^r \equiv LD / A_{iso}$$

Planar aromatic drug molecules tend to have their $\pi \rightarrow \pi^*$ transitions polarized in the plane of the chromophore. If the drug molecule is intercalated, then the drug and the DNA bases will be essentially coplanar, giving an $LD^r$ in the drug absorption region that has the same sign and magnitude as the DNA $LD^r$.[9] As can be seen in Figure 2.7, the $LD^r$ in the PTO absorption region has the same sign and approximately the same magnitude as the DNA $LD^r$ (250-290 nm), indicating that the planes of the base pairs and the dye are parallel, owing to intercalation.[10]

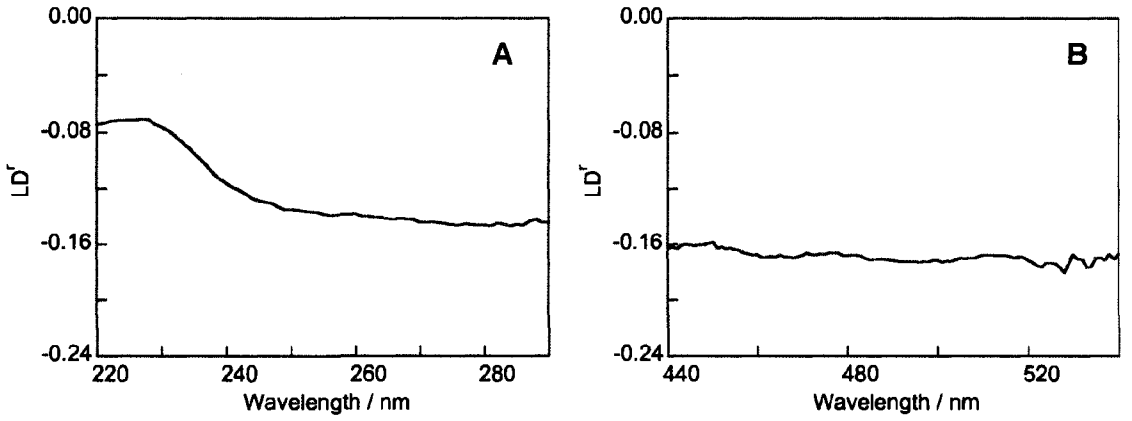


**Figure 2.7: Reduced linear dichroism of PTO and double-stranded calf thymus DNA in (A) the DNA region and (B) the dye region. For more details, see Chapter 4.**

Linear dichroism spectroscopy has also been used to study the structure of the molecular electric wire M-DNA,[11] to determine whether or not DNA was released from bacteriophage T5 after dye binding,[12] to investigate the alignment of DNA in agarose gels,[13] and to study the structure of RecA protein-DNA complex filaments using fluorescence detection.[14]

To observe LD, the sample must be completely or partially aligned. Examples of alignment techniques are flow orientation, electric field orientation, squeezed gel orientation, liquid crystal orientation, and absorption into stretched polymers. In our experiments we employed flow orientation in a cylindrical Couette cell, as it is the most common method for aligning DNA. To achieve significant alignment using this technique, the DNA strand must be sufficiently long, i.e. contain at least 1000-1500 base pairs.[15]

Our laboratory technician G. Cuglietta, the employees of the machine shop at the University of Ottawa and I designed and constructed the Couette apparatus, shown in Figure 2.8A,B. The inner and outer cylinders, made of fused silica, were purchased from the University of Michigan's Department of Chemical Engineering but were originally fabricated by KineOptics (Slidell, LA). The outer cylinder, which is mounted on a platform as seen in Figure 2.8B, is fixed and the inner cylinder

rotates, creating a laminar flow. The orientation direction is tangential to this flow, and the incident light is perpendicular to the orientation direction. The sample is placed in the annular gap between the two cylinders, and the DNA is oriented by the flow of the solution. A schematic illustration of flow orientation in a Couette cell is shown in Figure 2.8C. With our apparatus, the rotational speed of the inner cylinder can be adjusted using a dial without numbers, requiring a tachometer to measure the rpm. In our experiments, the rotational speed of the inner cylinder was between 80 and 90 rpm.

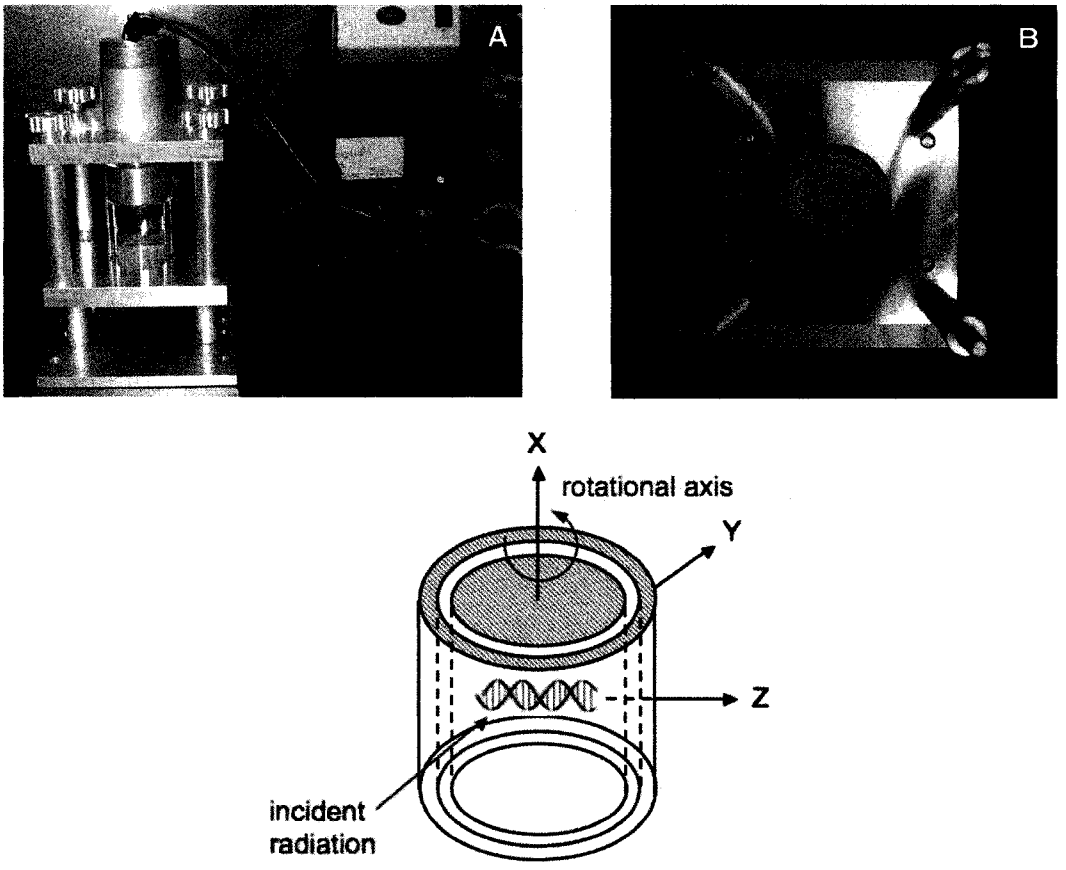


**Figure 2.8: (A) Couette apparatus designed and constructed at the University of Ottawa. (B) Outer cylinder mounted on a platform. (C) Schematic illustration of flow orientation in a Couette cell with radial incident light.[1]**

## 2.3. Time-Resolved Fluorescence Spectroscopy

Fluorescence refers to the return of an excited state to its ground state ($S_0$) via the emission of a photon without any flipping of electron spins, generally occurring from the lowest-energy singlet state ($S_1$). The process involves states of the same multiplicity, making it spin-allowed. As a consequence, fluorescence occurs rapidly, with rate constants between $10^6$-$10^{12}$ $s^{-1}$. Time-resolved fluorescence (TRF) techniques allow one to measure the fluorescence lifetime of an excited species, which is the average time that a fluorophore remains in the excited state. The fluorescence lifetime ($\tau_F$) can be expressed (Equation 2-15) in terms of the fluorescence quantum yield ($\Phi_F$) and the radiative lifetime ($\tau_{rad}$)

**Equation 2-15**
$$\tau_F = \Phi_F \tau_{rad} = \frac{1}{k_{rad} + \sum k_{nr}}$$

where $k_{rad}$ is the inverse of the radiative lifetime and $k_{nr}$ is the rate of non-radiative decay of the singlet state. The radiative lifetime is an intrinsic property that is more or less constant, unlike the fluorescence lifetime that is affected by environmental effects.

A typical fluorescence emission rate is $10^8$ $s^{-1}$, meaning a fluorescence lifetime around 10 nanoseconds.[16] To monitor time-resolved fluorescence, the excitation pulse must be significantly shorter than the fluorescence decay, hence the use of pulsed lasers. In contrast to steady-state fluorescence spectroscopy where the intensity depends on the fluorophore concentration, the fluorescence lifetime of any given species is usually independent of concentration. In comparison to time-resolved absorption techniques that measure differences in transmitted light, TRF techniques are extremely sensitive, arising from the lack of background emission.

The dominant mode of excited state deactivation in cyanine dyes is believed to be radiationless deactivation through rotations around the internuclear double bond joining the two ring systems.[17-20] Upon intercalation in DNA, this deactivation

mode is suppressed and the fluorescence lifetime increases, as expected from inspection of Equation 2-15. As an example, the lifetime of the cyanine dye PTO is < 70 ps in buffer and increases to 1.9 ns in double-stranded calf thymus DNA (*vide infra*). Thus fluorescence lifetimes can provide information on the environment of the chromophore; in this example the fluorescence lifetime reports on the mobility of the dye.

### 2.3.1. Optical System for Time-Resolved Fluorescence

Our picosecond (ps) laser system is a cavity dumped active/passive mode-locked $Nd^{3+}$:YAG (yttrium-aluminium-garnet) system that provides around 3-5 mJ/pulse at 1064 nm. Its optical layout is shown in Figure 2.9.

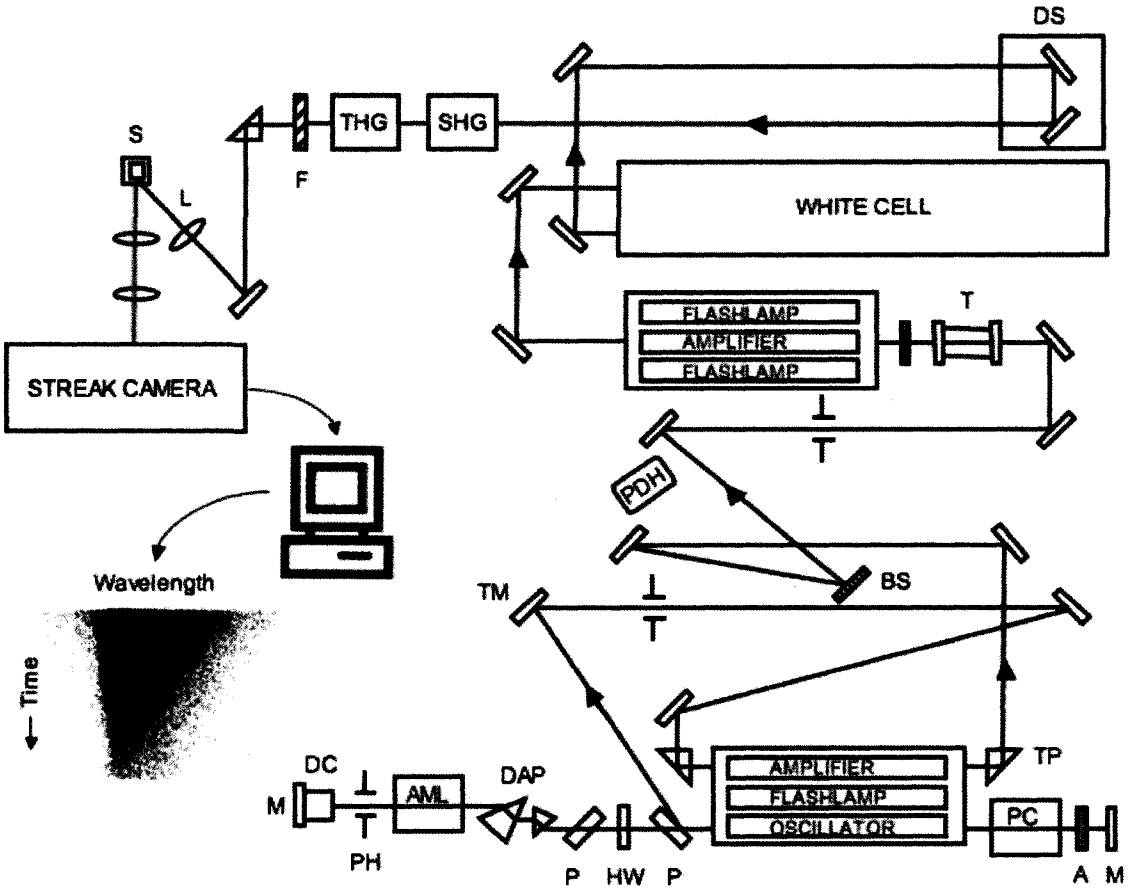


**Figure 2.9: Schematic diagram of the optical layout of our picosecond laser system. M: mirror, DC: dye cell, PH: pinhole, AML: acousto-optic mode-locker, DAP: delay adjustment prism, P: polarizer, HW: half wave plate, PC: Pockels cell, A: apodizer, TM: turning mirror, TP: 90° turning prism, BS: beam splitter, PDH: pin diode head, T: telescope, DS: delay stage, SHG: second harmonic generator, THG: third harmonic generator, F: filter, L: lens, S: sample. Adapted from Continuum.[21]**

The laser head consists of the laser medium ($Nd^{3+}$ doped YAG) and the flashlamp that excites the lasing medium through optical pumping. The oscillator uses mode-locking of a saturable dye absorber to produce a train of 1064 nm pulses (Figure 2.10A), where each individual pulse has a full width at half maximum of 35 ps. An active acousto-optic mode-locker is used in conjunction with the

passive dye mode-locker and, as a consequence, misshots are eliminated and the output energy is stabilized. The cavity dumping technique (Figure 2.10B) is used to select one of the pulses in the pulse train (Figure 2.10C). The electro-optic Pockels cell is triggered by a photodiode that senses the intensity buildup in the cavity. When the intensity reaches the correct level, a polarizer ejects the selected output pulse. The pulse is passed through a pinhole (for spatial filtering) and then directed through an amplifier, which amplifies it by a factor of 10. It is directed to a beam splitter, where 20% of the light is utilized in the remainder of our setup. A very small part of the remaining pulse (<1%) is transmitted to a pin diode head, triggering the streak camera. A telescope expands the beam before it is amplified by an external amplifier. For our 20 ns sweep time scale, the streak camera delay time is 110 ns. This delay is achieved optically by reflecting the pulse off of mirrors, including those in the White cell. This optical delay unit can produce delays between 13 and 93 ns, depending on the number of times the pulse is reflected. As a reference, light passing through air takes 3.0 ns to travel 1 meter. The pulse is directed through a potassium dihydrogen phosphate crystal, generating 532 nm light. In addition to the second harmonic, it is also possible to generate the third (355 nm) and fourth harmonics (266 nm) by using the appropriate harmonic generators. The selected wavelength of light is focused on the sample by a lens. The light emitted from the sample is collected and collimated by a lens, and a second lens focuses the light into the streak camera.

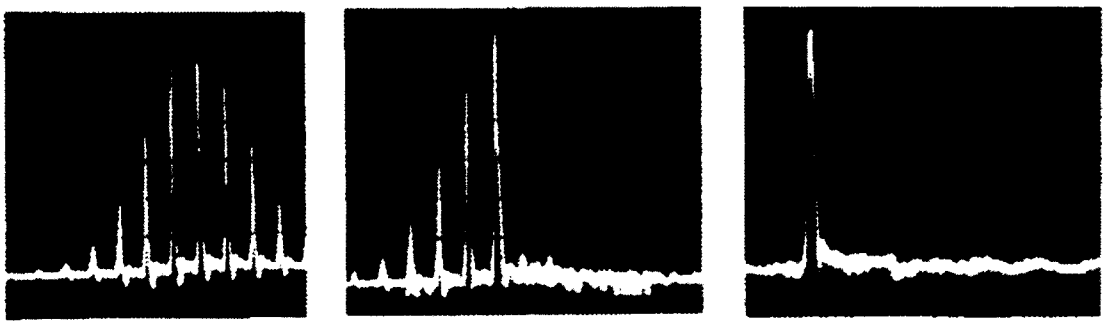

**Figure 2.10: (A) The full pulse train in the resonator without cavity dumping. (B) Train when dumped. (C) The single switched out pulse. Adapted from Continuum.[21]**

There are two common detection methods used in time-resolved fluorescence: single photon counting and streak camera detection. Our TRF system uses streak camera detection. The various elements of a typical electronic streak camera are illustrated in Figure 2.11. The light emitted from the sample enters the spectrograph, which separates it into its component wavelengths. It is then focused onto the photocathode, where it is converted into photoelectrons. The photoelectrons are accelerated (via accelerating electrodes) to the deflection plates. When the photoelectrons pass through the deflection plates, a sweep voltage is applied, causing them to be swept vertically. The swept electron image is multiplied at the micro-channel plate and subsequently reaches the phosphor screen, where it is reconverted to an optical image. This image is registered by a charge-coupled device through a fiber reducer, and the video signal is converted to a digital signal. The horizontal positions of the photoelectrons exiting the photocathode are retained during their trajectories, thus the horizontal axis of the phosphor screen represents the wavelength of emitted light. An advantage of using a streak camera is that it obtains three-dimensional (wavelength, time and intensity) data in a single measurement. An example of acquired data is shown in Figure 2.9, where the horizontal axis is the wavelength, the vertical axis is the time, and the colour of each pixel represents the intensity.

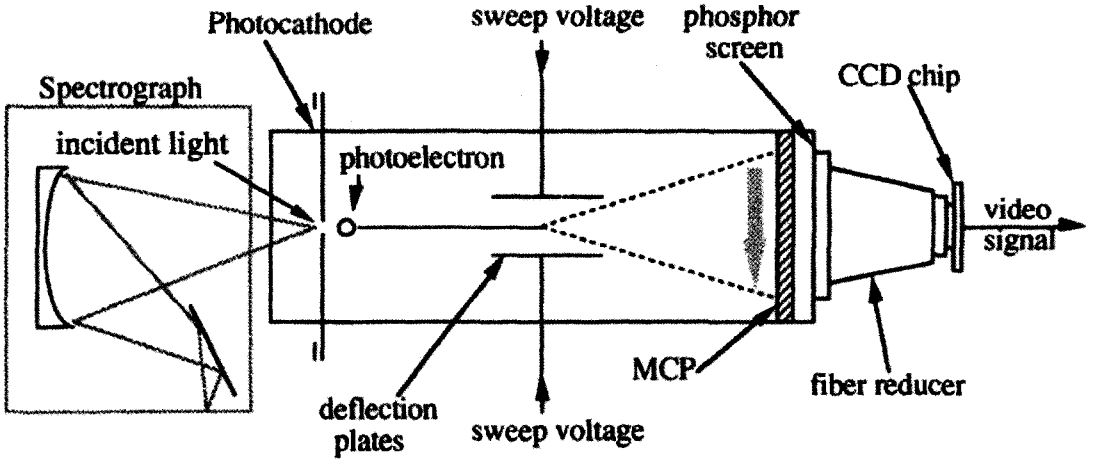


**Figure 2.11: Schematic diagram of an electronic streak camera. MCP: micro-channel plate, CCD: charge-coupled device. Adapted from Watanabe *et al.*[22]**

## 2.4. Molecular Dynamics Simulations

Molecular modeling uses computer-based methods to study the behaviour of molecular systems, placing an emphasis on the graphical representation of the molecular structures. Gaussian is the most popular and widely used software package for *ab initio* electronic structure calculations. AMBER (**A**ssisted **M**odel **B**uilding with **E**nergy **R**efinement) was first introduced in the late 1970's and is now one of the most widely used molecular modeling packages.[23] AMBER has been used to model DNA conformational changes,[24-27] to examine ion distributions of isolated DNA duplexes and DNA clusters,[28] and to study enzyme reaction mechanisms.[29,30] Another leading molecular dynamics (MD) simulation package is CHARMM (**C**hemistry at **HAR**vard **M**acromolecular **M**echanics). CHARMM has a reputation for being efficient but frequently evoking user frustration. It is program-oriented rather than problem-oriented, requiring the user to either type commands into an interpreter or write scripts that are then input to the program. For simplicity, we chose the AMBER software package.

All of the information that follows was gathered from references St-Amant[31] and Leach.[32] Quantum mechanical methods consider the electrons in a system, and as a consequence the calculations are lengthy. Alternatively, molecular mechanics (MM), also known as force field methods, are used for calculations on systems containing a large number of atoms. In MM there are no electrons, rather there are atoms bearing partial charges, and the energy is a function of the atomic coordinates. MM works so well because its two assumptions are valid, the first being the Born-Oppenheimer approximation. If this approximation were not valid, it would be impossible to treat the energy as a function of the atomic coordinates. However, we can make this assumption since we know that the ignored electrons will instantaneously re-adjust to the positions of the relatively slower-moving nuclei. The second assumption is that parameters are transferable. Since functional groups in chemistry are transferable, it is reasonable to assume that validated

parameters for small systems can be used to study much larger systems, comprising the small systems.

All force fields have four basic components, which are contained in the following functional form:

$$V(r^N) = \sum_{bonds} \frac{k_i}{2}(l_i - l_{i,0})^2 + \sum_{angles} \frac{k_i}{2}(\theta_i - \theta_{i,0})^2 + \sum_{torsions} \frac{V_n}{2}(1 + \cos(n\omega - \gamma))$$
$$+ \sum_{i=1}^{N} \sum_{j=i+1}^{N} \left( 4\varepsilon_{ij} \left[ \left( \frac{\sigma_{ij}}{r_{ij}} \right)^{12} - \left( \frac{\sigma_{ij}}{r_{ij}} \right)^{6} \right] + \frac{q_i q_j}{4\pi\varepsilon_0 r_{ij}} \right)$$

where $V(r^N)$ represents the potential energy, which is a function of the positions ($r$) of $N$ atoms. The first term uses a harmonic potential to model the interaction between pairs of bonded atoms, and $l_i$ represents the bond length while $l_{i,0}$ represents the reference bond length, and $k_i$ represents the bond's force constant. A harmonic potential is also used to model angle bending (the second term) as the potential near a bond angle's reference value, $\theta_{i,0}$, is more or less harmonic. The third term is a torsional potential, where $\omega$ is the torsion angle, $n$ is the multiplicity of the torsion (the number of minima between 0 and 360°), $\gamma$ is a phase factor, and $V_n$ is the 'barrier' height. The last term deals with non-bonded interactions between all pairs of atoms that are either in different molecules or are in one molecule but separated by at least three bonds. Non-bonded interactions are modeled using a Lennard-Jones potential for the van der Waals interactions and a Coulomb potential for the electrostatic interactions, where $r_{ij}$ is the distance between atoms, $\sigma_{ij}$ is the distance at which the energy is zero, $\varepsilon_{ij}$ is the well depth, $q_i$ is the partial atomic charge, and $\varepsilon_0$ is the permittivity of free space. To more adequately describe hydrogen bonding, some force fields replace the Lennard-Jones 6-12 term with a reparameterized 10-12 potential. However, the majority of force fields do not use an explicit hydrogen-bonding term as they assume that the van der Waals and electrostatic interactions will properly account for hydrogen-bonding.

In our simulations, the TIP3P model,[33] which is one of the most common water models, was used to explicitly describe the water molecules. It is a three

point model (the three atoms) where each water molecule is kept in a rigid geometry and the interactions between molecules are calculated using pairwise Coulombic and Lennard-Jones expressions. The software places the water molecules on the points of an evenly spaced lattice, and if a lattice point is occupied by the biomolecule then no solvent molecule is placed there. Since it is impossible to simulate bulk water, periodic boundary conditions are used where a small box (containing the solute and solvent) is replicated infinitely in all directions. If a particle exits the box from one side then it reenters from the other side, thus the number of particles inside the central box is constant. To prevent the biomolecule from interacting with its own image in an adjacent box, there must be an adequate number of water molecules between the biomolecule and the edges of the box, i.e. the box must be sufficiently large. The distance between the solute and the box boundary is typically between 8 and 12Å. However, a box is not the ideal shape since it contains an unnecessary amount of water molecules, which will significantly slow down the calculation. A more efficient shape is a truncated octahedron, which is what we employed in our studies.

A gradient is a vector that is the first derivative of the energy with respect to each internal degree of freedom. The negative of a gradient is the force acting on each internal degree of freedom. Gradients are used to quickly find the nearest minimum on a potential energy surface (PES).

In the steepest descent method, the displacement towards the minimum is based entirely on the value of the gradient, as seen in Equation 2-16.

**Equation 2-16**

$$x_{k+1} = x_k - \lambda_k \frac{g_k}{|g_k|}$$

where $x$ is the vector that contains all the values of the internal degrees of freedom, $g$ is the gradient vector, $k$ corresponds to the current geometry, and $\lambda_k$ is the step size. This method is reliable, but slow when the forces are appreciable. In addition, there will be problems when the forces become very small, i.e. in regions where the PES is shallow.

The conjugate gradients method is useful when the forces acting on a system are small, as it ensures that consecutive steps are orthogonal to one another (Equation 2-17).

**Equation 2-17** $$x_{k+1} = x_k - g_k + \gamma_k(x_k - x_{k-1})$$

where $\gamma_k$ is a scalar constant given by Equation 2-18.

**Equation 2-18** $$\gamma_k = \frac{g_k \bullet g_k}{g_{k-1} \bullet g_{k-1}}$$

In our optimizations, we first employed the steepest descent method, which is good when large forces are present, followed by the conjugate gradients method, which is far more efficient with small forces.

In general, any property of a system can be represented by $A(p^N(t),r^N(t))$, where A is the instantaneous value of the property, and $p^N(t)$ and $r^N(t)$ represent the momenta and positions, respectively, of the N particles in the system at time t. The value that we measure experimentally is the time average, given by Equation 2-19.

**Equation 2-19** $$A_{average} = \lim_{\tau \to \infty} \frac{1}{\tau} \int_0^{\tau} A(p^N(t),r^N(t))dt$$

Integrating Newton's equations of motion over the time period $\tau$ gives the time-averaged values of A. Molecular dynamics computes the 'real' dynamics of a system, which can be used to calculate time-averaged properties. Molecular dynamics is deterministic, i.e. a particular set of initial conditions will always generate the same trajectory. Since the force field depends on the distance between atoms, the equations of motion must be constantly evaluated. This is done using very short time steps, which are typically between 1 and 10 femtoseconds, and are normally run over approximately 1 nanosecond. At each step, the forces acting on each atom are calculated and are used, in conjunction with the current positions and velocities, to produce new positions and velocities. The atoms are

then moved to their new positions and the procedure is repeated, generating a trajectory.

As the size of a system increases, the number of bonds, bond angles and torsions increases linearly while the number of non-bonded interactions increases quadratically. As a result, calculating the non-bonded interactions takes the most time. A cutoff is used so that non-bonded interactions are only calculated for electrically neutral groups that are within a certain distance of one another. For electrically neutral groups, the leading term in the electrostatic interaction is the dipole-dipole interaction that depends on $1/r^3$, so any interactions outside the cutoff are weak interactions and will not result in significant errors. Checking at each time step to see whether two groups fall within the cutoff distance would defeat the purpose of having a cutoff as this is CPU-demanding. Instead, a non-bonded neighbour list is created every x time steps (x is typically between 10 and 20) and any groups that are within the cutoff distance plus an offset distance are put on the list. When calculating the non-bonded interactions, only groups on the non-bonded list are examined to see if they fall within the cutoff distance. The typical value of a cutoff is around 10 Å.

The DNA phosphate backbone is negatively charged and is surrounded by positive counterions. Since charge-charge interactions depend on 1/r, using a 10 Å cutoff can introduce significant errors in the electrostatic contribution to the MM energy. This problem is avoided by using the Ewald method, which computes all electrostatic contributions out to infinity using periodic boundary conditions.

The initial geometry can be the X-ray structure or structures obtained from NMR data or theoretical modeling. In our simulations the DNA structures were generated using the NUCGEN utility embedded in AMBER, which is a program that generates Cartesian coordinates of standard A- and B-form nucleic acid duplexes. An initial set of velocities is also required, which is generated randomly by selecting from a Maxwell-Boltzmann distribution at the temperature of interest (Equation 2-20).

**Equation 2-20**

$$p(v_{ix}) = \left(\frac{m_i}{2\pi k_B T}\right)^{1/2} \exp\left[-\frac{1}{2}\frac{m_i v_{ix}^2}{k_B T}\right]$$

The initial velocities are then adjusted so that the total momentum of the system is zero, to ensure that the system does not drift away. The initial forces acting on the particles may be quite high, due to flawed experimental data or poorly added hydrogen atoms or water molecules, so the steepest descent and conjugate gradients methods are used to remove any large forces. During this initial minimization, the solute (DNA and dye in our case) is kept relatively fixed in its initial conformation using a force constant. If a restrained atom moves from its initial position then a force will act to bring it back to that position. A second minimization is then performed on the entire system, without any restraints. Once at a minimum on the PES, random velocities are assigned and the system is equilibrated before beginning the MD simulation. During the MD simulation, a time step must be chosen that smoothly describes the continual stretching of the harmonic oscillator. Consequently, the time step must be approximately one-tenth the time of the highest frequency vibration, i.e. ~$10^{-15}$ s. In order to increase the time step without losing information of great chemical interest, vibrations involving H atoms are frozen using the SHAKE procedure.[34] This procedure iteratively calculates the magnitude of the constraint forces until all the constraints, i.e. the H bonds or bond angles being frozen, are obeyed and the frozen internal coordinates are in fact frozen. As a result, a time step of approximately 2 femtoseconds can now be employed, making the MD simulation twice as efficient. MD simulations can be run at constant pressure by changing the volume of the simulation cell. The protocol for setting up simulations of DNA oligomers and dyes that was followed in this thesis is given in Section 2.5.

## 2.5. Appendix: Protocol for Setting Up our AMBER Simulations

The following protocol was used in this thesis to set up simulations of DNA oligomers and dyes.

1. Optimize the dye using the B3LYP/6-31G* hybrid density functional method with the Gaussian 03[35] series of the program.
2. Construct an input file that defines the DNA bases and specifies whether the DNA is A- or B-form, and run NUCGEN using that file to generate the Cartesian coordinates of the DNA.
3. LEaP is a program that reads in force field, topology and coordinate data and produces the files that are required for minimization and molecular dynamics. Load the Cartesian coordinates of the DNA into the graphical interface of LEaP, called xleap. Import the dye residue into xleap. Highlight the dye and move/rotate it into the desired position between the bases/base pairs.
4. Add the counterions using the addions command.
5. Save the topology and coordinate files.
6. Add a truncated octahedral box of water around the DNA using the solvateoct command with a 10 Å buffer of water molecules (described by the TIP3P model[33]) around the DNA in each direction.
7. Save the topology and coordinate files for the solvated DNA.
8. Keep the solute (dye and DNA) relatively fixed using a force constant, and minimize the positions of the water and the counterions.
9. Minimize the entire system (without any restraints).
10. Heat the system, at constant volume, from 0 to 300K over 20 ps with weak restraints on the solute.
11. Switch from using constant volume to constant pressure so that the density of water can relax. Remove the restraints on the solute. Run the 2 ns molecular dynamics simulation.

## 2.6. References


1. Rodger, A.; Nordén, B., *Circular Dichroism & Linear Dichroism*. Oxford University Press: Oxford, 1997; p 150.

2. Woody, R. W., Theory of Circular Dichroism of Proteins. In *Circular Dichroism and the Conformational Analysis of Biomolecules*, Fasman, G. D., Ed. Plenum Press: New York, 1996; pp 25-67.

3. Matsuoka, Y.; Nordén, B., Linear dichroism studies of nucleic acid bases in stretched poly(vinyl alcohol) film. Molecular orientation and electronic transition moment directions. *J. Phys. Chem.* **1982**, 86, (8), 1378-1386.

4. Mikelsons, L.; Carra, C.; Shaw, M.; Schweitzer, C.; Scaiano, J. C., Experimental and theoretical study of the interaction of single-stranded DNA homopolymers and a monomethine cyanine dye: nature of specific binding. *Photochem. Photobiol. Sci.* **2005**, 4, (10), 798-802.

5. JASCO Corporation, Model J-810 Spectropolarimeter Hardware/Function Manual. 1999; pp 1-5.

6. Richards, A. D.; Rodger, A., Synthetic metallomolecules as agents for the control of DNA structure. *Chem. Soc. Rev.* **2007**, 36, (471-483).

7. Granzhan, A.; Ihmels, H.; Viola, G., 9-Donor-substituted acridizinium salts: versatile environment-sensitive fluorophores for the detection of biomacromolecules. *J. Am. Chem. Soc.* **2007**, 129, (5), 1254-1267.

8. Ardhammar, M.; Nordén, B.; Kurucsev, T., DNA-Drug Interactions. In *Circular Dichroism: Principles and Applications*, 2nd ed.; Berova, N.; Nakanishi, K.; Woody, R. W., Eds. Wiley-VCH: New York, 2000; pp 741-768.

9. Nordén, B.; Kurucsev, T., Analysing DNA complexes by circular and linear dichroism. *J. Mol. Recognit.* **1994**, 7, (2), 141-156.

10. Lerman, L. S., The structure of the DNA-acridine complex. *Proc. Natl. Acad. Sci. U.S.A.* **1963**, 49, (1), 94-102.

11. Shin, J.-S.; Kim, J.-M.; Lee, H. M.; Kim, J.-H.; Lee, H.; Kim, S. K., Property of the M-DNA probed by a minor groove binding dye 4',6-diamidino-2-phenylindole. *Biophys. Chem.* **2007**, 125, 403-410.

12. Eriksson, M.; Härdelin, M.; Larsson, A.; Bergenholtz, J.; Åkerman, B., Binding of intercalating and groove-binding cyanine dyes to bacteriophage T5. *J. Phys. Chem. B* **2007**, 111, (5), 1139-1148.

13. Cole, K. D.; Gaigalas, A.; Åkerman, B., Single-molecule measurements of trapped and migrating circular DNA during electrophoresis in agarose gels. *Electrophoresis* **2006**, 27, 4396-4407.

14. Morimatsu, K.; Takahashi, M., Structural analysis of RecA protein-DNA complexes by fluorescence-detected linear dichroism: Absence of structural change of filament for pairing of complementary DNA strands. *Anal. Biochem.* **2006**, 358, 192-198.

15. Rodger, A., Linear dichroism. *Methods Enzymol.* **1993**, 226, 232-258.

16. Lakowicz, J. R., *Principles of Fluorescence Spectroscopy.* 2nd ed.; Kluwer Academic/Plenum Publishers: New York, 1999.

17. Carlsson, C.; Larsson, A.; Jonsson, M.; Albinsson, B.; Nordén, B., Optical and photophysical properties of the oxazole yellow DNA probes YO and YOYO. *J. Phys. Chem.* **1994**, 98, (40), 10313-10321.

18. Paerschke, H.; Süsse, K.-E.; Welsch, D.-G., Investigation of vibronic energy relaxation of polymethin cyanine dyes by picosecond spectroscopy. *Chem. Phys. Lett.* **1979**, 66, (2), 376-380.

19. Sundström, V.; Gillbro, T., Viscosity dependent radiationless relaxation rate of cyanine dyes. A picosecond laser spectroscopy study. *Chem. Phys.* **1981**, 61, 257-269.

20. Ponterini, G.; Momicchioli, F., Trans-cis photoisomerization mechanism of carbocyanines: experimental check of theoretical models. *Chem. Phys.* **1991**, 151, 111-126.

21. Continuum, Operation and Maintenance Manual: PY61 Series Laser. pp 2-1 to 2-6.

22. Watanabe, M.; Koishi, M.; Roehrenbeck, P. W., Development and characteristics of a new picosecond fluorescence lifetime system. *Proc. SPIE* **1993**, 1885, 155-164.

23. Case, D. A.; Cheatham III, T. E.; Darden, T.; Gohlke, H.; Luo, R.; Merz, K. M., Jr.; Onufriev, A.; Simmerling, C.; Wang, B.; Woods, R. J., The Amber biomolecular simulation programs. *J. Comput. Chem.* **2005**, 26, (16), 1668-1688.

24. Somsen, O. J. G.; Trinkunas, G.; de Keijzer, M.; van Hoek, A.; van Amerongen, H., Local diffusive dynamics in DNA: A time-resolved fluorescence and molecular-dynamics study of dinucleotides with 2-aminopurine. *J. Lumin.* **2006**, 119-120, 100-104.

25. Kannan, S.; Kohlhoff, K.; Zacharias, M., B-DNA under stress: over- and untwisting of DNA during molecular dynamics simulations. *Biophys. J.* **2006**, 91, (8), 2956-2965.

26. Real, A. N.; Greenall, R. J., B→A→B transitions in a molecular dynamics trajectory of low salt DNA solution. *J. Mol. Model.* **2000**, 6, 654-658.

27. Song, C.; Xia, Y.; Zhao, M.; Liu, X.; Li, F.; Ji, Y.; Huang, B.; Yin, Y., The effect of salt concentration on DNA conformation transition: a molecular-dynamics study. *J. Mol. Model.* **2006**, 12, 249-254.

28. Long, H.; Kudlay, A.; Schatz, G. C., Molecular dynamics studies of ion distributions for DNA duplexes and DNA clusters: salt effects and connection to DNA melting. *J. Phys. Chem. B.* **2006**, 110, (6), 2918-2926.

29. Yan, S. F.; Wu, M.; Geacintov, N. E.; Broyde, S., Altering DNA polymerase incorporation fidelity by distorting the dNTP binding pocket with a bulky carcinogen-damaged template. *Biochemistry* **2004**, 43, (24), 7750-7765.

30. Dodson, M. L.; Lloyd, R. S., Backbone dynamics of DNA containing 8-oxoguanine: importance for substrate recognition by base excision repair glycosylases. *Mutat. Res.* **2001**, 487, 93-108.

31. St-Amant, A., *CHM4141 course notes*. University of Ottawa: 2004.

32. Leach, A. R., *Molecular Modelling: Principles and Applications*. 2nd ed.; Prentice Hall: Harlow, 2001; p 744.

33. Jorgensen, W. L.; Chandrasekhar, J.; Madura, J. D.; Impey, R. W.; M.L., K., Comparison of simple potential functions for simulating liquid water. *J. Chem. Phys.* **1983**, 79, (2), 926-935.

34. van Gunsteren, W. F.; Berendsen, H. J. C., Algorithms for macromolecular dynamics and constraint dynamics. *Mol. Phys.* **1977**, 34, (5), 1311-1327.

35. Frisch, M. J.; Trucks, G. W.; Schlegel, H. B.; Scuseria, G. E.; Robb, M. A.; Cheeseman, J. R.; Montgomery, J., J.A.; Vreven, T.; Kudin, K. N.; Burant, J. C.; Millam, J. M.; Iyengar, S. S.; Tomasi, J.; Barone, V.; Mennucci, B.; Cossi, M.; Scalmani, G.; Rega, N.; Petersson, G. A.; Nakatsuji, H.; Hada, M.; Ehara, M.; Toyota, K.; Fukuda, R.; Hasegawa, J.; Ishida, M.; Nakajima, T.; Honda, Y.; Kitao, O.; Nakai, H.; Klene, M.; Li, X.; Knox, J. E.; Hratchian, H. P.; Cross, J. B.; Adamo, C.; Jaramillo, J.; Gomperts, R.; Stratmann, R. E.; Yazyev, O.; Austin, A. J.; Cammi, R.; Pomelli, C.; Ochterski, J. W.; Ayala, P. Y.; Morokuma, K.; Voth, G. A.; Salvador, P.; Dannenberg, J. J.; Zakrzewski, V. G.; Dapprich, S.; Daniels, A. D.; Strain, M. C.; Farkas, O.; Malick, D. K.; Rabuck, A. D.; Raghavachari, K.; Foresman, J. B.; Ortiz, J. V.; Cui, Q.; Baboul, A. G.; Clifford, S.; Cioslowski, J.; Stefanov, B. B.; Liu, G.; Liashenko, A.; Piskorz, P.; Komaromi, I.; Martin, R. L.; Fox, D. J.; Keith, T.; Al-Laham, M. A.; Peng, C. Y.; Nanayakkara, A.; Challacombe, M.; Gill, P. M. W.; Johnson, B.; Chen, W.; Wong, M. W.; Gonzalez, C.; Pople, J.A. *Gaussian 03*, Revision B.04; Gaussian, Inc.: Pittsburgh, 2003.

# 3. The Interactions of Cyanine Dyes with Single-Stranded DNA Homopolymers

## 3.1. Introduction

The interaction of dyes with DNA is widely used in analytical biochemistry, microscopy, and many other imaging applications. Previous work in our laboratory has shown that the fluorescence lifetimes of intercalated dyes, particularly PicoGreen® (PG), can be used to distinguish single- from double-stranded DNA (ssDNA and dsDNA, respectively), and ultimately to monitor DNA damage.[1,2] Unfortunately, the structure of PicoGreen is proprietary, making it impossible to combine experimental studies with computational methods. However, the structure of PicoGreen is known to resemble the monomethine cyanine dye thiazole orange (TO).

Several monomethine cyanine dyes have proven useful as sensors for DNA and its structural changes. One of the biggest advantages of using these dyes is that they are virtually non-fluorescent in solution, but undergo dramatic increases in fluorescence upon binding to DNA. For example, the fluorescence quantum yield of TO increases by a factor of ~3,000 upon binding to nucleic acids.[3] But the nature of the association process is not always clear; this is particularly true of single-stranded DNA.

Netzel *et al.* examined the relationship between emission quantum yields of cyanine dyes and duplex DNA base content, and found that quinolinium cyanine dyes such as TO and oxazole yellow (YO) seem to selectively bind to GC-rich regions in calf thymus DNA (CT DNA), while pyridinium cyanine dyes appear to bind to AT-rich regions.[4] However, there was no definitive proof as the lifetimes of these dyes varied significantly in the different types of DNA, and the bi- and triexponential decays indicated more than one mode of binding. Other studies involving the measurement of equilibrium constants for TO and TO- and YO-derivatives showed no dependence on duplex base content.[5,6]

There is also no conclusive evidence regarding the association of cyanine dyes and ssDNA. Rye *et al.* found that TOTO (TO dimer) and ethidium homodimer associate with ssDNA in a complex that is just as stable as the dye/dsDNA

complex,[7] but did not examine the DNA base-specificity of the dyes. Nygren *et al.* found that TO binds with high affinity as a monomer with poly(dA) in an intercalation complex, and possesses a high fluorescence quantum yield; those authors suggested that purines offer more surface area than pyrimidines for hydrophobic interactions.[5] Prodhomme *et al.* determined fluorescence quantum yields and absorption and emission spectral shifts of TO-derivatives (TO-PRO-1 and TO-MET) in the presence of poly(dA), poly(dT) and a few ss oligonucleotides but could only conclude that there are various local interactions between the dyes and the ssDNA.[8] Their study of 2 and 3 oligonucleotides for TO-PRO-1 and TO-MET, respectively, indicated that as the purine content of the oligonucleotide increased, so did the fluorescence quantum yield. Simon *et al.* found that the fluorescence quantum yields of YO and YOYO in ssDNA 30-mers decreased in the order G»A>C≈T and A>G»T»C, respectively.[9] However, there was no ICD for any of the YO/DNA complexes (indicating either no, or extremely weak, association) and the YOYO ICD in $(dA)_{30}$•$(dT)_{30}$ resembled that of YOYO in the individual strands rather than that of YOYO in poly(dA)•poly(dT), thus the relationships found for these short oligonucleotides are not valid for polynucleotides. In an attempt to establish whether or not PG binding to ssDNA is base-specific, recent work in our laboratory involved the study of fluorescence quantum yields and lifetimes of PG in homopolymers and CT DNA, and found that the dye binds preferentially between alternating GC base pairs in dsDNA and between two different bases, one of them being G or T, in ss CT DNA.[10] The only problem is that since the exact structure of PG is unknown, it is impossible to directly relate the base specificity of PG with other cyanine dyes such as TO and YO.

Detecting DNA damage with rapid screening methods could be utilized in a wide range of applications, including health-related, as well as to monitor regulatory aspects of food authenticity related to γ-irradiation of food, a common practice aimed at disinfection and increased shelf life.[11] During this applied work it became evident that designing good sensors for screening DNA damage requires an intimate understanding of the interaction of dyes with both single- and double-

stranded DNA. The work reported in this chapter deals with ssDNA homopolymers and provides a system that is amenable to a number of spectroscopic techniques, as well as a computational approach. Earlier work in this laboratory[12] indicated that dyes that experience structural mobility restrictions from interacting with DNA are the preferred type of molecular sensor for these types of analytical applications; the selection of this N-propyl pyridinium derivative of TO (PTO) reflects this conclusion. Changes in the chemical shifts of the $^1$H NMR spectrum of a TOTO/dsDNA complex indicate dye intercalation;[13] we anticipate that TO and its derivatives will also intercalate. It has been shown using various techniques that at dye:DNA base mixing ratios up to 0.20, YO monointercalates in dsDNA with the long axis of the dye parallel to the long axis of the base pair pocket.[14] It has been postulated that all of the quinoline dyes (YO- and TO-derivatives) should behave in the same manner, i.e. also be intercalators.[4] Thus we anticipated that the TO-derivative PTO would also intercalate in DNA, and that its extra positive charge (relative to YO and TO) should help the association.

In this work, we have examined the interaction of PTO with DNA homopolymers using steady-state and time-resolved fluorescence spectroscopy, circular dichroism and UV-Visible absorption spectroscopy, and computational methods. As the interaction of TO and PG with DNA has been well-studied, we looked at the circular dichroism of these dye/ssDNA complexes and the molecular modeling of TO/ssDNA so that we could compare them with those of the N-propyl pyridinium derivative of TO to gain further insight into the association of PTO with DNA.

This project was an extension of work initiated by a postdoctoral fellow in our laboratory, Dr. C. Schweitzer. The molecular dynamics simulations were done in collaboration with a postdoctoral fellow in our laboratory, Dr. C. Carra, with aid from Dr. M. Shaw. Some of the measurements presented in this chapter were performed by M. Antonic who worked in our laboratory under my supervision as part of the Undergraduate Research Scholarship program at the University of Ottawa. I am grateful for her help.

## 3.2. Results

### 3.2.1. Absorption Spectroscopy

The structures of the cyanine dyes that were studied are shown in Scheme 3.1. Aggregation of cyanine dyes is rather common.[5,15-20] Even at low concentrations such as 1 μM, TO and its N-propyl pyridinium derivative (PTO) were present as both the monomeric and aggregated species, as can be seen in Figure 3.1 and Figure 3.2 where the data have been reduced to "nominal" extinction coefficients to facilitate the comparison. The concentrations of the dye stock solutions were determined by measuring the absorption of a diluted dye solution (a concentration where no aggregation occurs) and using the extinction coefficient of 73 900 $M^{-1}cm^{-1}$ for PTO (510.5 nm)[21] and 63 000 $M^{-1}cm^{-1}$ for TO (500 nm).[5] The nominal extinction coefficients for Figure 3.1 and Figure 3.2 were then determined by diluting the stock solution and calculating the extinction coefficients as if no aggregation had occurred. This wide concentration range required cuvettes with pathlengths ranging from 1 to 10 mm.

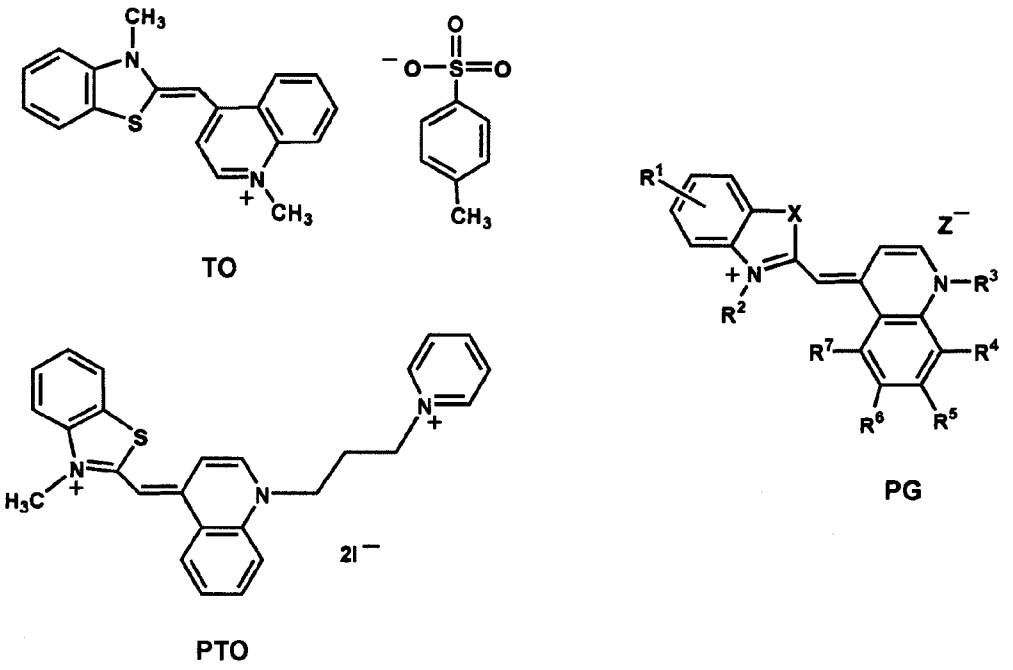


**Scheme 3.1: Structures of the cyanine dyes under study. Top left: thiazole orange (TO); bottom left: N-propyl pyridinium derivative of TO (PTO); right: PicoGreen (PG). In the case of PG, X is either S or O. Many different substituents ($R^n$) can be found on the conjugated rings. The counterion $Z^-$ is chloride, iodide, perchlorate, and/or various sulfonates.[22,23]**

In the case of PTO, the band with a characteristic maximum at 508 nm is the monomer absorption band, which decreased as the dye concentration increased, indicating that significant aggregation occurs at concentrations exceeding 10-20 μM. The aggregates are responsible for the shoulder around 481 nm, which increased as the dye concentration increased and eventually shifted to a distinct absorption maximum at 478 nm due to higher-order aggregates. Note that at 1 μM PTO (a concentration where there should be little or no aggregation) there is a shoulder that represents the upper limit to the contribution from a monomer vibrational band (*vide infra*). It is known that cyanine dyes form higher-order aggregates.[17] As there is no isosbestic point, PTO is most likely present as more than one type of aggregate at high concentration. As the absorption band of the

aggregates is blue-shifted relative to that of the monomer, these aggregates are most likely H-aggregates, i.e. face-to-face aggregates that are stacked with little or no offset.[18,19,24]

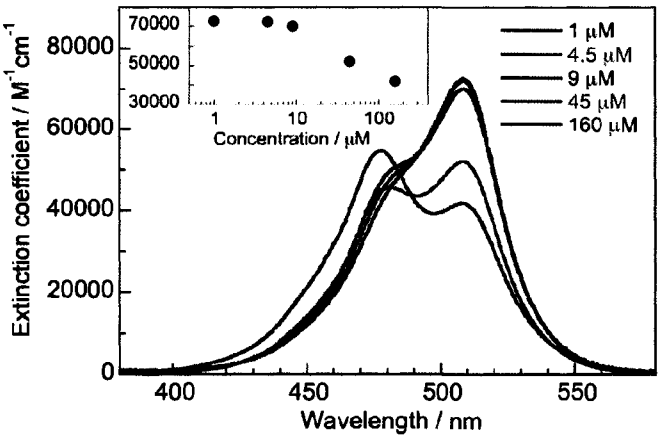


***Figure 3.1: Absorption spectra of PTO at different concentrations in 10 mM Tris buffer (pH 7.4) at 20°C. The insert shows the extinction coefficient at 508 nm as a function of the dye concentration in a semi-log plot.***

Like PTO, TO aggregates, although its 501 nm monomer maximum decreased much more rapidly as the dye concentration increased. Possible reasons for the more rapid TO aggregation are (i) unlike PTO, TO is not very water-soluble, (ii) the bigger PTO side group (N-propyl pyridinium) slows down aggregation compared to TO (with a methyl side group) and (iii) the two positive charges in PTO inhibit aggregation compared to TO (with one positive charge). The stock TO solution was prepared by dissolving TO in DMSO then diluting it to 1:30 DMSO:water. The monomer extinction coefficient of the 160 μM TO solution is greater than that of the 45 μM TO solution (Figure 3.2), most likely due to the contribution of the shoulder of the 160 μM TO aggregate absorption band. Similarly to PTO, there was no isosbestic point, indicating the presence of multiple aggregated species.

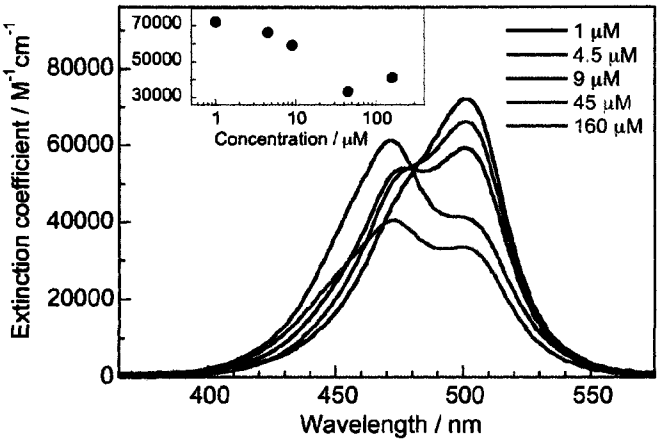


**Figure 3.2: Absorption spectra of TO at different concentrations in 10 mM Tris buffer (pH 7.4) at 20°C. The insert shows the extinction coefficient at 501 nm as a function of TO concentration in a semi-log plot.**

Much of the fluorescence and induced circular dichroism work was performed using 20 μM dye solutions; this concentration represents a compromise between reducing aggregate formation, and performing most of the work under conditions of good signal-to-noise ratio.

The spectra of Figure 3.3 indicate that PTO behaved differently with different ssDNA homopolymers. Only poly(dA) caused a pronounced shift in the monomer band, from 508 nm to ~515 nm (for 200 μM poly(dA)), suggesting a more delocalized structure due to a stronger interaction relative to the other ssDNA homopolymers. Poly(dG) caused a significant decrease in extinction coefficient, indicating intercalation, brought on by a strong interaction between the ligand in-plane transitions and the transition moments of nearby costacked nucleobases.[25] Both poly(dC) and poly(dT) seemed to enhance the short wavelength band, indicative of aggregation. If some homopolymer association–for poly(dC) and poly(dT)–involves dye aggregates, other results (*vide infra*) suggest that such complexes are not fluorescent.

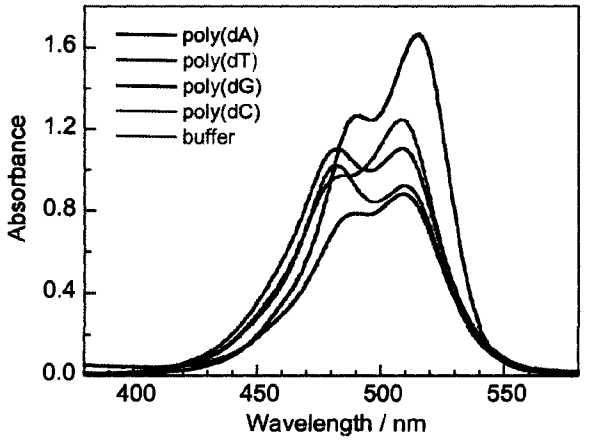


**Figure 3.3: Absorption spectra of 20 μM PTO in the presence of various single-stranded DNA polymers (200 μM) in 10 mM Tris buffer (pH 7.4) at 20°C.**

### 3.2.2. Steady-State Fluorescence Spectroscopy

The steady-state fluorescence of PTO shows dramatic intensity differences depending on the DNA homopolymer present, and virtually no fluorescence in the absence of DNA, Figure 3.4. It is believed that cyanine dyes undergo rapid deactivation from the singlet excited state by rotation around the internuclear double bond joining the two ring systems,[26-30] a long established decay mechanism for alkenes.[31] This energy releasing mechanism dramatically reduces fluorescence. However, if the dye was intercalated, the two bases would restrict its rotational freedom, forcing it to dissipate its energy predominantly through emission via fluorescence. This rationale has been used to explain the fluorescence enhancement of cyanine dyes upon binding to nucleic acids.[3,26,32] From this perspective, the data of Figure 3.4 suggest that poly(dG) and poly(dA) restrict the rotational freedom of the dye, while poly(dC) and poly(dT) do not.

As indicated above, poly(dC) and poly(dT) appear to enhance dye aggregation, as measured in their absorption spectra. The data in Figure 3.4 suggest that such aggregates are not fluorescent, which is consistent with their assignment as H-aggregates.[33,34]

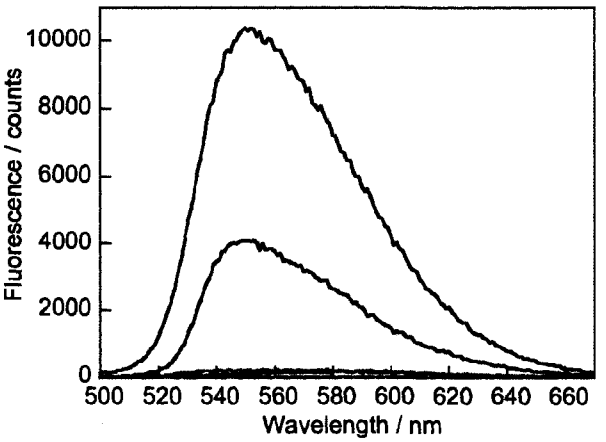


**Figure 3.4: Fluorescence of 20 μM PTO in the presence of 200 μM homopolymers in 10 mM Tris buffer (pH 7.4), excited at 355 nm. The relative intensities are 100: 39: 2.3: 1.8 and 0.5 for poly(dG), poly(dA), poly(dC), poly(dT), and buffer alone, respectively. Recorded at room temperature for poly(dG) (blue), poly(dA) (black), poly(dC) (green) and poly(dT) (red). The dye alone (purple) blends with the baseline.**

In the concentration range that we were using, both TO and its N-propyl pyridinium derivative (PTO) were always present in both monomeric and aggregate forms (see section 3.2.1). The same was true even in the presence of DNA. This made the determination of binding constants non-trivial. Since these species, with unknown individual extinction coefficients, were always present we had no way of determining accurate binding constants using absorption spectroscopy.

In an attempt to estimate the binding constants, the concentration dependence of the fluorescence of PTO with poly(dA) and poly(dG) was studied. The integrated fluorescence of PTO with poly(dA), shown in Figure 3.5A, reached a plateau around 18 μM poly(dA), indicating a binding stoichiometry of one dye molecule per 4 bases and an equilibrium constant around $10^5\ M^{-1}$ at room temperature. At DNA concentrations above 18 μM, there were ample intercalation sites and thus all dye was intercalated, giving the maximum fluorescence intensity.

At DNA concentrations below 18 μM, the fluorescence intensity was less than maximal thus the dye must have used other (less restrictive) binding modes, such as groove binding or electrostatic associations. Unlike poly(dA), there was no plateau in the PTO fluorescence when the dye was titrated with poly(dG), as seen in Figure 3.5B. This indicates that in the concentration range studied, more than one mode of binding is occurring even when there are free intercalation sites, for example at 180 μM poly(dG) the dye:base ratio is 1:40. The data shows a downward curvature, indicating that if higher concentrations of DNA were added then a plateau would eventually be reached. The equilibrium constant for binding of PTO to poly(dG) was estimated to be around $10^4$ $M^{-1}$ (in terms of moles of bases) at room temperature.

Nygren *et al.* used chemometric methods to determine TO binding constants of 6.3 x $10^4$, 2.5 x $10^3$ and 200 $M^{-1}$ for poly(dG) and poly(dA), poly(dC) and poly(dT), respectively.[5] We measured the binding constants of the TO-derivative PTO for poly(dA) and poly(dG), which were around $10^4$-$10^5$ $M^{-1}$ at room temperature.

Values for poly(dC) and poly(dT) association with monomeric PTO must be at least 2 orders of magnitude lower than that of the dye with the polypurines, given the very low fluorescence observed (see Figure 3.4). This is consistent with TO, which has binding constants for the polypyrimidines 1-2 orders of magnitude smaller than those for the polypurines.[5]

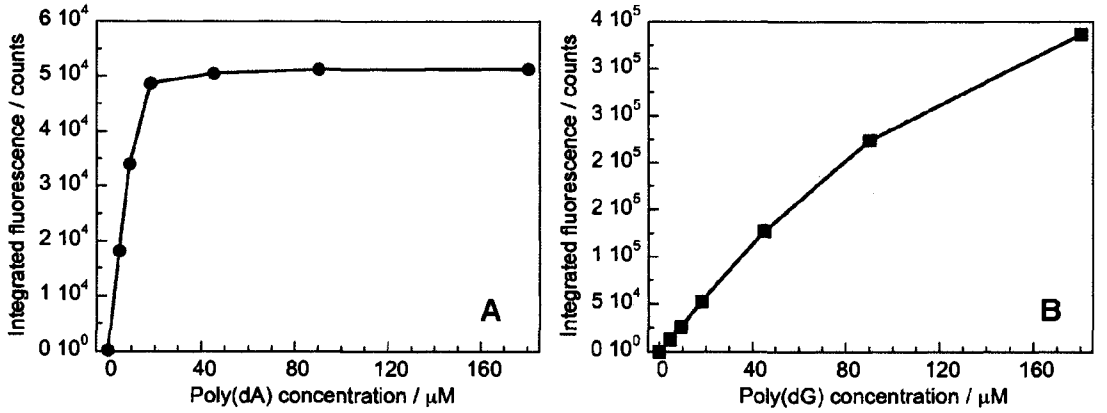


**Figure 3.5: Integrated fluorescence (over 500-700 nm emission) of 4.5 μM PTO in 10 mM Tris buffer (pH 7.4) at room temperature, excited at 355 nm, as a function of: (A) poly(dA) and (B) poly(dG) concentration. The lines are only present to guide the eye.**

To ensure that the fluorescence of the PTO/DNA complexes was stable, their fluorescence was monitored over time. As seen in Figure 3.6, there were initial changes in the integrated fluorescence. The integrated fluorescence stabilized after approximately 1200 seconds thus all measurements should be done after a 20 minute stabilization period.

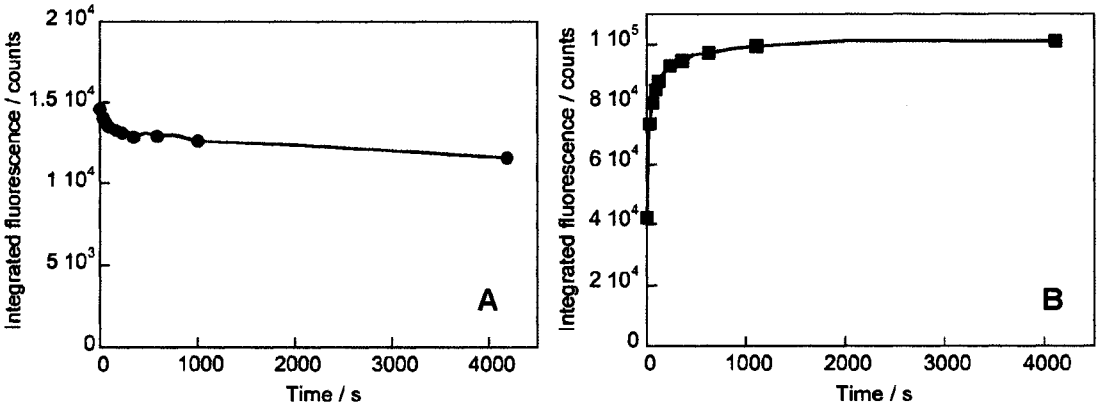


**Figure 3.6: Integrated fluorescence of 4.5 μM PTO in 10 mM Tris buffer (pH 7.4) at room temperature, excited at 355 nm, as a function of time for: (A) 100 μM poly(dA) over its 535-545 nm emission and (B) 100 μM poly(dG) over its 545-555 nm emission. The lines are only present to guide the eye.**

### 3.2.3. Time-Resolved Fluorescence Spectroscopy

Similar to the steady-state fluorescence experiments, it was observed in the time-resolved fluorescence work that PTO emits more strongly in the presence of poly(dG) and poly(dA) than in poly(dC) and poly(dT). Time-resolved fluorescence spectroscopy provides both kinetic data and "snapshots" of the spectra. The fluorescence spectra monitored in the 100 ps following laser excitation are shown in Figure 3.7. The relatively higher intensity in poly(dA) (compared with the steady-state spectra of Figure 3.4) is due to the shorter dye fluorescence lifetime in poly(dA) that led to a weaker integrated signal in the case of Figure 3.4.

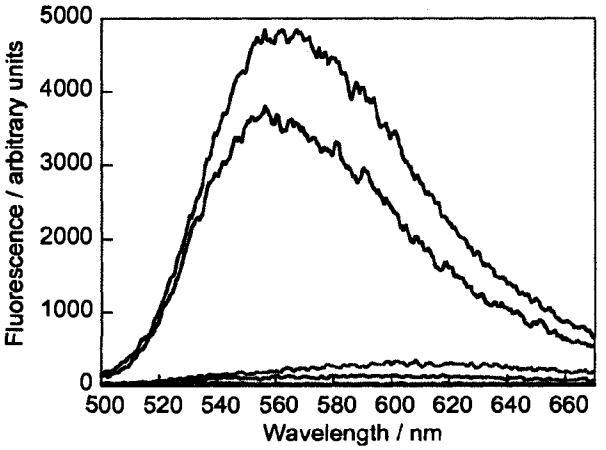


**Figure 3.7: Fluorescence of 20 μM PTO in the presence of 200 μM homopolymers in 10 mM Tris buffer (pH 7.4), 10 mm path length, excited with a picosecond laser at 355 nm and recorded within the first 100 ps following excitation. Recorded at room temperature for poly(dG) (blue), poly(dA) (black), poly(dT) (red) and poly(dC) (green). The dye alone (purple) blends with the baseline.**

The fluorescence decays of PTO with poly(dC) and poly(dT) were weak, dominated by a component with a lifetime of *ca.* 0.3 ns (Table 3.1). This suggests a very weak and loose association, perhaps largely determined by a combination of hydrophobic effects and electrostatic forces, given the two positive charges in PTO. Complexes of PTO with both poly(dA) and poly(dG) showed strong emission, in agreement with the steady-state data of Figure 3.4. In the absence of DNA, PTO exhibited extremely weak emission with a relative intensity of < 5 counts (for both steady-state and time-resolved fluorescence, Figure 3.4 and Figure 3.7, respectively) with the time-resolved trace largely following the instrument response function, suggesting $\tau < 70$ ps. The association geometry of the long lifetime component is unclear, although it is unlikely to reflect aggregates, since emission was extremely weak in systems (poly(dC) and poly(dT)) that appeared to favour aggregation. Further, there was no hint of a short wavelength band (or shoulder) in either the steady-state or time-resolved spectra (see Figure 3.4 and Figure 3.7).

We speculate that some association geometries severely hinder bond rotation and result in longer lived emission.

Note that the fluorescence decay of PTO in poly(dA) was the only one that could be fitted to a single exponential (Table 3.1).

**Table 3.1: Fluorescence decay data for PTO in the presence of DNA homopolymers[a]**

| Poly- | $\tau_1$ / ns | $A_1$ (%) | $\tau_2$ / ns | $A_2$ (%) | Rel. int.[b] |
|---|---|---|---|---|---|
| dG | 0.72 | 38 | 3.4 | 62 | 42 |
| dA | 0.48 | 100 | - | - | (100) |
| dC | 0.28 | 59 | 2.8 | 41 | 3 |
| dT | 0.27 | 78 | 2.3 | 22 | 8 |

[a] Typical errors are around 0.05 ns for lifetimes with pre-exponential factors exceeding 40%, but can be as large as 0.3 ns for pre-exponential factors around 20%. [b] Based on the time-resolved emission immediately after laser excitation.

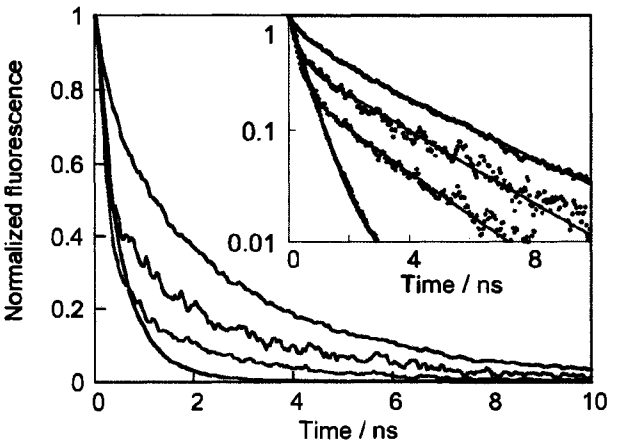


**Figure 3.8: Fluorescence decays following 35 ps laser excitation (355 nm) of buffered (pH 7.4) solutions containing 20 μM PTO and 200 μM homopolymers. Recorded at room temperature for poly(dG) (blue), poly(dA) (black), poly(dT) (red) and poly(dC) (green). Inset: semi-log plot.**

### 3.2.4. Circular Dichroism

Upon addition of a dye to DNA, one would expect the CD signal in the DNA region to remain unchanged unless perturbations in the DNA helix had occurred. PTO only had a significant effect on the DNA region in the case of poly(dA) (see Figure 3.9) and the decrease in the CD signal was probably due to a minor loss of secondary structure (note the high base:dye ratio), but it was consistent with our results which indicated that PTO intercalates readily into poly(dA) (*vide infra*). Interestingly, for the polypyrimidines and even for poly(dG), where all other results indicated significant association with PTO, there did not appear to be any significant change in helix structure caused by the addition of dye. Note that these experiments had to be carried out at lower dye:DNA concentrations to achieve acceptable optical properties in the DNA region.

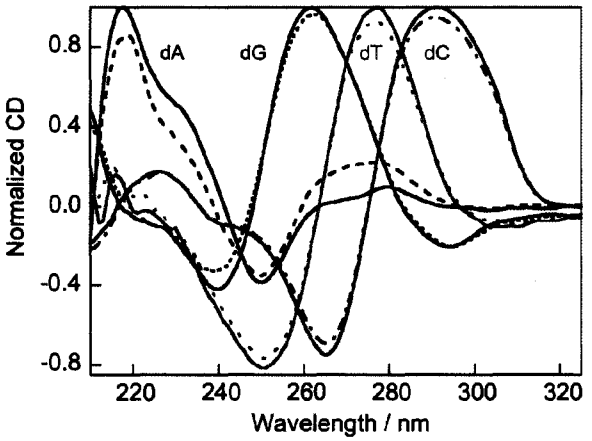


**Figure 3.9: Circular dichroism from 35 μM DNA homopolymers with (dashed line) and without (full line) 3.5 μM PTO in 10 mM Tris buffer (pH 7.4), 10 mm path length, recorded at 20°C for poly(dA) (black), poly(dG) (blue), poly(dC) (green) and poly(dT) (red).**

### 3.2.5. Induced Circular Dichroism

Achiral molecules, such as PTO, placed in a chiral environment may show induced circular dichroism (ICD) due to coupling of the electrical transition moments of the guest molecule and of the chiral host.[25] Induced circular dichroism of the same solutions as in Figure 3.4 and Figure 3.7 showed very weak signals for PTO with poly(dC) and poly(dT) (Figure 3.10) indicative of inefficient association, consistent with the fluorescence results. In contrast, PTO complexes involving both poly(dA) and poly(dG) led to strong ICD signals. For the latter, two minima were observed, indicative of more than one type of binding, consistent with the titration results (see section 3.2.2). For the nondegenerate case, the ICD spectrum should be essentially identical to the corresponding absorption spectrum; it can be either positive or negative.[25] The ICD peaks – at 480 nm and 526 nm – of PTO in poly(dG) differed from the absorbance peaks – at 489 and 508 nm – indicating that the ICD was not simply the nondegenerate case; more than one type of binding was occurring. Only in the case of poly(dA) was the ICD signal fairly simple, except for a small feature at around 500 nm. This suggests a single or highly dominant mode of binding. This ICD signal may incorporate some exciton coupling between two or more intercalated chromophores.

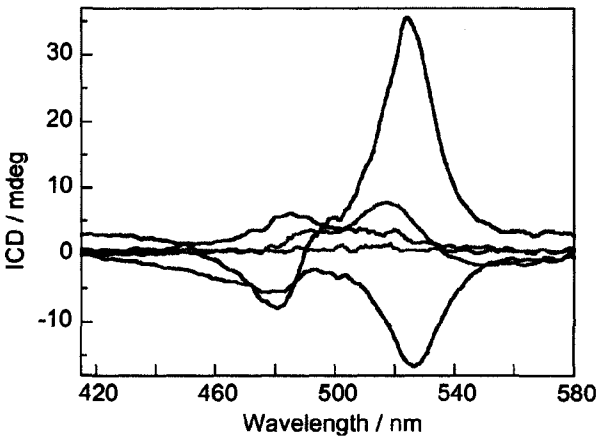


**Figure 3.10: Induced circular dichroism from 20 μM PTO in the presence of 200 μM DNA homopolymers in 10 mM Tris buffer (pH 7.4), 10 mm optical path. Recorded at 20°C for poly(dA) (black), poly(dG) (blue), poly(dC) (green), poly(dT) (red) and the dye in buffer alone (purple).**

It has been reported that symmetrical cyanine dyes can form face-to-face dimers that assemble end-to-end within the minor groove of DNA.[35] It is possible that in the cases of poly(dC) and poly(dT) the weak ICD signals may incorporate some contribution from dye aggregates associated with the backbones of the DNA homopolymers. It was found that at low dye concentrations (3.5 μM), PTO did not show any association with the polypyrimidines (see Figure 3.11) while at higher dye concentrations (20 μM) there was evidence of complexation (see Figure 3.10). This further supports our hypothesis that PTO associates with the polypyrimidines as an aggregate. In contrast, ICD signals whose shapes were independent of dye concentration were observed for PTO with the polypurines (see Figure 3.10 and Figure 3.11), indicating association of the dye monomer.

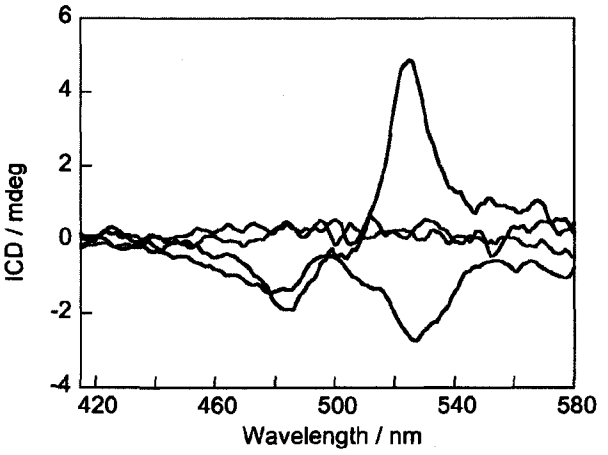


**Figure 3.11: Induced circular dichroism from 3.5 μM PTO in the presence of 35 μM DNA homopolymers in 10 mM Tris buffer (pH 7.4), 10 mm optical path. Recorded at 20°C for poly(dA) (black), poly(dG) (blue), poly(dC) (green) and poly(dT) (red).**

Comparison of the ICD of TO (Figure 3.12) and of PTO (Figure 3.11) with poly(dA) shows that both dyes underwent the same interaction with the DNA strand. The peak and the trough of the TO ICD were blue-shifted by several nanometers relative to those of the PTO ICD, but this is expected as the TO monomer absorption maximum (501 nm) is also blue-shifted compared to that of PTO (508 nm). Nygren *et al.* have reported that TO binds as a monomer to poly(dA), as both a monomer and a dimer to poly(dG), and mostly as a dimer to poly(dC) and poly(dT).[5] If TO and PTO bind to poly(dA) as monomers, then the +/- excitons (two bands of equal magnitude where the longer wavelength band is positive and the shorter wavelength band is negative) must be due to excitonic coupling between dye monomers and the DNA backbone rather than coupling between dye molecules in a single intercalation site. The ICD of TO and poly(dG) is more complicated, with two longer wavelength peaks and a shorter wavelength trough, shown in Figure 3.12, suggesting more than one mode of binding, in agreement with the results of Nygren *et al.* Although PTO also appears to bind to poly(dG) in more than one manner, its ICD spectrum differs from that of TO, therefore the orientations of

the bound chromophores must differ in the two cases. As with 3.5 μM PTO: 35 μM DNA, there was no TO ICD upon addition of the dye to poly(dC) or poly(dT), as seen in Figure 3.12. Similarly to PTO, bound TO dimers exhibited minimal fluorescence in poly(dC) and poly(dT).[5] These results reinforce the idea that PTO associates with the polypyrimidines as a non-fluorescent dimer/aggregate.

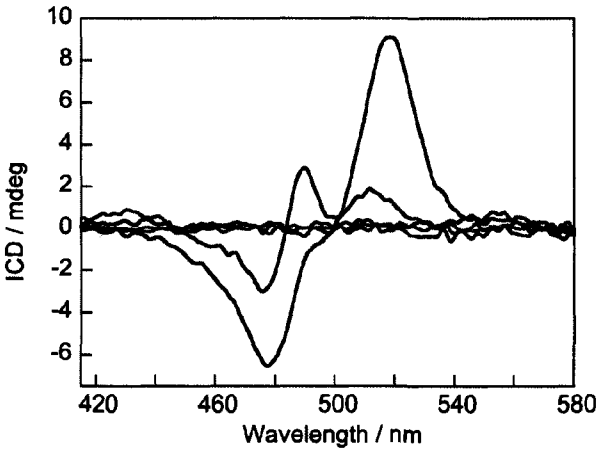


**Figure 3.12: Induced circular dichroism from 7 μM TO in the presence of 70 μM DNA homopolymers in 10 mM Tris buffer (pH 7.4), 10 mm optical path. Recorded at 20°C for poly(dA) (black), poly(dG) (blue), poly(dC) (green), poly(dT) (red) and the dye in buffer alone (purple).**

The ICD of PG with poly(dT) and poly(dG) (see Figure 3.13) resembled that of PTO and TO with poly(dA) (see Figure 3.11 and Figure 3.12), although they lack the small feature around 500 nm. Previous work in our laboratory, based on circular dichroism and fluorescence spectroscopy, led to the conclusion that PG binds to poly(dG) and poly(dT) as a dimer.[10] Although the ICD spectra are similar, the PG complexes decay with biexponential kinetics while PTO/poly(dA) decays monoexponentially. Either PTO binds to poly(dA) as a monomer and the +/- exciton results from coupling between the dye and the DNA backbone, or PTO binds as a dimer with a single mode of intercalation and the +/- exciton results from coupling between intercalated dye molecules. The former hypothesis agrees with the

TO/poly(dA) results of Nygren *et al.*[5] while the latter hypothesis agrees with the PG and poly(dG) and poly(dT) results.[10] The weak steady-state fluorescence, immeasurable fluorescence lifetimes (≤0.05 ns) and lack of ICD suggested a loose association between PG and poly(dA) and poly(dC).[10] In the presence of poly(dC) and poly(dT), PTO showed similar fluorescence characteristics although weak ICD was observed at dye concentrations of 20 μM but not at 3.5 μM. Although the general structure of PG is similar to that of TO and PTO, the fact that PG associates strongly with poly(dG) and poly(dT) but not poly(dA) and poly(dC) indicates that its substituents play a significant role in its binding specificity, which differs from that of TO and PTO that bind strongly to poly(dA) and poly(dG) but weakly to poly(dC) and poly(dT).

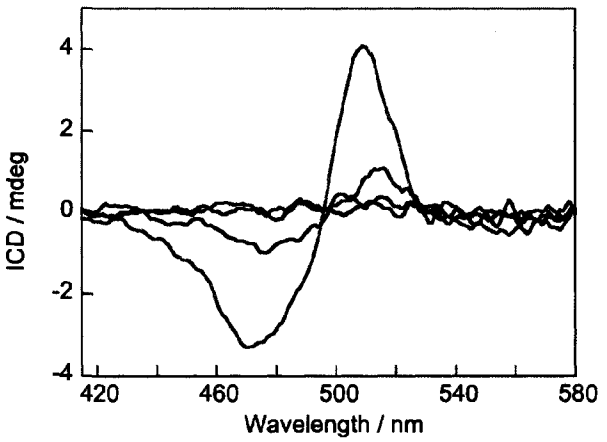


**Figure 3.13: Induced circular dichroism from 7 μM PG in the presence of 70 μM DNA homopolymers in 10 mM Tris buffer (pH 7.4), 5 mm optical path. Recorded at 20°C for poly(dA) (black), poly(dG) (blue), poly(dC) (green) and poly(dT) (red).**

### 3.2.6. The Effect of PTO on RNA Homopolymers

For poly(rC) there was no change whatsoever in the RNA region upon addition of PTO, which is not surprising since the ICD of PTO indicated no association between the dye and the RNA (see next paragraph). PTO had a large

effect on the RNA region of poly(rA) and a lesser effect on poly(rU), in both cases indicating a loss of secondary structure caused by intercalation. Intercalation of PTO in poly(rA) is consistent with the above-mentioned results where PTO intercalated readily into poly(dA). On the other hand, intercalation of PTO in poly(rU) contradicts the weak association observed for PTO with poly(dT); most likely the methyl group of thymine, which uracil lacks, causes these differences. Note that these experiments had to be carried out at lower dye:RNA concentrations (7:70 μM) to achieve acceptable optical properties in the RNA region.

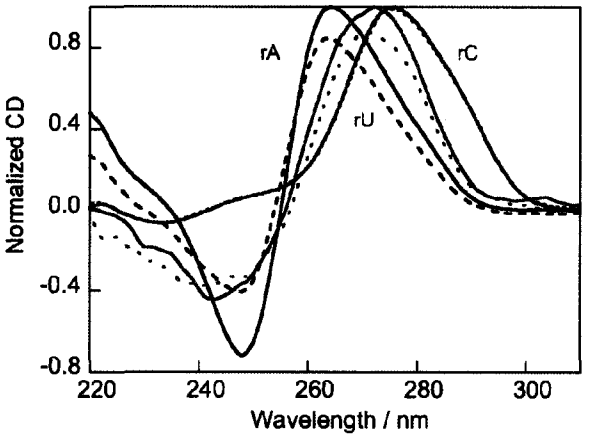


**Figure 3.14: Circular dichroism from 70 μM RNA homopolymers with (dashed line) and without (full line) 7 μM PTO in 10 mM Tris buffer (pH 7.4), 5 mm path length, recorded at 20°C for poly(rA) (black), poly(rC) (green) and poly(rU) (red).**

When PTO was complexed with poly(rA), it showed ICD extrema at the same wavelengths (within 2 nm) as PTO and poly(dA), see Figure 3.15 and Table 3.2. The signs of the major peak and trough were identical for both cases. However, the small feature at around 500 nm was positive in the case of the polydeoxyribonucleotide and negative for the polyribonucleotide, demonstrating its dependence on the hydroxyl group of the sugar. For 7 μM PTO and 70 μM poly(rC), no ICD was observed. Although 20 μM PTO and 200 μM poly(dC) exhibited weak ICD, 3.5 μM PTO and 35 μM poly(dC) showed no ICD, in agreement

with the poly(rC) complex. These results further support the idea that PTO associates with polypyrimidines as an aggregate. The ICD observed with PTO and poly(rU) indicates an association with higher order aggregates, which showed an absorption maximum at 478 nm (see Figure 3.1). Although PTO appears to associate with both poly(dT) and poly(rU) as an aggregate, the ICD of PTO with poly(rU) was blue-shifted, and of opposite sign, relative to that with poly(dT). These differences are most likely an effect of the methyl group of thymine, which uracil lacks.

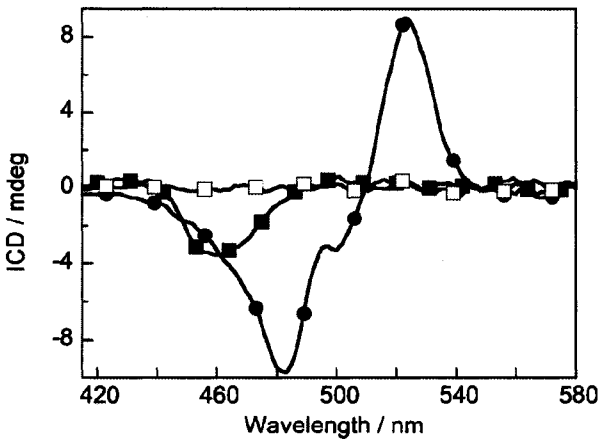


**Figure 3.15: Induced circular dichroism from 7 μM PTO in the presence of 70 μM RNA homopolymers in 10 mM Tris buffer (pH 7.4), 5 mm optical path. Recorded at 20°C for poly(rA) (●), poly(rC) (□) and poly(rU) (■).**

**Table 3.2: Induced circular dichroism data for PTO[a] in the presence of DNA[b] and RNA[c] homopolymers**

| Poly- | Location of peak(+) or trough(-) / nm |
|---|---|
| dA | 481(-), 498[d](+), 524(+) |
| rA | 483(-), 500(-), 523(+) |
| dC (200 μM) | 485(+) |
| dC(35 μM) | none |
| rC | none |
| dT | 492[d](+),517(+) |
| rU | 460(-) |

[a]1:10 dye:DNA base ratio

[b]Concentration of the DNA homopolymers was 200 μM

[c]Concentration of the RNA homopolymers was 70 μM

[d] Shoulder rather than a peak

### 3.2.7. Computational Studies

Computational studies provide a unique insight into the nature of the dye-DNA interaction. Although the general structure of PG is known (see Scheme 3.1), its exact structure is proprietary, making it impossible to study computationally. PTO and TO each have two *E-Z* isomers and a low barrier of rotation around the bond joining the benzothiazole and quinoline rings, hence all the conformers were considered and fully optimized (*in vacuo*) by B3LYP/6-31G*, Figure 3.16 and Figure 3.17. The ground state geometries of PTO and TO chosen for the majority of the MD simulations were the most stable structures by 4.1 and 4.18 kcal $mol^{-1}$, respectively, between the two possible conformations of their respective *trans* isomers. These structures were confirmed as the dominant structures using $^1H$ NMR, COSY and NOE experiments (data presented in Section 3.5.5). Note the similarity in energies for each conformer of PTO and its equivalent of TO. A few calculations were done with the second most stable structure of PTO, as discussed in section 3.2.7.5. It was found that the cross peak

patterns in the NOESY spectra were the same for both TOTO/dsDNA and free TOTO, indicating that the conformation does not change upon intercalation.[13] Thus one can assume that the most stable TO and PTO structures in solution will also be the most stable in DNA. As TOTO is simply a covalently linked dimer of TO and PTO is a TO-derivative, we have assumed that the most stable TO and PTO structures in solution will also be the most stable in DNA for the purposes of our calculations.

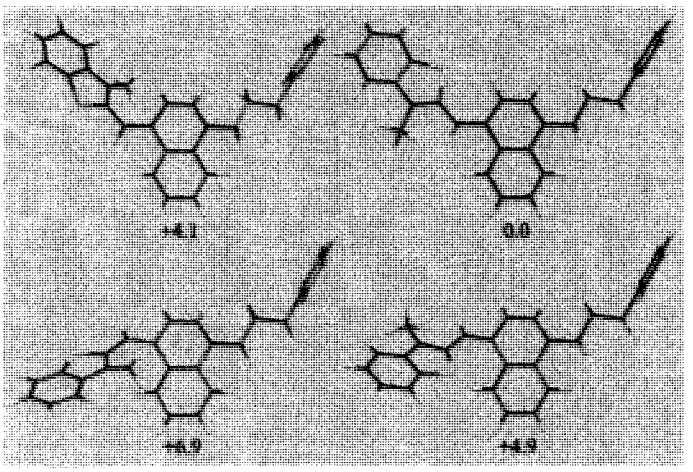


**Figure 3.16: Isomers and conformers of PTO showing relative energy minima (in kcal $mol^{-1}$) for the optimized structures.**

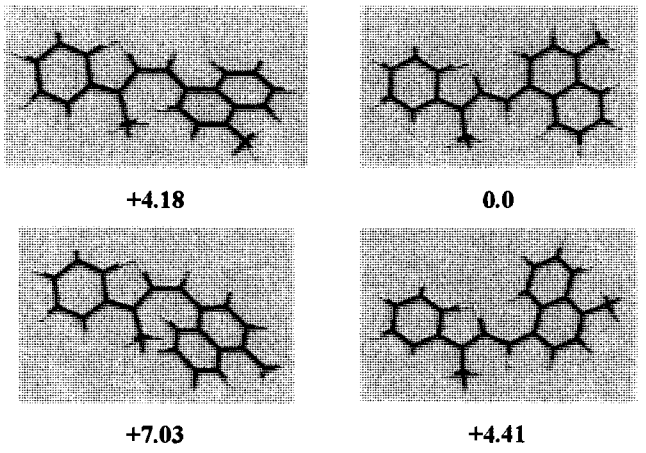


**Figure 3.17: Isomers and conformers of TO showing relative energy minima (in kcal $mol^{-1}$) for the optimized structures.**

The DNA oligomers consisted of 10 bases to coincide with the experimental conditions, where a 1:10 dye:base ratio was employed. The modeling was carried out by inserting the dye, either PTO or TO, in an arbitrary position near the center of the 10 base chain, i.e. between the $5^{th}$ and $6^{th}$ base. As such, each 2 ns simulation required 10 days of CPU time, thus it was not feasible to place the dye in the proximity of the DNA and monitor its intercalation as this would require extremely long simulations. In order to provide a complete description of the system, several orientations between the dye and the DNA oligomers were considered. These consisted of placing the benzothiazole moiety between the bases, the quinoline moiety between the bases, both the benzothiazole and the quinoline moieties between the bases, or the pyridinium moiety between the bases (PTO only). Table 3.3 in the Discussion section (Section 3.3.2) summarizes the observations that follow.

The simulations involve the dye, the DNA oligomer, the counterions, and approximately 4000 water molecules (Figure 3.18A). To visualize things more easily in this thesis, the water molecules were removed graphically (as seen in Figure 3.18B), but they were always present during the simulation. In addition, a ribbon was added to the DNA phosphate backbone, as shown in Figure 3.18C.

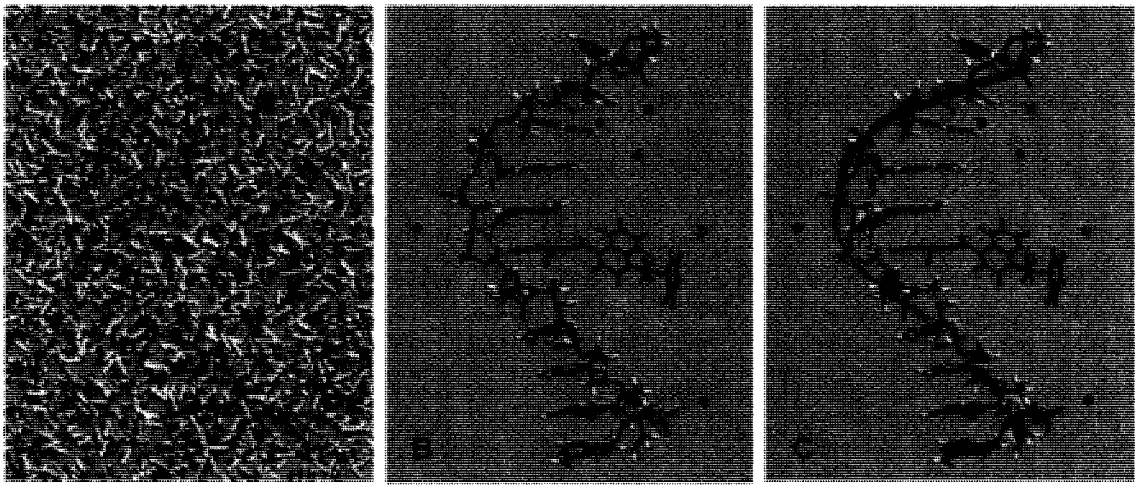

**Figure 3.18: (A) Visualization of the complete system (dye, DNA, counterions and water). (B) Visualization where the water molecules in (A) have been removed. (C) Visualization where a ribbon has been added to the DNA phosphate backbone in (B). Blue and red circles are the counterions, and the dye is green.**

An example of "snapshots" of a molecular dynamics trajectory is shown in Figure 3.19, taken in 250 picosecond intervals. Due to the large number of simulations in this thesis, it is only feasible to show the initial (for example Figure 3.19A) and final (for example Figure 3.19I) orientations of the dye/DNA complexes.

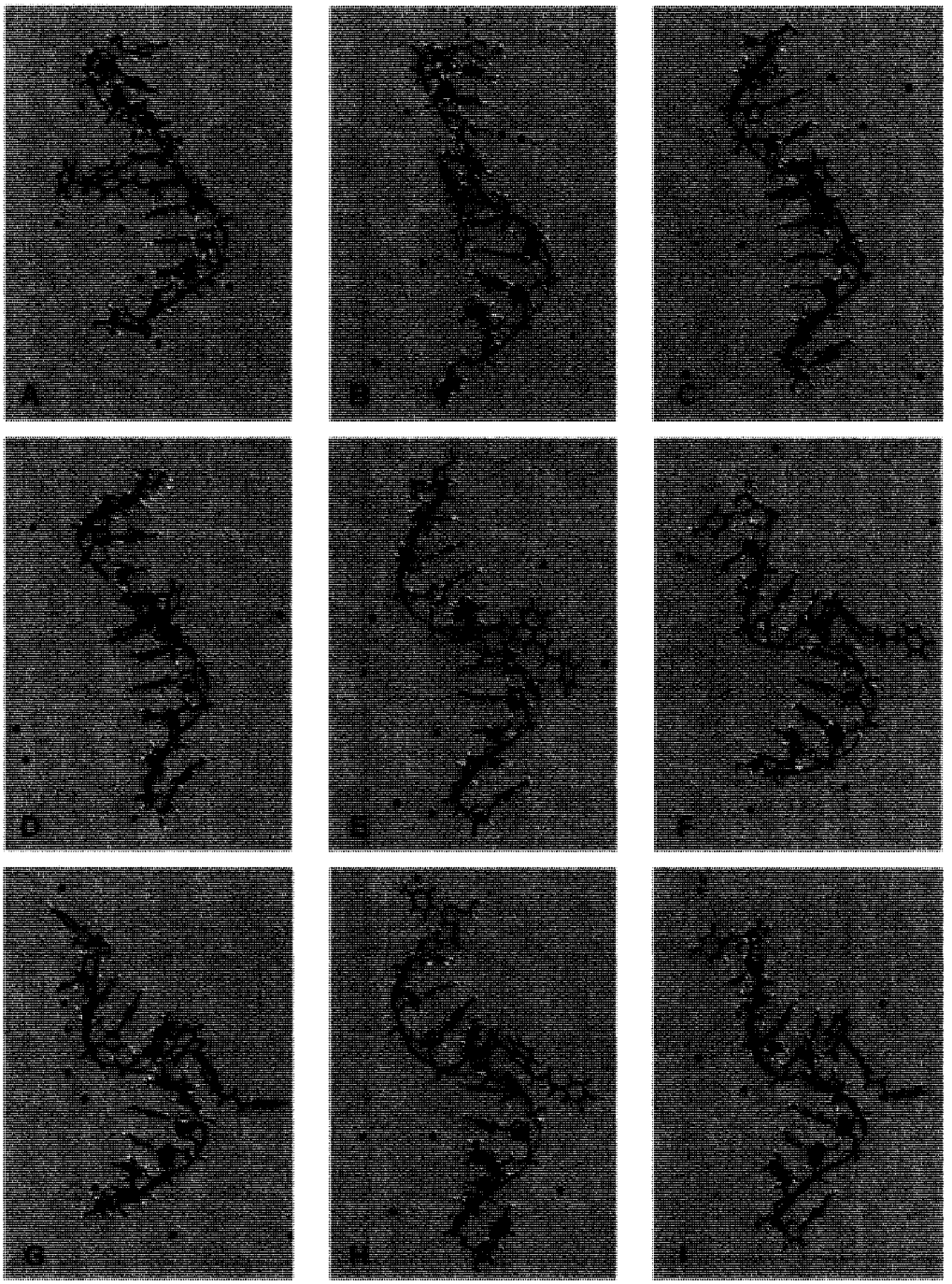

**Figure 3.19: Representative simulation at (A) 0, (B), 250, (C) 500, (D) 750, (E) 1000, (F) 1250, (G) 1500, (H) 1750, and (I) 2000 picoseconds.**

### 3.2.7.1. Intercalation via the Benzothiazole Moiety

When inserting the PTO benzothiazole moiety between the bases of the DNA oligomers, 4 orientations were considered for each oligomer, as illustrated in Figure 3.20.

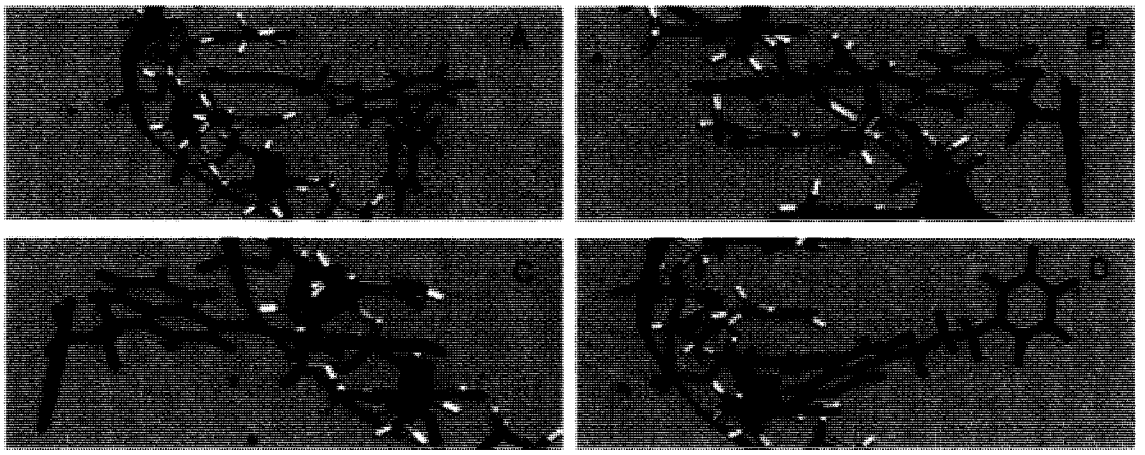


**Figure 3.20: Illustration of the modes of insertion of the PTO benzothiazole moiety between the two central bases of DNA oligomers, shown here for $(dT)_{10}$. (A) Benzothiazole aromatic H's are near the backbone. (B) Benzothiazole $CH_3$ is near the backbone. (C) Benzothiazole S is near the backbone. (D) Orientation in (A) that was rotated 180°.**

When the benzothiazole moiety of PTO was placed between the bases of $(dA)_{10}$, in 2 of the 4 simulations there was a shift, leaving the quinoline intercalated, as shown in Figure 3.21B. In the other 2 simulations the benzothiazole remained intercalated while the rest of the dye moved around. In one of these cases a $\pi$-stacking interaction between the quinoline and the pyridinium moieties was evident, as seen in Figure 3.21D. Note that in this work, $\pi$-stacking refers to stacking between 2 or more $\pi$-systems.

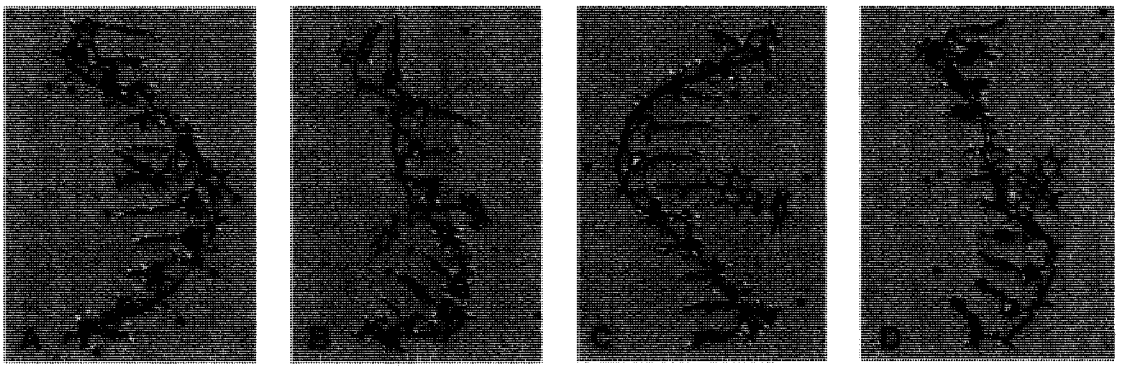

**Figure 3.21: Initial (A) conformation of PTO/$(dA)_{10}$, and after 2 ns (B), showing the quinoline moiety intercalated between A bases. Initial (C) conformation of PTO/$(dA)_{10}$, and after 2 ns (D), showing the benzothiazole moiety intercalated and $\pi$-stacking between the quinoline and the pyridinium moieties.**

In 2 of the 4 cases where the benzothiazole moiety of PTO was placed between the bases of $(dG)_{10}$, the dye shifted so that the quinoline moiety was intercalated, as shown in Figure 3.22B. In the other 2 cases, the dye moved around slightly but its orientation remained very close to the starting guess, with a slight elongation of the oligomer, as seen in Figure 3.22D.

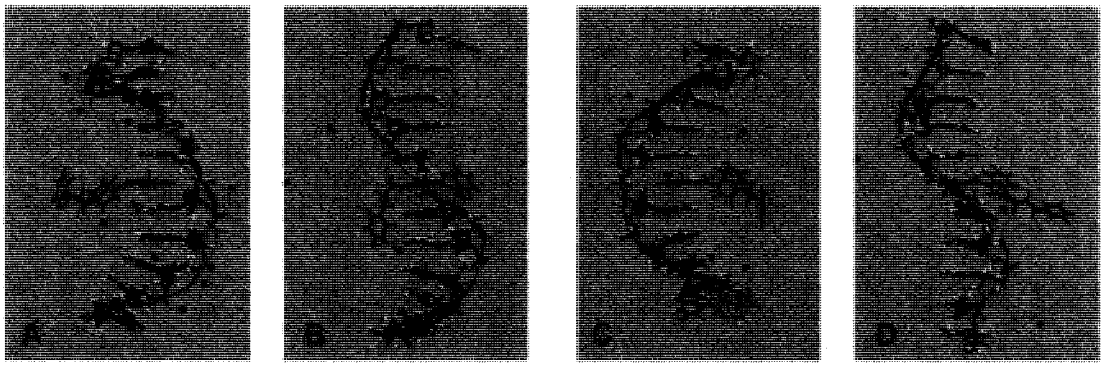


**Figure 3.22: Initial (A) conformation of PTO/$(dG)_{10}$, and after 2 ns (B), showing the quinoline moiety intercalated between G bases. Initial (C) conformation of PTO/$(dG)_{10}$, and after 2 ns (D), showing the benzothiazole intercalated in a manner similar to the initial orientation.**

When the quinoline moiety was intercalated, $\pi$-stacking between the dye and the DNA bases was evident. Although both oligomers showed a similar association with PTO, there was some indication of a more organized arrangement in the case of $(dG)_{10}$, as shown in Figure 3.23.

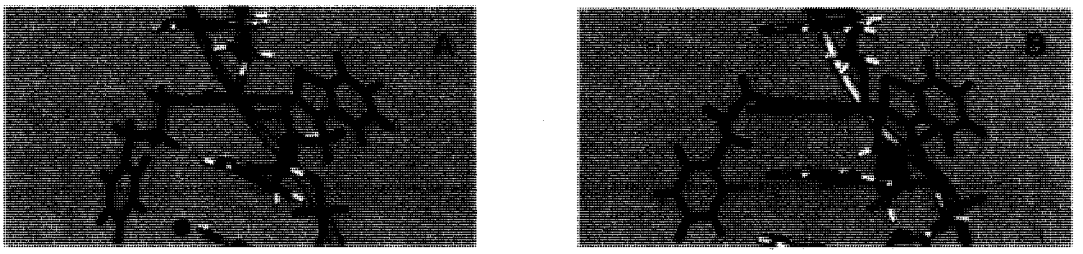


**Figure 3.23: Close-ups of (A) the final PTO/$(dA)_{10}$ structure (from Figure 3.21B) after 2 ns and (B) the final PTO/$(dG)_{10}$ structure (from Figure 3.22B) after 2 ns.**

In every simulation involving insertion of the PTO benzothiazole moiety between the bases of $(dA)_{10}$ or $(dG)_{10}$, PTO remained intercalated. In 50% of the cases, the benzothiazole shifted within 1 ns so that the quinoline moiety was intercalated. In the other 50% of the cases, the dye moved around slightly but remained close to the starting guess.

When inserting the TO benzothiazole moiety between the bases of the DNA oligomers, 4 orientations were considered for each oligomer, as illustrated in Figure 3.24.

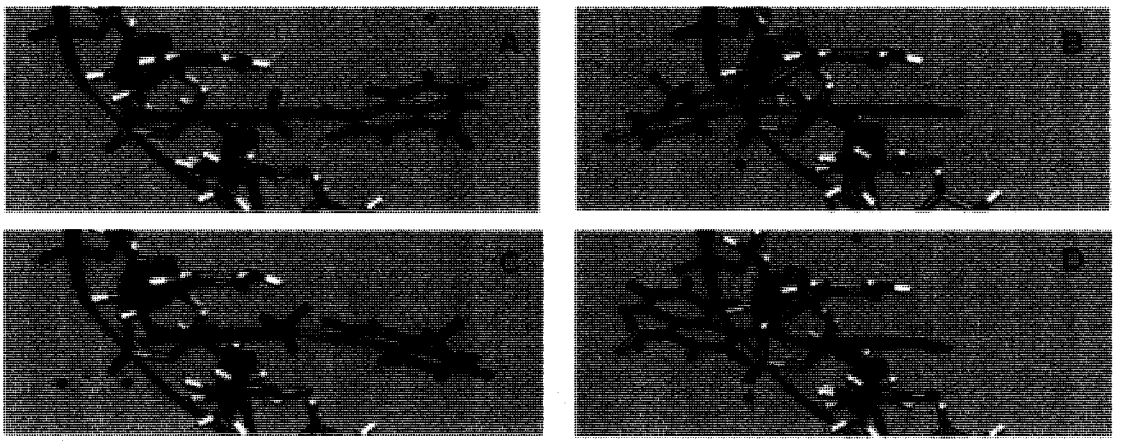


**Figure 3.24: Illustration of the modes of insertion of the TO benzothiazole moiety between the two central bases of DNA oligomers, shown here for $(dC)_{10}$. (A,B) Benzothiazole $CH_3$ is perpendicular to the intercalation pocket (going into the plane of the paper); in (B) the quinoline moiety is much closer to the DNA backbone than in (A). (C,D) Benzothiazole $CH_3$ is perpendicular to the intercalation pocket (coming out of the plane of the paper); in (D) the quinoline moiety is much closer to the DNA backbone than in (C).**

When the benzothiazole moiety of TO was inserted between the bases of $(dA)_{10}$, in all 4 cases the benzothiazole interacted with one base in the intercalation site while the quinoline interacted with the other. In 3 of the 4 cases, this orientation caused the DNA strand to bend significantly, as seen in Figure 3.25B, and would presumably lead to complete dissociation if not for $\pi$-stacking interactions. In 2 of these 3 cases the quinoline became intercalated before forming the final complex where each moiety interacted with a base (data not shown). In 1 of the 4 cases, one of the bases flipped out of the helix so that it was perpendicular to the other bases, as seen in Figure 3.25D. This arrangement of the DNA strand more closely resembles intercalation than that shown in Figure 3.25B.

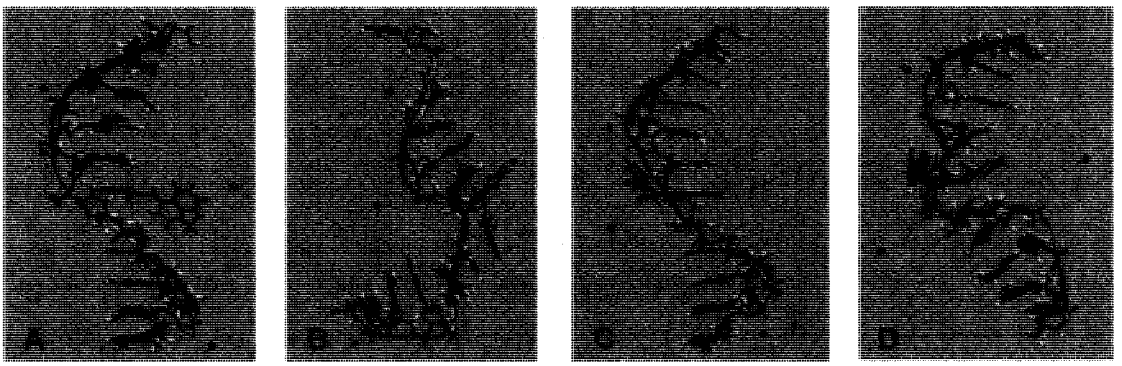


**Figure 3.25: Initial (A) conformation of TO/$(dA)_{10}$, and after 4 ns (B), showing the dye partly dissociated. Initial (C) conformation of TO/$(dA)_{10}$, and after 6 ns (D), showing both the benzothiazole and the quinoline moieties interacting with A bases while one base was flipped out of the helix.**

In 2 of the 4 cases involving the benzothiazole moiety of TO intercalated in $(dG)_{10}$, the dye remained in place and there was a slight elongation of the oligomer, as shown in Figure 3.26B. In the other two cases both moieties were positioned between the bases. In one of these cases the dye partly dissociated, causing the DNA to become extremely bent (data not shown). In the other case the DNA strand maintained its structure during the 4 ns simulation, although it did undergo some elongation, as seen in Figure 3.26D.

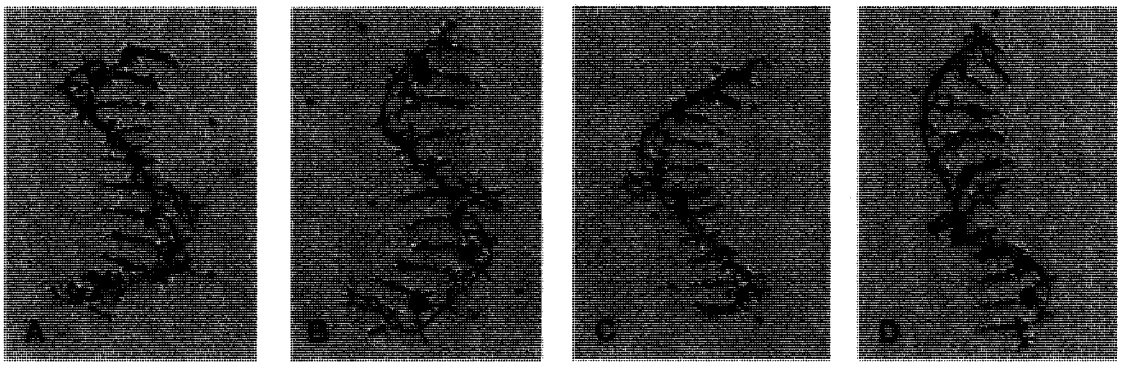


**Figure 3.26: Initial (A) conformation of TO/$(dG)_{10}$, and after 2 ns (B), showing the benzothiazole moiety intercalated between G bases. Initial (C) conformation of TO/$(dG)_{10}$, and after 4 ns (D), showing both the benzothiazole and quinoline moieties interacting with G bases.**

Only in 25% of the cases did TO remain intercalated in the purine oligomers but, unlike PTO, the intercalated moiety never shifted to being the quinoline but remained the benzothiazole moiety. In 50% of the cases studied, the TO benzothiazole moiety interacted with one base and the quinoline with the other, causing the DNA to bend. It is believed that such orientations would lead to complete dissociation if not for $\pi$-stacking interactions. In the other 25% of the cases, the TO benzothiazole moiety interacted with one base and the quinoline moiety interacted with the other base while the overall helical structure of the DNA was essentially maintained, rather than collapsing around the dye or losing the helicity.

When studying PTO and $(dC)_{10}$, the dye was placed in similar orientations to the corresponding initial guesses for $(dA)_{10}$ and $(dG)_{10}$. After a few hundred picoseconds, in 2 of the 4 cases studied, the dye dissociated from the oligomer, as seen in Figure 3.27B. In one of the remaining cases, the dye stayed close to its starting orientation (not shown).

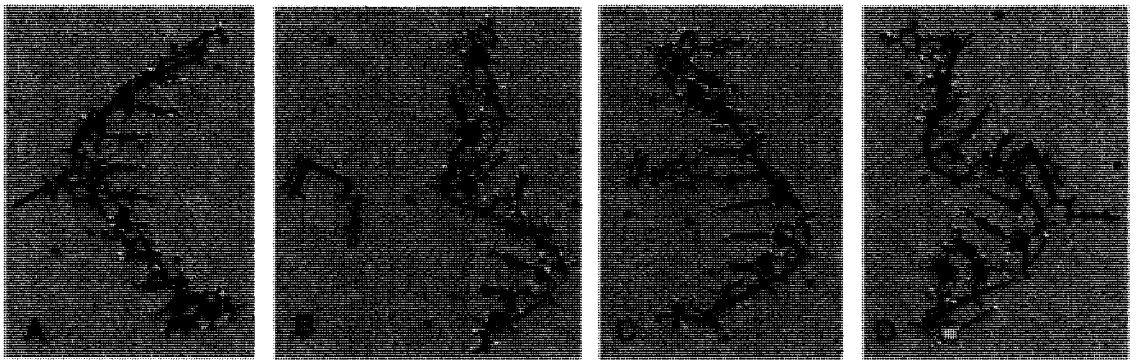

**Figure 3.27: Initial (A) conformation of PTO/$(dC)_{10}$, and after 2 ns (B), showing the dye dissociated. Initial (C) conformation of PTO/$(dC)_{10}$, and after 2 ns (D), showing the dye partly dissociated.**

In the last case, the dye partly dissociated but was held near the DNA due to an interaction with one of the bases, as shown in Figure 3.27D. A close-up is shown in Figure 3.28.

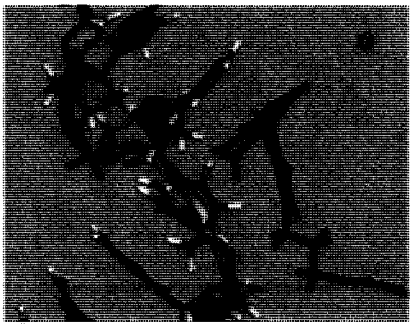

**Figure 3.28: Close-up of the final PTO/$(dC)_{10}$ structure (from Figure 3.27) after 2 ns.**

When the benzothiazole moiety of PTO was placed between two T bases, in 2 of the 4 cases the dye dissociated although it stayed near the DNA oligomer, as shown in Figure 3.29B, presumably due to electrostatic interactions. In one case the dye dissociated almost immediately and in the other dissociation occurred after several hundred picoseconds. In one of the two remaining cases, the dye stayed close to its starting orientation (not shown). In the last case, the benzothiazole moiety interacted with one base while the quinoline moiety interacted with the other, as seen in Figure 3.29D, an orientation that would presumably lead to complete dissociation if not for $\pi$-stacking interactions.

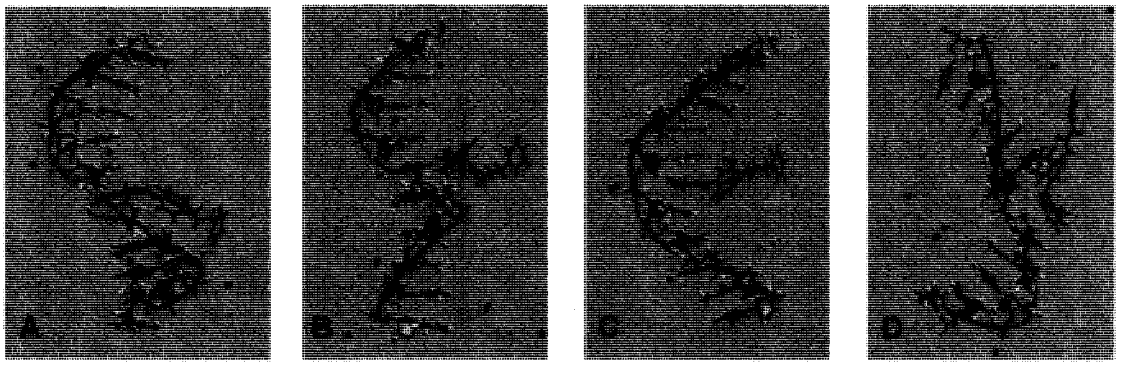


**Figure 3.29: Initial (A) conformation of PTO/$(dT)_{10}$, and after 2 ns (B), showing the dye dissociated. Initial (C) conformation of PTO/$(dT)_{10}$, and after 2 ns (D), showing the dye partly dissociated.**

In 50% of the cases involving the intercalation of the benzothiazole moiety of PTO into $(dC)_{10}$ or $(dT)_{10}$, the dye left the single strand within the first few hundred picoseconds. In 25% of the cases the dye partly dissociated but was held in the proximity of the DNA strand, presumably due to $\pi$-stacking or electrostatic interactions. In the last 25% of the cases the dye remained close to its starting orientation. These simulations reveal the absence of a strong association as found for PTO with $(dA)_{10}$ or $(dG)_{10}$.

Intercalation of the TO benzothiazole moiety in $(dC)_{10}$ led to almost immediate dissociation in 1 of the 4 cases, but the dye remained in the proximity of the DNA oligomer, presumably due to electrostatic interactions (data not shown). In 2 of the 4 cases, both moieties interacted with a C base, resulting in bending of the DNA and partial dissociation. The more extreme case is shown in Figure 3.30B. In the last case, after approximately 1 ns there was a shift from having the benzothiazole moiety intercalated to having both moieties in the intercalation site. This situation continued for 3 ns, at which point the quinoline moiety became intercalated and, simultaneously, one of the bases flipped out of the DNA helix so that it was perpendicular to the other bases. The dye remained in this position during the next 2 ns of the simulation (i.e. 4-6 ns), as seen in Figure 3.30D.

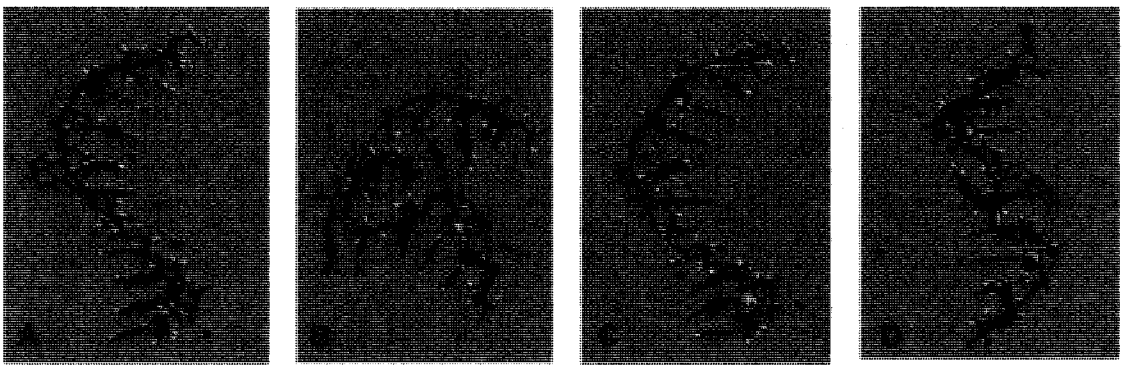

**Figure 3.30: Initial (A) conformation of TO/$(dC)_{10}$, and after 4 ns (B), showing the dye partly dissociated. Initial (C) conformation of TO/$(dC)_{10}$, and after 6 ns (D), showing the quinoline moiety intercalated while one base was flipped out of the helix.**

In 2 of the 4 cases involving the insertion of the TO benzothiazole moiety between the bases of $(dT)_{10}$, the benzothiazole moiety remained intercalated; the quinoline moiety moved around slightly although the dye's orientation did not change greatly from the starting position, as seen in Figure 3.31B. In another case, TO partly dissociated and each moiety interacted with a base (data not shown), as seen for other dye-DNA combinations, for example Figure 3.29D. In the last case, the intercalated moiety switched from the benzothiazole to the quinoline, which underwent a $\pi$-stacking interaction with one base. Electrostatic interactions between the dye and the DNA strand caused the strand to bend towards the dye, as shown in Figure 3.31D.

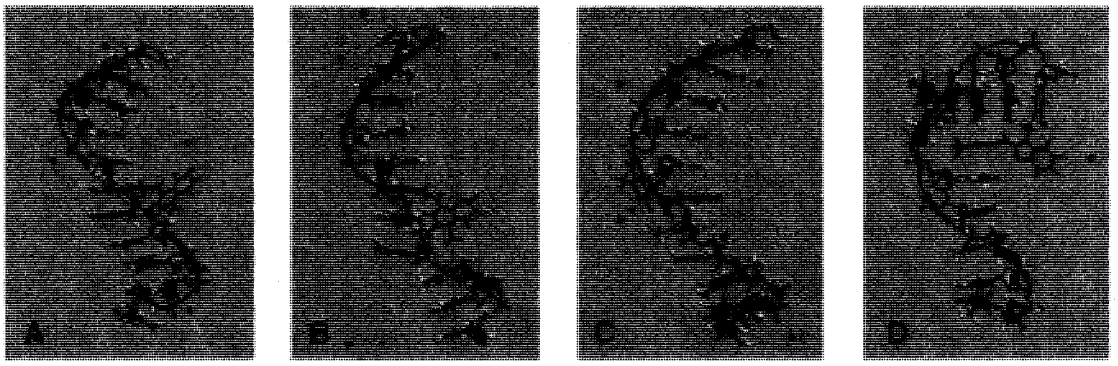


**Figure 3.31: Initial (A) conformation of TO/$(dT)_{10}$, and after 2 ns (B), showing the dye in a position similar to the starting orientation. Initial (C) conformation of TO/$(dT)_{10}$, and after 4 ns (D), showing the dye partly dissociated and a significant bending of the DNA strand.**

Only in 1 of the 8 cases involving the intercalation of the TO benzothiazole moiety in $(dC)_{10}$ or $(dT)_{10}$ did the dye leave the single strand. The dissociation occurred almost immediately, but the dye stayed in the proximity of the DNA strand, presumably due to electrostatic associations. In 4 of the 8 cases the dye underwent partial dissociation; complete dissociation was most likely prevented by $\pi$-stacking interactions. In the other 3 cases the dye remained intercalated, with either the benzothiazole or the quinoline moiety between the bases.

### 3.2.7.2. Intercalation via the Quinoline Moiety

When studying the intercalation of PTO via the insertion of the quinoline moiety, only one starting orientation (shown in Figure 3.32) was chosen for each dye-DNA combination. Initial results involving the intercalation of the PTO benzothiazole moiety indicated that the preferred mode of intercalation for PTO involves the quinoline moiety between the bases (evidenced by shifting of the benzothiazole to intercalate the quinoline), thus less emphasis was placed on calculations where the starting orientation consisted of the quinoline moiety between the bases.

**Figure 3.32: Illustration of the mode of insertion of the PTO quinoline moiety between the two central bases of DNA oligomers, shown here for $(dT)_{10}$.**

When the quinoline moiety of PTO was placed between the bases of the $(dA)_{10}$ strand, the other two moieties moved around slightly while the quinoline moiety remained between the bases, and rotation around the methine bond was prevented. At the end of the 2 ns simulation, the helical DNA structure remained intact and $\pi$-stacking was observed between the dye and the bases, shown in Figure 3.33B.

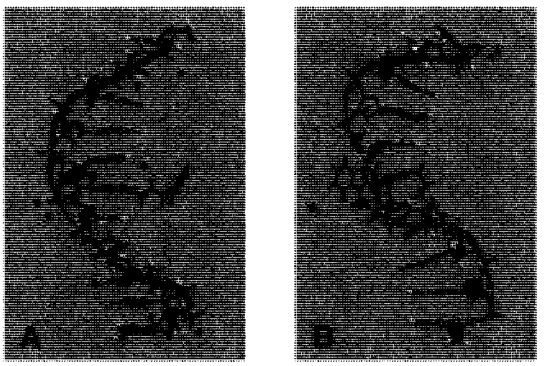


**Figure 3.33: Initial (A) conformation of PTO/$(dA)_{10}$, and after 2 ns (B), showing the dye in a position similar to the starting orientation.**

During the insertion of the PTO quinoline moiety into $(dG)_{10}$, the dye was initially placed with the benzothiazole moiety too close to the bases hence both the benzothiazole and the quinoline moieties were intercalated, as shown in Figure 3.34A. During the optimization, the benzothiazole moiety shifted to the position between the bases and this was the starting orientation for the molecular dynamics simulation, seen in Figure 3.34B. Interestingly, within the first few hundred picoseconds there was a shift which placed the quinoline moiety between the bases and this orientation persisted during the rest of the simulation, as shown in Figure 3.34C, supporting the idea that the quinoline is the preferred moiety for intercalation in single-stranded homopolymers. Another simulation was run where the quinoline moiety was correctly inserted between the G bases, and the dye remained close to the starting orientation (data not shown).

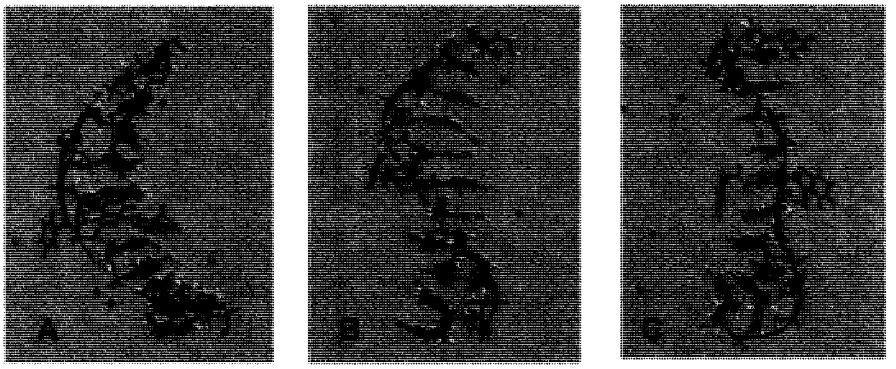

**Figure 3.34: Structure before optimization (A); initial (B) conformation of PTO/$(dG)_{10}$ and after 2 ns (C) of molecular dynamics simulation, showing the quinoline moiety intercalated.**

Since the initial modeling results involving the intercalation of the TO benzothiazole moiety did not show a tendency to shift towards the intercalation of the quinoline moiety, various modes of insertion of the TO quinoline moiety were examined. When inserting the TO quinoline moiety between the bases of the DNA oligomers, 4 orientations were considered for each oligomer, as illustrated in Figure 3.35.

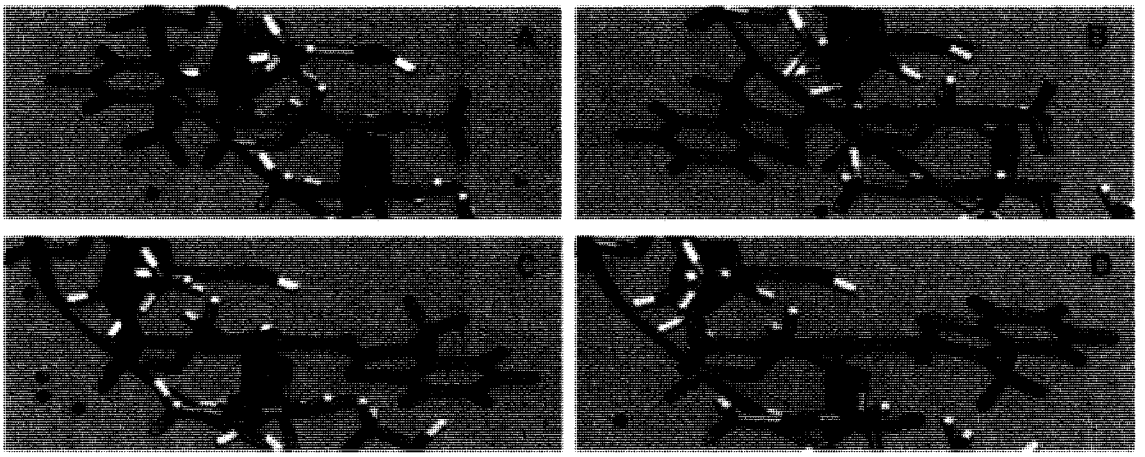

**Figure 3.35: Illustration of the modes of insertion of the TO quinoline moiety between the two central bases of DNA oligomers, shown here for $(dT)_{10}$.**
**(A,B) Benzothiazole moiety is near the DNA backbone; in (A) the methine H is going into the plane of the paper while in (B) it is coming out of the plane of the paper. (C,D) Benzothiazole moiety is further away from the DNA backbone compared to (A) and (B); in (C) the methine H is going into the plane of the paper while in (D) it is coming out of the plane of the paper.**

In 2 of the 4 cases where the quinoline moiety of TO was placed between the bases of $(dA)_{10}$, the dye remained close to the starting orientation. In one of these two cases, one of the bases flipped out of the helix, see Figure 3.36B, without affecting the stacking arrangement of the DNA strand. In 1 of the 2 remaining cases, each moiety of TO interacted with a base in the intercalation site and caused significant bending of the DNA (data not shown) as seen in previous examples (see Section 3.2.7.1). In the last case, the intercalated moiety shifted from the quinoline to the benzothiazole, as seen in Figure 3.36D.

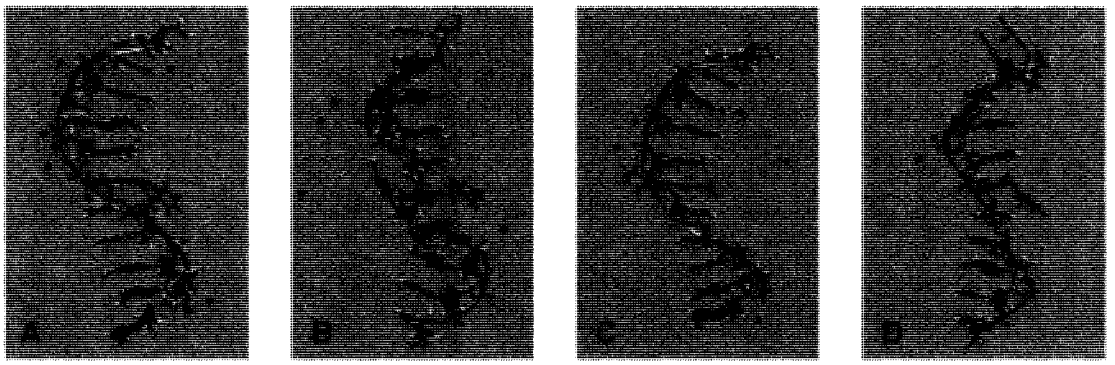


**Figure 3.36: Initial (A) conformation of TO/$(dA)_{10}$, and after 2 ns (B), showing the quinoline moiety intercalated and one base flipped out from the DNA helix. Initial (C) conformation of TO/$(dA)_{10}$, and after 2 ns (D), showing the benzothiazole moiety intercalated.**

In 2 of the 4 instances where the TO quinoline moiety was intercalated in $(dG)_{10}$, the dye remained close to the starting position but caused a slight elongation of the DNA strand, as seen in the example in Figure 3.37B. In the other 2 instances, both TO moieties moved into the intercalation site, as seen in the example in Figure 3.37D, and did not significantly alter the DNA structure.

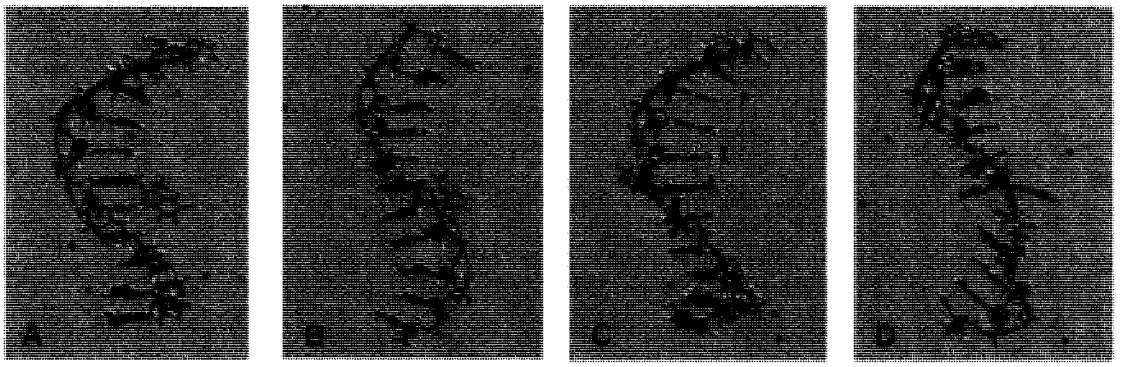


**Figure 3.37: Initial (A) conformation of TO/$(dG)_{10}$, and after 4 ns (B), showing the quinoline intercalated and the DNA strand elongated. Initial (C) conformation of TO/$(dG)_{10}$, and after 2 ns (D), showing both moieties interacting with G bases.**

In 7 of the 8 cases where the quinoline moiety of TO was intercalated between either A or G bases, the dye remained intercalated during the 2 ns simulation. Of these 7 cases, 4 resulted in a final orientation resembling the starting orientation. In 1 of these 7 cases there was a shift that intercalated the benzothiazole moiety. In the last 2 of these cases, both the quinoline and the benzothiazole moieties ended up between the bases without disrupting the structure of the DNA strand. Only in 1 case did the dye dissociate partially from the DNA, suggesting a relatively strong association between TO and the polypurine oligomers.

When the PTO quinoline moiety was placed between two bases in $(dC)_{10}$, the benzothiazole moiety interacted with one base in the intercalation site while the quinoline moiety interacted with the other, resulting in partial dissociation and twisting of the DNA strand, shown in Figure 3.38B. Near the beginning of the simulation involving PTO and $(dT)_{10}$, the dye dissociated but remained in the proximity of the DNA strand due to an interaction between the benzothiazole moiety and one base, which switched to an interaction between the quinoline moiety and that same base, see Figure 3.38D. Although intercalation of the PTO quinoline moiety is favourable for $(dA)_{10}$ and $(dG)_{10}$, it does not appear to be so for $(dC)_{10}$ and $(dT)_{10}$.

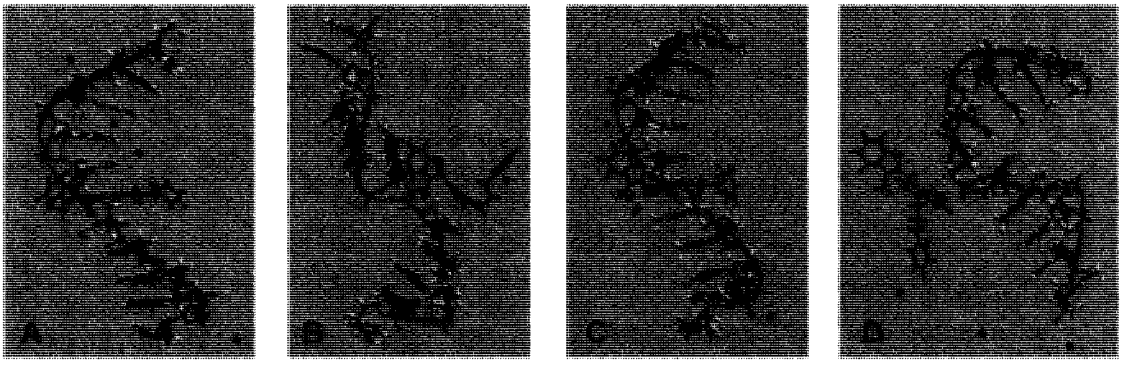

**Figure 3.38: Initial (A) conformation of PTO/$(dC)_{10}$, and after 2 ns (B), showing the dye partly dissociated. Initial (C) conformation of PTO/$(dT)_{10}$, and after 4 ns (D), showing the dye unintercalated but interacting with a base.**

When studying the intercalation of the quinoline moiety of TO in $(dC)_{10}$, some interesting observations were made in one particular case. Firstly, the dye remained close to the starting orientation for the first 1.5 ns. Then each moiety interacted with a base (an observation seen with other dye/DNA combinations), shown in Figure 3.39B. But between 2 and 3 ns, the dye dissociated completely. This indicates that, in general, when both moieties are interacting with the two bases in the intercalation site, the dye may dissociate if the simulation were run for a longer period of time. As each 2 ns simulation requires 10 days of CPU time, longer simulations were not possible for every orientation studied.

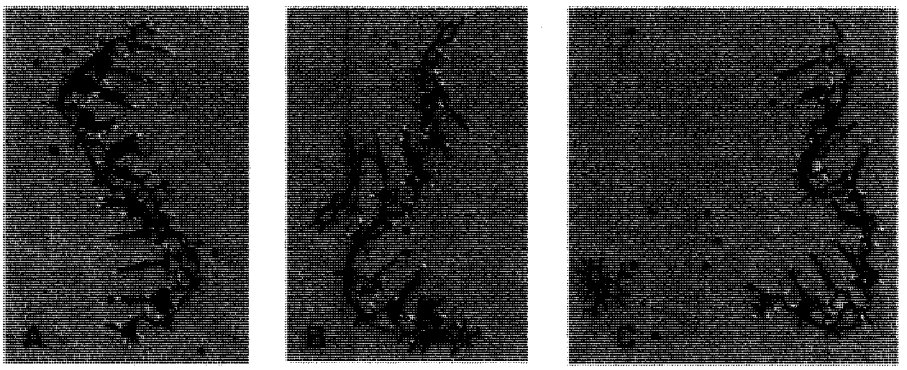


**Figure 3.39: Initial (A) conformation of TO/$(dC)_{10}$, and after 2 ns (B) showing both the benzothiazole and the quinoline moieties interacting with C bases, and after 3 ns (C) showing the dye completely dissociated from the DNA strand.**

In one of the cases involving the intercalation of the TO quinoline moiety into $(dC)_{10}$, the dye remained close to the starting orientation during the 2 ns simulation (data not shown). In another case, the dye partially dissociated and the quinoline and the benzothiazole moieties associated with the C bases, shown in Figure 3.40B. In the last case, the dye spent almost all of the 4 ns simulation with both moieties interacting with the two C bases, but at the very end switched to having the benzothiazole moiety intercalated, as seen in Figure 3.40D. This demonstrates that not all partially dissociated dye/DNA complexes will result in complete dissociation.


**Figure 3.40: Initial (A) conformation of TO/$(dC)_{10}$, and after 4 ns (B) showing both the benzothiazole and the quinoline moieties interacting with C bases. Initial (C) conformation of TO/$(dC)_{10}$, and after 4 ns (D) showing the benzothiazole moiety between C bases.**

In the first simulation involving the intercalation of the TO quinoline moiety in $(dT)_{10}$, the dye remained close to the starting orientation (data not shown). In the second simulation, there was an almost immediate shift, leaving the benzothiazole moiety intercalated (data not shown). In the third case, there was also a shift which resulted in the benzothiazole moiety being intercalated, but in addition one of the bases in the intercalation site flipped out of the DNA helix so that the benzothiazole moiety interacted with three bases while the quinoline moiety interacted with a fourth base in the DNA strand, as seen in Figure 3.41B. In the last case, during the majority of the 4 ns simulation both moieties interacted with T bases, and at the very end of the simulation it was mostly just the quinoline moiety interacting with one T base, shown in Figure 3.41D. If this simulation were run longer it might lead to complete dissociation of the dye.

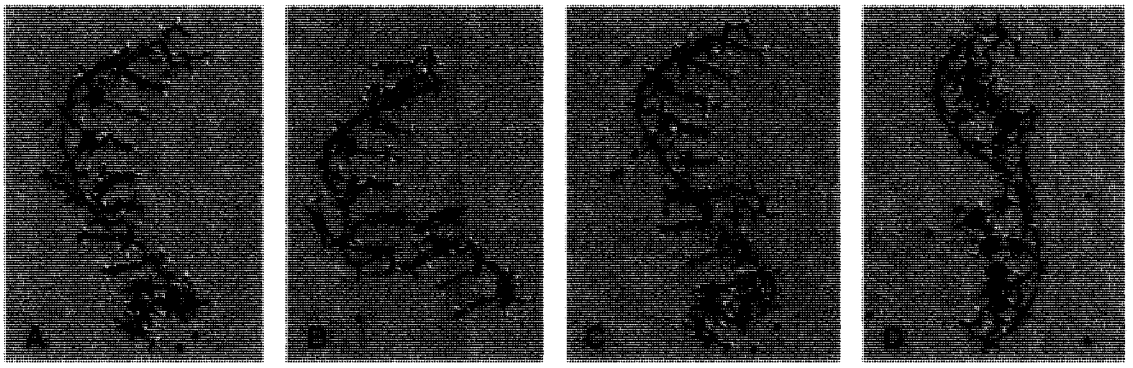


**Figure 3.41: Initial (A) conformation of TO/$(dT)_{10}$, and after 6 ns (B) showing both the benzothiazole and the quinoline moieties interacting with T bases. Initial (C) conformation of TO/$(dT)_{10}$, and after 4 ns (D) showing the quinoline moiety interacting with T bases.**

When the quinoline moiety of TO was inserted between the bases of either $(dC)_{10}$ or $(dT)_{10}$, in 3 of the 8 cases the dye dissociated, either completely or partially. In the remaining cases, 2 remained close to the starting orientation while 3 exhibited a shift that placed the benzothiazole moiety between the bases. Like

PTO, these results indicate a weaker association for TO with the polypyrimidine oligomers than with the polypurine oligomers.

### 3.2.7.3. Intercalation of Both the Benzothiazole and Quinoline Moieties

In an attempt to gather more information regarding the preferred moiety for intercalation, simulations were run where both the benzothiazole and the quinoline moieties were placed between the bases of the various DNA oligomers. These simulations were only done with PTO, and there were two different modes of insertion, illustrated in Figure 3.42.

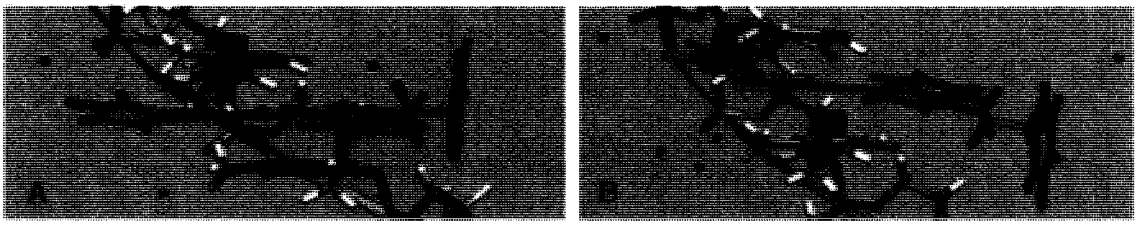


**Figure 3.42: Illustration of the modes of insertion of both the PTO benzothiazole and quinoline moieties between the two central bases of DNA oligomers, shown here for $(dT)_{10}$. (A) Benzothiazole moiety is near the DNA backbone and the benzothiazole $CH_3$ is coming out of the plane of the paper.**
**(B) Benzothiazole moiety is near the DNA backbone and the benzothiazole $CH_3$ is going into the plane of the paper.**

In the first of the two cases involving PTO and $(dA)_{10}$, initially both the benzothiazole and quinoline moieties interacted with the bases in the intercalation site, but during the 4 ns simulation there was a shift that resulted in quinoline intercalation, as seen in Figure 3.43B. In the second case, there was a shift to intercalate the quinoline moiety and the dye stayed in this position for most of the 2 ns simulation but at the very end it shifted again so that both the quinoline and the benzothiazole moieties were interacting with the bases in the intercalation site. During the next 2 ns, both moieties associated with the two bases, partially dissociating and causing a large degree of twisting of the DNA strand, shown in Figure 3.43D.

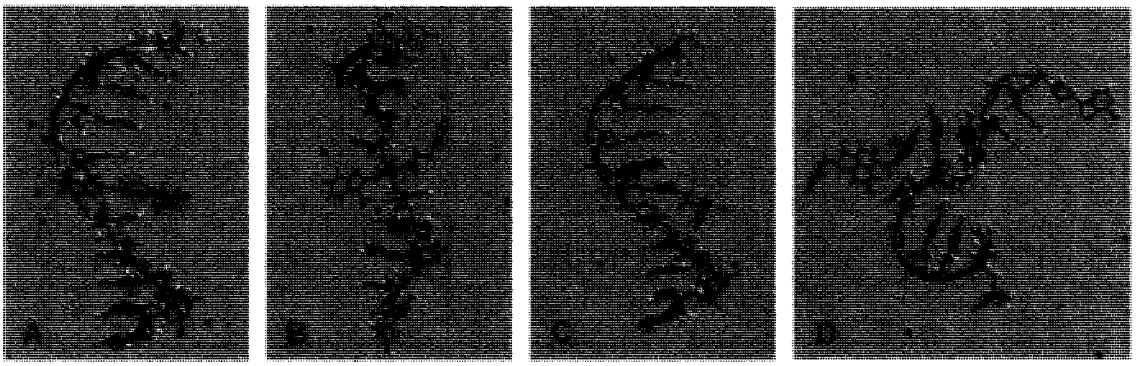

**Figure 3.43: Initial (A) conformation of PTO/$(dA)_{10}$, and after 4 ns (B) showing the quinoline moiety intercalated. Initial (C) conformation of PTO/$(dA)_{10}$, and after 4 ns (D) showing the dye partly dissociated.**

In both cases involving PTO and $(dG)_{10}$, there was a shift from having both the benzothiazole and the quinoline moieties between the bases to only the quinoline moiety being intercalated, shown in Figure 3.44B.

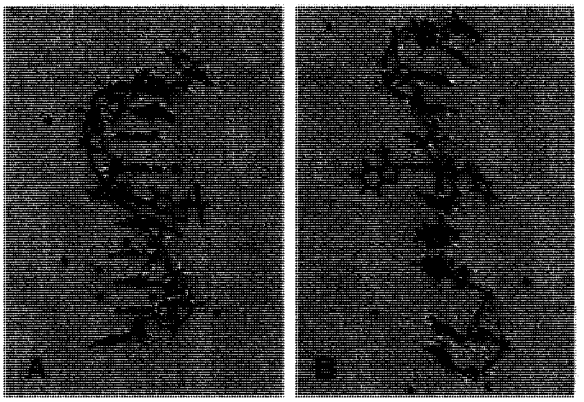


**Figure 3.44: Initial (A) conformation of PTO/$(dG)_{10}$, and after 2 ns (B) showing the quinoline moiety intercalated.**

In 3 of the 4 cases involving the intercalation of the PTO benzothiazole and quinoline moieties in $(dA)_{10}$ and $(dG)_{10}$, there was a shift that placed the quinoline moiety between the bases. These findings suggest that intercalation of the quinoline moiety is preferred. In the fourth case the dye was partly dissociated.

When both the benzothiazole and the quinoline moieties of PTO were placed between the bases of $(dC)_{10}$, in both cases both moieties initially stayed in place. In the first case, this interaction continued, causing a bending of the DNA strand and partial dissociation of the dye, as seen in Figure 3.45B. In the second case, one base flipped out of the helix so that it was perpendicular to the other bases, and the benzothiazole moiety moved into the intercalation site, shown in Figure 3.45D.

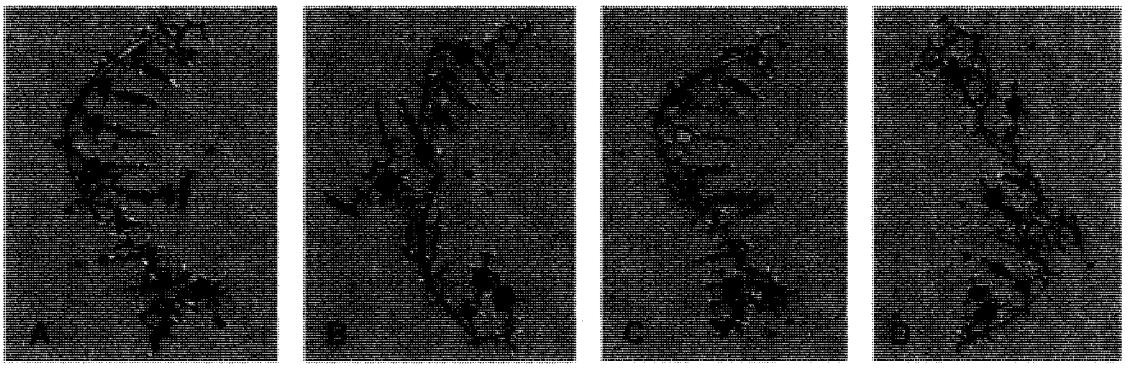


**Figure 3.45: Initial (A) conformation of PTO/$(dC)_{10}$, and after 4 ns (B) showing the dye partly dissociated. Initial (C) conformation of PTO/$(dC)_{10}$, and after 4 ns (D) showing the benzothiazole moiety intercalated and one base flipped out of the helix.**

In the first case where both the benzothiazole and the quinoline moieties were placed between the bases of $(dT)_{10}$, the dye maintained this interaction during the 4 ns simulation, resulting in partial dissociation and bending of the DNA strand, shown in Figure 3.46B. In the second case, there was an almost immediate shift to place the quinoline moiety between the bases and this arrangement persisted during the first 2 ns of the simulation. Between 2 and 6 ns, there was a shift that placed the benzothiazole moiety between the T bases, and eventually both the benzothiazole and the quinoline moieties interacted with the bases, resulting in bending of the DNA strand, as seen in Figure 3.46D.

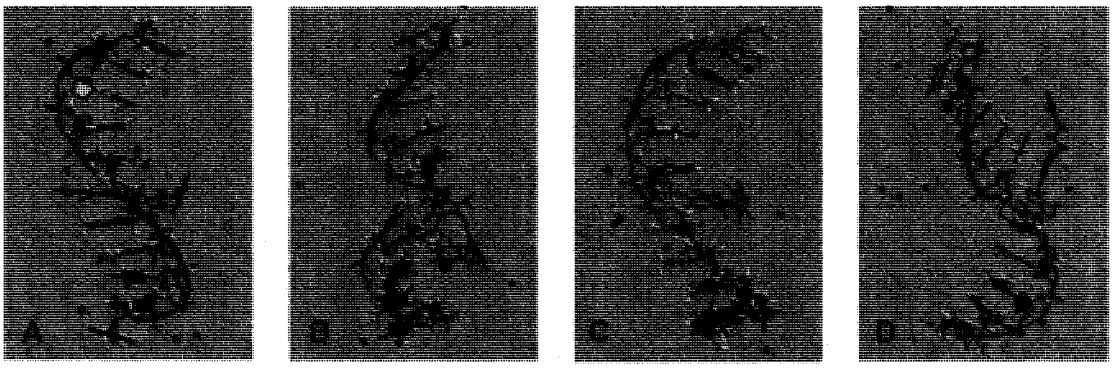

**Figure 3.46: Initial (A) conformation of PTO/$(dT)_{10}$, and after 4 ns (B) showing the dye partly dissociated. Initial (C) conformation of PTO/$(dT)_{10}$, and after 6 ns (D) showing the dye partly dissociated.**

When inserting both the benzothiazole and the quinoline moieties of PTO between the bases of either $(dC)_{10}$ or $(dT)_{10}$, in 3 of the 4 situations examined the dye dissociated partly, presumably held near the DNA strand by $\pi$-stacking interactions. In the other case, the benzothiazole moiety shifted into the intercalation site. These results are consistent with the other computational findings, which indicated a weak and loose association of the dye with $(dC)_{10}$ and $(dT)_{10}$.

### 3.2.7.4. Intercalation via the Pyridinium Moiety of PTO

The pyridinium moiety of PTO has the most flexibility due to the alkyl chain that connects it to the rest of the molecule. As such, we hypothesized that inserting this moiety would most likely lead to the dye dissociating from the DNA strand. In addition, it is known that intercalation is the preferred mode of binding for flat polyaromatic ligands with large enough surface areas and the appropriate sterics; the criteria for intercalation is a minimum of two fused ring systems,[36] which the pyridinium moiety does not fulfill. Nevertheless, the pyridinium moiety was intercalated in two different fashions for the simulations, as shown in Figure 3.47, to investigate whether this mode of insertion would lead to dissociation.

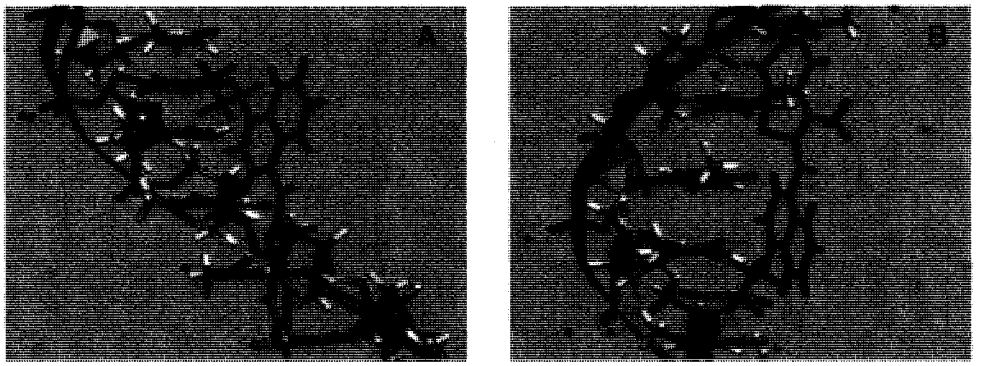


**Figure 3.47: Illustration of the modes of insertion of the PTO pyridinium moiety between the two central bases of DNA oligomers, shown here for $(dT)_{10}$.**
**(A) Benzothiazole moiety is closer to the 3'-T than the 5'-T.**
**(B) Benzothiazole moiety is closer to the 5'-T than the 3'-T.**

In the first instance where the PTO pyridinium moiety was intercalated into $(dA)_{10}$, the dye dissociated approximately 1 ns into the simulation but stayed in the proximity of the DNA strand (shown in Figure 3.48B), presumably due to electrostatic associations. In the second instance, the bases in the intercalation site opened up and both the pyridinium and the quinoline moieties each interacted with a base for the duration of the 4 ns simulation. This $\pi$-stacking interaction caused an elongation of the DNA strand and disruption of its helicity, seen in Figure 3.48D.

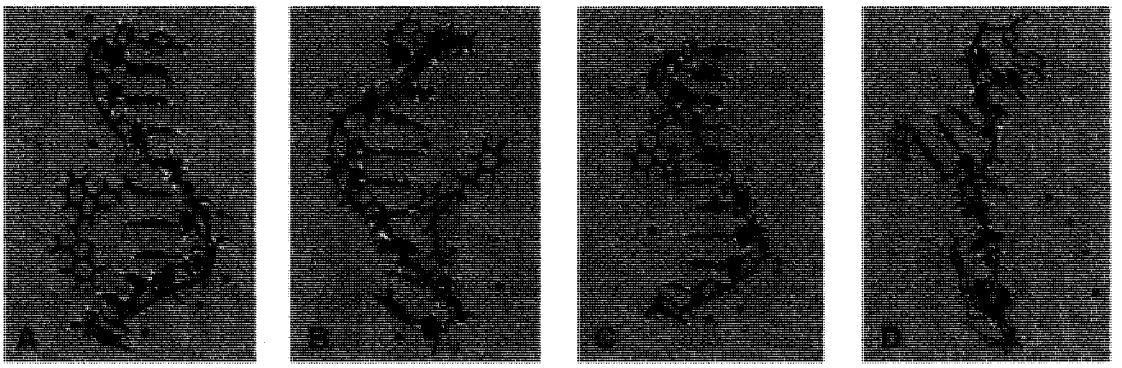


**Figure 3.48: Initial (A) conformation of PTO/$(dA)_{10}$, and after 2 ns (B) showing the dye dissociated. Initial (C) conformation of PTO/$(dA)_{10}$, and after 4 ns (D) showing both the pyridinium and the quinoline moieties interacting with A bases.**

In the first case where the PTO pyridinium moiety was inserted between the central bases of $(dG)_{10}$, there was a shift, which placed the quinoline moiety between the two bases. There was a subsequent interaction between the benzothiazole moiety and one of the bases, resulting in both the benzothiazole and the quinoline moieties interacting with the two bases and disruption of the DNA structure, shown in Figure 3.49B. In the second case, similar shifts occurred although the final orientation placed the benzothiazole moiety between the bases, as seen in Figure 3.49D.

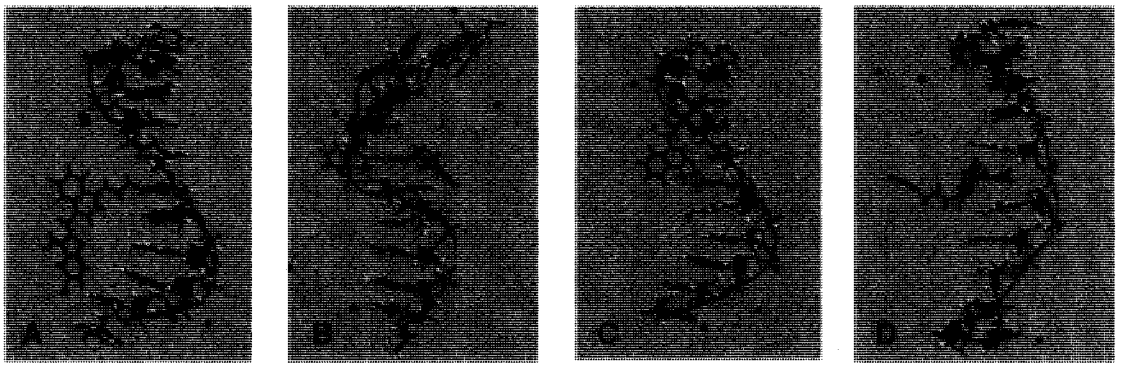


**Figure 3.49: Initial (A) conformation of PTO/$(dG)_{10}$, and after 4 ns (B) showing both the benzothiazole and the quinoline moieties interacting with G bases. Initial (C) conformation of PTO/$(dG)_{10}$, and after 4 ns (D) showing the benzothiazole moiety intercalated.**

In both instances where the pyridinium moiety of PTO was intercalated in $(dC)_{10}$, the bases in the intercalation site opened up and there were shifts that eventually left both the benzothiazole and the quinoline moieties interacting with C bases, shown in Figure 3.50B and Figure 3.50D. Presumably this orientation would lead to dissociation if it were not for $\pi$-stacking effects.

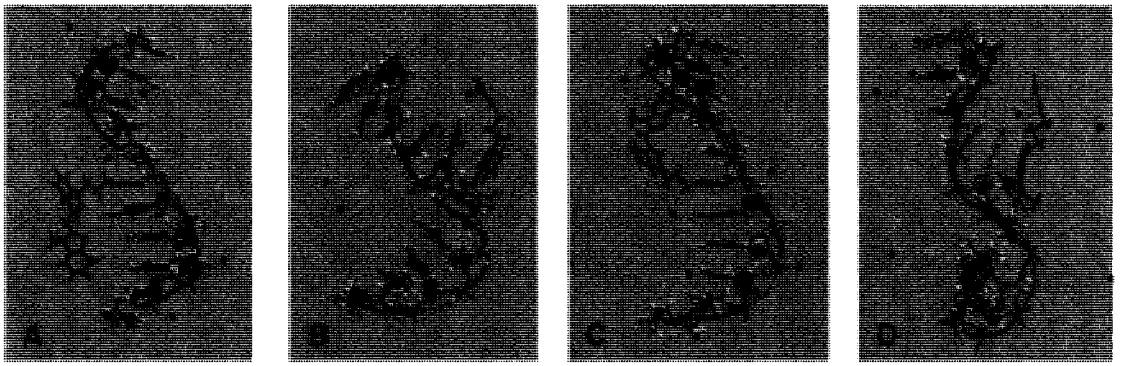

**Figure 3.50: Initial (A) conformation of PTO/$(dC)_{10}$, and after 4 ns (B) showing the dye partly dissociated. Initial (C) conformation of PTO/$(dC)_{10}$, and after 4 ns (D) showing the dye partly dissociated.**

When the pyridinium moiety of PTO was intercalated in $(dT)_{10}$, in the first case the dye almost immediately dissociated from the DNA but stayed in its proximity, presumably due to electrostatic interactions, and after 2 ns the dye interacted with the 5'-T and this π-stacking association lasted for 2 ns, shown in Figure 3.51B. In the second case, the dye dissociated from the DNA strand after approximately 1 ns, but stayed in its proximity due to a π-stacking interaction with one T base, shown in Figure 3.51D.

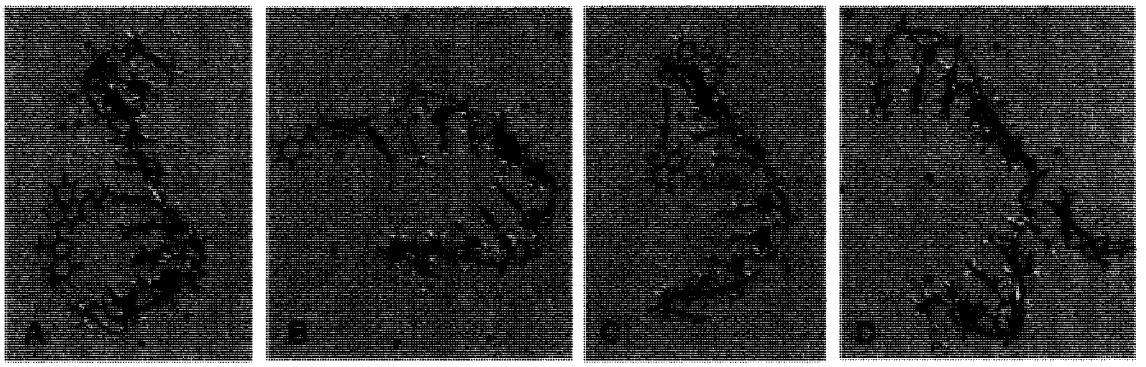

**Figure 3.51: Initial (A) conformation of PTO/$(dT)_{10}$, and after 4 ns (B) showing the dye dissociated but interacting with the 5'-T. Initial (C) conformation of PTO/$(dT)_{10}$, and after 4 ns (D) showing the dye dissociated but still interacting with a base.**

The PTO pyridinium moiety consists of only one aromatic ring and has significant flexibility, thus it seems unlikely that this moiety would become intercalated. As anticipated, insertion of the pyridinium moiety into various DNA oligomers resulted in dissociation or partial dissociation in all of the orientations modeled. However, there was one exception where the dye remained intercalated, but the intercalated moiety was not the pyridinium, it was the benzothiazole.

### 3.2.7.5. Computational Studies Involving the PTO Structure that is Second Lowest in Energy

Only a few calculations were performed using the PTO structure that is second lowest in energy. Its mode of insertion between the DNA bases is shown in Figure 3.52.

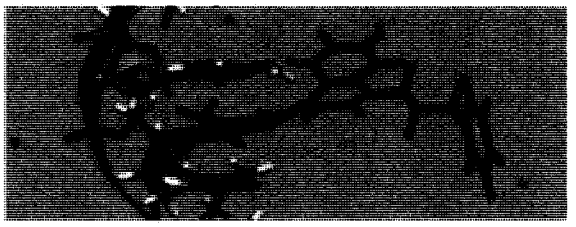

**Figure 3.52: Illustration of the mode of insertion of the PTO benzothiazole moiety between the two central bases of DNA oligomers, shown here for $(dC)_{10}$. The PTO structure is the second lowest in energy.**

When the PTO structure that was second lowest in energy was intercalated in $(dA)_{10}$, there was a shift, which placed the quinoline moiety between the bases. The quinoline moeity interacted primarily with the base above it, causing the DNA strand to bend, as shown in Figure 3.53B. Intercalation of PTO in $(dG)_{10}$ caused the DNA to become very bent and the benzothiazole and quinoline moieties interacted with 2 of the central G bases, as seen in Figure 3.53D.

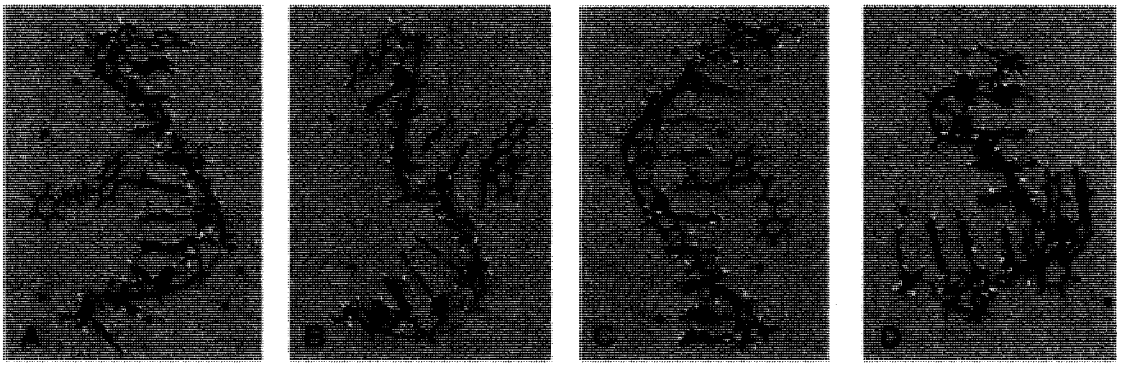

**Figure 3.53: Initial (A) conformation of PTO/$(dA)_{10}$, and after 2 ns (B) showing the dye partially dissociated. Initial (C) conformation of PTO/$(dG)_{10}$, and after 4 ns (D) showing the dye partly dissociated and interacting with G bases.**

When the PTO benzothiazole moiety was placed between the bases of $(dC)_{10}$, the pyridinium moiety wiggled around for the first 3 ns and then the dye dissociated but remained in the proximity of the DNA strand, as seen in Figure 3.54B. During the simulation involving PTO and $(dT)_{10}$, the benzothiazole moiety remained in its original insertion position (between bases 4 and 5) and the pyridinium moiety interacted with the sixth base in the strand, bending the DNA, as seen in Figure 3.54D. This orientation might lead to dissociation of the dye if the simulation were run for a longer period of time.

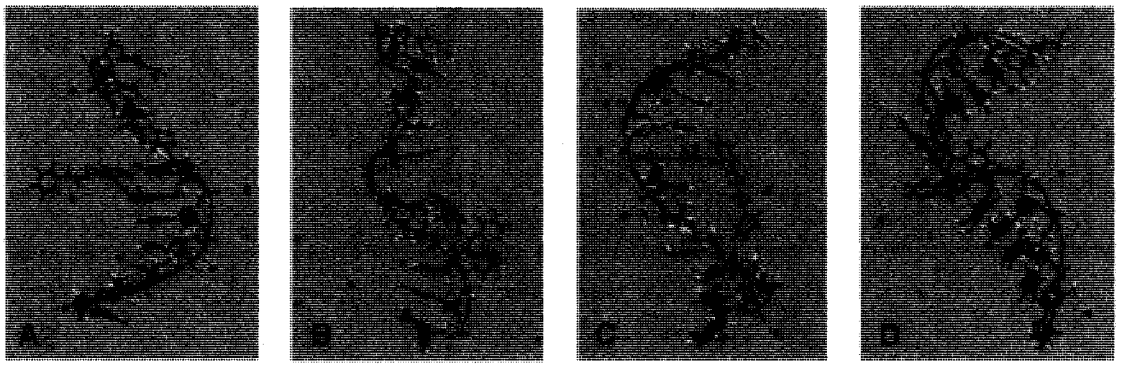

**Figure 3.54: Initial (A) conformation of PTO/$(dC)_{10}$, and after 4 ns (B) showing the dye dissociated. Initial (C) conformation of PTO/$(dT)_{10}$, and after 2 ns (D) showing the benzothiazole moiety between two T bases and the pyridinium moiety interacting with another base.**

The modeling of the second most stable PTO structure and the DNA oligomers was too superficial to draw any conclusions, however it appears that it does not follow the same trends as the most stable structure. In all 4 cases studied, there appeared to be weak interactions (or dissociation) between the dye and the DNA strands. These results suggest that the second most stable PTO structure does not intercalate in DNA, although further studies would be required before making any conclusions.

## 3.3. Discussion

### 3.3.1. Experimental Studies

When PTO was added to single-stranded DNA homopolymers, the only homopolymer that caused a significant shift (towards the red) in the monomer absorption band was poly(dA), suggesting a more delocalized structure due to a stronger interaction. However, the PTO/poly(dG) solution showed a decrease in extinction coefficient, indicative of intercalation. In general, intercalation of a dye between the DNA base pairs results in a shift of the absorption maximum towards longer wavelengths and an accompanying decrease in extinction coefficient, although exceptions exist.[37] These results suggest that PTO intercalates in poly(dA) and poly(dG).

It was anticipated that intercalation would lead to increased dye fluorescence due to hindered rotation around the central methine bond, as has been proposed for oxazole yellow bound to DNA.[26] The intense steady-state and time-resolved fluorescence exhibited by PTO in the presence of poly(dA) and poly(dG) support dye intercalation.

Poly(dA) appears to be the only homopolymer upon which PTO affects secondary structure, as evidenced by changes in its circular dichroism spectrum, once again indicating dye intercalation. However, strong induced circular dichroism of the dye was observed in the presence of poly(dG) in addition to poly(dA), suggesting a strong interaction with both of the single strands.

All of the above-mentioned observations concerning PTO and the polypurines indicate a strong dye-DNA association, specifically intercalation.

Addition of poly(dC) and poly(dT) to PTO enhanced the short wavelength absorption band, indicating aggregation. However, if the polypyrimidines were associating with dye aggregates, other results (*vide infra*) indicated that such complexes were not fluorescent.

The lack of a strong fluorescence signal for PTO and poly(dC) or poly(dT) suggested that the dye was not intercalated, and could expend its excitation energy

non-radiatively. The weak time-resolved fluorescence signals, dominated by a component with a relatively short lifetime (*ca.* 0.3 ns), suggest a very weak and loose association between PTO and the polypyrimidines.

At low concentrations (3.5 μM PTO / 35 μM DNA), the dye did not undergo induced CD in the presence of the polypyrimidines. At higher concentrations (20 μM PTO / 200 μM DNA), the dye displayed weak ICD, most likely from dye aggregates associated with the homopolymers.

The above-mentioned experimental results indicate a weak and loose association between PTO and the polypyrimidines.

Comparison of the findings on the association of PTO and TO with DNA homopolymers, in addition to the conclusions drawn from the published results of Nygren *et al.*[5] on the binding of TO to DNA, indicate that the two dyes behave very similarly: monomer association with poly(dA), at least two binding modes with poly(dG), and dimeric/aggregate association with poly(dC) and poly(dT). As these two dyes differ only in the substituent on the quinoline ring, the results demonstrate the unimportance of the pyridinium moiety in the association process.

The trends observed for PTO and TO do not follow those observed for PG. Although the general structure of PG is similar to that of TO and PTO, the fact that PG associates strongly with poly(dG) and poly(dT) but not poly(dA) and poly(dC) indicates that its substituents play a significant role in its binding specificity, which differs from that of TO and PTO which both bind strongly to poly(dA) and poly(dG) but weakly to poly(dC) and poly(dT).

Of the three RNA homopolymers studied, complexes involving PTO and poly(rC) and poly(rA) showed the same CD and ICD characteristics as the corresponding dye/DNA complexes. On the other hand, PTO/poly(rU) behaved differently from PTO/poly(dT), showing a strong association between dye aggregates and the polyribonucleotide, most likely due to the methyl group present on thymine but not on uracil.

### 3.3.2. Computational Studies

The results of all of the molecular dynamics simulations involving the DNA oligomers and the most stable structures of PTO and TO are summarized in Table 3.3.

**Table 3.3: Summary of computational results involving DNA oligomers and the most stable structures of PTO and TO.**

| **Initial intercalated moiety:** | **$(dA)_{10}$** |
|---|---|
| PTO benzothiazole (Figure 3.21) | Dye remained intercalated in all 4 cases (intercalated moiety was the benzothiazole in 2 cases and the quinoline in 2 cases). |
| PTO quinoline (Figure 3.33) | In the 1 case, dye remained close to the starting orientation. |
| PTO benzothiazole and quinoline (Figure 3.43) | In 1 case, shifted to intercalate the quinoline moiety.<br>In 1 case, dye partly dissociated. |
| PTO pyridinium (Figure 3.48) | In 1 case, dye dissociated.<br>In 1 case, dye partly dissociated. |
| TO benzothiazole (Figure 3.25) | In 3 cases, dye partly dissociated.<br>In 1 case, dye remained intercalated (both moieties were in the intercalation site with one base flipped out of the helix). |
| TO quinoline (Figure 3.36) | In 3 cases, dye remained intercalated (intercalated moiety was the benzothiazole in 1 case and the quinoline in 2 cases).<br>In 1 case, dye partly dissociated. |
| | **$(dG)_{10}$** |
| PTO benzothiazole (Figure 3.22) | Dye remained intercalated in all 4 cases (intercalated moiety was the benzothiazole in 2 cases and the quinoline in 2 cases). |
| PTO quinoline (Figure 3.34) | In 1 case, accidentally started out with benzothiazole moiety intercalated and shifted so that the quinoline moiety was intercalated. When quinoline was properly inserted, dye remained close to the starting orientation. |
| PTO benzothiazole and quinoline (Figure 3.44) | In both cases, shifted to intercalate the quinoline moiety. |

| **Initial intercalated moiety:** | **$(dG)_{10}$ (continued)** |
|---|---|
| PTO pyridinium (Figure 3.49) | In 1 case, dye partly dissociated.<br>In 1 case, shifted to intercalate the benzothiazole moiety. |
| TO benzothiazole (Figure 3.26) | In 2 cases, dye remained close to the starting orientation.<br>In 1 case, dye partly dissociated.<br>In 1 case, dye remained intercalated (both moieties were in the intercalation site but DNA maintained its structure). |
| TO quinoline (Figure 3.37) | In all 4 cases, dye remained intercalated (intercalated moiety was the quinoline in 2 cases, and both moieties in 2 cases where the DNA maintained its structure). |
| **Initial intercalated moiety:** | **$(dC)_{10}$** |
| PTO benzothiazole (Figure 3.27) | In 2 cases, dye dissociated.<br>In 1 case, dye partly dissociated.<br>In 1 case, dye remained close to the starting orientation. |
| PTO quinoline (Figure 3.38) | In the 1 case, dye partly dissociated. |
| PTO benzothiazole and quinoline (Figure 3.45) | In 1 case, dye partly dissociated.<br>In 1 case, dye remained intercalated (benzothiazole moiety was in the intercalation site with one base flipped out of the helix). |
| PTO pyridinium (Figure 3.50) | In both cases, dye partly dissociated. |
| TO benzothiazole (Figure 3.30) | In 1 case, dye dissociated.<br>In 2 cases, dye partly dissociated.<br>In 1 case, quinoline intercalated with one base flipped out of the helix. |
| TO quinoline (Figure 3.39 and Figure 3.40) | In 1 case, dye dissociated.<br>In 1 case, dye partly dissociated.<br>In 2 cases, dye remained intercalated (intercalated moiety was the benzothiazole in 1 case and the quinoline in the other). |

| **Initial intercalated moiety:** | **$(dT)_{10}$** |
|---|---|
| PTO benzothiazole (Figure 3.29) | In 2 cases, dye dissociated.<br>In 1 case, dye partly dissociated.<br>In 1 case, dye remained close to the starting orientation. |
| PTO quinoline (Figure 3.38) | In the 1 case, dye dissociated. |
| PTO benzothiazole and quinoline (Figure 3.46) | In 2 cases, dye partly dissociated. |
| PTO pyridinium (Figure 3.51) | In both cases, dye dissociated. |
| TO benzothiazole (Figure 3.31) | In 2 cases, dye partly dissociated.<br>In 2 cases, dye remained close to the starting orientation. |
| TO quinoline (Figure 3.41) | In 1 case, dye partly dissociated.<br>In 3 cases, dye remained intercalated (intercalated moiety was the benzothiazole in 2 cases and the quinoline in the other). |

In this discussion the insertion of the PTO pyridinium moiety was disregarded as it is expected to dissociate. In 14 of the 15 cases, PTO remained intercalated in $(dA)_{10}$ and $(dG)_{10}$, consistent with the experimental spectral results. When the benzothiazole moiety was intercalated, or both the benzothiazole and quinoline moieties were intercalated, there was a tendency of the dye to shift, resulting in preferential intercalation of the quinoline moiety. However, when the quinoline moiety was positioned between the bases of $(dA)_{10}$ or $(dG)_{10}$, no shift was observed. These results suggest that intercalation of the quinoline moiety is preferred. Eleven of the 16 simulations involving TO and $(dA)_{10}$ and $(dG)_{10}$ oligomers show a strong association between the dye and the DNA strand, although there did not appear to be a preference for intercalation of a specific moiety.

Others have experimentally demonstrated that intercalating molecules stretch (by the spacing of one base pair) and significantly unwind the DNA double helix.[37] In this work, elongation and unwinding of the single-stranded helix was seen

in many of the simulations where the dye remained intercalated, demonstrating the ability of the AMBER 8 software to replicate true dye-DNA interactions.

In many of the simulations involving dye intercalation in $(dC)_{10}$ or $(dT)_{10}$, the dye dissociated, either completely or partially, during the 2 ns simulation. This occurred in 11 of the 14 PTO cases and in 8 of the 16 TO cases. These findings suggest that both PTO and TO do not associate as strongly to $(dC)_{10}$ or $(dT)_{10}$ as they do to $(dA)_{10}$ or $(dG)_{10}$, which is consistent with the experimental spectral results. In the cases where the dyes remained intercalated, they showed no preference for having a specific moiety between the bases.

Spielmann *et al.* used NOE-derived distance restraints in restrained molecular dynamics calculations and found that TOTO bis-intercalates in the CTAG•CTAG site of $d(5'\text{-CGCTAGCG-}3')_2$ with the benzothiazole moiety between the pyrimidines and the quinoline moiety between the purines.[32] Although PTO did show the tendency to place the quinoline ring between the bases of $(dA)_{10}$ and $(dG)_{10}$, TO did not. In the few instances where PTO and TO remained intercalated in $(dC)_{10}$ and $(dT)_{10}$, neither dye showed a preference for having the benzothiazole moiety between the bases.

## 3.4. Conclusions

The results of the molecular dynamics simulations agree remarkably well with the experimental results. Analysis of the data suggests highly specific binding in the cases of PTO and TO to poly(dG) and poly(dA), consistent with the strong fluorescence and ICD signals observed. Further, in the case of PTO/poly(dA), the strong association suggested by the computational results is further supported by the single exponential fit to the fluorescence decay, by the rather simple Cotton effects observed by ICD, and by the fact that poly(dA) is the only homopolymer that causes a significant shift of the monomer dye absorption spectrum. Similar strong association is indicated by calculations with PTO and poly(dG) (Figure 3.23), although in this case both the ICD and fluorescence lifetime data indicate that more than one form of association may be involved. The preference for association involving the quinoline ring is also consistent with the limited restriction of the rotation around the methine bond. Nygren *et al.*[5] found that TO binds with high affinity as a monomer with poly(dA) and with calf thymus ssDNA in an intercalation complex, and shows a high fluorescence quantum yield. However, they found that TO binds as a monomer as well as a dimer to poly(dG) and that both species are fluorescent. Comparison of ICD spectra indicate that TO and PTO bind to poly(dA) very similarly, and that both TO and PTO associate with poly(dG) via more than one mode of binding but the orientations of the bound chromophores differ. Thus it is likely that the TO-derivative PTO behaves similarly to TO, leading to strongly fluorescent poly(dG) and poly(dA) complexes.

It is interesting that PTO in both poly(dC) and poly(dT) shows virtually no emission and weak ICD, but the absorbance indicates that the homopolymers promote dye aggregation. This may be due to the homopolymers stabilizing the aggregates themselves (or dimers) or providing a nucleation centre for dye aggregation. Nygren *et al.* found that TO associates with poly(dC) and poly(dT) as a virtually non-fluorescent dimer,[5] consistent with the behaviour of PTO with these

homopolymers. If the PTO aggregates associate with the DNA, clearly they lead to little changes in the homopolymer helix, as suggested by the CD data of Figure 3.9.

The fact that poly(dG) and poly(dA) show selective association suggests that π-interactions (rather than only hydrophobic effects) play a dominant role. This is consistent with the calculations that show π-stacking with relatively minor helical distortions; note that only PTO in poly(dA) causes some changes in the CD signals in the DNA region (Figure 3.9). Further, the final structures seem to indicate a hindered, but not frozen, rotation of the benzothiazole ring around the bond joining it to the quinoline ring.

In conclusion, the calculations, in combination with the spectroscopic data, provide a unique understanding of the interactions between a cyanine dye and DNA homopolymers. Such information can contribute to the design of new dyes that are more effective in binding to a specific base or sequence of bases. This research could play a role in the development of dye-based methodologies to detect/monitor DNA damage.[2]

## 3.5. Materials and Methods

### 3.5.1. Materials

The Tris buffer solutions were prepared in 18 MΩ water (Millipore Corporation) with Trizma Pre-Set Crystals (reagent grade, pH 7.4) and $Na_2EDTA$ (Sigma Grade) from Sigma-Aldrich, and NaCl (optical grade) from Alfa Aesar. PTO is commercially available from Dr. Todor Deligeorgiev at the University of Sofia, Bulgaria. Thiazole orange tosylate (for fluorescence, ≥98.0% by HPLC) was purchased from Fluka, PicoGreen dsDNA quantitation reagent was from Invitrogen, and DMSO (HPLC grade) was obtained from OmniSolv. Poly(dA), poly(dT), and poly(dC) were obtained from Midland Certified Reagent Company, and poly(dG) was purchased from BioCorp. For poly(dA) most of the material had between 125 and 350 bases; poly(dT) was longer, with most of the material between 900 and 1200 bases. The size of poly(dC) was not available, and poly(dG) was 40 bases in length. Quartz Suprasil cuvettes (Hellma or Luzchem Research Inc.) with a 10 mm optical path were employed in all the experiments.

### 3.5.2. Solution Preparation

A stock buffer solution of pH 7.4 was prepared containing 0.01 M Tris, 0.001 M EDTA, and 0.1 M NaCl. All DNA concentrations were determined by absorption spectroscopy using the following 260 nm extinction coefficients: 15 100 $M^{-1}cm^{-1}$ for poly(dA), 11 700 $M^{-1}cm^{-1}$ for poly(dG), 8 700 $M^{-1}cm^{-1}$ for poly(dT) and 7 400 $M^{-1}cm^{-1}$ for poly(dC). The concentrations of the dye stock solutions were determined by measuring the absorption of a diluted dye solution (a concentration where no aggregation occurs) and using the extinction coefficient of 73 900 $M^{-1}cm^{-1}$ for PTO (510.5 nm),[21] and 63 000 $M^{-1}cm^{-1}$ for TO (500 nm).[5] The PG concentration was estimated using the reported extinction coefficient of 70 000 $M^{-1}cm^{-1}$.[38] The PTO and DNA stock solutions were prepared in buffer and subsequently diluted in buffer when the dye:DNA solutions were prepared. The DNA stock solutions were shaken for 1 h (to ensure dissolution of the DNA) and allowed to fully dissolve

overnight before use, and stored at -4°C, or at -20°C for long-term storage. The dyes, as received from the suppliers, were kept at -20°C. A stock solution of TO was made by dissolving the dye in DMSO and then adding buffer to produce a 1:30 DMSO:buffer solution which was subsequently diluted in buffer when the dye:DNA solutions were prepared. Diluting the stock solution and calculating the extinction coefficients with the assumption that no aggregation had occurred constituted the "nominal" extinction coefficient determination used in Figure 3.1 (*vide infra*). The dye:DNA base ratio is defined as the number of chromophores per base. A 1:10 dye:DNA base ratio was used to ensure that the dominant binding mode would be that of intercalation. Dye/DNA concentrations in the final PTO mixtures were (20/200) μM, except when looking at the CD signal in the DNA region where the dye/DNA concentrations were (3.5/35) μM. In order to record both the CD and ICD of the same solution, dye/DNA concentrations of (7/70) μM were used for TO and PG. For each experiment, freshly prepared solutions using the stocks were made. Experiments were carried out at room temperature, except for the CD work where the temperature was kept fixed at 20°C.

### 3.5.3. Instrumentation

Absorption spectra were recorded using a Varian Cary-50 with a scan rate of 600 nm/min. Steady-state fluorescence spectroscopy was carried out using a Photon Technology International luminescence spectrometer operated in the CW mode. Fluorescence emission spectra were recorded upon 355 nm excitation using a 1 s integration time and 1 nm integration step. The excitation slits were either 1 or 1.5 nm while the emission slits were 4 nm. When determining the binding constants, equal volumes of ssDNA and 9 μM PTO were added to the 4.5 μM dye solution.

Time-resolved studies were made with the third harmonic of a Continuum PY-61 Nd:YAG laser ($\lambda$= 355 nm, fwhm = 35 ps, pulse energy $\leq$ 4 mJ), using a Hamamatsu C4334 streak camera and Hamamatsu Photoluminescence Measurement Software U4790 version 2.2 for luminescence detection.

Circular dichroism experiments were performed on a Jasco J-810 spectrometer with a 150 W Xenon lamp. The instrumental parameters were a 0.1 nm data pitch, continuous scanning mode, 50 nm/min scan speed, 4 s response, and 1 nm bandwidth. The buffer solution spectrum was used as a blank, which was subtracted from the CD signals.

### 3.5.4. Computational Details

The two *E-Z* isomers of PTO and TO each have two conformations, which were fully optimized by the B3LYP/6-31G* hybrid density functional method, with the Gaussian 03[39] series of the program. Only the geometry of the most stable (and second most stable for PTO) conformation (*vide infra*) was used to generate the appropriate input for the MD simulations.

The molecular dynamics calculations were carried out with the AMBER 8 package[40] using the parm99 force field[41] for the ssDNA fragments and a General Amber Force Field[42] parameterized by fitting HF/6-31G* atom-centered point charges for PTO and TO. During the modeling, the nonbonding interactions were cut off at 10 Å and the Ewald method was used to treat long-range electrostatic interactions. The canonical structures of the ssDNA fragment, composed of 10 bases, were generated using the NUCGEN utility embedded in AMBER. To maintain the neutrality of the system, 9 $Na^+$ counterions were added in the proximity of the $PO_4^-$ groups of the ssDNA; for PTO two $Cl^-$ atoms were located closely to the N's of the dye, formally positively charged, and for TO one $Cl^-$ atom was added. The ssDNA/dye complex was modeled in an octahedron periodic box with a 10 Å buffer of water molecules explicitly described by the TIP3P model.[43] The solvent molecules (approximately 4000 water molecules) are omitted in the pictures to allow a better visualization of the solute. The equilibration of the system was performed as follows. An initial optimization of 2000 cycles, the first 1000 by steepest descent and the rest with a conjugate gradient method, with the ssDNA and dye restrained, to relax the solvent. Then a further optimization of 2000 cycles (without any restraints) was carried out to lead to a final relaxed geometry. The first equilibration was carried out with a weak restraint on the ssDNA-dye for 20 ps at constant

volume, constantly increasing the temperature from 0 to 300 K. Finally, the equilibration was continued to 2 ns at a constant pressure of 1 atm, and the temperature was kept constant with the Langevin temperature equilibration scheme using a collision frequency of 1.0 $ps^{-1}$.[44] During the MD calculation, hydrogen vibrations were kept frozen by using SHAKE bond constraints,[45] allowing a longer time step of 2 fs without introducing any instability.

### 3.5.5. NMR

$^1H$ and NOESY NMR were recorded with the assistance of Dr. G. Facey on an AVANCE 500 NMR spectrometer. COSY spectra were recorded with the assistance of Dr. G. Facey on an INOVA 500 NMR spectrometer.

#### 3.5.5.1. PTO

$^1H$-NMR (500 MHz, DMSO-d6) δ 9.08 (d, 2H), 8.80 (d, 1H), 8.60 (t, 1H), 8.56 (d, 1H), 8.17 (m, 3H), 8.06 (d, 1H), 8.00 (t, 1H), 7.81 (d, 1H), 7.76 (t, 1H), 7.63 (t, 1H), 7.44 (t, 1H), 7.37 (d, 1H), 6.95 (s, 1H), 4.80 (t, 2H), 4.71 (t, 2H), 4.04 (s, 3H), 2.56 (t, 2H).

NOEs between δ 8.80 and 6.95, 7.81; 8.06 and 7.44; 8.00 and 7.76; 7.81 and 4.04, 7.63; 7.76 and 8.00, 8.80; 6.95 and 4.04, 8.80; 4.80 and 9.08, 2.56; 4.71 and 8.57, 8.17, 2.56; 4.04 and 6.95, 7.81; 2.56 and 4.80, 4.71, 8.17.

The COSY of TO is shown in Figure 3.55, and a close-up of the aromatic region is shown in Figure 3.56.

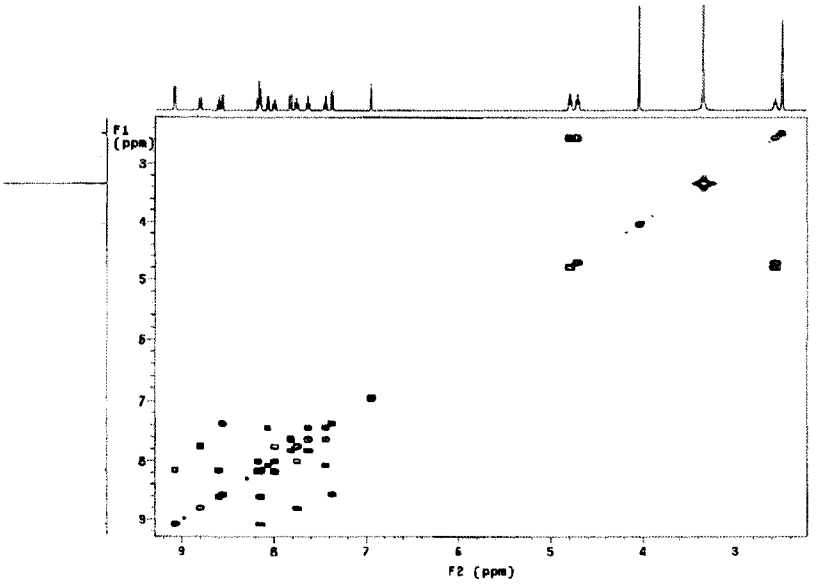


**Figure 3.55: PTO COSY.**

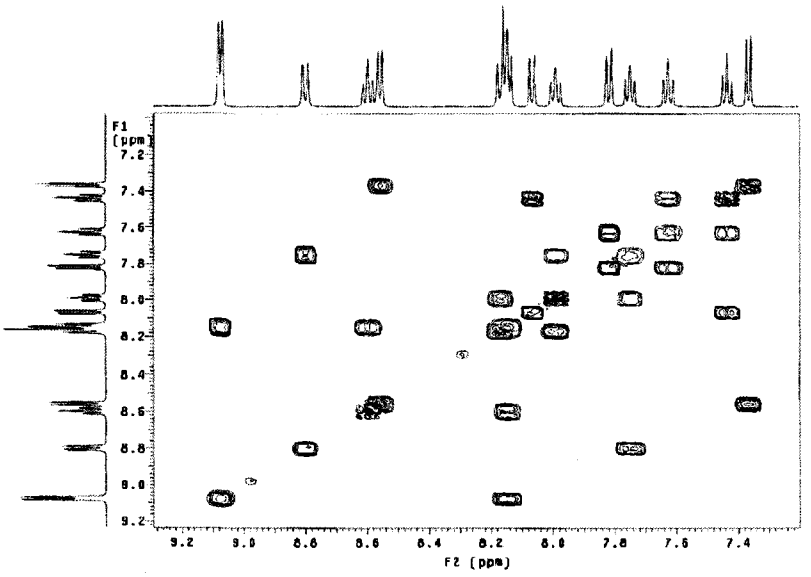


**Figure 3.56: Close-up of the aromatic region of the PTO COSY.**

### 3.5.5.2. TO

$^1$H-NMR (500 MHz, DMSO-d6) δ 8.81 (d, 1H), 8.61 (d, 1H), 8.02 (m, 3H), 7.78 (m, 2H), 7.66 (t, 1H), 7.47 (d, 2H), 7.41 (t, 1H), 7.36 (d, 1H), 7.12 (d, 2H), 6.93 (s, 1H), 4.17 (s, 3H), 4.01 (s, 3H), 2.28 (s, 3H).

NOEs between δ 6.93 and 8.81, 4.01; 4.17 and 8.61, 8.02; 4.01 and 7.78, 6.93.

The COSY of TO is shown in Figure 3.57, and a close-up of the aromatic region is shown in Figure 3.58.

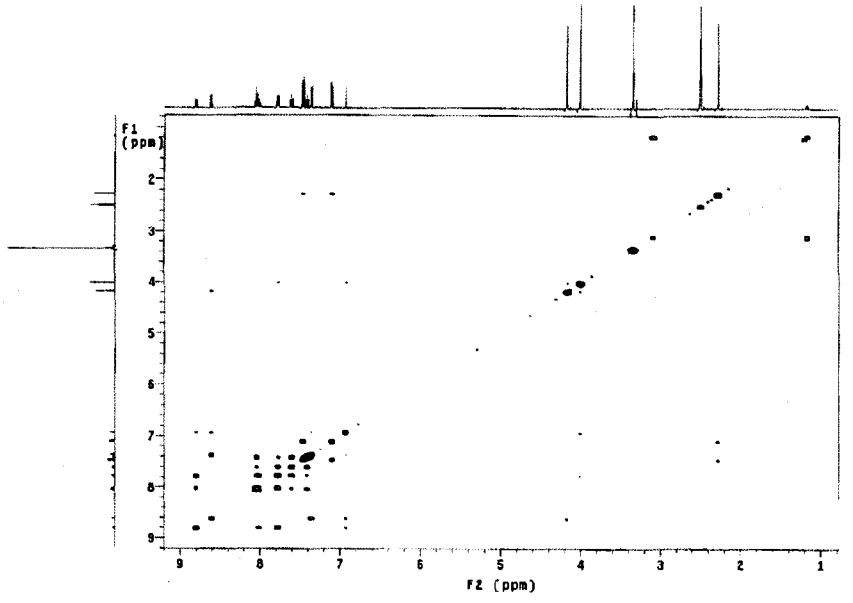


**Figure 3.57: TO COSY.**

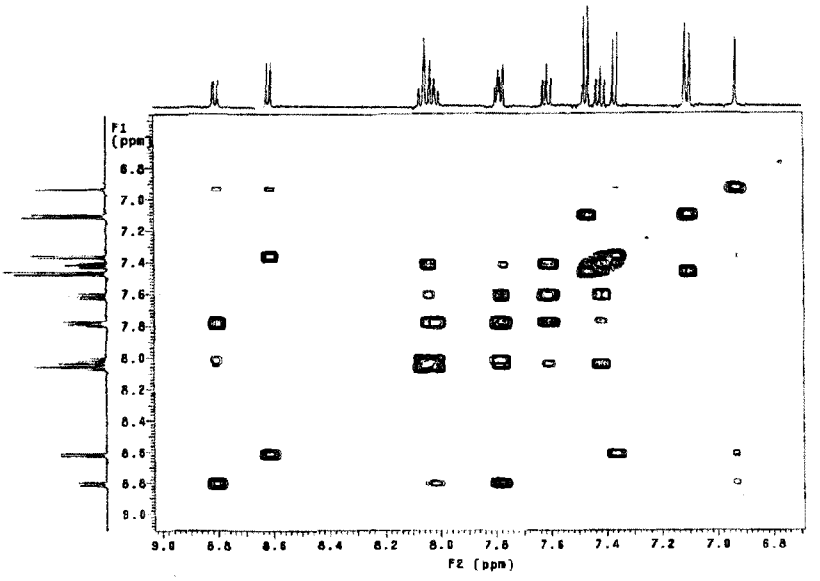


**Figure 3.58: Close-up of the aromatic region of the TO COSY.**

## 3.6. References


1. Cosa, G.; Focsaneanu, K.-S.; McLean, J. R. N.; Scaiano, J. C., Direct determination of single-to-double stranded DNA ratio in solution applying time-resolved fluorescence measurements of dye-DNA complexes. *Chem. Commun.* **2000,** 8, 689-690.

2. Cosa, G.; Vinette, A. L.; McLean, J. R. N.; Scaiano, J. C., Novel DNA damage detection technique applying time-resolved fluorescence measurements. *Anal. Chem.* **2002,** 74, (24), 6163-6169.

3. Lee, L. G.; Chen, C.-H.; Chiu, L. A., Thiazole orange: a new dye for reticulocyte analysis. *Cytometry* **1986,** 7, 508-517.

4. Netzel, T. L.; Nafisi, K.; Zhao, M.; Lenhard, J. R.; Johnson, I., Base-content dependence of emission enhancements, quantum yields, and lifetimes for cyanine dyes bound to double-strand DNA: photophysical properties of monomeric and bichromophoric DNA stains. *J. Phys. Chem.* **1995,** 99, (51), 17936-17947.

5. Nygren, J.; Svanvik, N.; Kubista, M., The interactions between the fluorescent dye thiazole orange and DNA. *Biopolymers* **1998,** 46, 39-51.

6. Petty, J. T.; Bordelon, J. A.; Robertson, M. E., Thermodynamic characterization of the association of cyanine dyes with DNA. *J. Phys. Chem. B.* **2000,** 104, (30), 7221-7227.

7. Rye, H. S.; Glazer, A. N., Interaction of dimeric intercalating dyes with single-stranded DNA. *Nucleic Acids Res.* **1995,** 23, (7), 1215-1222.

8. Prodhomme, S.; Demaret, J.-P.; Vinogradov, S.; Asseline, U.; Morin-Allory, L.; Vigny, P., A theoretical and experimental study of two thiazole orange derivatives with single- and double-stranded oligonucleotides, polydeoxyribonucleotides and DNA. *J. Photochem. Photobiol. B: Biol.* **1999,** 53, 60-69.

9. Simon, L. D.; Abramo, K. H.; Sell, J. K.; McGown, L. B., Oxazole yellow dye interactions with short DNA oligomers of homogeneous base composition and their hybrids. *Biospectroscopy* **1998,** 4, 17-25.

10. Schweitzer, C.; Scaiano, J. C., Selective binding and local photophysics of the fluorescent cyanine dye PicoGreen in double-stranded and single-stranded DNA. *Phys. Chem. Chem. Phys.* **2003,** 5, 4911-4917.

11. Mikelsons, L.; Scaiano, J. C., Will my strawberries glow in the dark? *Canadian Chemical News, October issue* **2004**, 18-19.

12. Cosa, G.; Focsaneanu, K.-S.; McLean, J. R. N.; McNamee, J. P.; Scaiano, J. C., Photophysical properties of fluorescent DNA-dyes bound to single- and double-stranded DNA in aqueous buffered solution. *Photochem. Photobiol.* **2001,** 73, (6), 585-599.

13. Jacobsen, J. P.; Pedersen, J. B.; Hansen, L. F.; Wemmer, D. E., Site selective bis-intercalation of a homodimeric thiazole orange dye in DNA oligonucleotides. *Nucleic Acids Res.* **1995,** 23, (5), 753-760.

14. Larsson, A.; Carlsson, C.; Jonsson, M.; Albinsson, B., Characterization of the binding of the fluorescent dyes YO and YOYO to DNA by polarized light spectroscopy. *J. Am. Chem. Soc.* **1994,** 116, (19), 8459-8465.

15. Ogul'chansky, T. Y.; Losytskyy, M. Y.; Kovalska, V. B.; Yashchuk, V. M.; Yarmoluk, S. M., Interactions of cyanine dyes with nucleic acids. XXIV. Aggregation of monomethine cyanine dyes in presence of DNA and its manifestation in absorption and fluorescence spectra. *Spectrochim. Acta A* **2001,** 57, 1525-1532.

16. Nygren, J.; Andrade, J. M.; Kubista, M., Characterization of a single sample by combining thermodynamic and spectroscopic information in spectral analysis. *Anal. Chem.* **1996,** 68, (10), 1706-1710.

17. West, W.; Pearce, S., The dimeric state of cyanine dyes. *J. Phys. Chem.* **1965,** 69, (6), 1894-1903.

18. Hannah, K. C.; Armitage, B., DNA-templated assembly of helical cyanine dye aggregates: a supramolecular chain polymerization. *Acc. Chem. Res.* **2004,** 37, (11), 845-853.

19. Mishra, A.; Behera, R. K.; Behera, P. K.; Mishra, B. K.; Behera, G. B., Cyanines during the 1990s: a review. *Chem. Rev.* **2000,** 100, (6), 1973-2011.

20. Armitage, B. A., Cyanine dye-DNA interactions: intercalation, groove binding, and aggregation. *Top. Curr. Chem.* **2005,** 253, 55-76.

21. Timtcheva, I.; Maximova, V.; Deligeorgiev, T.; Zaneva, D.; Ivanov, I., New asymmetric monomethine cyanine dyes for nucleic-acid labelling: absorption and fluorescence spectral characteristics. *J. Photochem. Photobiol. A: Chem.* **2000,** 130, (1), 7-11.

22. Yue, S. T.; Singer, V. L.; Roth, B. L.; Mozer, T. J.; Millard, P. J.; Jones, L. J.; Jin, X.; Haugland, R. P.; Poot, M. "Substituted unsymmetrical cyanine dyes with selected permeability", World Intellectual Property Organization, WO 96/13552. 1996.

23. Haugland, R. P.; Yue, S. T.; Millard, P. J.; Roth, B. L. "Cyclic-substituted unsymmetrical cyanine dyes", United States Patent Office, US5436134. 1995.

24. Emerson, E. S.; Conlin, M. A.; Rosenoff, A. E.; Norland, K. S.; Rodriguez, H.; Chin, D.; Bird, G.R., The Geometrical Structure and Absorption Spectrum of a Cyanine Dye Aggregate. *J. Phys. Chem.* **1967,** 71, (8), 2396-2403.

25. Ardhammar, M.; Nordén, B.; Kurucsev, T., DNA-Drug Interactions. In *Circular Dichroism: Principles and Applications*, 2nd ed.; Berova, N.; Nakanishi, K.; Woody, R. W., Eds. Wiley-VCH: New York, 2000; pp 741-768.

26. Carlsson, C.; Larsson, A.; Jonsson, M.; Albinsson, B.; Nord*n, B., Optical and photophysical properties of the oxazole yellow DNA probes YO and YOYO. *J. Phys. Chem.* **1994,** 98, (40), 10313-10321.

27. Paerschke, H.; Süsse, K.-E.; Welsch, D.-G., Investigation of vibronic energy relaxation of polymethin cyanine dyes by picosecond spectroscopy. *Chem. Phys. Lett.* **1979,** 66, (2), 376-380.

28. Sundström, V.; Gillbro, T., Viscosity dependent radiationless relaxation rate of cyanine dyes. A picosecond laser spectroscopy study. *Chem. Phys.* **1981,** 61, 257-269.

29. Ponterini, G.; Momicchioli, F., Trans-cis photoisomerization mechanism of carbocyanines: experimental check of theoretical models. *Chem. Phys.* **1991,** 151, 111-126.

30. Rullière, C., Laser action and photoisomerisation of 3,3'-diethyl oxadicarbocyanine iodide (DODCI): influence of temperature and concentration. *Chem. Phys. Lett.* **1976,** 43, (2), 303-308.

31. Saltiel, J., Perdeuteriostilbene. The role of phantom states in the cis-trans photoisomerization of stilbenes. *J. Am. Chem. Soc.* **1967,** 89, (4), 1036-1037.

32. Spielmann, H. P.; Wemmer, D. E.; Jacobsen, J. P., Solution structure of a DNA complex with the fluorescent bis-intercalator TOTO determined by NMR spectroscopy. *Biochemistry* **1995,** 34, (27), 8542-8553.

33. Seifert, J. L.; Connor, R. E.; Kushon, S. A.; Wang, M.; Armitage, B. A., Spontaneous assembly of helical cyanine dye aggregates on DNA nanotemplates. *J. Am. Chem. Soc.* **1999,** 121, (13), 2987-2995.

34. Chowdhury, A.; Wachsmann-Hogiu, S.; Bangal, P. R.; Raheem, I.; Peteanu, L. A., Characterization of chiral H and J aggregates of cyanine dyes formed by DNA templating using Stark and fluorescence spectroscopies. *J. Phys. Chem. B* **2001,** 105, (48), 12196-12201.

35. Garoff, R. A.; Litzinger, E. A.; Connor, R. E.; Fishman, I.; Armitage, B. A., Helical aggregation of cyanine dyes on DNA templates: effect of dye structure on formation of homo- and heteroaggregates. *Langmuir* **2002,** 18, (16), 6330-6337.

36. Barton, D., Sir; Nakanishi, K.; Meth-Cohn, C., *Comprehensive natural products chemistry.* Elsevier: Amsterdam; New York, 1999; Vol. 7, p 417-476.

37. Bloomfield, V. A.; Crothers, D. M.; Tinoco, I., Jr., Interaction and Reaction with Drugs. In *Nucleic Acids: Structures, Properties, and Functions*, University Science Books: Sausalito, 2000; pp 535-596.

38. Singer, V. L.; Jones, L. J.; Yue, S. T.; Haugland, R. P., Characterization of PicoGreen reagent and development of a fluorescence-based solution assay for double-stranded DNA quantitation. *Anal. Biochem.* **1997,** 249, (2), 228-238.

39. Frisch, M. J.; Trucks, G. W.; Schlegel, H. B.; Scuseria, G. E.; Robb, M. A.; Cheeseman, J. R.; Montgomery, J., J.A.; Vreven, T.; Kudin, K. N.; Burant, J. C.; Millam, J. M.; Iyengar, S. S.; Tomasi, J.; Barone, V.; Mennucci, B.; Cossi, M.; Scalmani, G.; Rega, N.; Petersson, G. A.; Nakatsuji, H.; Hada, M.; Ehara, M.; Toyota, K.; Fukuda, R.; Hasegawa, J.; Ishida, M.; Nakajima, T.; Honda, Y.; Kitao, O.; Nakai, H.; Klene, M.; Li, X.; Knox, J. E.; Hratchian, H. P.; Cross, J. B.; Adamo, C.; Jaramillo, J.; Gomperts, R.; Stratmann, R. E.; Yazyev, O.; Austin, A. J.; Cammi, R.; Pomelli, C.; Ochterski, J. W.; Ayala, P. Y.; Morokuma, K.; Voth, G. A.; Salvador, P.; Dannenberg, J. J.; Zakrzewski, V. G.; Dapprich, S.; Daniels, A. D.; Strain, M. C.; Farkas, O.; Malick, D. K.; Rabuck, A. D.; Raghavachari, K.; Foresman, J. B.; Ortiz, J. V.; Cui, Q.; Baboul, A. G.; Clifford, S.; Cioslowski, J.; Stefanov, B. B.; Liu, G.; Liashenko, A.; Piskorz, P.; Komaromi, I.; Martin, R. L.; Fox, D. J.; Keith, T.; Al-Laham, M. A.; Peng, C. Y.; Nanayakkara, A.; Challacombe, M.; Gill, P. M. W.; Johnson, B.; Chen, W.; Wong, M. W.; Gonzalez, C.; Pople, J. A. *Gaussian 03*, Revision B.04; Gaussian, Inc.: Pittsburgh, 2003.

40. Case, D. A.; Darden, T. A.; Cheatham III, T. E.; Simmerling, C. L.; Wang, J.; Duke, R. E.; Luo, R.; Merz, K. M.; Wang, B.; Pearlman, D. A.; Crowley, M.; Brozell, S.; Tsui, V.; Gohlke, H.; Mongan, J.; Hornak, V.; Cui, G.; Beroza, P.; Schafmeister, C.; Caldwell, J. W.; Ross, W. S.; Kollman, P. A. *AMBER 8*, University of California, San Francisco, 2004.

41. Wang, J.; Cieplak, P.; Kollman, P. A., How well does a restrained electrostatic potential (RESP) model perform in calculating conformational energies of organic and biological molecules? *J. Comput. Chem.* **2000,** 21, 1049-1074.

42. Wang, J.; Wolf, R. M.; Caldwell, J. W.; Kollman, P. A.; Case, D. A., Developing and testing of a general AMBER force field. *J. Comput. Chem.* **2004,** 25, (9), 1157-1174.

43. Jorgensen, W. L.; Chandrasekhar, J.; Madura, J. D.; Impey, R. W.; M.L., K., Comparison of simple potential functions for simulating liquid water. *J. Chem. Phys.* **1983,** 79, (2), 926-935.

44. Pastor, R. W.; Brooks, B. R.; Szabo, A., An analysis of the accuracy of Langevin and molecular dynamics algorithms. *Mol. Phys.* **1988,** 65, 1409-1419.

45. van Gunsteren, W. F.; Berendsen, H. J. C., Algorithms for macromolecular dynamics and constraint dynamics. *Mol. Phys.* **1977,** 34, (5), 1311-1327.

# 4. The Interactions of Cyanine Dyes with Double-Stranded DNA

## 4.1. Introduction

There is still much to be discovered regarding the antitumor activity of DNA-reactive drugs, such as the relationship between the structure of the drug/DNA complex and the biological response. The main groups of clinically significant DNA reactive compounds have been identified as: alkylating agents, DNA strand breaking agents, and intercalating agents.[1] Intercalators affect the topological conformation of DNA and interfere with its ability to act as a template in replication and transcription.[2] Molecules that hinder the functions of nucleic acids are important in antibiotic and cancer chemotherapy.[3] In addition to nonlethal effects, the association of small molecules with nucleic acids can lead to cell death.[4] In this chapter the effects of intercalating cyanine dyes on double-stranded (ds) DNA will be examined.

Asymmetric cyanine dyes have been used in a variety of applications, such as the quantitation and sizing of DNA restriction fragments in gels,[5] the quantitation of dsDNA in solution,[6] reticulocyte analysis using flow cytometry,[7] in a fluorescent intercalator displacement assay for determining DNA binding affinity and sequence selectivity,[8] and in high-sensitivity two-colour detection of dsDNA in agarose gels.[9] It has been suggested that as the use of high sensitivity fluorescence detection equipment becomes more commonplace, these dyes may replace radiolabels in the sensitive detection of DNA.[10] The key to their high sensitivity is their low background fluorescence: they are virtually non-fluorescent in solution and undergo dramatic increases in fluorescence upon binding to DNA. This property has enabled the detection of picograms of DNA in agarose gels[11] and 2-4 attomoles of DNA base pairs per band in fluorescence-detected capillary electrophoresis.[12]

It remains to be established whether or not the binding of cyanine dyes is sequence specific. A comparison of the fluorescence quantum yields of cyanine dyes and duplex DNA base content indicated that quinolinium cyanine dyes such as thiazole orange (TO) and oxazole yellow (YO) selectively bind to GC-rich regions in calf thymus DNA, while pyridinium cyanine dyes bind to AT-rich regions.[13] However,

there was no definitive proof as the lifetimes of the dyes varied considerably in the different types of DNA, and the bi- and triexponential decays suggested more than one mode of binding. On the other hand, equilibrium constants for TO and TO- and YO-derivatives did not show a dependence on duplex base content.[14,15] There is a linear relationship between the relative electrophoretic mobility of various dsDNA fragments prelabelled with dimeric dyes (homodimers of ethidium, TO and YO) and fragment size, and also between the fluorescence intensity of the dye/DNA complexes and the DNA concentration in base pairs, thus it was concluded that the binding of these dyes is independent of the DNA base pair composition.[10]

Müller and Crothers first proposed the technique of using surfactants to measure drug dissociation rates in 1968.[16] Since then, the technique has been used to measure the dissociation rates of various drugs from DNA.[17-22] Until recently, it was believed that the rate-limiting step was dissociation of the drug from the DNA, and that the only role of the anionic surfactant (which was assumed not to interact with the anionic sugar-phosphate backbone of DNA) was to sequester the drug and prevent it from reassociating with the DNA.[16-19] However, it has been shown that anionic surfactants increase the dissociation rate of cationic intercalators from DNA.[23] We have used this knowledge to study the effect of sodium dodecyl sulfate on dye dissociation from various dye/DNA complexes, and to determine their relative stabilities.

In the previous chapter, we used experimental spectroscopic techniques and computational methods to study the association of three cyanine dyes (PTO, TO, and PG) with single-stranded (ss) DNA homopolymers. That knowledge will be used in this chapter to investigate the more complex association of these cyanine dyes with double-stranded DNA. We have examined the interactions of the cyanine dyes with dsDNA (natural and synthetic) using UV-Visible absorption spectroscopy, circular dichroism and linear dichroism spectroscopy, steady-state and time-resolved fluorescence spectroscopy, detergent sequestration and computational methods. The experimental spectroscopic techniques identified differences between the dye complexes with ss- and dsDNA, and the computational

methods provided further insight into the association process. Interestingly, we found that hybridization of complementary DNA homopolymer single strands in the presence of intercalating cyanine dyes leads to the formation of a new type of stable dye/DNA complex that cannot be obtained by addition of the same molecule to the corresponding dsDNA. This may explain the mechanism of action of some drugs.

This project was a continuation of work initiated by a postdoctoral fellow in our laboratory, Dr. C. Schweitzer. The molecular dynamics simulations were done in collaboration with a postdoctoral fellow in our laboratory, Dr. C. Carra, with aid from Dr. M. Shaw. Some of the measurements presented in this chapter were performed by M. Antonic who worked in our laboratory under my supervision as part of the Undergraduate Research Scholarship program at the University of Ottawa. I am grateful for her help.

## 4.2. Results

### 4.2.1. Cyanine Dyes and CT DNA

#### 4.2.1.1. Absorption, CD and LD Spectroscopy

The structures of the cyanine dyes that were studied were shown in Scheme 3.1, and their absorption properties were discussed in Section 3.2.1. When the N-propyl pyridinium derivative of thiazole orange (PTO) was added to either ss or ds calf thymus (CT) DNA, both the monomer and aggregate absorption bands red-shifted (see Figure 4.1A), indicative of intercalation.[24] In addition, there was a decrease in the aggregate absorption band (481 nm in free PTO) and an increase in the monomer absorption band (508 nm in free PTO) which is consistent with monomer intercalation and suppression of dye aggregation, as has been postulated for the binding of thiazole orange (TO) to ds CT DNA.[25]

As with PTO, addition of CT DNA (ss or ds) to TO caused a red-shift of both the monomer and aggregate absorption bands, as well as an increase in the monomer absorption band intensity and a decrease in the aggregate absorption band intensity, consistent with previous results which found that binding of TO to ds CT DNA prevented dye aggregation.[25] If the extinction coefficients of monomeric and aggregate TO are similar in both ss and ds CT DNA, then Figure 4.1B indicates that there is a higher monomer:aggregate ratio in dsDNA compared to ssDNA. This is in contrast to PTO and CT DNA, where there is very little difference between the monomer:aggregate ratios in ss- and dsDNA.

The photophysical properties of PicoGreen® (PG) in buffer and in DNA have already been studied,[26] but they are included here to provide a comparison under the same experimental conditions. Of all the dyes, PG shows the least aggregation at 20 μM, both in buffer and in DNA, as seen in Figure 4.1C. TO and PG each have one positive charge, thus it appears that the substituents on PG hinder aggregation. As the PG dimer/aggregate shoulder is barely visible, its contribution to the absorption spectrum is minor and, upon complexation with both ss- and dsDNA, a

red-shift and a decrease in absorption occur, consistent with intercalation, which was already demonstrated to be its binding mode.[26]

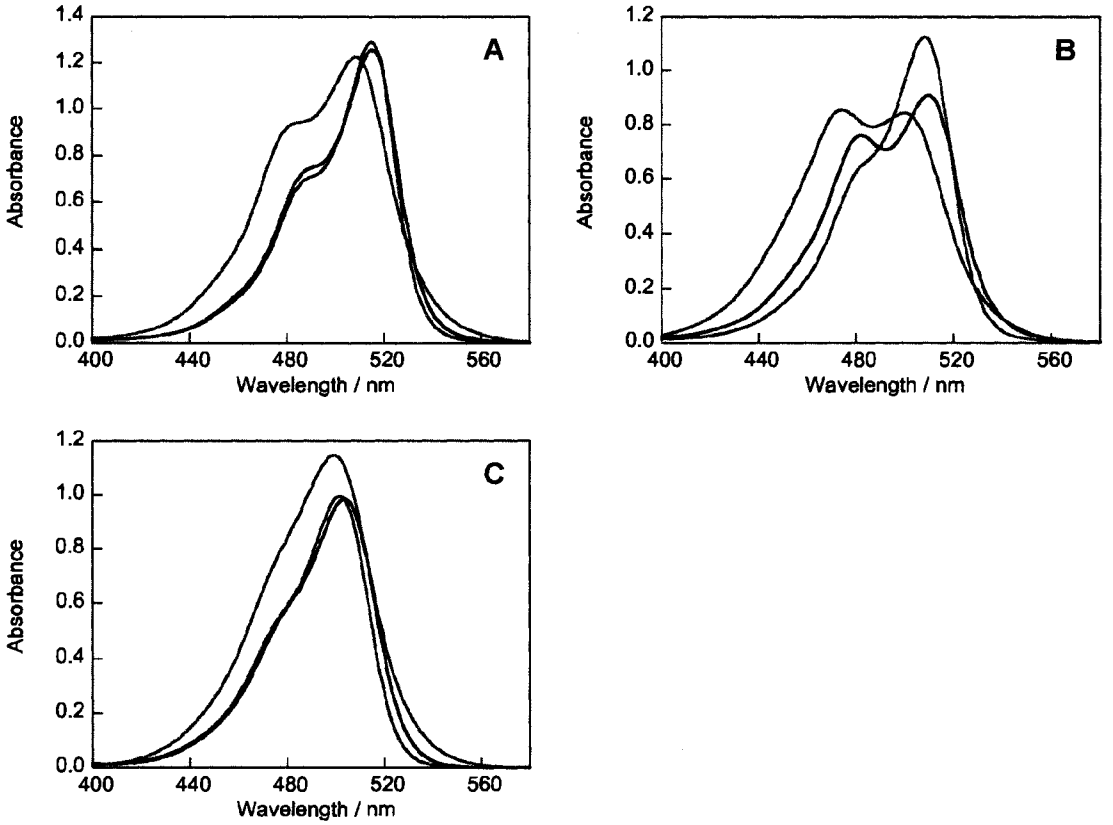


**Figure 4.1: Absorption spectra of 20 μM dye alone (purple) and in the presence of 200 μM dsDNA (red) or 200 μM ssDNA (black), all in 10 mM Tris buffer (pH 7.4) at room temperature. (A) PTO, (B) TO, (C) PG.**

When achiral molecules, such as the dyes studied here, are located in a chiral environment they may show induced circular dichroism (ICD) due to coupling of the electrical transition moments of the guest molecule and of the chiral host.[27] PTO shows a negative ICD signal whose shape is the same in both ss- and dsDNA, as seen in Figure 4.2B. The ICD spectra do not correspond to any of those observed for PTO with ss homopolymers (see Section 3.2.5), but the troughs around 487 and 510 nm are very similar to the absorption maxima (487 and

515 nm) of PTO in CT DNA, suggesting that the ICD arises from an interaction between two transition moments of unequal transition energies, i.e. the nondegenerate case.

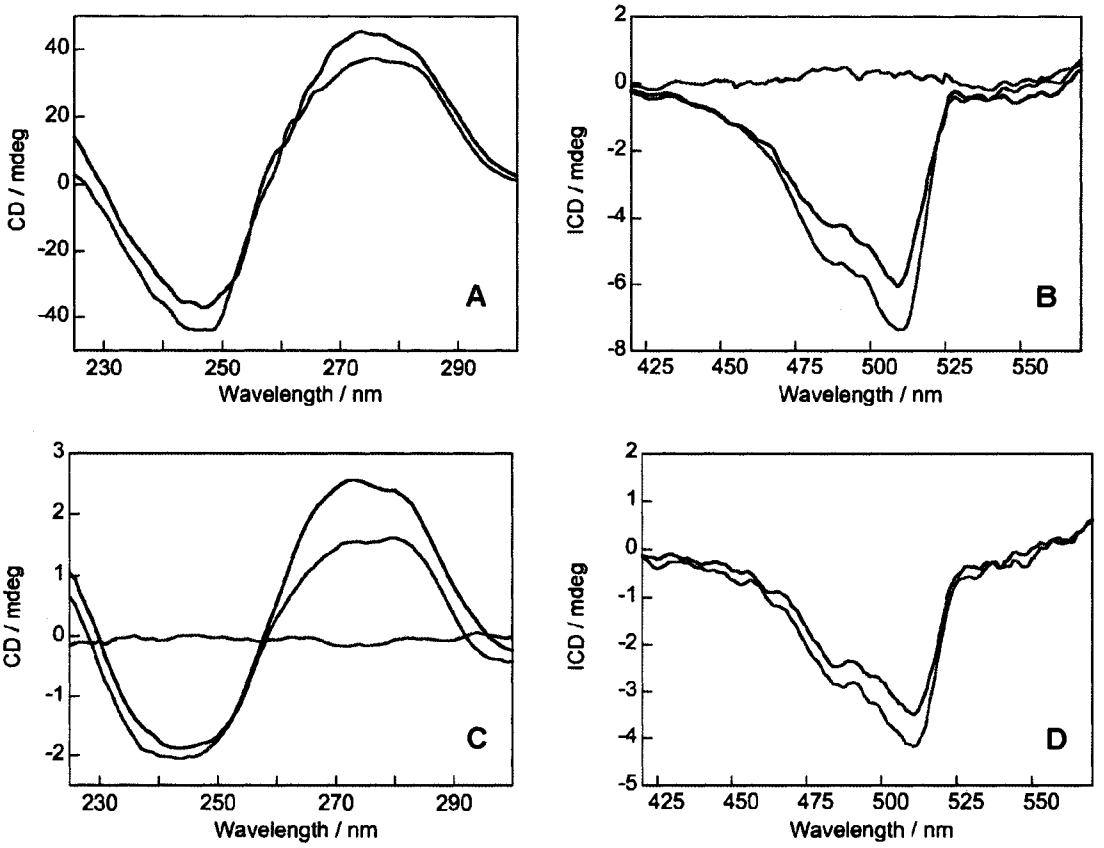


**Figure 4.2: (A) CD spectra of 200 μM dsDNA (red) and 200 μM ssDNA (black) in 10 mM Tris buffer (pH 7.4) at 20°C. (B) ICD and (C) CD spectra of 20 μM PTO alone (purple) and in the presence of 200 μM dsDNA (red) or 200 μM ssDNA (black) in 10 mM Tris buffer (pH 7.4) at 20°C. (D) ICD spectra of 10 μM PTO and 100 μM dsDNA in 10 mM Tris buffer (pH 7.4) at 20°C before (red) and after (green) thermal cycling. Recorded using a 10 mm path length for (A), (B) and (D) and a 1 mm path length for (C).**

Denaturation of ds B-form DNA only has a modest effect on its CD, i.e. the magnitudes of the CD bands above 230 nm only change slightly,[28] as seen in

Figure 4.2A. The CD spectra of CT DNA in the presence of PTO (Figure 4.2C) resemble those of the DNA alone, although the ratio of the long wavelength band (area between 257 and 300 nm) in ssDNA compared to dsDNA changes from 1.2 to 1.8 upon addition of the dye.

To see whether or not DNA renaturation is affected by the presence of the dye, the PTO/dsDNA complex was subjected to thermal cycling, i.e. heated at 95°C for 10 minutes (to denature the DNA) and then allowed to return to room temperature (to permit renaturation). The ratio of the area of the PTO ICD signal in dsDNA to that in ssDNA is 1.4 (Figure 4.2B). The ratio of the area of the PTO ICD signal in the PTO/dsDNA complex before and after thermal cycling is also 1.4 (Figure 4.2D), indicating that PTO prevents DNA renaturation.

The ICD spectra of TO with ss and ds CT DNA, Figure 4.3A, are both distinct from those of TO with ss DNA homopolymers (see Section 3.2.5). However, they do share some common features. In the presence of poly(dA), poly(dG), and ss and ds CT DNA, TO shows a trough around 477 nm. In the presence of poly(dA) and ss- and ds CT DNA, TO shows a peak around 518 nm. The trough around 497 nm observed in the ICD of TO/ds CT DNA was not observed when TO was complexed with any of the ss DNA homopolymers. However, TO/poly(dA) did exhibit a small negative feature around 500 nm so the trough may be due to a similar (more intense) interaction in TO/ds CT DNA. Although there are many different binding sites in CT DNA, these findings suggest that association of TO with A bases in both ss and ds CT DNA contribute to the observed ICD, and there may also be a contribution from TO binding to G bases. Even though the ICD signals of TO in ss and ds CT DNA have a similar peak and trough, the spectra are unique, indicating that TO binds somewhat differently to each one. The CD spectra (225-300 nm) of TO/ssDNA and TO/dsDNA (Figure 4.3B) resemble those of the DNA alone (Figure 4.2A), with the exception that the ratio of the short wavelength band for TO/dsDNA and TO/ssDNA is larger than the ratio for dsDNA and ssDNA alone.

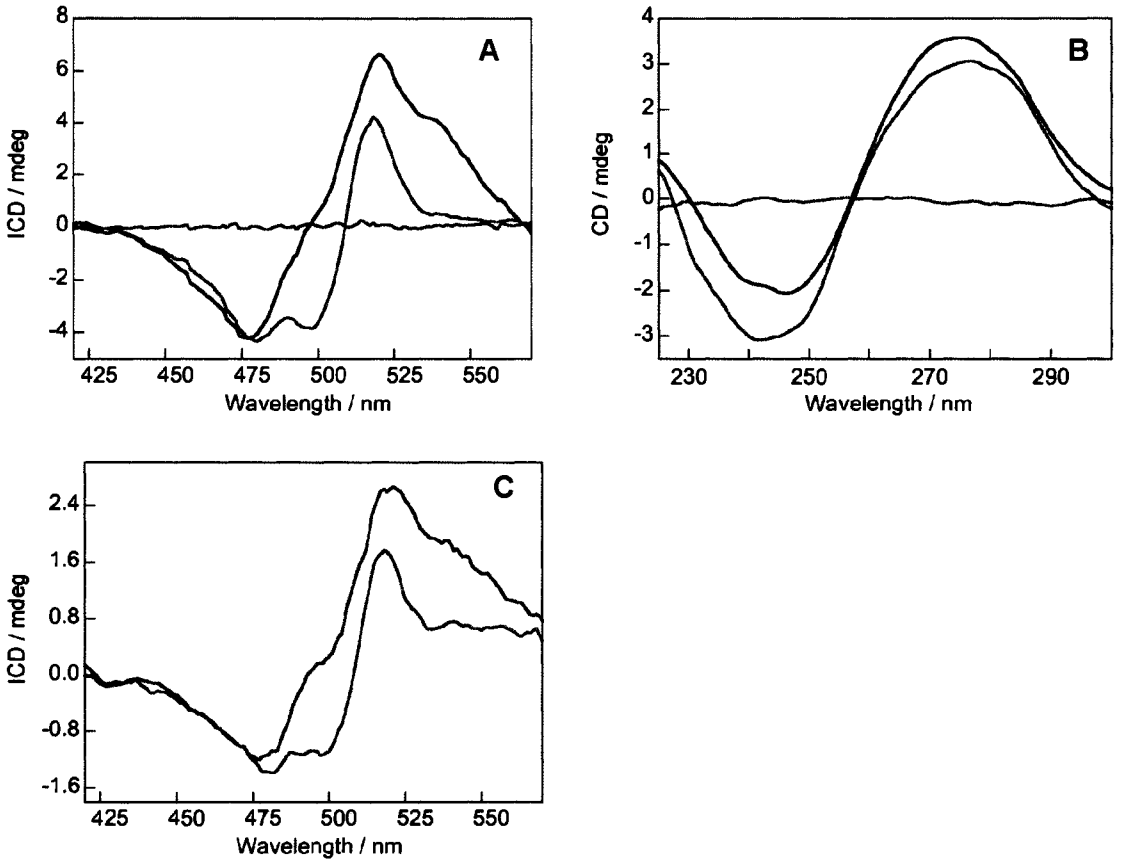


**Figure 4.3: (A) ICD and (B) CD spectra of 20 μM TO alone (purple) and in the presence of 200 μM dsDNA (red) or 200 μM ssDNA (black) in 10 mM Tris buffer (pH 7.4) at 20°C. (C) ICD spectra of 10 μM TO and 100 μM dsDNA in 10 mM Tris buffer (pH 7.4) at 20°C before (red) and after (green) thermal cycling. Recorded using 10 and 1 mm path lengths for ICD and CD, respectively.**

Thermal cycling altered the ICD of the TO/dsDNA complex, as shown in Figure 4.3C. The ICD of the TO/dsDNA solution that underwent thermal cycling resembles that of TO and ssDNA (Figure 4.3A), even 24 hours later, suggesting that the presence of the dye inhibits renaturation of the DNA. The effects of dyes on strand hybridization will be discussed further in Section 4.2.2.

The negative ICD signals of PG in ss- and dsDNA (see Figure 4.4A) are due to monomeric intercalation, as previously reported.[26,29] It was shown that PG binds

preferentially between alternating GC base pairs in dsDNA, and between two different bases, one of which is G or T, in ssDNA.[29] As with TO, the CD spectra of PG and CT DNA (Figure 4.4B) resembled those of the DNA alone, with the exception of increased intensity in the short wavelength band for PG/dsDNA relative to dsDNA.

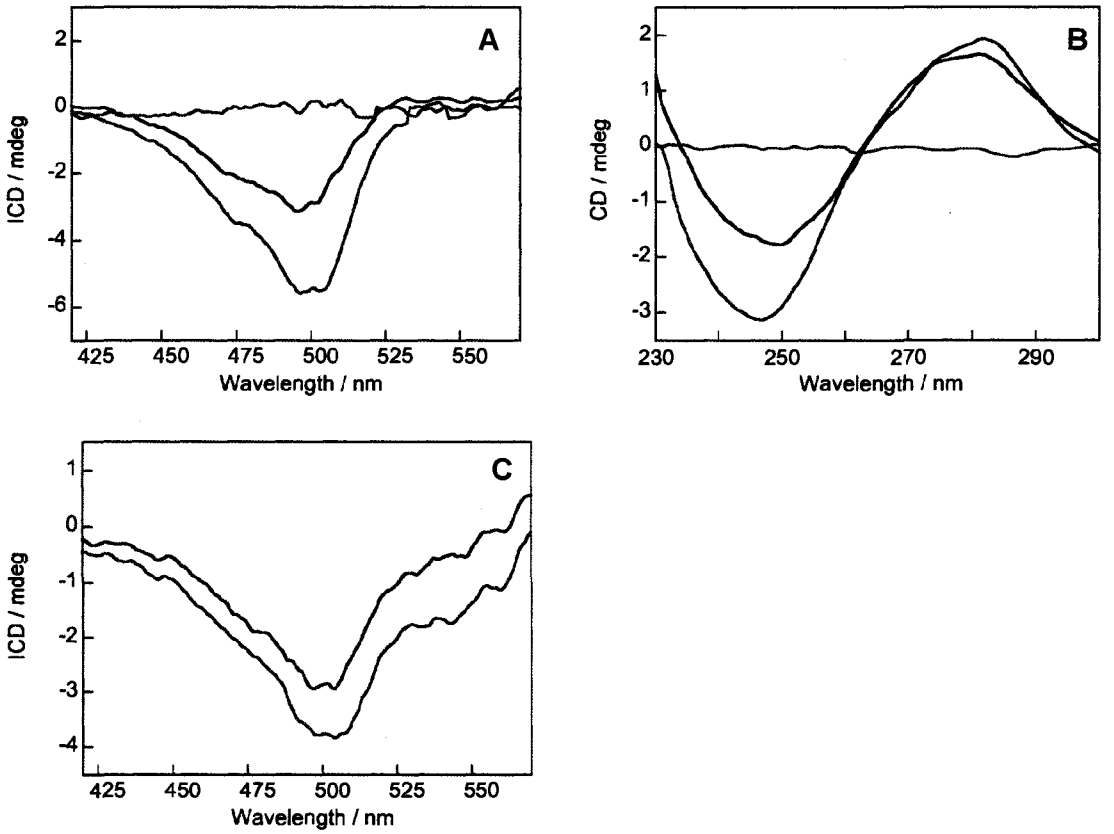


**Figure 4.4: (A) ICD and (B) CD spectra of 20 μM PG alone (purple) and in the presence of 200 μM dsDNA (red) or 200 μM ssDNA (black) in 10 mM Tris buffer (pH 7.4) at 20°C. (C) ICD spectra of 10 μM PG and 100 μM dsDNA in 10 mM Tris buffer (pH 7.4) at 20°C before (red) and after (green) thermal cycling. Recorded using 10 and 1 mm path lengths for ICD and CD, respectively.**

The ratio of the area of the PG ICD signal in dsDNA to that in ssDNA is 1.66 (Figure 4.4A). When comparing the PG/dsDNA complex before and after thermal

cycling (Figure 4.4C), a ratio of 1.64 is obtained for the area of the PG ICD signal, indicating that the dye hinders renaturation of the strands, as observed with the other two dyes and dsDNA.

In our laboratory, we designed a Couette apparatus for recording linear dichroism (LD). The sample is placed in the annular gap between two quartz cylinders. The inner cylinder rotates while the outer cylinder is fixed, producing a flow that aligns the sample. In the case of dsDNA, the DNA is aligned with the helix axis parallel to the flow. To test our Couette cell, the LD of ds CT DNA was recorded (Figure 4.5), and it is in excellent agreement with previously published spectra.[30-32] When DNA is denatured by lowering the pH of the DNA solution (pH < 3.5 in 0.1 M citrate buffer), its LD changes from a large negative signal to a very small positive one, indicating a more parallel than perpendicular orientation of the bases to the helix in acidic solution upon denaturation.[33] However, a high (0.1 M NaCl) salt concentration keeps the DNA in its native form under acidic conditions (pH 3.3) and thus it exhibits negative LD.[33] As can be seen in Figure 4.5, the LD observed for single-stranded CT DNA resembles that of the corresponding double-stranded CT DNA, although the area of the signal is approximately 26 times smaller. The negative LD indicates that the ssDNA is in its native form and the decreased intensity relative to dsDNA is due to a lower degree of orientation, owing to the flexibility of the single strands. To generate single-stranded DNA in our experiments, the double-stranded DNA was heat-denatured and then shock cooled in an ice bath (to prevent renaturation). However, we cannot rule out the possibility that partial renaturation occurred and that the negative LD signal is due to some contamination from double-stranded DNA.

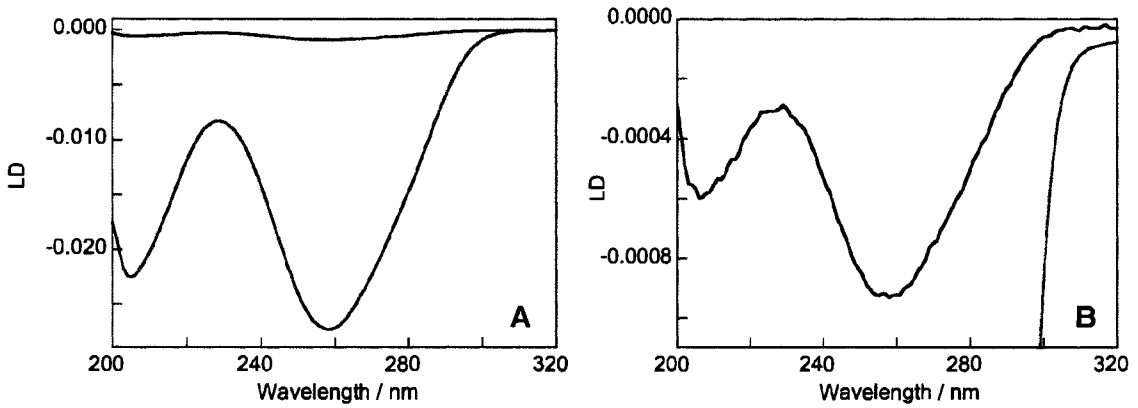


**Figure 4.5: (A) Linear dichroism spectra of 100 μM ds CT DNA (red) and 100 μM ss CT DNA (black) in 10 mM Tris buffer (pH 7.4), recorded at room temperature using a 6 mm optical path. (B) Close-up of the spectrum in (A), showing the weak LD signal of ss CT DNA.**

The bases in dsDNA are approximately perpendicular to the helical axis so their electronic transitions result in a negative LD.[34] As the LD signals of PTO with ss- and dsDNA (Figure 4.6A) are also negative (and have the same shape as the PTO absorption band), this indicates that the transition moment of bound PTO is perpendicular to the helical axis, which is consistent with intercalation.[35-37] When studying the binding of ligands to DNA, an increase in LD signifies enhanced DNA orientation due to lengthening and stiffening of the DNA.[38] The increased LD signals of the PTO/DNA complexes (Figure 4.6A) relative to those of the DNA without any dye (Figure 4.5) indicate that dye association lengthens and stiffens the DNA, consistent with intercalation.

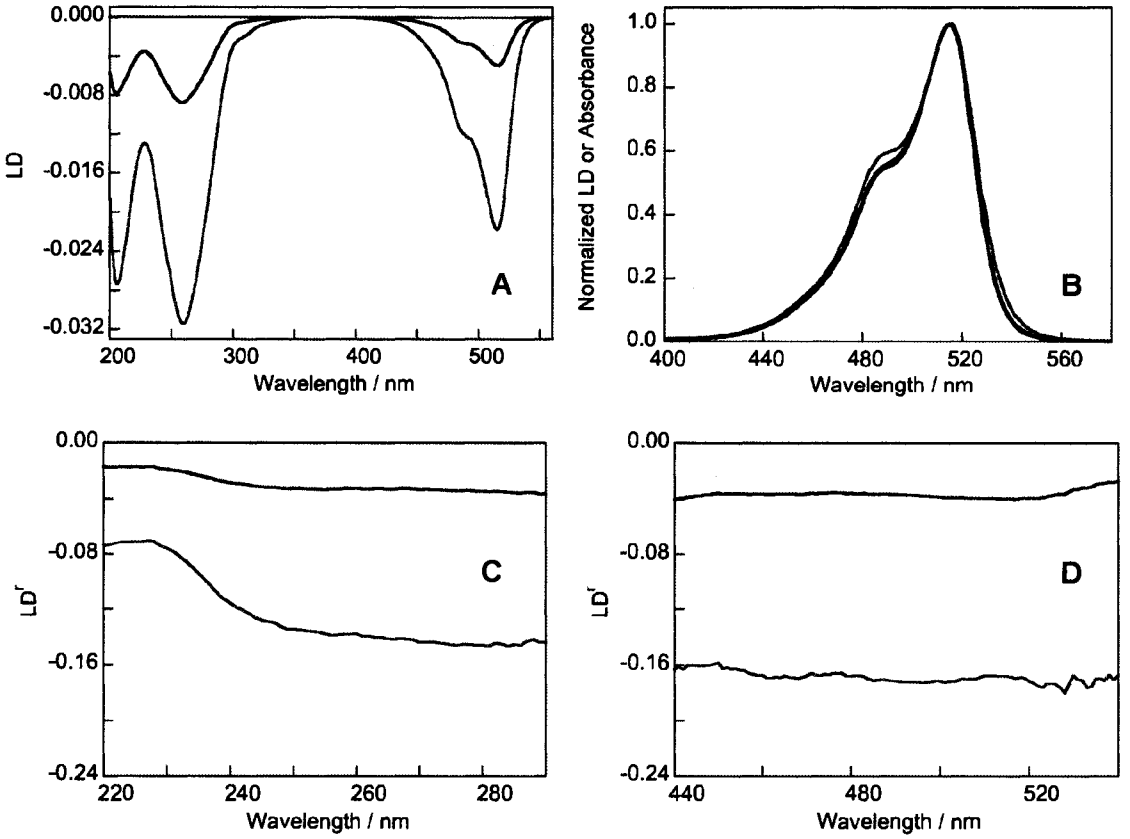


**Figure 4.6: (A) Linear dichroism spectra of 10 μM PTO alone (purple) and in the presence of 100 μM dsDNA (red) or 100 μM ssDNA (black) in 10 mM Tris buffer (pH 7.4), recorded at room temperature using a 6 mm optical path. (B) Normalized linear dichroism spectra (inverted) of 10 μM PTO with 100 μM dsDNA (red) or 100 μM ssDNA (black), as well as normalized absorbance spectra of 20 μM PTO with 200 μM dsDNA (blue) or 200 μM ssDNA (green); red, black and blue lines lie on top of one another. Reduced linear dichroism ($LD^r$) of the solutions in (A) shown in the DNA region (C) and the dye region (D).**

The LD signals of PTO with ss- and dsDNA in the visible region are very similar to the corresponding absorption spectra, as shown via normalization in Figure 4.6B. The normalized absorbance and LD of PTO/dsDNA are identical, and since the LD signal is due to bound dye, this indicates that both monomeric and

dimeric PTO are bound to the dsDNA. We were surprised by this observation, since it seemed unlikely to us that the face-to-face dimer (discussed in Chapter 3) would be able to intercalate. The normalized absorbance of PTO/ssDNA is slightly broader and contains a larger dimer contribution than the corresponding normalized LD. This indicates that some dimers are bound to the ssDNA while others are free in solution.

The reduced linear dichroism ($LD^r$) is defined as the LD divided by the isotropic absorbance. The reduced linear dichroism in the DNA region of PTO/dsDNA (Figure 4.6C) is characteristic of B-form DNA with an essentially constant $LD^r$ in the 250-290 nm region, and a more positive $LD^r$ around 230 nm, which corresponds to a weak out-of-plane $n \rightarrow \pi^*$ transition.[39] The similarity of the $LD^r$ amplitudes in the DNA region (Figure 4.6C) and in the dye region (Figure 4.6D) indicate that the planes of the base pairs and the dye are parallel, owing to intercalation.[40]

As with PTO, the negative LD signals of TO with ss- and dsDNA (Figure 4.7A and Figure 4.7B) indicate dye intercalation. The TO/ssDNA complex exhibits a decreased LD: the intensity of the LD signal of TO/ssDNA around 260 nm is approximately 38% that of ssDNA alone. A reduction in LD signifies a decrease in DNA base orientation, i.e. the DNA is bending, which could be due to either a decrease in the overall DNA orientation or to tilting of the DNA bases.[41] Thus it appears that TO bends ssDNA, as was observed in some of the molecular dynamics simulations (see Section 3.2.7). The similarity of the $LD^r$ amplitudes in the DNA region (Figure 4.7C) and in the dye region (Figure 4.7D) indicate that the planes of the base pairs and the dye are parallel, owing to intercalation, as was found for PTO. Comparison of the normalized LD and absorbance in the visible region (Figure 4.7E) shows that when TO associates with dsDNA, both the monomer and the dimer intercalate. In contrast, the normalized LD and absorbance of TO in ssDNA show significant differences, indicating that a significant amount (most likely the majority, judging by the extremely weak LD) of dye is present as the dimer/aggregate in solution, rather than intercalated.

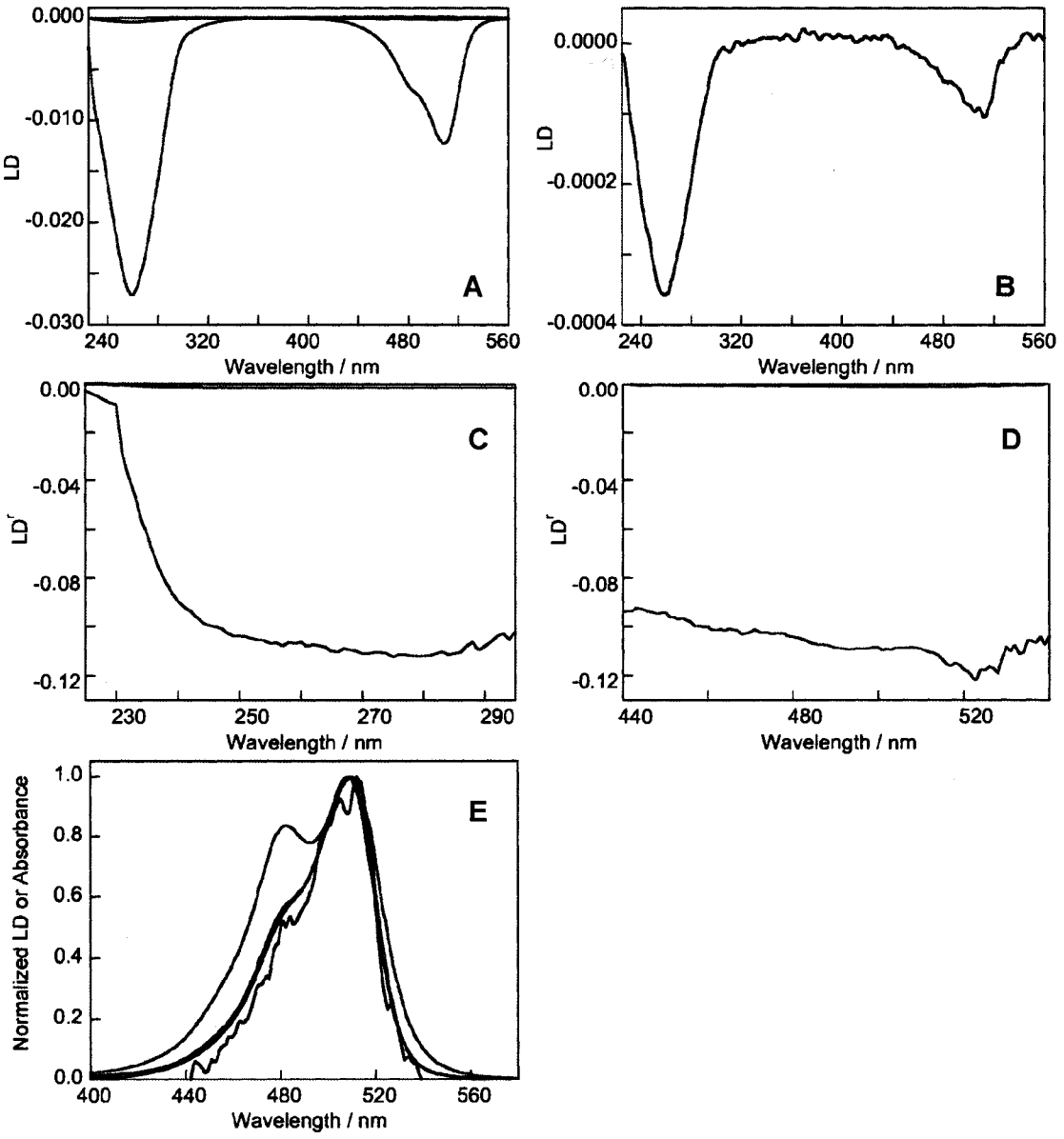


**Figure 4.7: (A) LD spectra of 10 μM TO alone (purple) and with 100 μM dsDNA (red) or 100 μM ssDNA (black) in 10 mM Tris buffer (pH 7.4), recorded at RT using a 6 mm optical path. (B) Close-up of the LD spectrum of TO/ssDNA from (A). $LD^r$ of the solutions in (A) shown in (C) the DNA region and (D) the dye region. (E) Normalized LD spectra of 10 μM TO with 100 μM dsDNA (red) or 100 μM ssDNA (black) as well as normalized absorbance spectra of 20 μM TO with 200 μM dsDNA (blue) or 200 μM ssDNA (green).**

As with the other two dyes, the negative LD signals of PG with ss- and dsDNA (Figure 4.8A and Figure 4.8B) indicate dye intercalation. The presence of PG decreases the LD of ssDNA: the intensity of the LD signal for PG/ssDNA around 260 nm is approximately 79% that of ssDNA on its own. Thus it appears that, like TO, PG bends the ssDNA. The similarity of the $LD^r$ amplitudes in the DNA region (Figure 4.8C) and in the dye region (Figure 4.8D) indicate that the planes of the base pairs and the dye are parallel, owing to intercalation, as was found for PTO and TO. However, the slightly more negative $LD^r$ in the dye region indicates that the dye is, on average, closer to a perpendicular orientation (relative to the DNA helical axis) than are the DNA bases.[35,42-44] The shape of the LD signal of PG with dsDNA in the visible region is essentially identical to that of the corresponding absorption spectrum, as shown via normalization in Figure 4.8E, indicating that all of the dye (mostly monomeric, a very small shoulder in the absorption region of the dimer) is bound to the dsDNA. The LD of PG/ssDNA is extremely weak thus one cannot tell from the normalized LD spectrum whether or not dimeric PG is bound to the ssDNA.

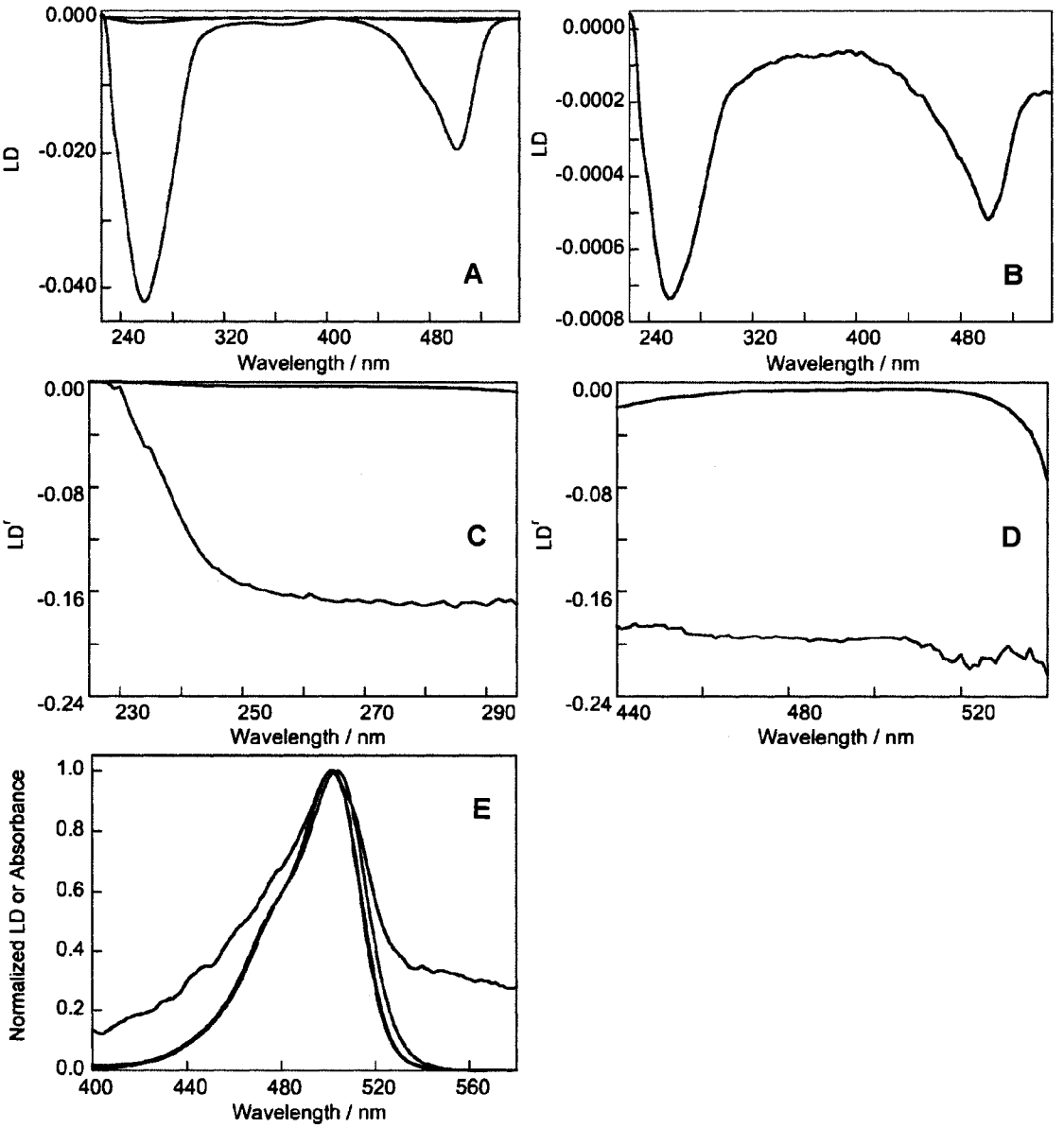


**Figure 4.8: (A) LD spectra of 10 µM PG alone (purple) and with 100 µM dsDNA (red) and 100 µM ssDNA (black) in 10 mM Tris buffer (pH 7.4), recorded at RT using a 6 mm optical path. (B) Close-up of the LD spectrum of PG/ssDNA from (A). $LD^r$ of the solutions in (A) shown in (C) the DNA and (D) the dye regions. (E) Normalized LD spectra of 10 µM PG with 100 µM dsDNA (red) and 100 µM ssDNA (black) as well as normalized absorbance spectra of 20 µM PG with 200 µM dsDNA (blue) and 200 µM ssDNA (green).**

#### 4.2.1.2. Steady-State and Time-Resolved Fluorescence Spectroscopy

In the PTO excitation spectrum there are peaks around ~475 nm and ~515 nm, as seen in Figure 4.9A. However, the peak around ~475 nm is most likely lamp fine structure while the peak around 515 nm is monomer fluorescence. PTO in dsDNA and in ssDNA emits at 535 nm and 537 nm, respectively, independent of the excitation wavelength (see Figure 4.9B-D), signifying that all excited species lead to monomer fluorescence. However, there is a very slight shoulder in each emission spectrum, which could be a (minor) contribution from the *cis* isomer via *cis-trans* isomerization, or a vibrational band (from the *trans* monomer). One reviewer suggested measuring the excitation spectrum of the DNA-bound dye to further distinguish between a potential vibrational band (which would be fluorescent) and the dimer (which would be non-fluorescent); unfortunately, the possibility of there being a fluorescent *cis* isomer makes this determination impossible. The aggregates that contribute to fluorescence must either transfer their energy to the monomer (the aggregate is significantly higher in energy) through FRET and the monomer fluoresces, or dissociate into monomers and then fluoresce. In all of the cases, the area under the fluorescence curve was 1.9 to 2.2 times larger for PTO/dsDNA than for PTO/ssDNA, consistent with the dye being more rotationally restricted in dsDNA compared to ssDNA. The fluorescence of PTO in buffer was negligible. Singlet excited state dye deactivation in solution via radiationless decay versus deactivation in DNA via fluorescence was discussed in Section 3.2.2.

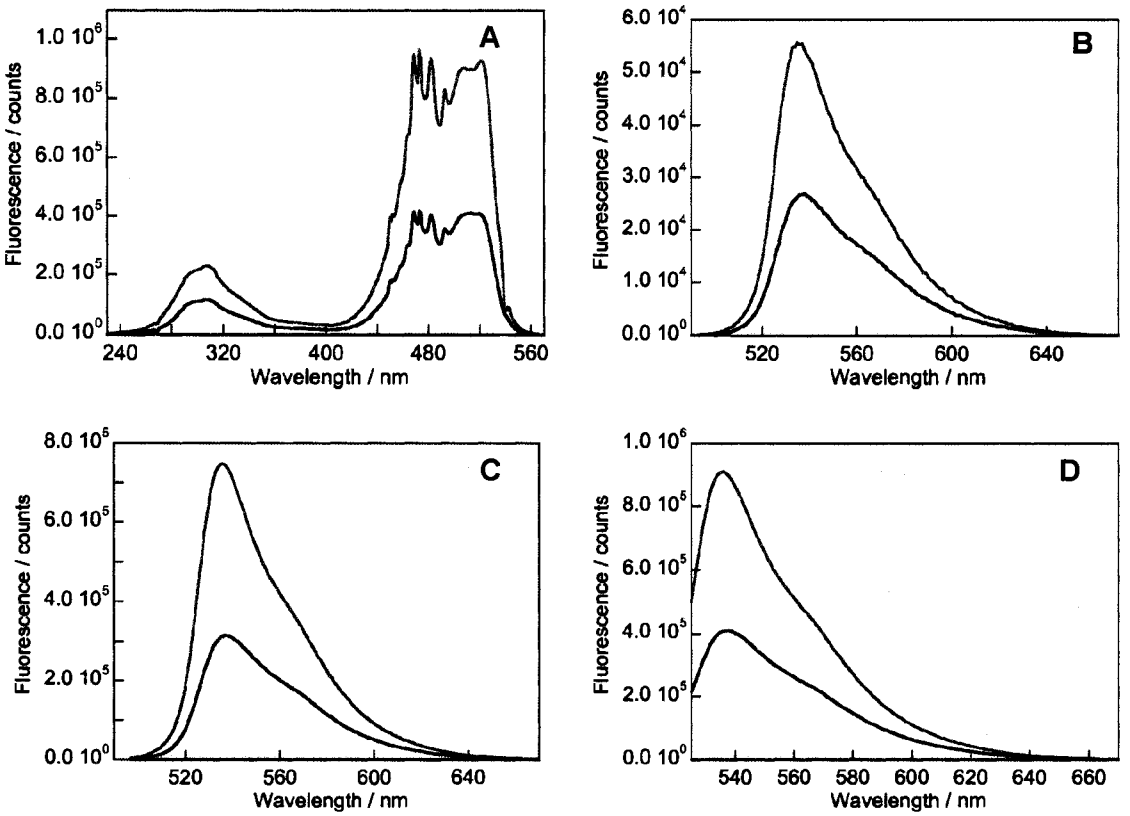


**Figure 4.9: Excitation (A) and emission (B-D) spectra of 20 μM PTO alone (purple, blends with baseline in all four cases) and in the presence of 200 μM dsDNA (red) or 200 μM ssDNA (black) in 10 mM Tris buffer (pH 7.4) at room temperature. Excitation spectra (A) were monitored at 537 nm for PTO and PTO/ssDNA and at 535 nm for TO/dsDNA; emission spectra were excited at 355 nm (B), 487 nm (C) and 515 nm (D).**

In the TO excitation spectrum there are peaks around ~475 nm (most likely lamp fine structure) and ~510 nm (monomer fluorescence), as seen in Figure 4.10A. TO in dsDNA and in ssDNA emits at 530 and 535 nm, respectively, independent of the excitation wavelength (see Figure 4.10B-D), signifying that all excited species lead to monomer fluorescence. However, there is a small shoulder in each emission spectrum, which could be a (minor) contribution from the *cis* isomer or a vibrational band (from the *trans* monomer). As with PTO, the TO

aggregates that contribute to fluorescence must either transfer their energy to the monomer through FRET and the monomer fluoresces, or dissociate into monomers and then fluoresce. In all of the cases, the area under the fluorescence curve was 3.6 to 5.1 times larger for TO/dsDNA than for TO/ssDNA, consistent with the dye being more rotationally restricted in dsDNA compared to ssDNA. The difference in the areas is approximately double that for PTO (a factor of 1.9 to 2.2).

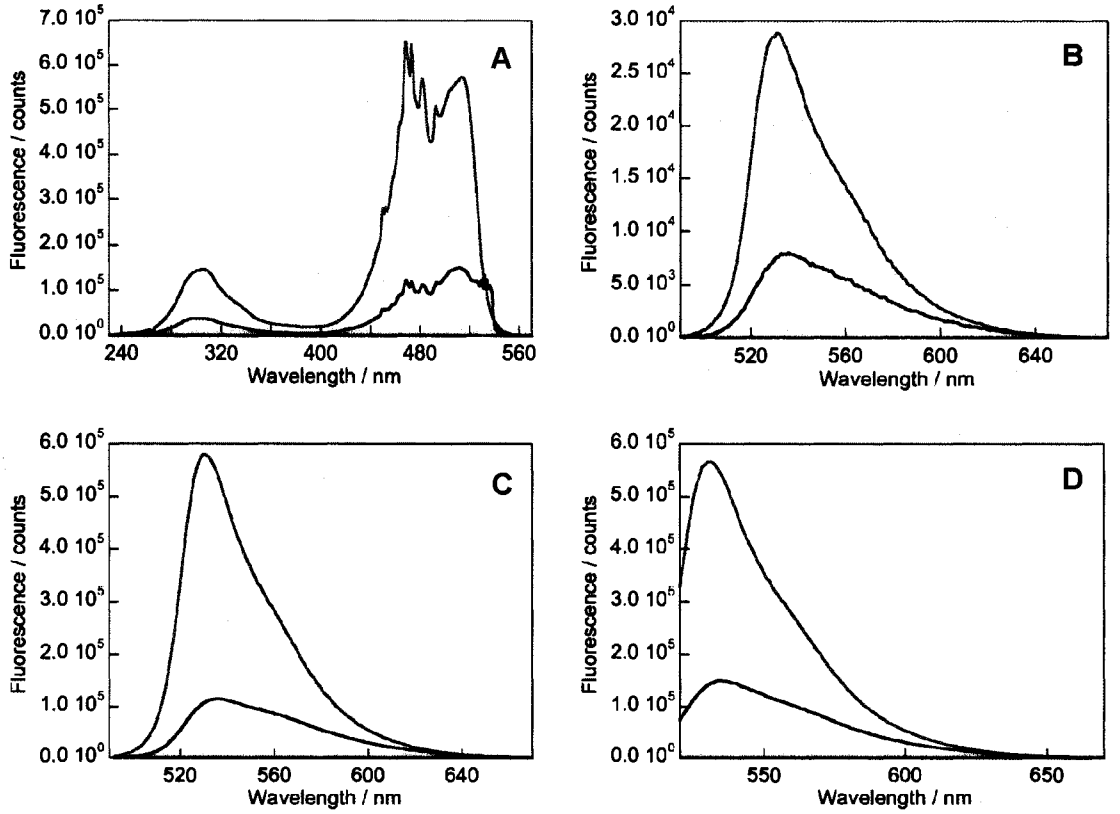


**Figure 4.10: (A) Excitation and (B-D) emission spectra of 20 µM TO alone (purple, blends with the baseline in all four cases) and in the presence of 200 µM dsDNA (red) or 200 µM ssDNA (black) in 10 mM Tris buffer (pH 7.4) at room temperature. Excitation spectra (A) were monitored at 530 nm for TO and TO/dsDNA and at 535 nm for TO/ssDNA; emission spectra were excited at 355 nm (B), 482 nm (C) and 510 nm (D).**

In the PG excitation spectrum there are peaks around ~475 nm (most likely lamp fine structure) and ~505 nm (monomer fluorescence), as seen in Figure 4.11A. PG in dsDNA and in ssDNA emits at 526 and 532 nm, respectively, independent of the excitation wavelength (see Figure 4.11B-D), signifying that all excited species lead to monomer fluorescence. Thus the PG aggregates must either transfer their energy to the monomer through FRET and the monomer fluoresces, or dissociate into monomers and then fluoresce. In all of the cases, the area under the fluorescence curve was 3.3 to 3.5 times larger for PG/dsDNA than for PG/ssDNA, consistent with the dye being more rotationally restricted in dsDNA compared to ssDNA. The difference in fluorescence falls in between that of PTO and TO.

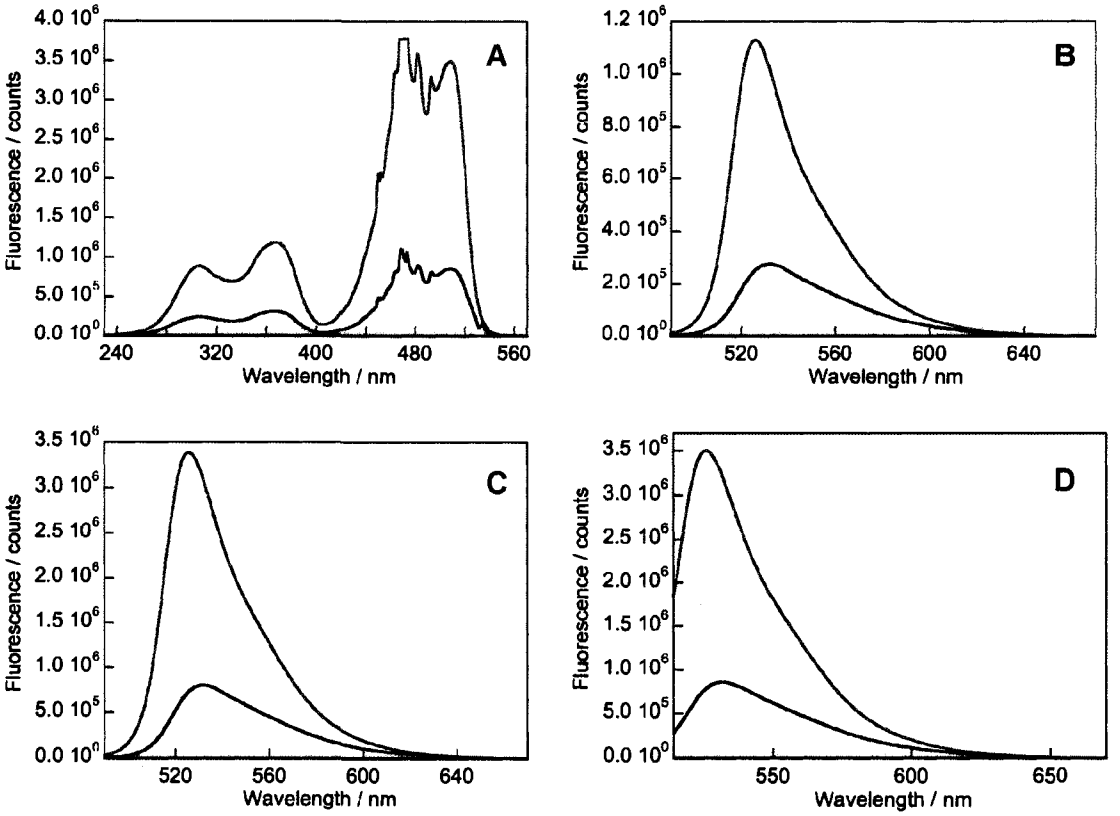


**Figure 4.11: (A) Excitation and (B-D) emission spectra of 20 μM PG alone (purple, blends with the baseline in all four cases) and in the presence of 200 μM dsDNA (red) or 200 μM ssDNA (black) in 10 mM Tris buffer (pH 7.4) at room temperature. Excitation spectra (A) were monitored at 532 nm for PG and PG/ssDNA and at 526 nm for PG/dsDNA; emission spectra were excited at 355 nm (B), 475 nm (C) and 504 nm (D).**

As was previously observed for PG,[26] the absorption bands of PTO and TO are slightly broader for the dye/ssDNA complex than for the dye/dsDNA complex, and significantly broader for the unbound dye (see Figure 4.12). The fluorescence emission of all three dyes is broader in ssDNA than in dsDNA (see Figure 4.12). The narrowing of the absorbance and fluorescence spectra upon complexation with DNA has been assigned to the loss of some of the equilibrated excited state rotational conformers upon going from buffer to DNA.[26]

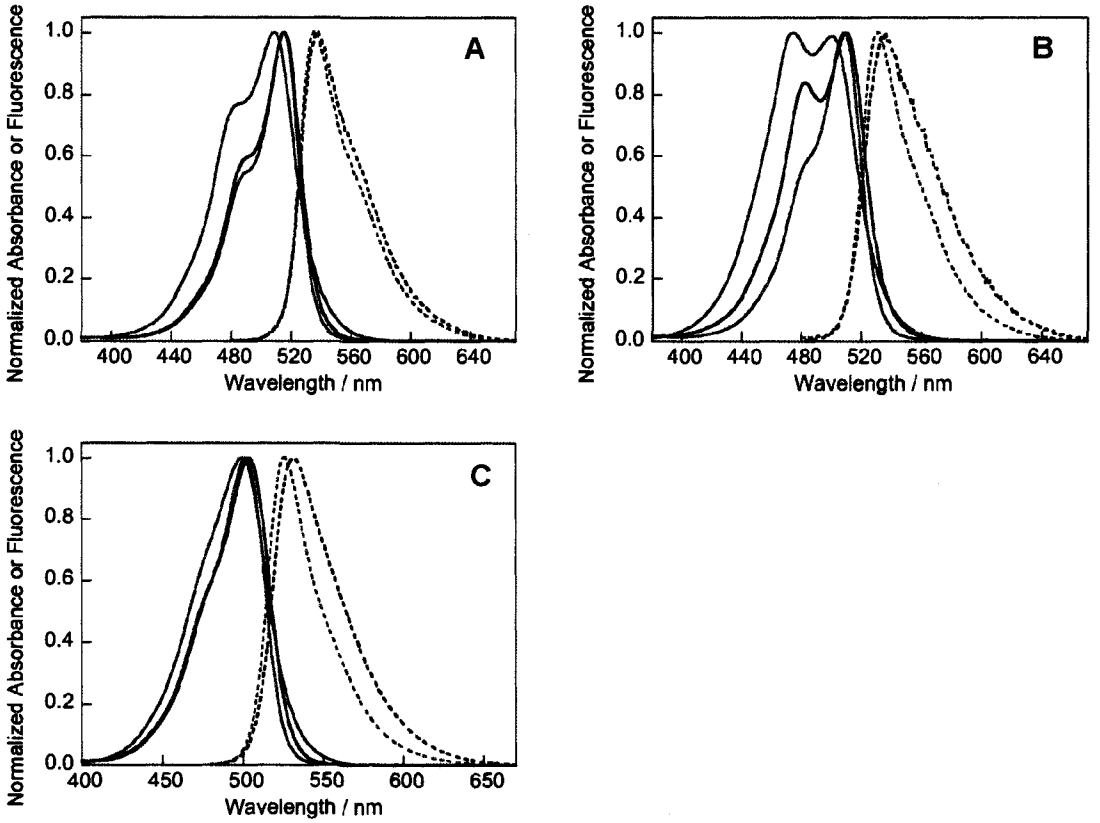


**Figure 4.12: Normalized absorption spectra (solid lines) and normalized fluorescence emission spectra (dashed lines, excited at 355 nm) of 20 μM dye alone (purple), with 200 μM dsDNA (red), and with 200 μM ssDNA (black) in 10 mM Tris buffer, recorded at room temperature using a 10 mm path length. (A) PTO, (B) TO, and (C) PG.**

Figure 4.13 shows the fluorescence decay signals of both PTO and TO in ss- and dsDNA, upon 355 nm laser excitation, at a 1:10 dye:base and dye:base pair ratio, respectively. In both ss- and dsDNA, PTO fluorescence decays biexponentially (see Table 4.1), even when a large excess of DNA base pairs are present and intercalation should be the dominant binding mode. This suggests that PTO binds to CT DNA in more than one intercalation site or in more than one position. These findings differ from those of PG with ds CT DNA, where PG decays monoexponentially with a 4.26 ns lifetime.[29] Although there is a very small shoulder

in the steady-state emission spectra of the PTO/DNA complexes (see Figure 4.9B-D), it seems unlikely that any of the components in the time-resolved decays arise from the *cis* isomer, as the pre-exponential factors are all 23% or larger, which is a substantial contribution. When the dye/base pair (d/b) ratio was 0.10 or lower for PTO in dsDNA, the fluorescence decays contained components with mean values of 3.11 ± 0.1 ns and 1.29 ± 0.09 ns. Upon increasing the ratio to 9 dye molecules per 10 base pairs, the fluorescence lifetimes decreased, most likely due to intermolecular quenching by nearby dye molecules. Interestingly, for the (20 μM PTO/ 200 μM ssDNA) complex, one fluorescence decay component closely resembles that of PTO in poly(dA), suggesting that PTO binds to A bases in ss CT DNA.

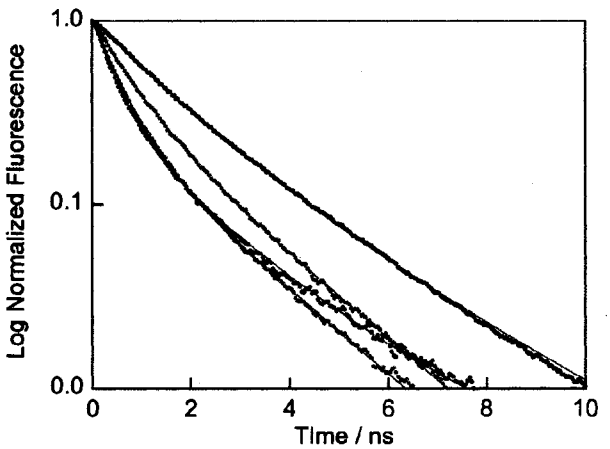


**Figure 4.13: Semi-log plot of the normalized fluorescence decays following 35 ps laser excitation (355 nm) of buffered (pH 7.4) solutions containing 20 μM dye and 200 μM CT DNA, recorded at room temperature for PTO/dsDNA (black), PTO/ssDNA (red), TO/dsDNA (purple) and TO/ssDNA (blue).**

**Table 4.1: Fluorescence decay data for cyanine dyes in the presence of double-stranded CT DNA.[a] Data for the dyes in the presence of single-stranded CT DNA is marked with a * in the d/b column.**

| Dye | d/b[b] | [dye] / μM | $\tau_1$ / ns | $A_1$ (%) | $\tau_2$ / ns | $A_2$ (%) | $\tau$ / ns[c] | $\tau$(dsDNA)/ $\tau$(ssDNA) |
|---|---|---|---|---|---|---|---|---|
| PTO | 0.02 | 20 | 1.14 | 30 | 3.16 | 70 | 2.19 | 1.3 |
| PTO | 0.02* | 20 | 1.03 | 45 | 3.09 | 55 | 1.66 | |
| PTO | 0.10 | 9 | 1.30 | 55 | 2.93 | 45 | 1.74 | - |
| PTO | 0.10 | 20 | 1.44 | 77 | 3.25 | 23 | 1.65 | 2.5 |
| PTO | 0.10* | 20 | 0.52 | 73 | 1.90 | 27 | 0.65 | |
| PTO | 0.90 | 20 | 0.78 | 41 | 1.87 | 59 | 1.17 | - |
| TO | 0.10 | 20 | 0.72 | 60 | 1.94 | 40 | 0.96 | 1.7 |
| TO[d] | 0.10* | 20 | 0.44 | 69 | 1.71 | 29 | 0.57 | |
| PG[e] | 0.16 | 11 | 4.5 | - | - | - | 4.5 | 2.7 |
| PG[e] | 0.16* | 11 | 1.16 | 51 | 3.09 | 49 | 1.67 | |

[a] Typical errors are around 0.05 ns for lifetimes with pre-exponential factors exceeding 40%, but can be as large as 0.2 ns for pre-exponential factors around 20%. [b] d/b represents the dye-to-base pair ratio for dsDNA and the dye-to-base ratio for ssDNA. [c] Average lifetime $\tau = (A_1k_1+A_2k_2)^{-1}$.
[d] Pre-exponential factors do not add up to 1 as a third component (5.56 ns, 2%) is required. [e] From reference 45.

The average lifetime of TO in dsDNA is significantly shorter than that of PTO in dsDNA; both average lifetimes are much shorter than that of PG in dsDNA (see Table 4.1). In contrast, the average lifetimes of TO and PTO in ssDNA were remarkably similar (for the same dye:DNA base concentration). They both had lifetime components with mean values of 0.48 ± 0.04 ns (71 ± 2%) and 1.80 ± 0.10 ns (28 ± 1%), although an extra component was needed to obtain an adequate fit for TO/ssDNA. These findings suggest that TO and PTO interact similarly with ss CT DNA, but differently with ds CT DNA.

For all three dyes, the average fluorescence lifetime is longer in dsDNA compared to ssDNA. However, PG is the only dye for which the fluorescence decay in dsDNA is monoexponential.[45]

#### 4.2.1.3. SDS Extractions

For the sodium dodecyl sulfate (SDS) experiments, the dye was added to the CT DNA the day before the experiment. The only exception was the 0 mM SDS solution, where the dye and DNA were mixed at the beginning of the fluorescence measurement. When PTO was injected into the CT DNA solution, there was an initial jump in fluorescence (see Figure 4.14) and then the fluorescence increased slightly over the next 60 seconds to reach its maximal value. This slight increase may be due to repositioning of bound dye molecules, from groove-bound to intercalated, as has been proposed for Δ,Δ-[μ-(11,11'-bi(dipyrido-[3,2-*a*:2',3'-*c*]-phenazinyl))(1,10-phenanthroline)$_4$Ru$_2$]$^{4+}$.[46] In all of the cases involving SDS, the change in fluorescence occurred within the first 1 or 2 seconds, making it impossible to measure the dye dissocation rate using the fluorimeter. In order to measure these rates, a stopped-flow apparatus is required. However, as free PTO is essentially non-fluorescent while bound PTO fluoresces, the measurements do report on the percentage of associated dye after SDS extraction. When SDS is absent, the fluorescence is maximal and one can assume that all dye is bound considering the low dye:base pair ratio (1:10). In the presence of 1 mM SDS, only 33% of PTO remains bound to the CT DNA. At SDS concentrations 2 mM and greater, there is negligible fluorescence thus all of the dye has been extracted from the DNA. These results agree with those of Westerlund *et al.*,[23] who demonstrated that surfactants play an active role in the extraction of cationic intercalators from DNA. The critical micelle concentration (CMC) for SDS in 0.1 M NaCl at 21°C is $1.5 \times 10^{-3}$ M,[47] although our buffer also contains 10 mM Tris and 1 mM EDTA which may change this number slightly. If we take the CMC to be 1.5 mM, then our results indicate that SDS concentrations above the CMC will extract all intercalated dye molecules.

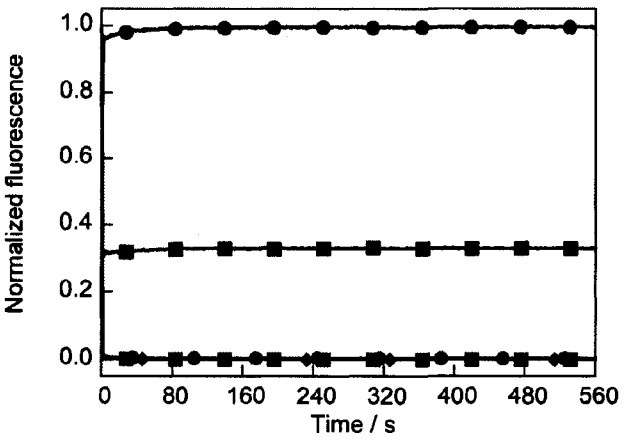


**Figure 4.14: Normalized (to the maximum intensity of the control) fluorescence of 3.5 μM PTO in the presence of 35 μM CT DNA in 10 mM Tris buffer (pH 7.4, 0.1 M NaCl), excited at 480 nm and monitored at 532 nm. Recorded at room temperature for 0 (●), 1 (■), 2 (red circles), 5 (blue squares) and 100 (green diamonds) mM SDS. Each trace is the average of 2 trials; the traces are continuous, the points simply identify the traces.**

When 2 or 100 mM SDS was added to PTO/CT DNA, the PTO ICD disappeared, as seen in Figure 4.15A, indicating dissociation of the dye from the DNA. This supports SDS removing PTO from the DNA, rather than quenching its fluorescence. Examination of the CD spectrum (Figure 4.15B) does not show an effect of SDS on the secondary structure of the DNA.

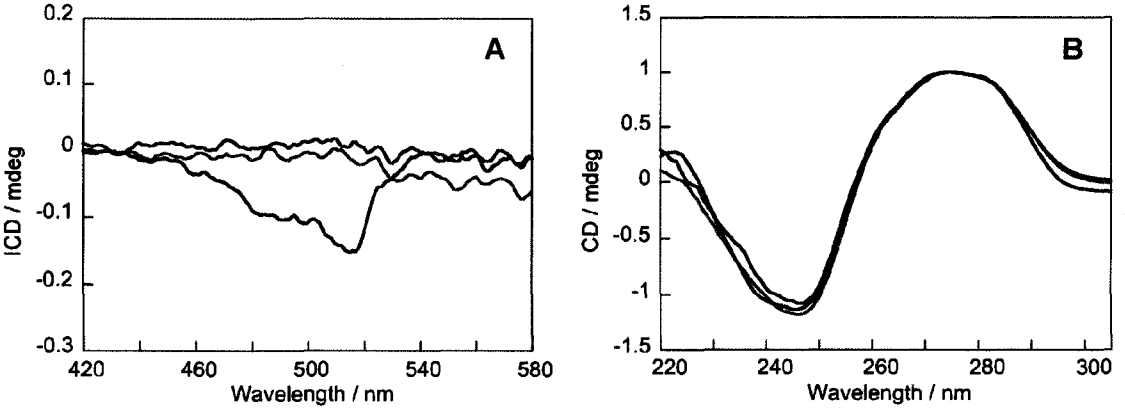


**Figure 4.15: (A) ICD and (B) CD of 7 μM PTO in the presence of 70 μM CT DNA in 10 mM Tris buffer (pH 7.4). Recorded at room temperature using a 1 mm path length for 0 (black), 2 (red) and 100 (blue) mM SDS.**

The effect of SDS on PTO absorption was examined, alone and complexed with dsDNA (Figure 4.16). Addition of SDS to the dye in buffer caused a slight red-shift (1 or 2 nanometers) of both the monomer absorption band and the shoulder (Figure 4.16A). There was also a slight increase in the monomer absorption band and a decrease in the shoulder, indicating that the anionic surfactant breaks up the dimers/aggregates. In the polar environment of the micelles, the dye should only be present in its monomeric form, thus the shoulder in the absorption spectrum (when SDS is present) represents a vibrational feature from the monomer. Consequently, in PTO/DNA solutions the absorbance around 487 nm consists of both a monomer vibrational band and a dimer band.

Upon addition of SDS to PTO/CT DNA, there was a blue-shift and an increase in absorbance for both the monomer absorption band and the dimer/aggregate shoulder, as shown in Figure 4.16B. As a general rule, intercalation in DNA causes a shift of the absorption maximum towards longer wavelengths and a decrease in extinction coefficient.[24] Since the opposite effect occurs, it suggests that SDS dissociates the dye from CT DNA, which is consistent with the fluorescence and ICD results. The same trends are also observed for PTO with poly(dA)•poly(dT) and poly(dG)•poly(dC), indicating that SDS dissociates the

dye from the double-stranded homopolymers. However, the change in absorbance (70% increase) for the PTO/poly(dG)•poly(dC) complex (Figure 4.16D) upon addition of SDS is much greater than in the other dye/DNA complexes, but this just reflects that PTO absorption is lower in poly(dG)•poly(dC) than in the other complexes as the absorbance intensity of the dye/poly(dG)•poly(dC)/SDS system resembles that of the other SDS systems.

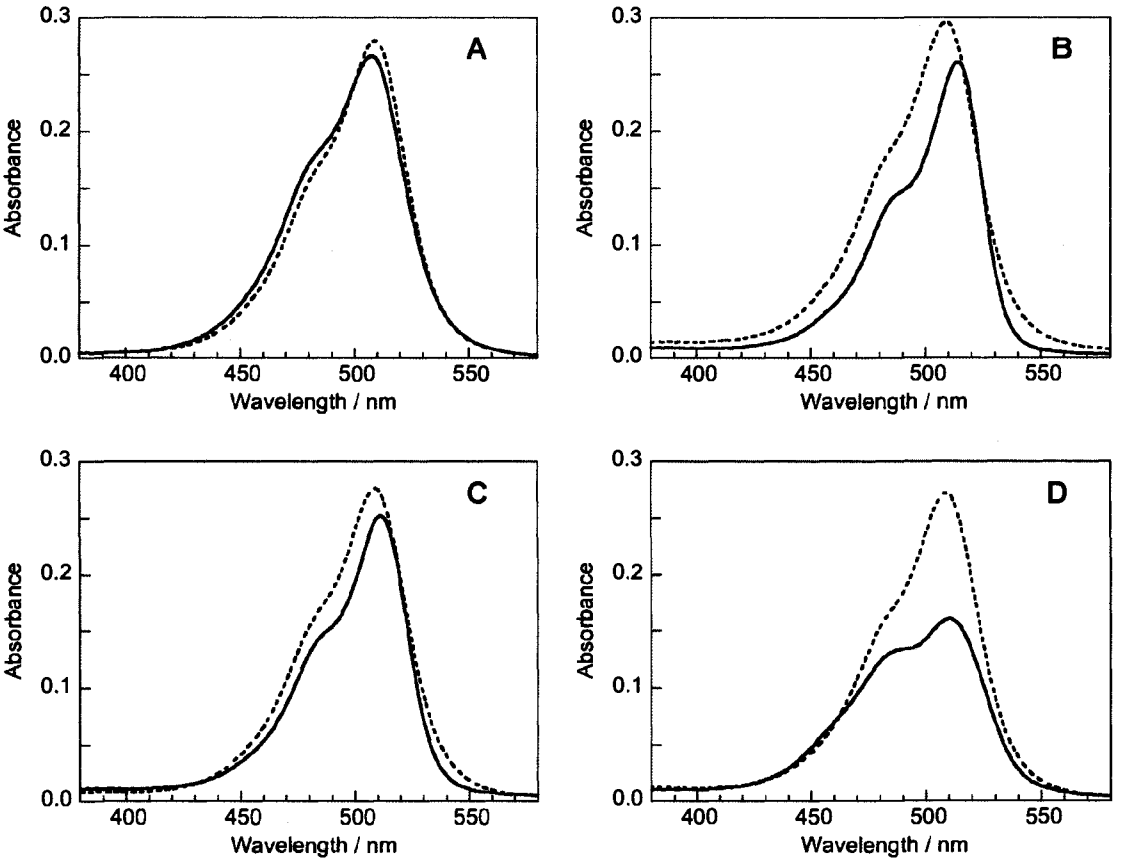


**Figure 4.16: Absorption spectra of (A) 3.5 µM PTO alone and in the presence of (B-D) 35 µM dsDNA in 10 mM Tris buffer (pH 7.4), recorded at room temperature using a 10 mm path length. (B) CT DNA; (C) poly(dA)•poly(dT); (D) poly(dG)•poly(dC). Full lines were recorded without SDS, and dashed lines were recorded in the presence of 5 mM SDS.**

The PicoGreen/CT DNA complex behaved similarly to PTO/CT DNA, in that for SDS concentrations 2 mM and greater, complete dye dissociation occurred, as seen in Figure 4.17. Like PTO, PG dissociation rates were too fast to measure on our fluorimeter. Comparison of Figure 4.14 and Figure 4.17 shows that 1 mM SDS was less effective at dissociating PG (67% residual fluorescence) than PTO (33% residual fluorescence), and PG dissociation using 1 mM SDS took longer than PTO dissociation, as evidenced by the slower fluorescence decrease.

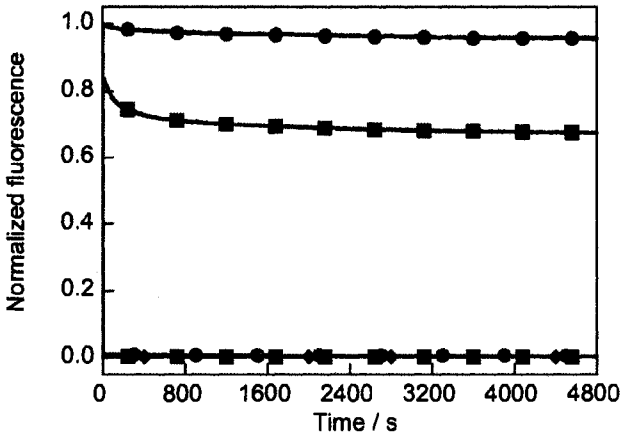


**Figure 4.17: Normalized (to the maximum intensity of the control) fluorescence of 3.5 μM PG in the presence of 35 μM CT DNA in 10 mM Tris buffer (pH 7.4, 0.1 M NaCl), excited at 480 nm and monitored at 524 nm. Recorded at room temperature for 0 (●), 1 (■), 2 (red circles), 5 (blue squares) and 100 (green diamonds) mM SDS.**

## 4.2.2. Hybridization Studies

### 4.2.2.1. Duplex Homopolymers

The CD spectra of the single-stranded homopolymers as well as the duplexes provided reference spectra in the absence of any dye. The spectra of poly(dA), poly(dT) and poly(dA)•poly(dT) (Figure 4.18A) match previously published spectra.[28,48] Comparison of the CD spectra of poly(dG) and of poly(dC) with spectra

in the literature[28,49] indicate that both single-stranded homopolymers exist as the self-complexed forms. However, when mixed together (and heated at 95°C and then allowed to return to room temperature) they form double-stranded poly(dG)•poly(dC), evidenced by the CD spectrum (Figure 4.18B) that resembles that in the literature.[49]

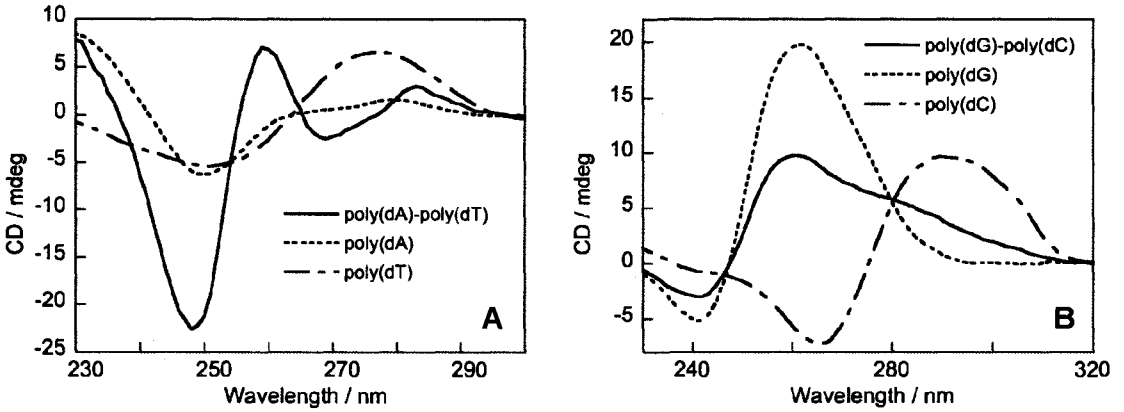


**Figure 4.18: Circular dichroism from DNA homopolymers in 10 mM Tris buffer (pH 7.4), 10 mm path length, recorded at 20°C for (A) 35 μM poly(dA)•poly(dT), 35 μM poly(dA), and 35 μM poly(dT) and (B) 20 μM poly(dG)•poly(dC), 40 μM poly(dG) and 40 μM poly(dC). The 20 μM poly(dG)•poly(dC) solution was heated at 95°C and then allowed to return to room temperature. The other solutions were not subjected to thermal cycling.**

### 4.2.2.2. PicoGreen and DNA Homopolymers

In the hybridization experiments, the dye was incubated with the DNA for 4 hours and the strands were allowed to hybridize for 17 hours while stored at room temperature and protected from light exposure. When PG was added to single-stranded poly(dA) and poly(dT) before hybridization of the strands, the dye exhibited negative ICD around 493 nm (shown in Figure 4.19A). A +/- exciton, which consists of two bands of equal magnitude where the longer wavelength band is positive and the shorter wavelength band is negative, was observed only in the

case where PG was added to poly(dT) before hybridization. However, the exciton signal differed from that of PG with single-stranded poly(dT) (discussed in Section 3.2.5) as the peak was red-shifted by approximately 4 nm and the trough was red-shifted by approximately 20 nm. When PG was added after hybridization of the strands, a unique signal was obtained, with a trough around 504 nm. After heating the PG/poly(dA)•poly(dT) complex to 90°C (to dissociate the dye from the DNA) and then allowing it to return to room temperature (to allow hybridization of the strands in the presence of the dye), a different ICD was observed which closely resembled that of the solution where the dye was added to poly(dT) before hybridization. This indicates that PG prefers to bind to poly(dT), in agreement with previous results.[29] Our findings suggest that a new complex is formed when the dye is present before hybridization of the single-stranded homopolymers compared to after hybridization.

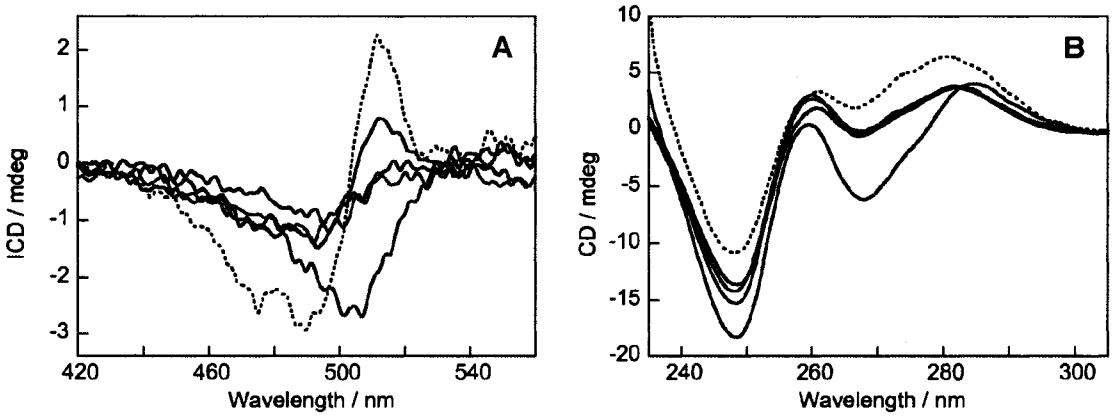


**Figure 4.19: (A) ICD and (B) CD from 3.5 μM PG / 35 μM poly(dA)•poly(dT) solutions in 10 mM Tris buffer (pH 7.4), 10 mm path length. Recorded at 20°C for [PG+poly(dT)]+polydA (black), [PG+poly(dA)]+poly(dT) (red), [PG+poly(dA)]+[PG+poly(dT)] (green) and [poly(dA)•poly(dT)]+PG (blue). The dashed line was recorded at 20°C after thermal cycling of the solution.**

Very similar CD spectra (Figure 4.19B) were obtained when (i) poly(dA) was added to poly(dT) incubated with PG, (ii) poly(dT) was mixed with poly(dA)

incubated with the dye, or (iii) both single strands were incubated with the dye. However, a different CD spectrum was observed for the complex where the dye was added after hybridization, specifically the long-wavelength peak was red-shifted and the ratio of the two peaks had changed. None of these spectra matched the spectrum of poly(dA)•poly(dT) (Figure 4.18A). These results suggest that addition of PG to poly(dA)•poly(dT) (either before or after hybridization) affects the secondary structure of the DNA, although the effects are different depending on when the dye was added.

The affinity of PG for these complexes was studied using SDS to enhance dissociation of the dye from the DNA. In the absence of SDS, when PG is added to poly(dA)•poly(dT) there is a jump in fluorescence as PG intercalates, followed by a slight (and slower) increase in fluorescence, as seen in Figure 4.20, which is presumably due to the movement of some dye molecules from groove-bound to intercalated. Addition of 1 mM SDS results in the dissociation of 10% and 76% of bound dye molecules from the complexes where the dye was added before and after hybridization, respectively. When the dye was added to poly(dA)•poly(dT), SDS concentrations of 1.5 mM, 2 mM, and 5 mM or greater caused 98%, 99% and 100% dissociation of the dye. A marked difference was observed when SDS was added to complexes where PG was incubated with the single strands before hybridization. Within the first 2 seconds of adding 1.5 mM SDS, there was a 58% drop in fluorescence, followed by a much slower decrease, which began to level off at a 94% loss of fluorescence after 6000 seconds. Similarly to the complex where PG was added after hybridization, addition of 2 and 100 mM SDS essentially dissociated all of the dye (98% and 100% dissociation, respectively) but, in contrast, took a much longer time to do so, as can be seen in Figure 4.20. These results indicate that two different complexes are formed, and that it is easier to extract PG from the complex where the dye was added after strand hybridization.

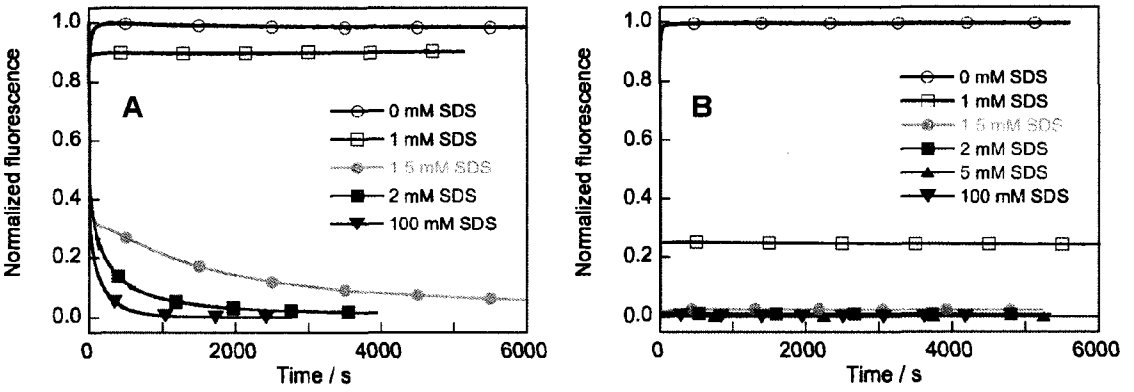


**Figure 4.20: Normalized (to the maximum intensity of the control) fluorescence of 3.5 μM PG in the presence of 35 μM poly(dA)•poly(dT) in 10 mM Tris buffer (pH 7.4), excited at 480 nm and monitored at 520 nm. Recorded at room temperature for (A) [PG+poly(dA)]+[PG+poly(dT)] and (B) [poly(dA)+poly(dT)]+PG.**

In contrast to PG and poly(dA)•poly(dT), the ICD of PG in poly(dG)•poly(dC) was not affected by the order of mixing. The ICD obtained when poly(dC) was added to poly(dG) incubated with PG was very similar to that obtained when PG was added to the hybridized strands, as seen in Figure 4.21A. The ICD was identical to that of PG with single-stranded poly(dG) (see Section 3.2.5), suggesting that the dye prefers binding between two G bases or between two GC base pairs, but not between two C bases (which did not show any ICD). Thermal cycling of the solution where PG was added after hybridization of the DNA did not change the shape of the ICD whatsoever, indicating that the dye is bound in the same manner as before thermal cycling.

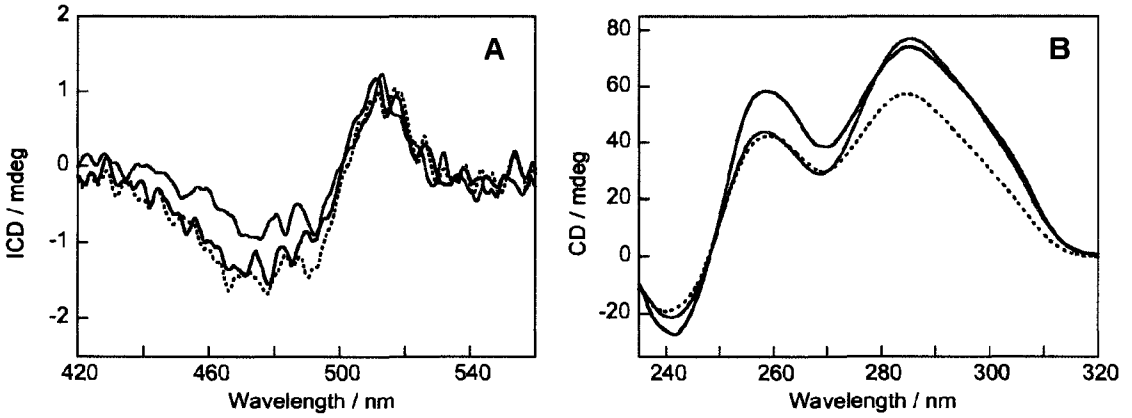


**Figure 4.21: (A) ICD and (B) CD from 20 μM PG / 200 μM poly(dG)•poly(dC) solutions in 10 mM Tris buffer (pH 7.4), 5 mm path length. Recorded at 20°C for [PG+poly(dG)]+poly(dC) (red) and [poly(dG)•poly(dC)]+PG (blue). The dashed line was recorded at 20°C after thermal cycling of the solution.**

The CD spectra of poly(dG)•poly(dC) in the presence of PG (Figure 4.21B) do not resemble that of the dsDNA alone (Figure 4.18B). Although the intensities of the 259 and 283 nm peaks differed, the 283 nm peak was more intense than the 259 nm peak for all of the PG/poly(dG)•poly(dC) solutions examined, which is opposite to that of the dsDNA alone and illustrates the effect of the dye on the DNA.

### 4.2.2.3. Thiazole Orange and DNA Homopolymers

When TO was added before hybridization of poly(dA) and poly(dT), the presence of the dye did not appear to have an effect on the complex that was formed since the ICD (Figure 4.22A) was essentially the same for the solutions where the dye was added before and after hybridization. The magnitude and shape of the ICD of the TO/poly(dA)•poly(dT) complex where the dye was added after hybridization was identical to that of TO and single-stranded poly(dA), suggesting that in double-stranded poly(dA)•poly(dT) TO prefers binding between two A bases, rather than binding between two T bases or two AT base pairs. However, when the dye was added to each strand before hybridization, the shape of the ICD resembled

that of TO/poly(dA) but the magnitude was about half, indicating that TO binds to A bases but other association processes also occur.

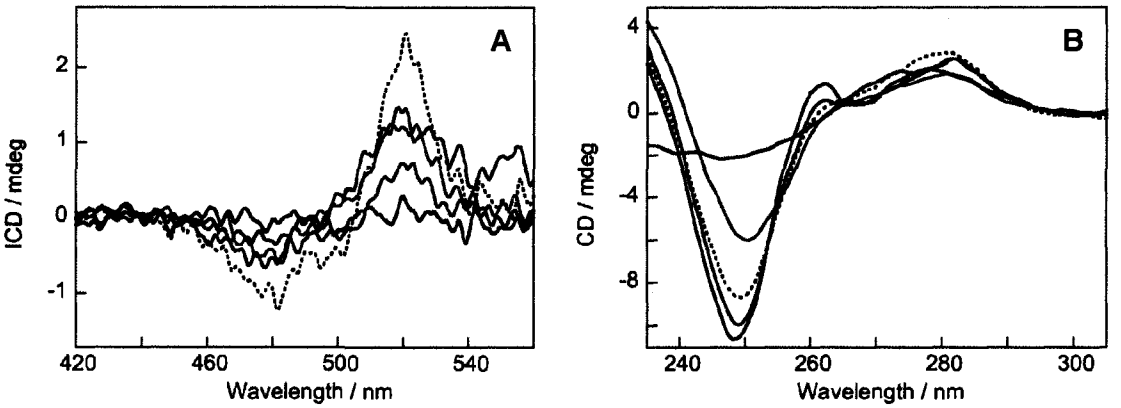


**Figure 4.22: (A) ICD and (B) CD from 3.5 μM TO / 35 μM DNA solutions in 10 mM Tris buffer (pH 7.4), 10 mm path length. Recorded at 20°C for TO+poly(dA) (red), TO+poly(dT) (black), [TO+poly(dA)]+[TO+poly(dT)] (green) and [poly(dA)•poly(dT)]+TO (blue). The dashed line was recorded at 20°C after thermal cycling of the solution.**

Regardless of when the dye was added, the dsDNA complexes both showed a CD trough at 247 nm (Figure 4.22B), characteristic of poly(dA)•poly(dT),[28] indicating that the strands globally hybridized. However, the ratio of the two peaks differed significantly from that of the DNA alone, showing that TO had an effect on the secondary structure of the DNA.

The shapes of the ICD of TO solutions where the dye was added before and after hybridization of poly(dG) and poly(dC) were very similar, as seen in Figure 4.23A. The spectra share some of the same characteristics as TO with single-stranded poly(dG) (see Section 3.2.5), specifically a trough at 476 nm and a peak at 490 nm. Although the magnitudes of the troughs are all roughly the same, the magnitude of the TO/poly(dG) 490 nm peak is approximately two times larger than that of TO/poly(dG)•poly(dC). Some differences between the TO/poly(dG) complex and the two TO/dsDNA complexes are that the long wavelength peak in

the single-stranded complex is around 511 nm while it is around 519 nm in the double-stranded complexes, and the ratios of the two peaks differ. As TO/poly(dC) does not show any ICD, it would seem that the observed ICD for the two TO/poly(dG)•poly(dC) complexes arises from an association between TO and G bases as well as TO and GC base pairs. Interestingly, upon thermal cycling of the solutions a unique ICD was obtained which does not resemble that of TO/poly(dG) or TO/poly(dC) or either complex before thermal cycling. This suggests that heating the complexes places the dye molecules in thermodynamically favourable orientations, which are similar to those of TO with single-stranded poly(dA) except red-shifted by 4-5 nm.

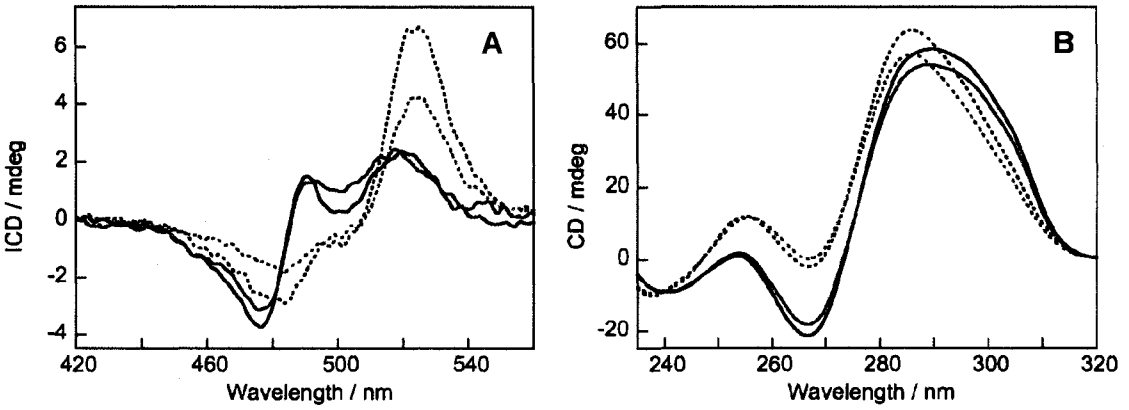


**Figure 4.23: (A) ICD and (B) CD from 7 µM TO / 70 µM poly(dG)•poly(dC) solutions in 10 mM Tris buffer (pH 7.4), 10 mm path length. Recorded at 20°C for [TO+poly(dG)]+[TO+poly(dC)] (red) and [poly(dG)•poly(dC)]+TO (blue). The dashed lines were recorded at 20°C after thermal cycling of the solutions.**

The CD of the TO complexes where the dye was added before and after hybridization of poly(dG) and poly(dC) are extremely similar (Figure 4.23B), and they undergo the same changes upon thermal cycling. Before thermal cycling of the complexes, the spectra more closely resembled the CD of poly(dC) than that of poly(dG)•poly(dC) (see Figure 4.18B), suggesting that the dye significantly altered the secondary structure of the DNA.

#### 4.2.2.4. N-Propyl Pyridinium Thiazole Orange and DNA Homopolymers

Addition of PTO to poly(dA) and/or poly(dT) before hybridization resulted in the formation of a new complex, as evidenced by its distinct ICD (Figure 4.24A). When the dye was added to hybridized poly(dA)•poly(dT) the ICD was relatively weak, but doubling the concentration gave a stronger negative signal that was identical in shape (data not shown). The ICD of PTO/poly(dA)•poly(dT) where the dye was added after hybridization does not correspond to either of the ICD signals observed for PTO with the single strands (see Section 3.2.5), thus the trough around 512 nm is most likely due to PTO intercalated between AT base pairs. The ICD spectra of the complexes where the dye was added before strand hybridization resemble the ICD spectrum of PTO with single-stranded poly(dA) although the intensities of the bands are different; the locations of the troughs and the peak differ by no more than 2 nm, and the shoulder in PTO/poly(dA) is a visible trough in the PTO/poly(dA)•poly(dT) complexes where the dye was added before hybridization. It appears as though PTO prefers binding between A bases in the presence of single strands of poly(dA) and poly(dT), even when incubated with poly(dT). Thermal cycling of the solution where the dye was added after hybridization produced an ICD that resembles the ICD of the solutions where the dye was incubated with the single strands before hybridization, although less intense.

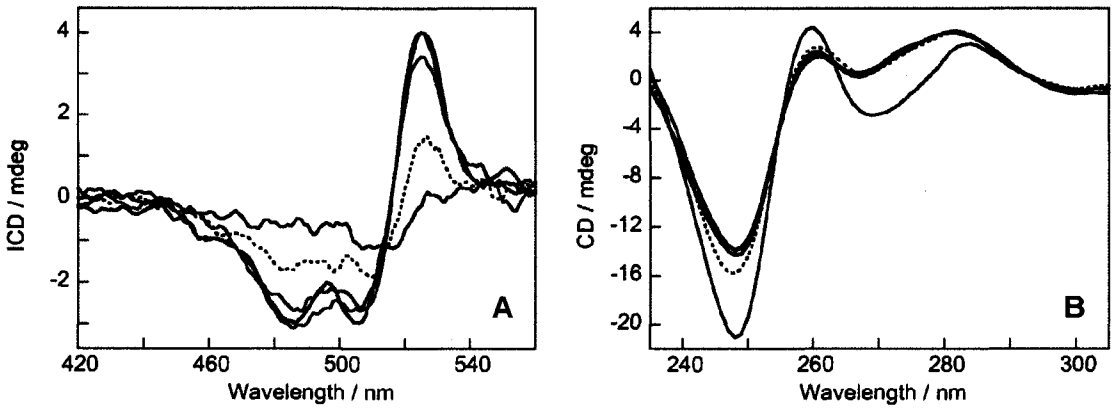


**Figure 4.24: (A) ICD and (B) CD from 3.5 μM PTO / 35 μM poly(dA)•poly(dT) solutions in 10 mM Tris buffer (pH 7.4), 10 mm path length. Recorded at 20°C for [PTO+poly(dT)]+polydA (black), [PTO+poly(dA)]+poly(dT) (red), [PTO+poly(dA)]+[PTO+poly(dT)] (green) and [poly(dA)•poly(dT)]+PTO (blue). The dashed line was recorded at 20°C after thermal cycling of the solution.**

The CD of the solution where PTO was added to hybridized poly(dA)•poly(dT) (Figure 4.24B) resembles that of the DNA alone (Figure 4.18A), suggesting that in this case the dye has little effect on the secondary structure of the DNA. However, when that solution was subjected to thermal cycling or when the dye was incubated with the single strand(s) before hybridization, a new complex was obtained, as evidenced by a different CD spectrum. This spectrum has a long-wavelength peak at 281 nm (compared to 283 nm for the complex where the dye was added after hybridization), no trough at 269 nm but it approaches zero at 267 nm, and the long-wavelength peak is more intense than the shorter-wavelength peak.

Dr. C. Schweitzer found that when the PTO/poly(dA)•poly(dT) solutions were left for two weeks at room temperature without protection from light, the DNA deteriorated (as seen by a significant decrease in the CD signal in the 200-300 nm region), but the ICD of the dye (450-550 nm) was still clearly apparent for both complexes and the ICD signals had not changed shape. This indicates that

although the DNA degraded, the dye remained associated in the same manner during the two-week period, demonstrating the extraordinary stability of the new dye/DNA complex, which did not evolve towards a "regular" intercalation complex.

When comparing PTO fluorescence in dye/DNA complexes involving ss- and dsDNA, it can be seen that the fluorescence intensity upon 450 nm excitation of PTO is clearly different in all four cases (Figure 4.25). An important observation is that the spectrum of the complex formed by hybridization of the single strands in the presence of the dye corresponds neither to that obtained by addition of the dye to previously hybridized DNA, nor to that of the individual single strands, nor to any combination of these.

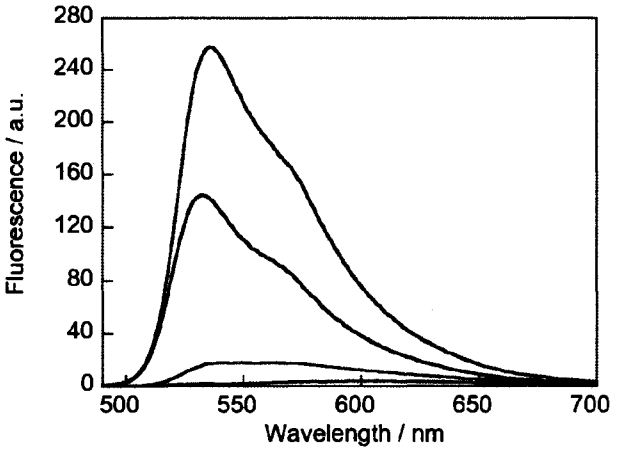


**Figure 4.25: Fluorescence of 6 μM PTO in the presence of 70 μM homopolymers in 10 mM Tris buffer (pH 7.4), excited at 450 nm. Recorded at room temperature for [PTO+poly(dA)]+ [PTO+poly(dT)] (green), [poly(dA)•poly(dT)]+PTO (blue), PTO+poly(dA) (red) and PTO+poly(dT) (black).**

Upon thermal cycling of the solution where the dye was added before hybridization of the strands, there was no significant change in the emission spectrum (Figure 4.26A). However, when the solution where the dye was added after hybridization was heated (dissociating the dye and denaturing the DNA) and

then allowed to return to room temperature (allowing renaturation in the presence of the dye), there was a 37% increase in the emission intensity (Figure 4.26B) as well as a shift of the fluorescence maximum from 531 nm to 534 nm (matching that of the solution where the dye was incubated with the ssDNA before hybridization). This indicates once again that a different complex is formed when the DNA strands hybridize in the presence of the dye compared to the complex formed when dye is added to hybridized DNA strands.

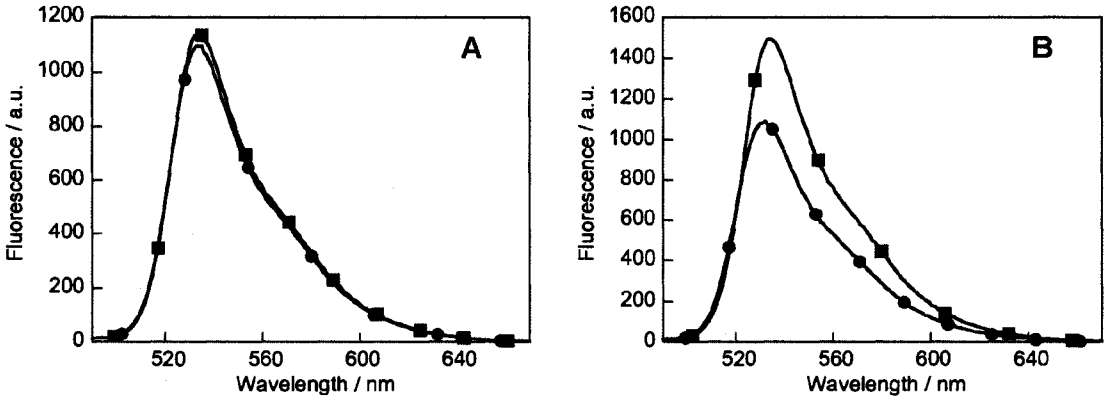


**Figure 4.26: Fluorescence of 3.5 μM PTO in the presence of 35 μM poly(dA)•poly(dT) in 10 mM Tris buffer (pH 7.4), excited at 355 nm. Recorded at room temperature (●) for solutions where the dye was added (A) before and (B) after strand hybridization. Solutions were then heated to 90°C, allowed to return to room temperature and their emission recorded (■).**

PTO fluorescence during strand hybridization was monitored as a function of time (Figure 4.27). The fluorescence emission was monitored for approximately 60 seconds before injection of either the dye or the complementary ssDNA, at which point, in all three cases, the fluorescence increased dramatically within 4 seconds. It was expected that upon formation of double-stranded DNA there would be a large increase in dye fluorescence as dsDNA is a more rigid environment than ssDNA. As noted in Chapter 3, the fluorescence was greater for PTO in poly(dA) than in poly(dT), as shown in Figure 4.27. When the dye was incubated with either poly(dA) or poly(dT) and the complementary strand was added, similar fluorescence

intensities were observed. In agreement with our previous results, when the dye was added to hybridized poly(dA)•poly(dT) the fluorescence intensity was less than that of the solutions where the dye was added before strand hybridization. Approximately six minutes after adding the dye to poly(dA)•poly(dT), the fluorescence had reached its maximal value. In a separate experiment (data not shown) the fluorescence emission of the PTO/ poly(dA)•poly(dT) complex where the dye was added after strand hybridization was monitored for 5000 seconds (83 minutes) and, after the initial increase, the intensity remained the same, thus it will never approach the intensity of the complexes where the dye was added before strand hybridization.

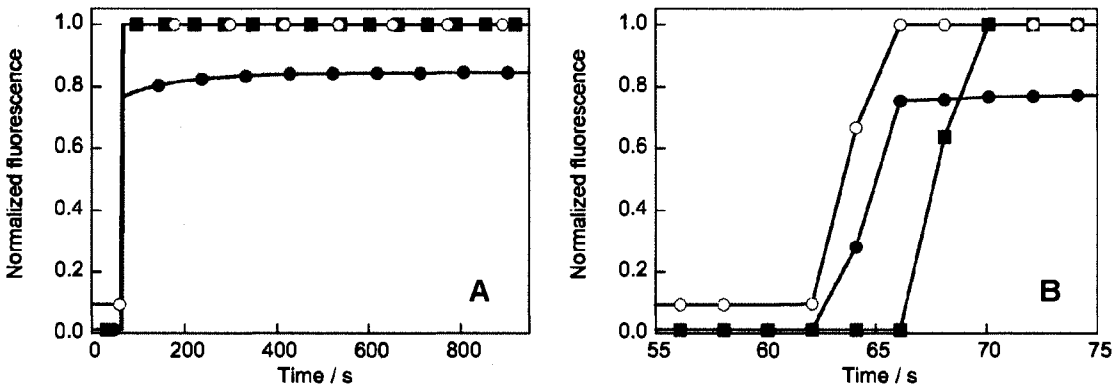


**Figure 4.27: (A) Normalized (to the maximum in all 3 cases) fluorescence of 5 µM PTO in the presence of 50 µM homopolymers in 10 mM Tris buffer (pH 7.4), excited at 480 nm and monitored at 532 nm. Recorded at room temperature for [poly(dA)•poly(dT)]+PTO (●), [PTO+poly(dA)]+poly(dT) (○) and [PTO+poly(dT)]+poly(dA) (■). (B) Close-up of the normalized fluorescence in the time period when the dye or complementary ssDNA was injected. The lines are only present to guide the eye.**

In the presence of 1 mM SDS, different amounts of dye were dissociated from poly(dA)•poly(dT) depending on whether the dye was added before or after hybridization of the DNA strands, as seen in Figure 4.28. Incubation of the dye with a single strand followed by hybridization with the complementary strand resulted in

a 30% loss of PTO fluorescence upon addition of 1 mM SDS, compared to a 75% loss when PTO had been added after hybridization, suggesting that the former dye/DNA complex is more stable than the latter. SDS concentrations of 2 or 2.5 mM decreased the PTO fluorescence by 96-98% in all three cases. SDS concentrations of 5 mM or greater reduced the fluorescence to essentially nothing in all three cases, indicating complete dissociation of intercalated PTO.

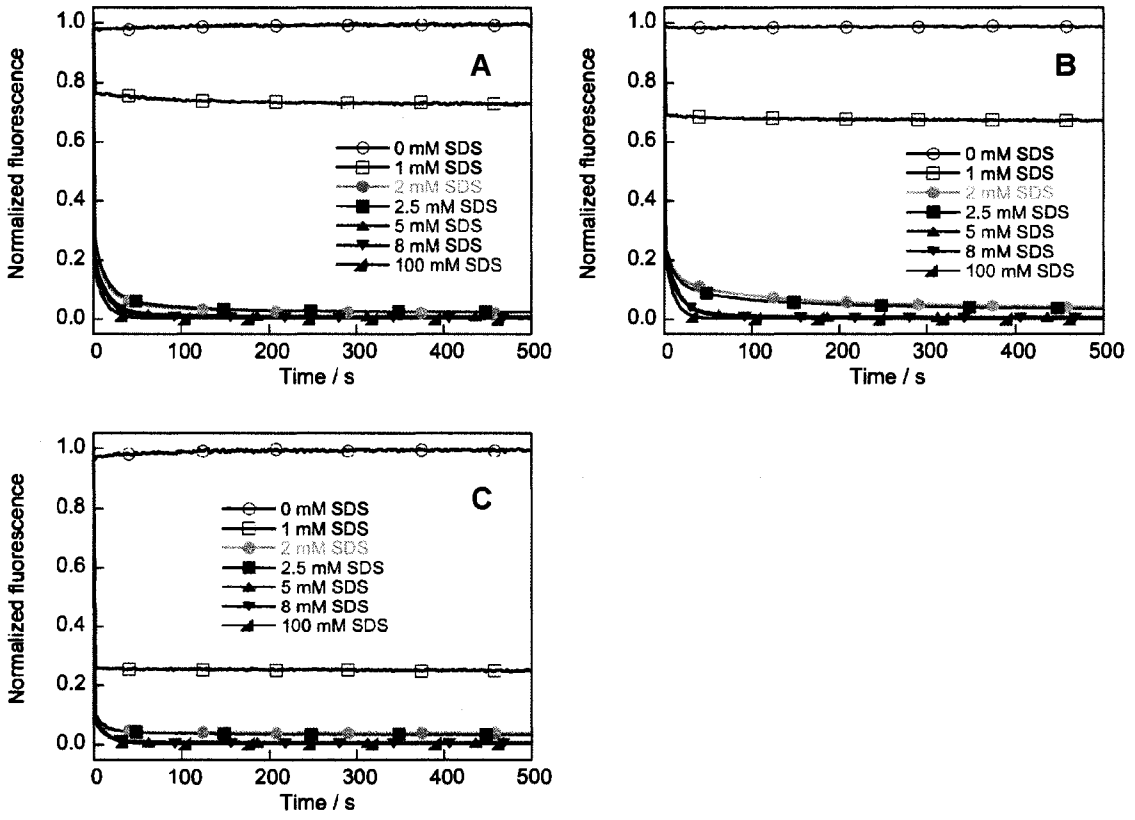


**Figure 4.28: Normalized (to the maximum intensity of the control) fluorescence of 5 μM PTO in the presence of 50 μM poly(dA)•poly(dT) in 10 mM Tris buffer (pH 7.4), excited at 480 nm and monitored at 532 nm. Recorded at room temperature for (A) [PTO+poly(dA)]+poly(dT), (B) [PTO+poly(dT)]+poly(dA), and (C) [poly(dA)•poly(dT)]+PTO.**

To ensure that PTO does not fluoresce in the presence of SDS, the fluorescence of PTO and SDS was monitored with and without poly(dA)•poly(dT). As can be seen in Figure 4.29, PTO fluorescence is negligible when only surfactant is present, and increases dramatically in the presence of DNA (although the fluorescence decreases over time as the dye is dissociated from the DNA by the SDS). The half-life of PTO fluorescence upon addition of SDS is approximately 8 seconds.

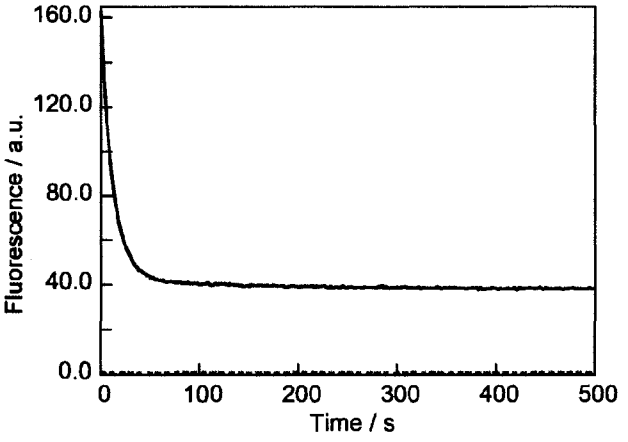


**Figure 4.29: Fluorescence of 5 μM PTO and 2.5 mM SDS in the absence (dashed red line, blends with the baseline) and presence (full black line) of 50 μM poly(dA)•poly(dT) in 10 mM Tris buffer (pH 7.4), excited at 480 nm and monitored at 532 nm. In the latter case, the dye was incubated with the dsDNA, followed by addition of SDS (at t = 0 s).**

These results, in addition to the ICD and fluorescence results in the absence of SDS, indicate that hybridization in the presence of PTO forms a complex that is distinct from that obtained when PTO is added to poly(dA)•poly(dT), and the former dye/DNA complex is more stable than the latter.

The hybridization experiments were also done with PTO and poly(dG)•poly(dC). The shapes of the ICD of PTO solutions where the dye was added before and after hybridization of poly(dG) and poly(dC) were very similar, as seen in Figure 4.30A. The spectra were distinct from those of PTO with the single strands (see Section 3.2.5), suggesting that the ICD arises from intercalation of PTO between two GC base pairs. As was found for TO, upon thermal cycling of the solutions a unique ICD was obtained which does not resemble that of PTO/poly(dG) or PTO/poly(dC) or either complex before thermal cycling. This suggests that heating the complexes places the dye molecules in thermodynamically favourable orientations, which are similar to those of PTO with single-stranded poly(dA) except red-shifted by 3-6 nm.

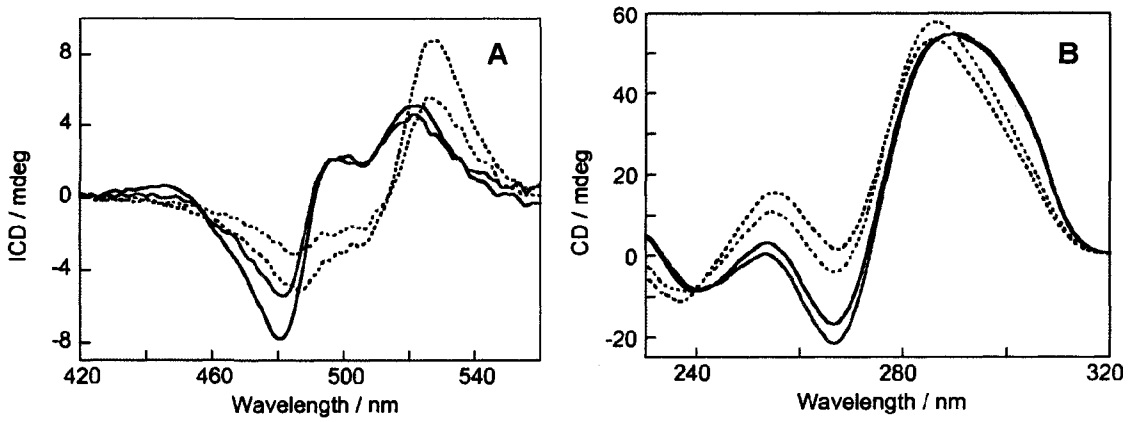


**Figure 4.30: (A) ICD and (B) CD from 7 μM PTO / 70 μM poly(dG)•poly(dC) solutions in 10 mM Tris buffer (pH 7.4), 10 mm path length. Recorded at 20°C for [PTO+poly(dG)]+[PTO+poly(dC)] (red) and [poly(dG)•poly(dC)]+PTO (blue). The dashed lines were recorded at 20°C after thermal cycling of the solutions.**

In summary, we have found that the presence of PG or PTO during hybridization of poly(dA) and poly(dT) results in the formation of a new (and more stable) type of complex, which cannot be obtained by addition of the dye to poly(dA)•poly(dT). The experimental evidence consists of unique CD and ICD, and an increased steady-state fluorescence intensity and a higher DNA affinity (measured using SDS to extract the dye) relative to the complex formed by adding the dye to hybridized poly(dA)•poly(dT). This effect was not observed for TO at all, nor for PG and PTO with poly(dG)•poly(dC). Upon thermal cycling of the complexes where the dye (TO or PTO) was added to poly(dG)•poly(dC) before and after hybridization, a unique ICD was obtained which did not resemble that of the dye/poly(dG) or dye/poly(dC) or either dye/poly(dG)•poly(dC) complex before thermal cycling. This suggests that heating the dye/poly(dG)•poly(dC) complexes places the dye molecules in thermodynamically favourable orientations, which are similar to those of the dyes with single-stranded poly(dA) except the spectra are red-shifted by a few nanometres.

### 4.2.3. Computational Studies

Computational studies proved very useful in the study of dye/DNA interactions involving ssDNA (see Chapter 3), thus they were also extended to dye/dsDNA complexes. The structure of PG is proprietary, thus it could not be studied computationally. As was discussed in Chapter 3, the isomers and conformers of PTO and TO were fully optimized (*in vacuo*) by B3LYP/6-31G* and the lowest energy structure for each dye (shown in Figure 4.31) was chosen for the simulations. Based upon the identical cross peak patterns in the NOESY spectra of TOTO/dsDNA and free TOTO, Jacobsen *et al.* concluded that the conformation of the dye does not change upon intercalation.[50] As TOTO is simply a covalently linked dimer of TO and PTO is a TO-derivative, we have assumed that the most stable TO and PTO structures in solution will also be the most stable in DNA for the purposes of our calculations.

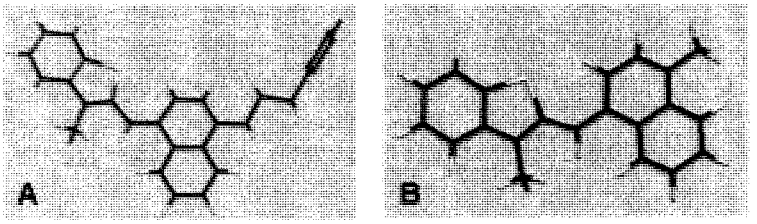


**Figure 4.31: (A) PTO and (B) TO optimized structures that are lowest in energy by 4.1 and 4.18 kcal mol$^{-1}$, respectively.**

The DNA oligomers consisted of 10 base pairs to coincide with the experimental conditions, where a 1:10 dye:base pair ratio was employed. The modeling was carried out by inserting the dye, either PTO or TO, in an arbitrary position near the center of the 10 base pair chain, i.e. between the 5$^{th}$ and 6$^{th}$ base pairs. As such, each 2 ns simulation required 10 days of CPU time, thus it was not feasible to place the dye in the proximity of the DNA and monitor its intercalation as this would require extremely long simulations. In order to provide a complete description of the system, several orientations between the dye and the DNA oligomers were considered. These consisted of placing the benzothiazole moiety

between the bases, the quinoline moiety between the bases, both the benzothiazole and the quinoline moieties between the bases (TO only), or the pyridinium moiety between the bases (PTO only). The DNA oligomers that were studied were $(dG)_{10}$•$(dC)_{10}$, $(dA)_{10}$•$(dT)_{10}$, and two duplexes with mixed base pairs. In addition, simulations of DNA renaturation were run, in the absence and presence of PTO and TO, to provide insight into the experimental hybridization results. Table 4.2 in the Discussion section (Section 4.3.2) summarizes the observations that follow.

#### 4.2.3.1. Intercalation via the Benzothiazole Moiety

When inserting the PTO benzothiazole moiety between the base pairs of the DNA oligomers, two orientations were considered for each oligomer, as illustrated in Figure 4.32.


**Figure 4.32: Illustration of the two different modes of insertion of the PTO benzothiazole moiety between the two central base pairs of DNA oligomers, shown here for $(dA)_{10}$•$(dT)_{10}$. (A) Benzothiazole $CH_3$ is between two pyrimidine bases while the benzothiazole S is between two purine bases. (B) Benzothiazole S is between two pyrimidine bases while the benzothiazole $CH_3$ is between two purine bases.**

When the PTO benzothiazole moiety was placed between the bases of $(dG)_{10}$•$(dC)_{10}$, in both cases the dye remained intercalated, as seen in Figure 4.33. However, in one case the benzothiazole moiety ended up between the G bases (Figure 4.33B) while in the other case it positioned itself between the C bases (Figure 4.33D).

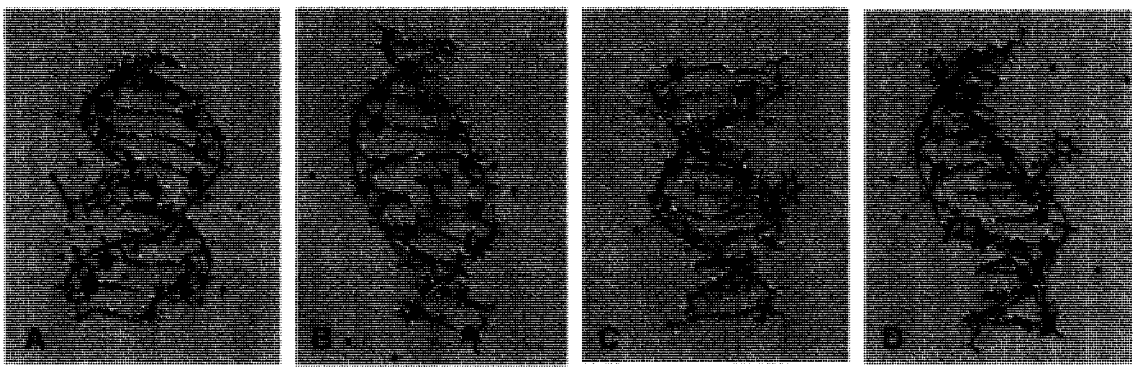


**Figure 4.33: Initial (A,C) conformations of PTO/$(dG)_{10}$•$(dC)_{10}$, and after 2 ns (B,D), showing the benzothiazole moiety intercalated.**

In one of the simulations where the PTO benzothiazole moiety was inserted in $(dA)_{10}\bullet(dT)_{10}$, the dye dissociated within the first few hundred picoseconds but stayed in the proximity of the DNA strand, presumably due to electrostatic interactions, as shown in Figure 4.34B. In the other simulation, the benzothiazole moiety remained intercalated, as seen in Figure 4.34D. For most of this simulation, the benzothiazole moiety was between the A bases, but around 2 ns it shifted so that it was between the T bases.

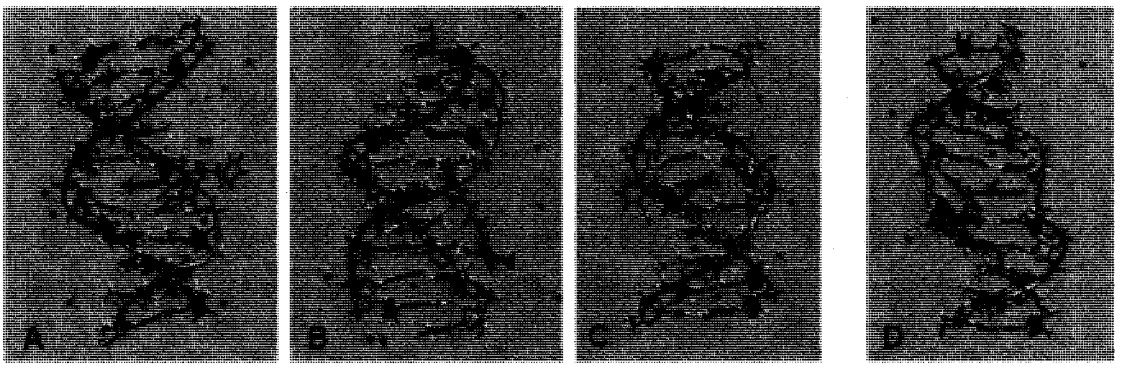


**Figure 4.34: Initial (A) conformation of PTO/$(dA)_{10}\bullet(dT)_{10}$, and after 2 ns (B), showing the dye dissociated. Initial (C) conformation of PTO/$(dA)_{10}\bullet(dT)_{10}$, and after 2 ns (D), showing the benzothiazole moiety intercalated.**

When inserting the TO benzothiazole moiety between the base pairs of the DNA oligomers, 4 orientations were considered for each oligomer, as illustrated in Figure 4.35.

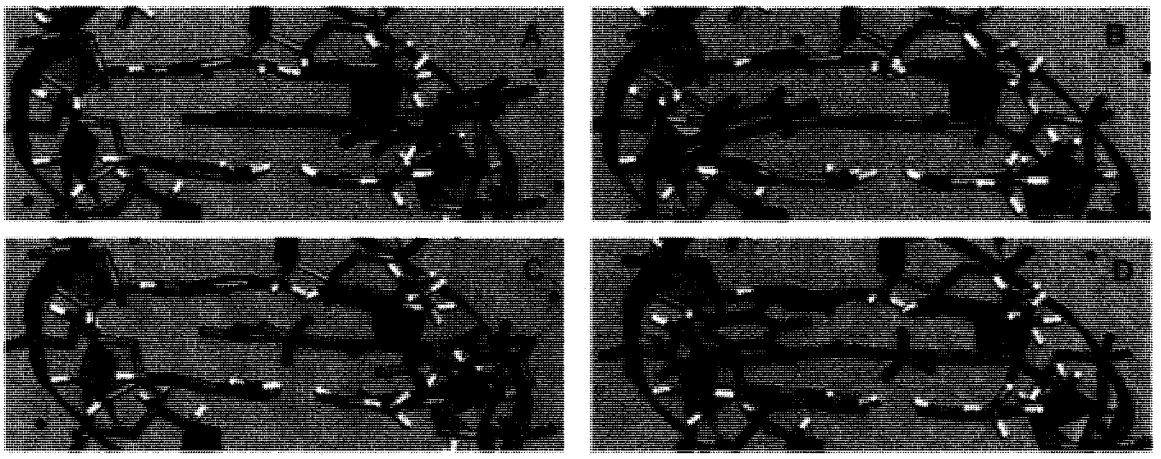


**Figure 4.35: Illustration of the modes of insertion of the TO benzothiazole moiety between the two central base pairs of DNA oligomers, shown here for $(dA)_{10}$•$(dT)_{10}$. (A,B) Benzothiazole $CH_3$ is perpendicular to the plane of the intercalation pocket (going into the plane of the paper); in (A) the quinoline moiety is near the pyrimidine strand while in (B) it is near the purine strand. (C,D) Benzothiazole $CH_3$ is perpendicular to the plane of the intercalation pocket (coming out of the plane of the paper); in (C) the quinoline moiety is near the pyrimidine strand while in (D) it is near the purine strand.**

When the TO benzothiazole moiety was placed between the bases of $(dG)_{10}$•$(dC)_{10}$, in 2 of the 4 cases studied the dye dissociated almost immediately but stayed in the proximity of the DNA (as seen in Figure 4.36B), presumably due to electrostatic interactions. In another case, there was an almost immediate shift that moved the benzothiazole moiety from its central position between the two GC base pairs to being solely between the two G bases, and this orientation persisted for 4 ns (data not shown). In the last case, within the first few hundred picoseconds, the benzothiazole moiety shifted so that it was between the two C bases and the quinoline moiety moved between the two G bases. The dye stayed in that orientation for the rest of the 2 ns simulation, as shown in Figure 4.36D, and lengthened the DNA helix by the spacing of approximately one base pair. In contrast to the results involving the dye and the single-stranded oligomers where insertion of both TO moieties between the bases frequently led to partial dissociation and bending of the DNA, intercalation of both moieties between the base pairs of this double-stranded oligomer appears to be very stable.

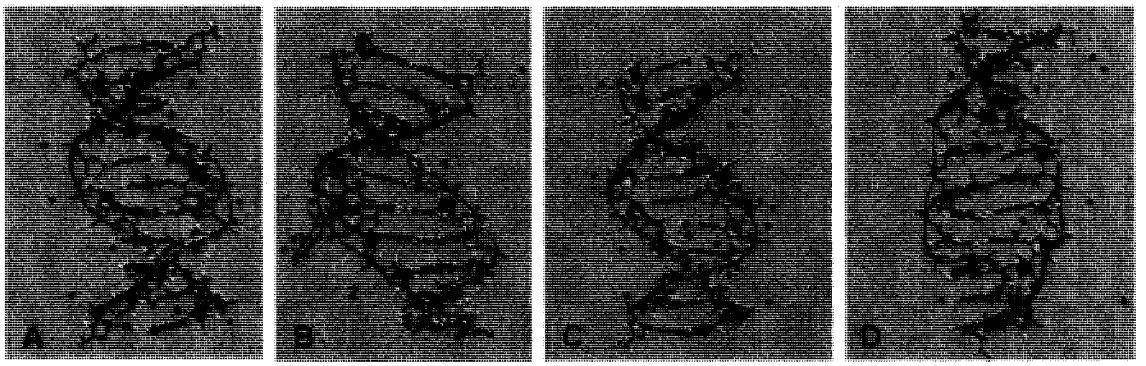


**Figure 4.36: Initial (A) conformation of TO/$(dG)_{10}$•$(dC)_{10}$, and after 2 ns (B), showing the dye dissociated. Initial (C) conformation of TO/$(dG)_{10}$•$(dC)_{10}$, and after 2 ns (D), showing both moieties intercalated.**

In the first case where the TO benzothiazole moiety was inserted in $(dA)_{10}$•$(dT)_{10}$, there was a shift within the first few hundred picoseconds that placed the quinoline moiety between the two base pairs. There was a subsequent shift that resulted in the quinoline moiety being positioned between the two A bases, as seen in Figure 4.37B. In another case, the dye dissociated within the first few hundred picoseconds but stayed in the proximity of the DNA strand, presumably due to electrostatic interactions (data not shown). In the final two cases, the benzothiazole moiety positioned itself between the two A bases while the quinoline moiety moved between the two T bases, as shown in Figure 4.37D.

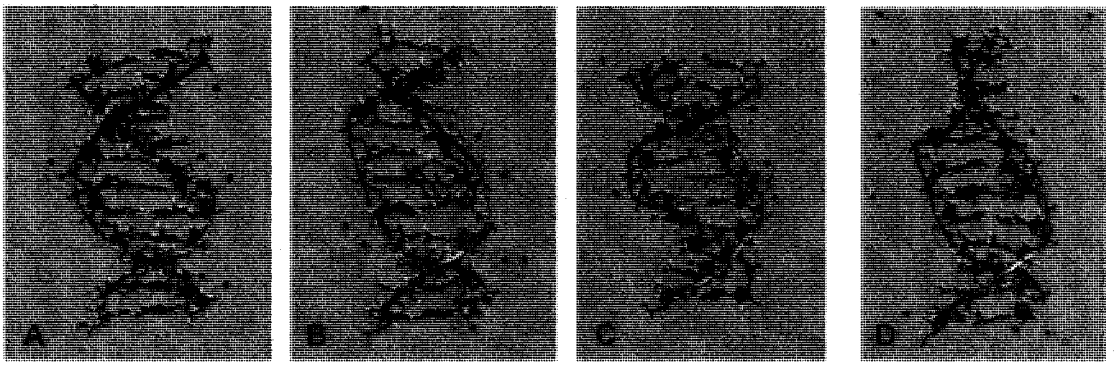


**Figure 4.37: Initial (A) conformation of TO/$(dA)_{10}$•$(dT)_{10}$, and after 2 ns (B), showing the quinoline moiety intercalated. Initial (C) conformation of TO/$(dA)_{10}$•$(dT)_{10}$, and after 2 ns (D), showing both moieties intercalated.**

#### 4.2.3.2. Intercalation via the Quinoline Moiety

When inserting the PTO quinoline moiety between the base pairs of the DNA oligomers, two orientations were considered for each oligomer, as illustrated in Figure 4.38.

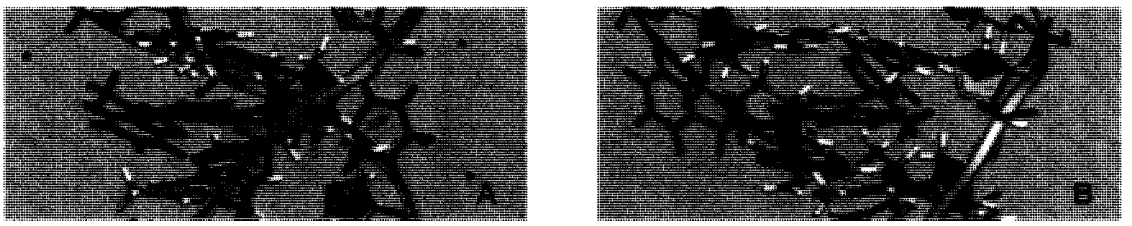


**Figure 4.38: Illustration of the two different modes of insertion of the PTO quinoline moiety between the two central base pairs of DNA oligomers, shown here for $(dA)_{10}\bullet(dT)_{10}$. In (A) the benzothiazole and pyridinium moieties are near the pyrimidine strand while in (B) they are near the purine strand.**

In both instances where the PTO quinoline moiety was inserted between the bases of $(dG)_{10}$•$(dC)_{10}$, the dye remained intercalated and lengthened the DNA duplex. In one instance, the quinoline moiety shifted from being between the two GC base pairs to being between the two G bases, as seen in Figure 4.39B. In the other instance, the quinoline moiety positioned itself between the two G bases, and near the end of the 2 ns simulation the benzothiazole moiety moved between the two C bases, as shown in Figure 4.39D.

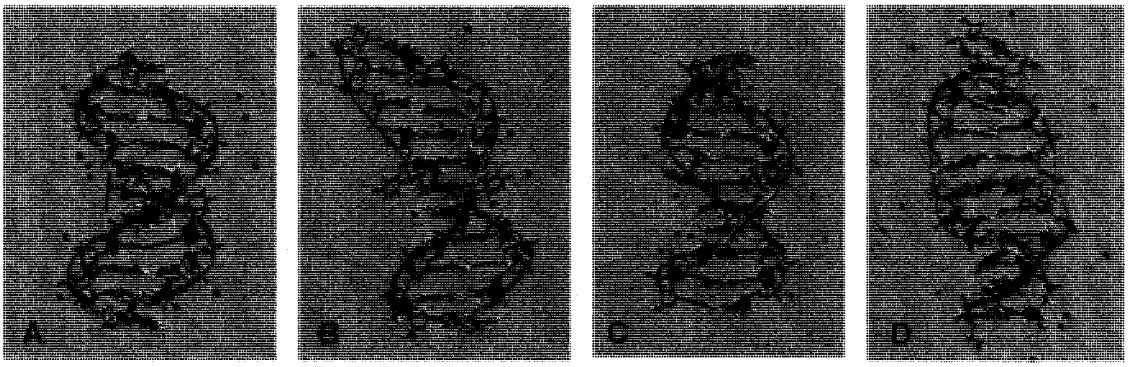


**Figure 4.39: Initial (A) conformation of PTO/$(dG)_{10}$•$(dC)_{10}$, and after 2 ns (B), showing the quinoline moiety intercalated. Initial (C) conformation of PTO/$(dG)_{10}$•$(dC)_{10}$, and after 2 ns (D), showing both moieties intercalated.**

In both instances where the PTO quinoline moiety was inserted between the bases of $(dA)_{10}$•$(dT)_{10}$, the dye remained intercalated. In one instance, the quinoline moiety shifted from being between the two AT base pairs to being between the two T bases (Figure 4.40B), and there was very little movement of the benzothiazole moiety during the 2 ns simulation. In the other instance, within the first few hundred picoseconds the quinoline moiety positioned itself between the two A bases and the benzothiazole moiety moved between the two T bases, as shown in Figure 4.40D.

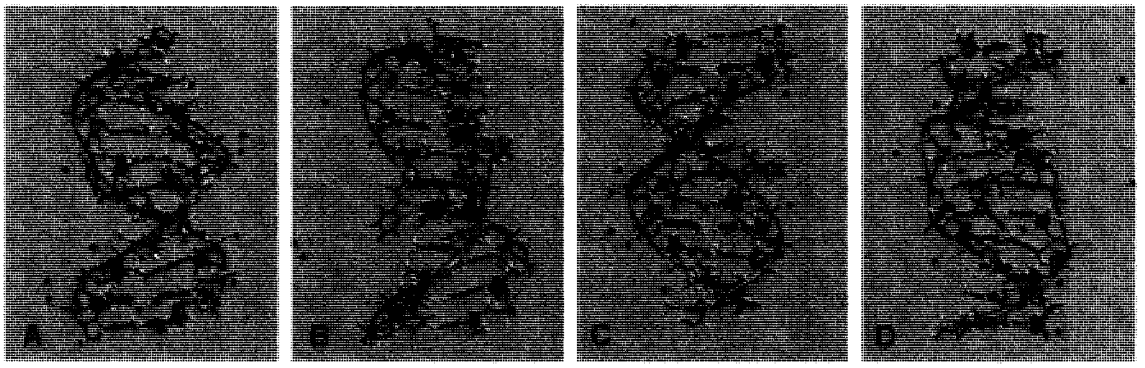


**Figure 4.40: Initial (A) conformation of PTO/$(dA)_{10}$•$(dT)_{10}$, and after 2 ns (B), showing the quinoline moiety intercalated. Initial (C) conformation of PTO/$(dA)_{10}$•$(dT)_{10}$, and after 2 ns (D), showing both moieties intercalated.**

When inserting the TO quinoline moiety between the base pairs of the DNA oligomers, four orientations were considered for each oligomer, as illustrated in Figure 4.41.

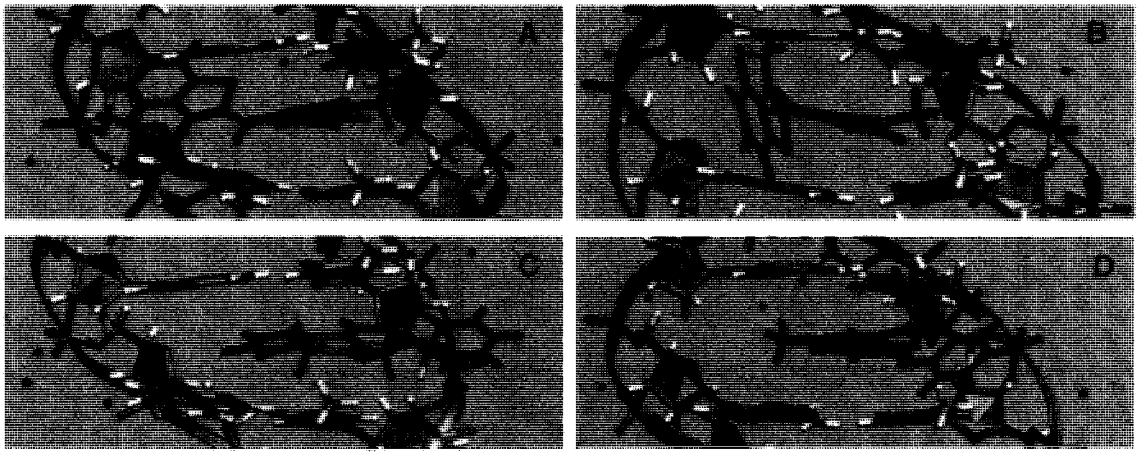


**Figure 4.41: Illustration of the modes of insertion of the TO quinoline moiety between the two central base pairs of DNA oligomers, shown here for $(dA)_{10}$•$(dT)_{10}$. (A,B) Quinoline $CH_3$ is near the pyrimidine strand; in (A) the benzothiazole S is closer to the 5'-A than is the benzothiazole $CH_3$ and in (B) the benzothiazole $CH_3$ is closer to the 5'-A than is the benzothiazole S. (C,D) Quinoline $CH_3$ is near the purine strand; in (C) the benzothiazole S is closer to the 3'-T than is the benzothiazole $CH_3$ and in (D) the benzothiazole $CH_3$ is closer to the 3'-T than is the benzothiazole S.**

In 3 of the 4 instances where the TO quinoline moiety was inserted between the base pairs of $(dG)_{10}$•$(dC)_{10}$, both moieties became intercalated, as seen in Figure 4.42B. In two of these instances the quinoline moiety was between the two C bases while the benzothiazole moiety was between the two G bases, and in the other instance it was the reverse. In all three instances, the DNA helix lengthened and the helicity was affected. In the last case, there was an immediate shift that moved the quinoline moiety from its position between the two GC base pairs to a position between the two G bases. This orientation persisted over the 4 ns simulation, as shown in Figure 4.42D.

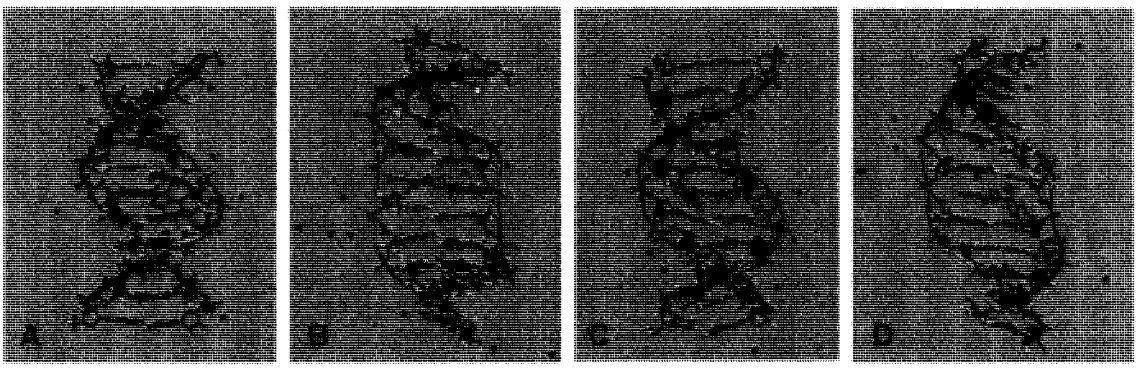


**Figure 4.42: Initial (A) conformation of TO/$(dG)_{10}$•$(dC)_{10}$, and after 2 ns (B), showing both moieties intercalated. Initial (C) conformation of TO/$(dG)_{10}$•$(dC)_{10}$, and after 4 ns (D), showing the quinoline moiety intercalated.**

Initial intercalation of the TO quinoline moiety in $(dA)_{10}\bullet(dT)_{10}$ led, over the 2 ns simulation, to both moieties being intercalated in 3 of the 4 cases studied. In two of these cases the quinoline moiety ended up between the two T bases while the benzothiazole moiety was between the two A bases, and in the other instance it was the reverse. One case is shown in Figure 4.43B, with a close-up shown in Figure 4.43E. In the last case, at the very beginning of the simulation, the quinoline moiety moved between the two A bases and the dye stayed in that orientation for the rest of the 2 ns simulation, as seen in Figure 4.43D (close-up shown in Figure 4.43F).

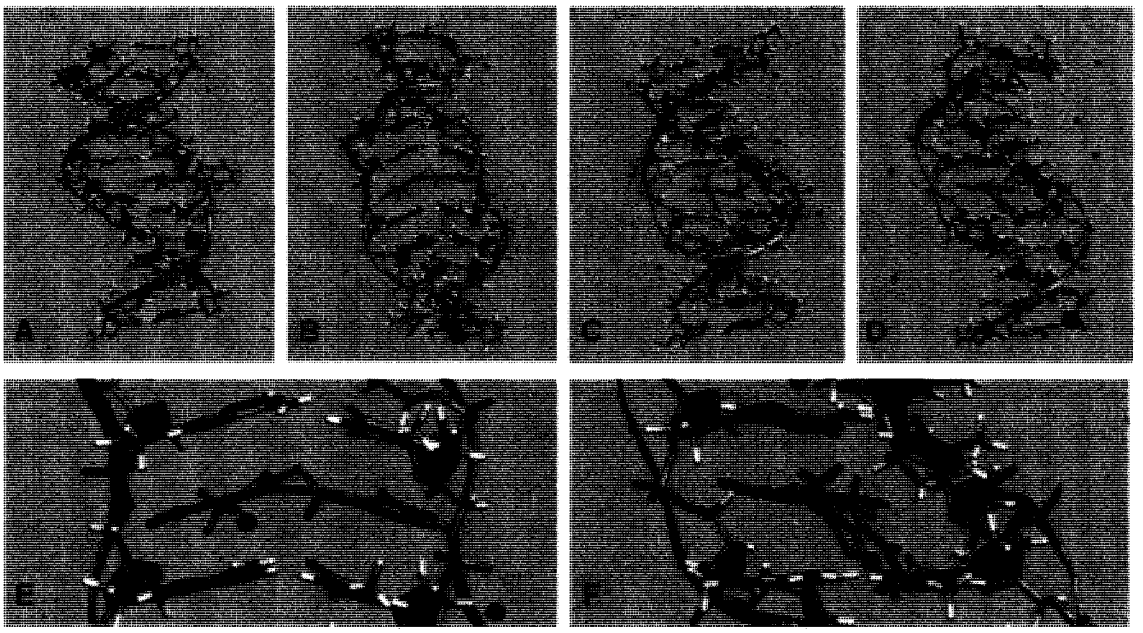


**Figure 4.43: Initial (A) conformation of TO/$(dA)_{10}\bullet(dT)_{10}$, and after 2 ns (B), showing both moieties intercalated. Initial (C) conformation of TO/$(dA)_{10}\bullet(dT)_{10}$, and after 2 ns (D), showing the quinoline moiety intercalated. (E) Close-up of the structure in (B). (F) Close-up of the structure in (D).**

#### 4.2.3.3. Intercalation of Both the Benzothiazole and Quinoline Moieties

Simulations were run where both the benzothiazole and the quinoline moieties were placed between the base pairs of the DNA oligomers. These simulations were only done with TO, and there were 4 different modes of insertion, illustrated in Figure 4.44.

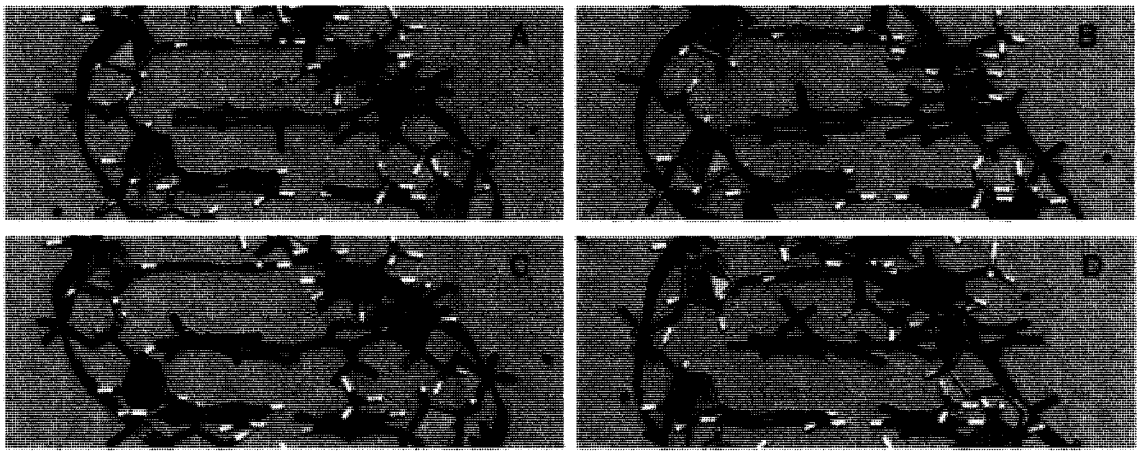


**Figure 4.44: Illustration of the modes of insertion of both the TO benzothiazole and quinoline moieties between the two central base pairs of DNA oligomers, shown here for $(dA)_{10}$•$(dT)_{10}$. (A,B) Quinoline moiety is between two pyrimidine bases while the benzothiazole moiety is between two purine bases; in (A) the methine H is going into the plane of the paper while in (B) it is coming out of the plane of the paper. (C,D) Benzothiazole moiety is between two pyrimidine bases while the quinoline moiety is between two purine bases; in (C) the methine H is going into the plane of the paper while in (D) it is coming out of the plane of the paper.**

In all 4 cases where both TO moieties were intercalated in $(dG)_{10}$•$(dC)_{10}$, both moieties remained between the base pairs, as seen in Figure 4.45. In one case, the quinoline moiety moved out of the intercalation site but then returned to its position between the bases (Figure 4.45D) – this occurred twice during the 3 ns simulation. During the simulations, there was an elongation of the DNA duplexes and their helicity was altered.

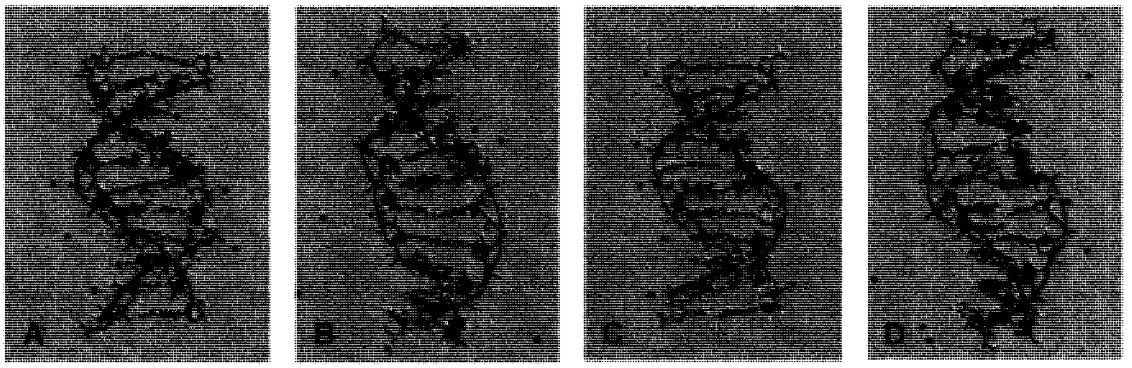


**Figure 4.45: Initial (A) conformation of TO/$(dG)_{10}$•$(dC)_{10}$, and after 2 ns (B), showing the dye close to the starting orientation. Initial (C) conformation of TO/$(dG)_{10}$•$(dC)_{10}$, and after 3 ns (D), showing both moieties intercalated.**

In all 4 cases where both TO moieties were intercalated in $(dA)_{10}\bullet(dT)_{10}$, the dye remained close to the starting orientation, as seen in Figure 4.46. During the 2 ns simulations, there was an elongation of the DNA duplexes and disruption of their helicity.

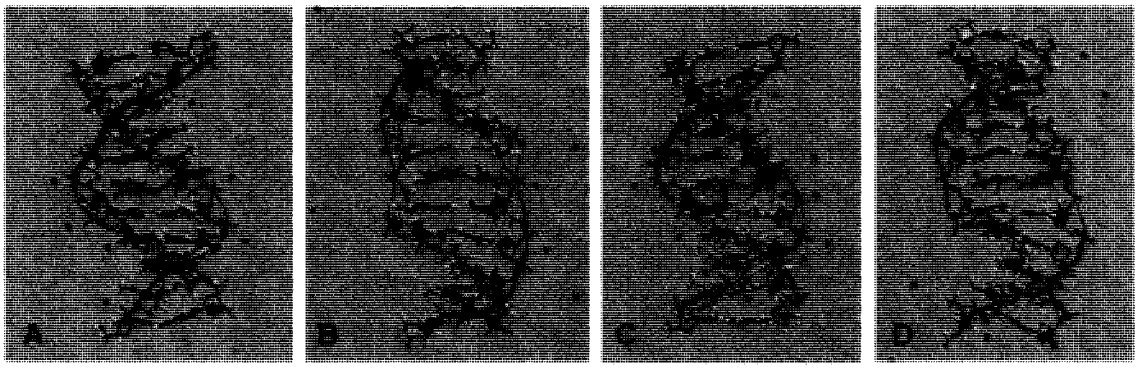


**Figure 4.46: Initial (A, C) conformations of TO/$(dA)_{10}\bullet(dT)_{10}$, and after 2 ns (B, D), showing the dye close to the starting orientation.**

### 4.2.3.4. Intercalation via the Pyridinium Moiety of PTO

As mentioned in Chapter 3, the pyridinium moiety of PTO has the most flexibility due to the alkyl chain connecting it to the rest of the molecule, and it does not fulfill the requirement for intercalation of having a minimum of two fused ring systems,[51] thus it was hypothesized that inserting this moiety between the DNA bases would most likely lead to dissociation of the dye from the DNA strand. This hypothesis is supported by the computational results involving PTO and single-stranded DNA oligomers (see Section 3.2.7.4). The validity of the hypothesis is investigated here by studying PTO and double-stranded DNA oligomers. The pyridinium moiety was intercalated in two different fashions for the simulations, as shown in Figure 4.47.

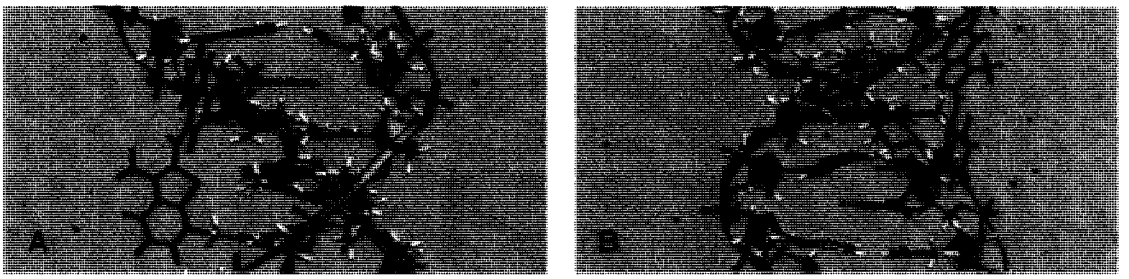


**Figure 4.47: Illustration of the modes of insertion of the PTO pyridinium moiety between the two central base pairs of DNA oligomers, shown here for $(dA)_{10}$•$(dT)_{10}$. (A) Benzothiazole moiety is closer to the 3'-A (and 5'-T) than the 5'-A (and 3'-T). (B) Benzothiazole moiety is closer to the 5'-A (and 3'-T) than the 3'-A (and 5'-T).**

In one of the simulations where the PTO pyridinium moiety was intercalated in $(dG)_{10}$•$(dC)_{10}$, the dye dissociated almost immediately but stayed in the proximity of the DNA strands, presumably due to electrostatic interactions, as seen in Figure 4.48B. In the other simulation, the pyridinium moiety remained intercalated throughout the 2 ns simulation, as shown in Figure 4.48D. During part of this simulation there was an interaction between the benzothiazole moiety and the DNA backbone. For most of the simulation the pyridinium moiety was between the two G bases, but near the end it moved between the two C bases.

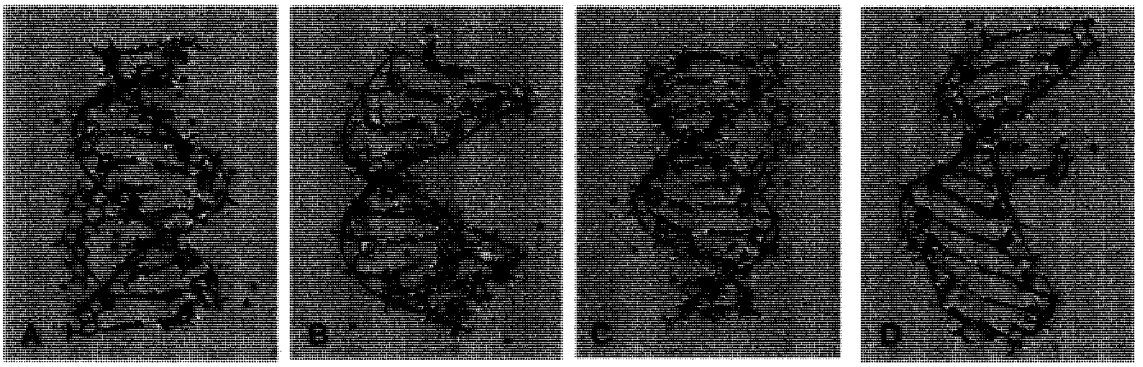


**Figure 4.48: Initial (A) conformation of PTO/$(dG)_{10}$•$(dC)_{10}$, and after 2 ns (B), showing the dye dissociated. Initial (C) conformation of PTO/$(dG)_{10}$•$(dC)_{10}$, and after 2 ns (D), showing the pyridinium moiety intercalated.**

In both simulations where the PTO pyridinium moiety was inserted between the bases of $(dA)_{10}\bullet(dT)_{10}$, the dye dissociated almost immediately but stayed in the proximity of the DNA strands, presumably due to electrostatic interactions, as seen in Figure 4.49. In one of the simulations, the dissociated dye moved from a position near the center of the DNA duplex to a position near the end of the duplex, and there was a $\pi$-stacking interaction between the quinoline moiety and the 5'-T, shown in Figure 4.49D. Note that in this work, $\pi$-stacking refers to stacking between 2 or more $\pi$-systems.

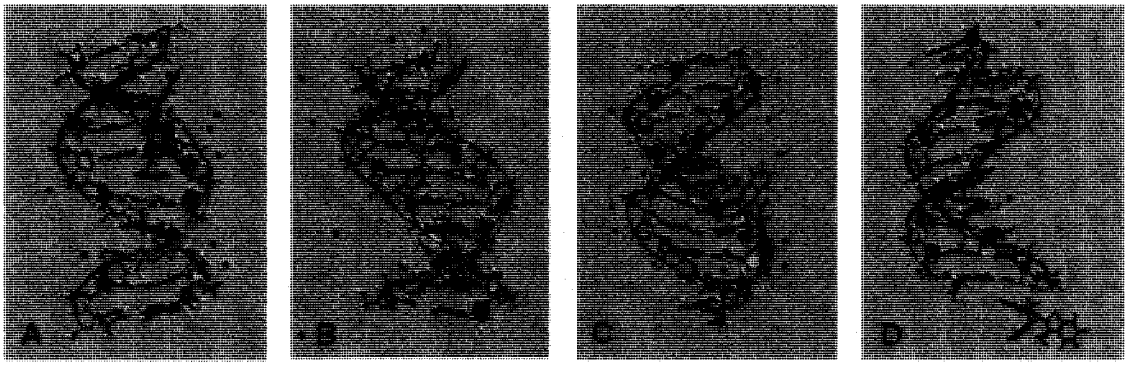


**Figure 4.49: Initial (A,C) conformations of PTO/$(dA)_{10}\bullet(dT)_{10}$, and after 2 ns (B,D), showing the dye dissociated.**

### 4.2.3.5. Intercalation in dsDNA with Mixed Base Pairs

As the experimental and computational findings involving PTO and TO indicated a strong association between the dyes and the single-stranded homopolymers poly(dA) and poly(dG) (see Chapter 3), we investigated whether or not the dyes showed a binding preference in double-stranded DNA containing mixed base pairs. The two 10-base pair duplexes that were examined are listed in Scheme 4.1.

5'-AAA ACC AAA A-3' (duplex 2G)
3'-TTT TGG TTT T-5'

5'-GGG GTT GGG G-3' (duplex 2A)
3'-CCC CAA CCC C-5'

**Scheme 4.1: Nomenclature of duplexes containing mixed base pairs.**

When inserting PTO between the base pairs of the DNA oligomers, three orientations were considered for each oligomer, as illustrated in Figure 4.50.

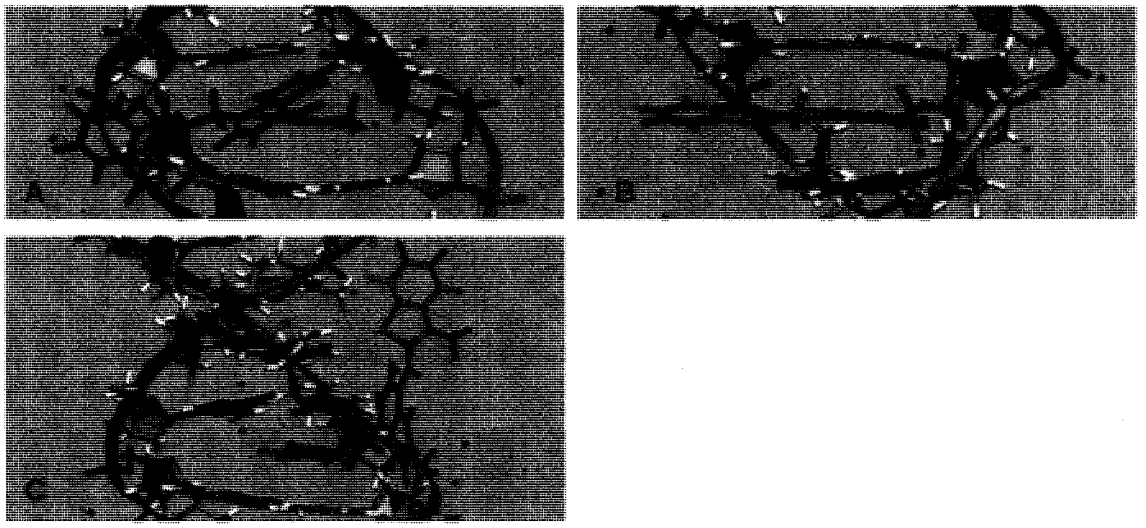


**Figure 4.50: Illustration of the modes of insertion of PTO between the two central base pairs of DNA oligomers containing mixed base pairs, shown here for duplex 2G. (A) Benzothiazole moiety is between the base pairs; the benzothiazole $CH_3$ is perpendicular to the intercalation pocket (this view is on an angle) and the pyridinium moiety is near the G bases. (B) Quinoline moiety is between the base pairs; both the benzothiazole and the pyridinium moieties are near the G bases; the methine H is coming out of the plane of the paper. (C) Pyridinium moiety is between the base pairs; benzothiazole moiety is closer to the 3'-A (and 5'-T) than the 5'-A (and 3'-T).**

When the PTO benzothiazole moiety was intercalated in duplex 2G, it remained intercalated but shifted away from the G bases, towards the C bases, during the 2 ns simulation. In addition, during the last half of the simulation there was a $\pi$-stacking interaction between the quinoline and pyridinium moieties, as seen in Figure 4.51B. When the PTO quinoline moiety was intercalated, during the 2 ns simulation the quinoline moiety positioned itself between the two C bases and the benzothiazole moiety moved between the two G bases (Figure 4.51D). This extended the length of the DNA duplex and disrupted its helicity. When the PTO pyridinium moiety was initially inserted between the bases of duplex 2G, the dye dissociated almost immediately but stayed in the proximity of the DNA duplex, presumably due to electrostatic interactions (Figure 4.51F).

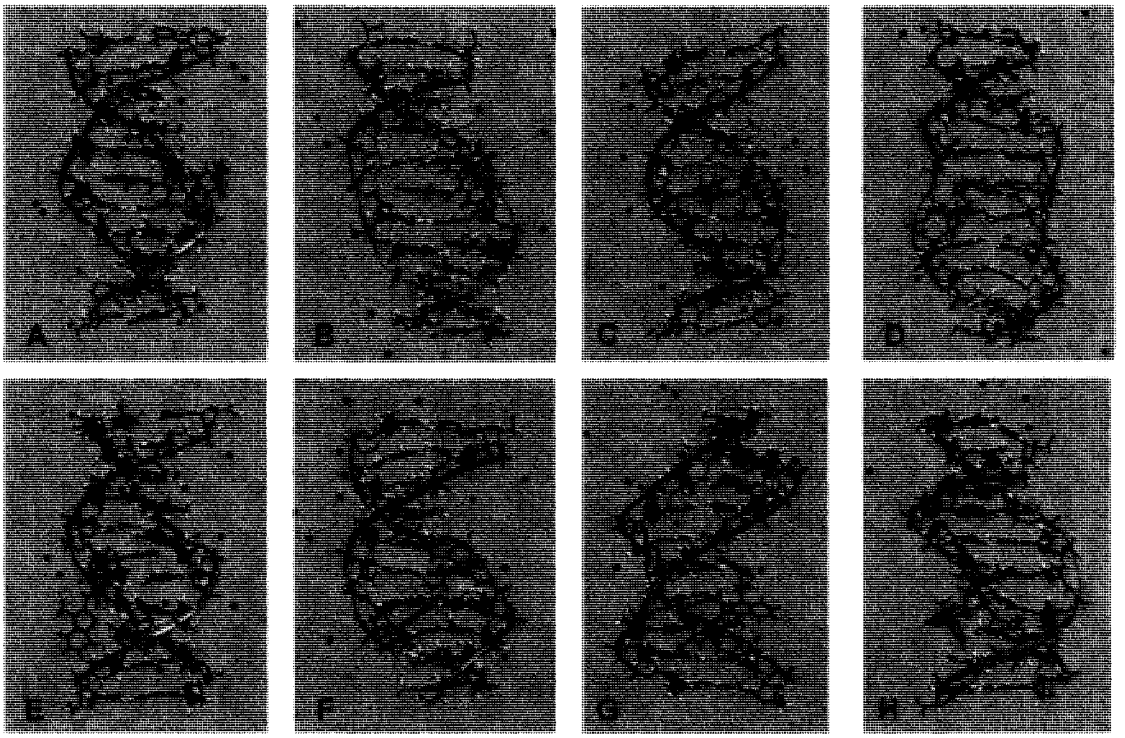


**Figure 4.51: Initial (A) conformation of PTO/duplex 2G, and after 2 ns (B), showing the benzothiazole moietiy intercalated. Initial (C) conformation of PTO/duplex 2G, and after 2 ns (D), showing both moieties intercalated. Initial (E) conformation of PTO/duplex 2G, and after 2 ns (F), showing the dye dissociated. (G,H) Alternate views of the structure in F, showing the dye dissociated.**

As with PTO/duplex 2G, the PTO benzothiazole moiety remained intercalated during the 2 ns simulation when it was inserted in duplex 2A, as shown in Figure 4.52B. Although the pyridinium moiety moved around during the simulation, the angle between the benzothiazole and the quinoline moieties remained relatively fixed. The same phenomenon was observed during the simulation where the quinoline moiety was initially placed between the base pairs (Figure 4.52C), i.e. the quinoline moiety remained intercalated, there was a relatively fixed orientation between the quinoline and the benzothiazole moieties, and there was movement of the pyridinium part of the molecule. In both cases, there was a shift from the central position to one where the intercalated moiety was between the two A bases. When the pyridinium moiety was inserted between the base pairs of duplex 2A, within the first few hundred picoseconds there was a shift that placed the pyridinium moiety between the two T bases. Around 1.5 ns, the dye dissociated but remained in the proximity of the DNA (Figure 4.52F), presumably due to electrostatic interactions.

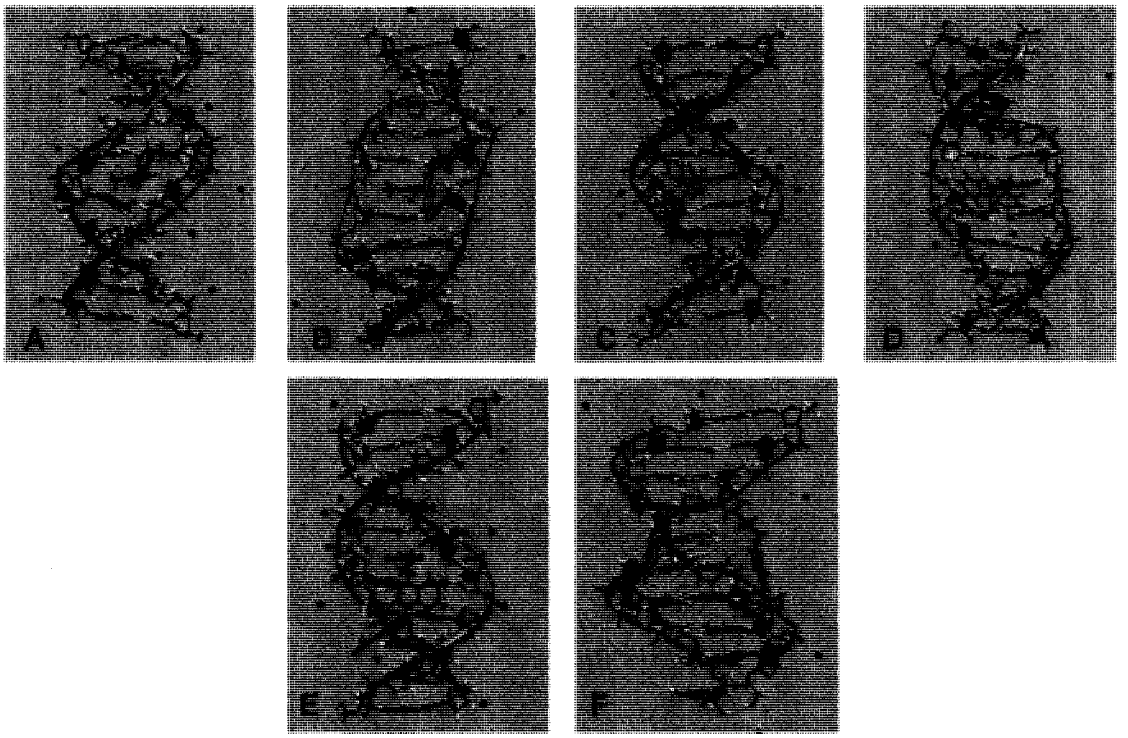


**Figure 4.52: Initial (A) conformation of PTO/duplex 2A, and after 2 ns (B), showing the benzothiazole moietiy intercalated. Initial (C) conformation of PTO/duplex 2A, and after 2 ns (D), showing the quinoline moiety intercalated. Initial (E) conformation of PTO/duplex 2A, and after 2 ns (F), showing the dye dissociated.**

When inserting TO between the base pairs of the DNA oligomers, three orientations were considered for each oligomer, as illustrated in Figure 4.53.

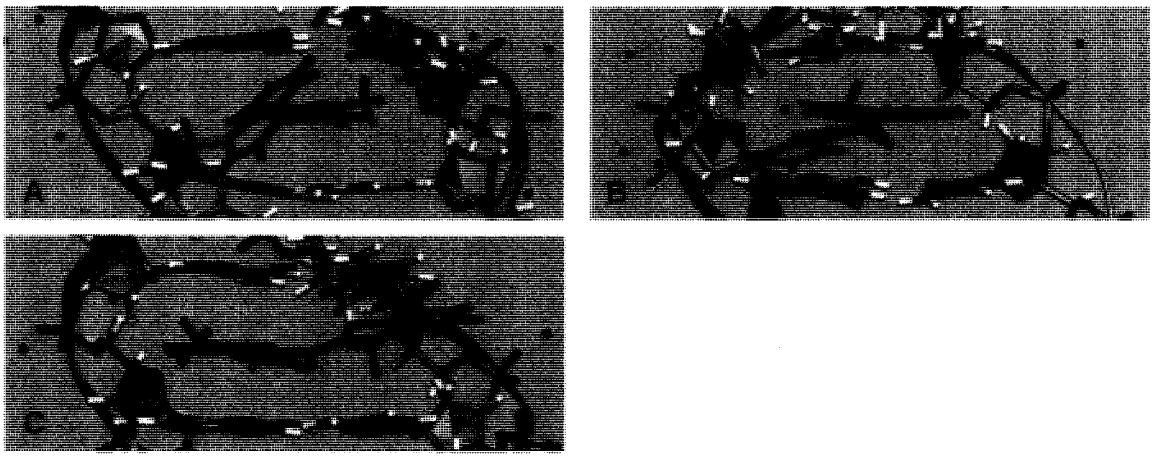


**Figure 4.53: Illustration of the modes of insertion of TO between the two central base pairs of DNA oligomers containing mixed base pairs, shown here for duplex 2G. (A) Benzothiazole moiety is between the base pairs; the benzothiazole $CH_3$ is perpendicular to the intercalation pocket (this view is on an angle) and the quinoline moiety is near the G bases. (B) Quinoline moiety is between the base pairs; the benzothiazole moiety is near the G bases; the quinoline $CH_3$ is going into the plane of the paper. (C) Quinoline moiety is between the two G bases and the benzothiazole moiety is between the two C bases; the methine H is going into the plane of the paper.**

In the simulation where the TO benzothiazole moiety was inserted between the two central base pairs of duplex 2G, after the optimization the benzothiazole moiety had moved between the 2 C bases (Figure 4.54A) and this was the starting point for the molecular dynamics simulation. In both cases where one TO moiety was initially intercalated in duplex 2G, after 2 ns both TO moieties were between the bases, as seen in Figure 4.54B and Figure 4.54D, and the DNA duplex had lengthened. In both cases, the intercalated moiety positioned itself between the two C bases and the other moiety moved between the two G bases.

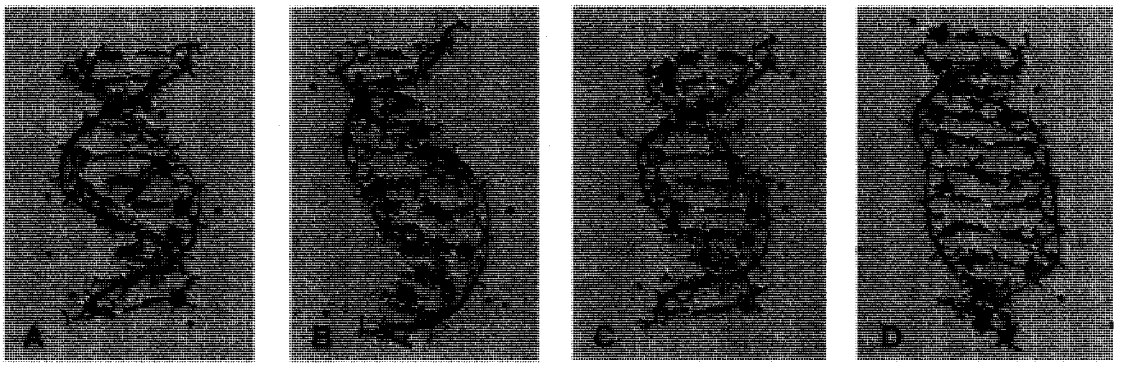


**Figure 4.54: Initial (A,C) conformations of TO/duplex 2G, and after 2 ns (B,D), showing both moieties intercalated.**

In both cases where one TO moiety was placed between the two central base pairs of duplex 2A, both moieties ended up being intercalated (Figure 4.55). In the case where the benzothiazole moiety was inserted in duplex 2A this occurred immediately, while it occurred near the end of the 2 ns simulation when the quinoline moiety was inserted. In both cases the moiety that was initially placed between the bases shifted to position itself between the two T bases while the other moiety oriented itself between the two A bases.

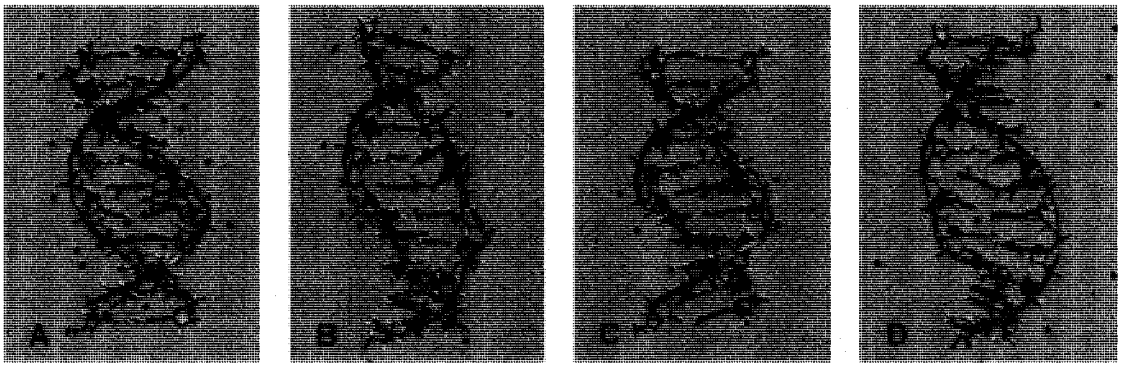


**Figure 4.55: Initial (A,C) conformations of TO/duplex 2A, and after 2 ns (B,D), showing both moieties intercalated.**

When both TO moieties were initially inserted between the central base pairs of duplex 2G or duplex 2A, they remained intercalated during the 2 ns simulation, as seen in Figure 4.56. The presence of the dye disrupted the structure of the DNA duplex, especially in the case of TO and duplex 2G, and lengthened the helix.

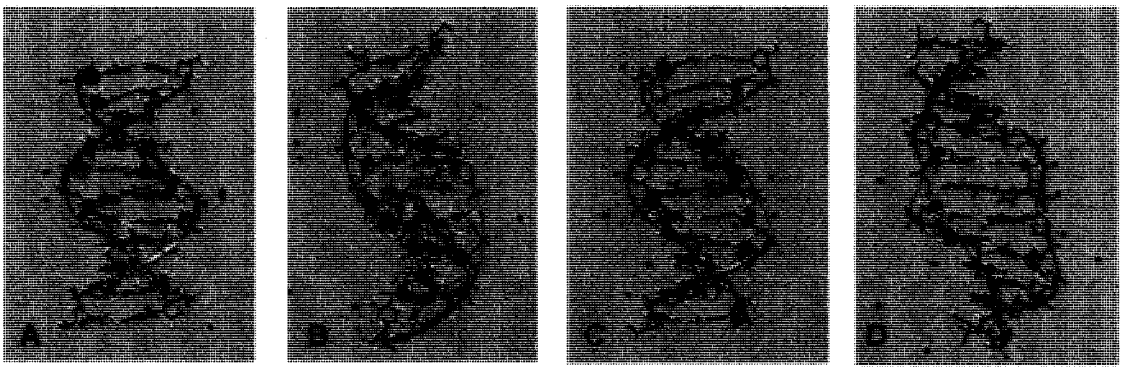


**Figure 4.56: Initial (A) conformation of TO/duplex 2G, and after 2 ns (B), showing both moieties intercalated. Initial (C) conformation of TO/duplex 2A, and after 2 ns (D), showing both moieties intercalated.**

#### 4.2.3.6. DNA Renaturation

To gain insight into the findings of the hybridization experiments (Section 4.2.2), computational simulations were run which mimicked DNA renaturation. As a control, the simulations were first run in the absence of dye. To increase the probability of forming a properly renatured duplex, the bases at the ends of each strand were different from the rest of the bases in the strand, as shown in Scheme 4.2, to prevent incorrect base pairing.

5'-GAA AAA AAA G-3' (renat-AT)
3'-CTT TTT TTT C-5'

5'-TGG GGG GGG T-3' (renat-GC)
3'-ACC CCC CCC A-5'

**Scheme 4.2: Nomenclature of duplexes used in the renaturation simulations.**

The starting orientation was obtained by running a minimization *in vacuo* with a nonbonded cutoff of 999 Å (essentially running without a cutoff since the cutoff is larger than the extent of the system), which pushed the two strands apart, as seen in Figure 4.57A for renat-AT, due to the large repulsive charge on the two chains. To aid in the strand separation, the temperature was increased from 0-300K and 0-900K for renat-AT and renat-GC, respectively. The top three base pairs were constrained during the minimization, as the rate-limiting step in renaturation is a nucleation event (the formation of one or more correct base pairs), followed by a zippering reaction where the rest of the base pairs sequentially form,[52] and we wanted to simulate the zippering reaction. Two nanoseconds into the simulation involving renat-AT, 12 of the 20 bases had formed base pairs, i.e. 6 consecutive base pairs were present, as shown in Figure 4.57B. After a total of 4 ns, 9 base pairs had formed, as seen in Figure 4.57C. Running the simulation for a total of 8 ns or using slightly different starting orientations (data not shown), did not result in complete renaturation thus the present starting orientation (Figure 4.57A) was used for the renaturation simulations of renat-AT in the presence of the dyes.

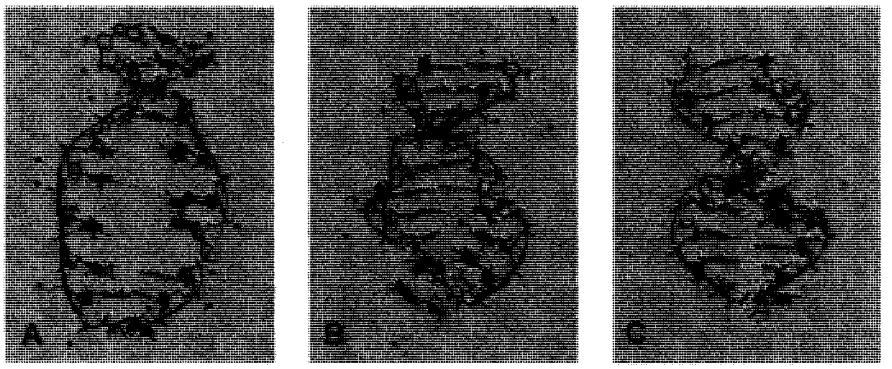


**Figure 4.57: Initial (A) conformation of renat-AT, and after 2 ns (B) and 4 ns (C), showing DNA renaturation.**

When modeling the renaturation of renat-GC, after 2 ns 16 of the 20 bases had formed base pairs hence there were 8 base pairs, as seen in Figure 4.58B. After 4 ns no new base pairs had formed (Figure 4.58C). As with renat-AT, running the simulation for a longer period of time (total of 7 ns) or using slightly different starting orientations (data not shown), did not result in complete renaturation thus the present starting orientation (Figure 4.58A) was used for the simulations of renat-GC renaturation in the presence of the dyes.

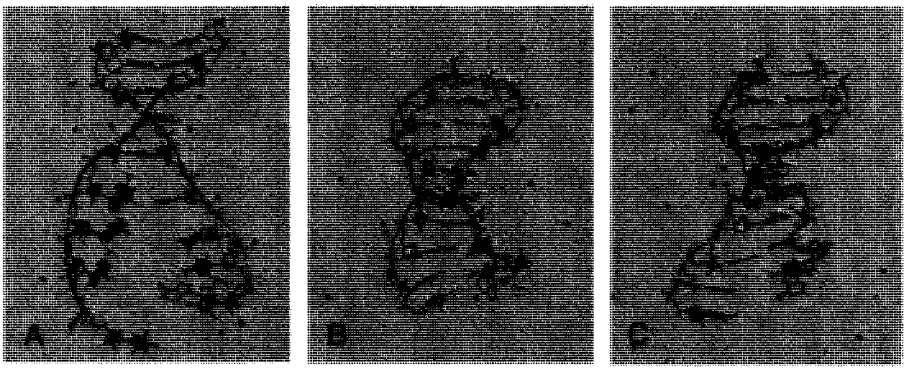


**Figure 4.58: Initial (A) conformation of renat-GC, and after 2 ns (B) and 4 ns (C), showing the renaturing of the DNA.**

#### 4.2.3.7. DNA Renaturation in the Presence of a Dye

The starting orientations for these simulations consisted of the initial structures shown in Section 4.2.3.6 plus the dye residues. Consequently, the simulations involving PTO and TO had two and one $Cl^-$ atom(s), respectively, added close to the N's of the dye to maintain the neutrality of the system. The dye molecules were placed in 4 different ways in the gap between the strands.

In the first simulation involving the renaturation of renat-AT in the presence of PTO, 4 base pairs were present initially (Figure 4.59A) and during the 4 ns simulation, no new base pairs formed. During the first 2 ns, the PTO quinoline moiety interacted with one of the T bases, as seen in Figure 4.59B. During the next 2 ns, both the quinoline and benzothiazole moieties interacted with T bases and then there was a shift that resulted in only the benzothiazole moiety interacting with a T base, as shown in Figure 4.59C. At the end of the 4 ns simulation the two strands were far apart, demonstrating the ability of the dye to affect renaturation.

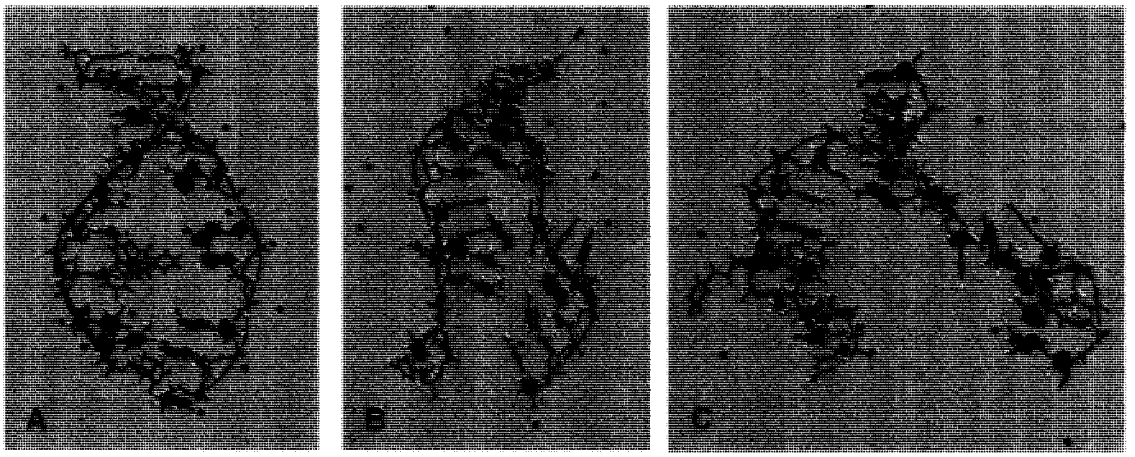


**Figure 4.59: Initial (A) conformation of PTO/renat-AT, and after 2 ns (B), showing the quinoline moiety interacting with a T base, and after 4 ns (C), showing the DNA strands far apart while the benzothiazole moiety interacts with a T base.**

In the second renaturation modelling, for most of the 2 ns simulation the PTO benzothiazole and pyridinium moieties each interacted with an A base while the quinoline moiety showed an association with a T base, which brought the two DNA strands closer together. Around 2 ns, only the benzothiazole moiety was interacting with a base, as seen in Figure 4.60B. During the next 2 ns, the benzothiazole moiety maintained its interaction with the A base, preventing renaturation at the centres of the two strands, as shown in Figure 4.60C.

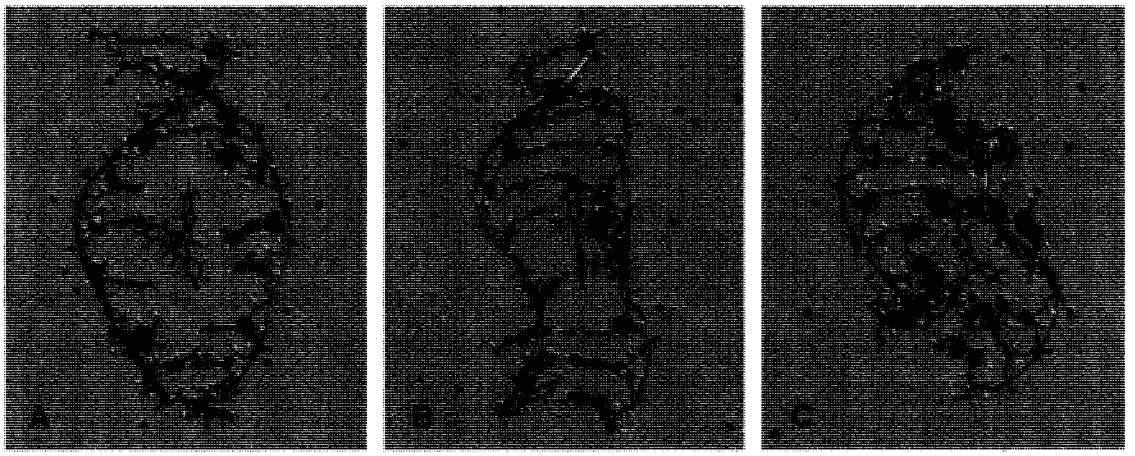


**Figure 4.60: Initial (A) conformation of PTO/renat-AT, and after 2 ns (B), showing the benzothiazole moiety interacting with an A base, and after 4 ns (C), showing the dye interfering with renaturation.**

In the third case where PTO was placed in between the renat-AT strands, the quinoline moiety immediately moved between two T bases. Approximately 1 ns into the simulation, only one T base was interacting with the quinoline moiety. At the end of 2 ns, there were 4 base pairs at one end and 3 base pairs at the other, as seen in Figure 4.61B. Subsequently, the quinoline moiety resumed its association with the two T bases and around 3 ns the benzothiazole moiety interacted with an A base. Eventually the quinoline moiety moved away from the T bases, as shown in Figure 4.61C. After 4 ns, there were 6 base pairs at one end and 3 base pairs at the other, demonstrating once again how the dye inhibits complete renaturation.

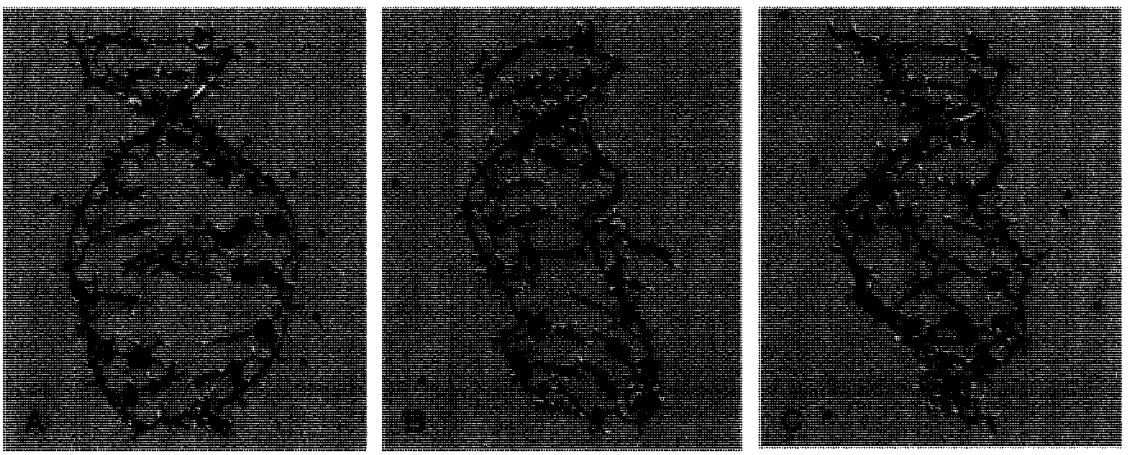

**Figure 4.61: Initial (A) conformation of PTO/renat-AT, and after 2 ns (B), showing the quinoline moiety interacting with a T base, and after 4 ns (C), showing the dye hindering renaturation.**

In the last simulation involving renat-AT and PTO, the PTO benzothiazole moiety showed an attraction for one of the A bases during the first 2 ns of the simulation and the DNA strands were quite twisted (Figure 4.62B). During the next 2 ns, the benzothiazole moiety underwent π-interactions with the A base as well as a nearby T base. There were 4 base pairs formed at one end, and 3 at the other. One of the A bases flipped out so that it was no longer π-stacked with the other A bases, as seen in Figure 4.62C.

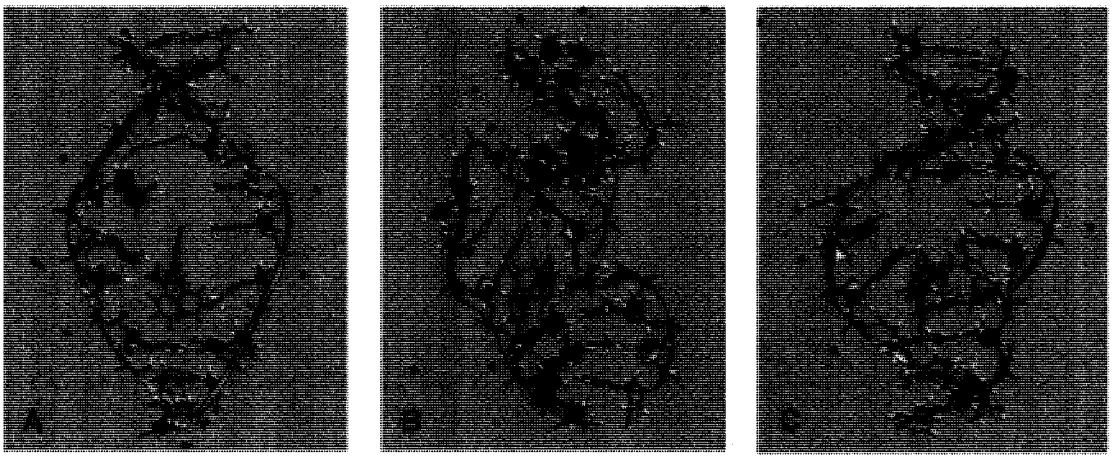


**Figure 4.62: Initial (A) conformation of PTO/renat-AT, and after 2 ns (B), showing the benzothiazole moiety interacting with an A base, and after 4 ns (C), showing the dye interfering with renaturation.**

In the first simulation involving the renaturation of renat-AT in the presence of TO, the benzothiazole moiety interacted with a T base and the quinoline moiety positioned itself between two A bases, as seen in Figure 4.63B. Six base pairs were present after 2 ns. Between 2 and 4 ns, the dye continued its associations with the bases but no new base pairs were formed and the bases at one end of the strands were twisted, as shown in Figure 4.63C.

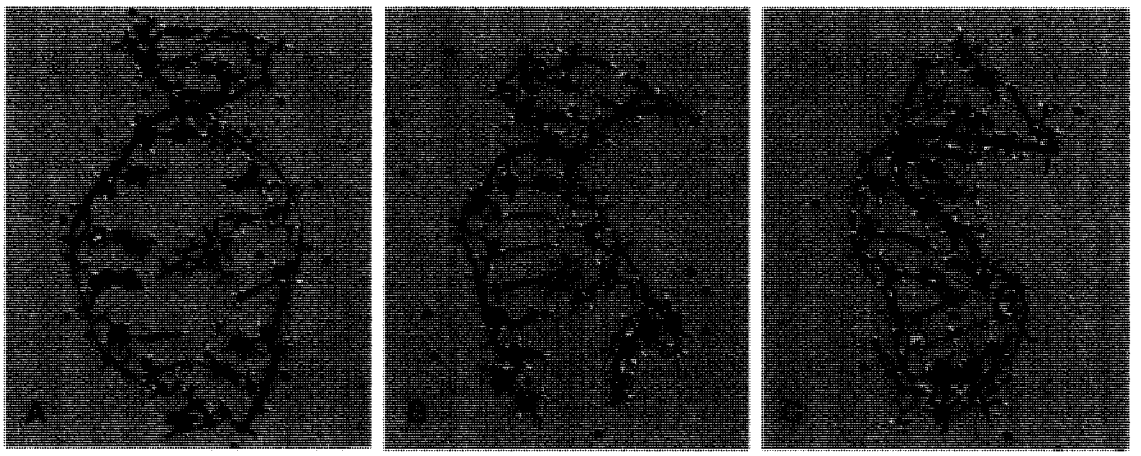

**Figure 4.63: Initial (A) conformation of TO/renat-AT, and after 2 ns (B), showing the benzothiazole moiety interacting with a T base and the quinoline moiety between two A bases, and after 4 ns (C), showing the dye hindering renaturation.**

In the second instance where TO was placed between the two strands, the benzothiazole moiety interacted with a T base, bringing the strands closer together. Approximately 1 ns into the simulation, the benzothiazole moiety associated with an A base (in addition to the T base), as shown in Figure 4.64B. The benzothiazole moiety continued its interactions with the A and T bases, and around 3 ns the quinoline moiety associated with a T base. At the end of the 4 ns simulation, the DNA bases had not paired up properly, as seen in Figure 4.64C.

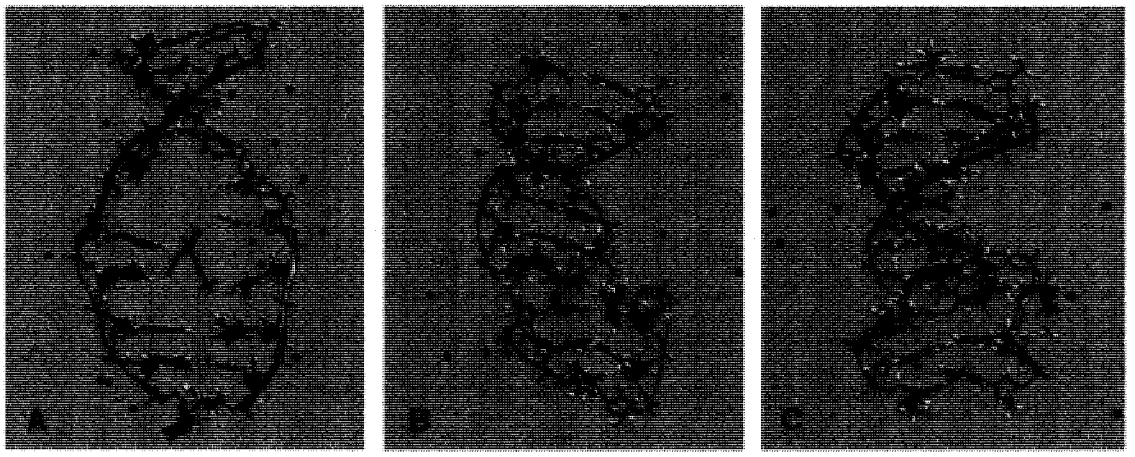

**Figure 4.64: Initial (A) conformation of TO/renat-AT, and after 2 ns (B), showing the benzothiazole moiety interacting with a T base and an A base, and after 4 ns (C), showing incomplete renaturation.**

In another simulation involving TO and renat-AT, the benzothiazole moiety immediately positioned itself between two T bases and remained there for approximately 1.5 ns. The benzothiazole moiety then briefly showed an attraction for an A base and then it interacted with a T base (Figure 4.65B). During the next 2 ns of the simulation, the benzothiazole moiety moved between two A bases and the quinoline moiety interacted with a T base. As can be seen in Figure 4.65C, one of the strands is more elongated than the other, resulting in improper base pairing.

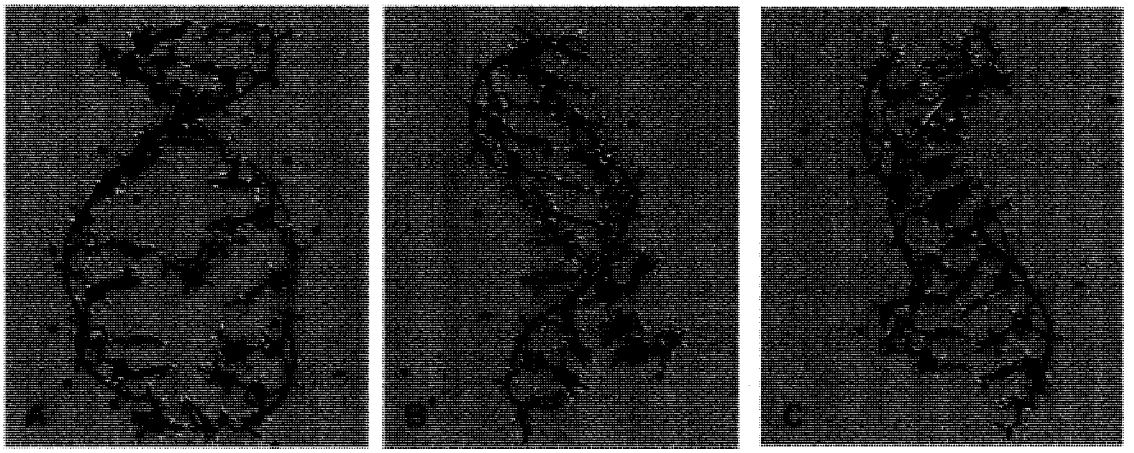

**Figure 4.65: Initial (A) conformation of TO/renat-AT, and after 2 ns (B), showing the benzothiazole moiety interacting with a T base, and after 4 ns (C), showing improper base pairing.**

In the last case involving TO and renat-AT, the TO benzothiazole moiety interacted with an A base during the first 2 ns of the simulation and caused that strand to become twisted. Meanwhile the quinoline moiety positioned itself between two nearby T bases, as shown in Figure 4.66B. During the next 2 ns of the simulation, the two moieties maintained their associations, and the two strands moved farther apart and became bent, as seen in Figure 4.66C.

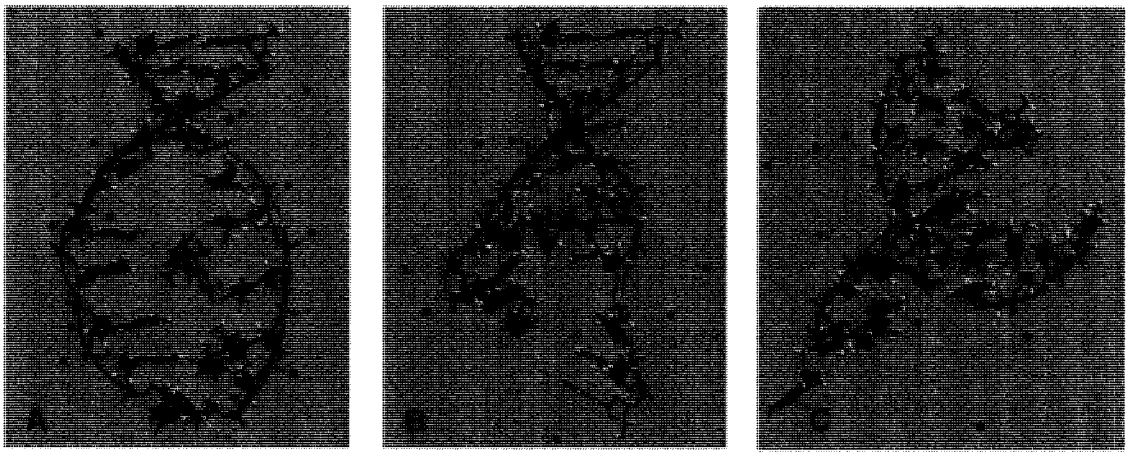

**Figure 4.66: Initial (A) conformation of TO/renat-AT, and after 2 ns (B), showing the quinoline moiety between two T bases and the benzothiazole moiety interacting with an A base, and after 4 ns (C), showing the dye preventing renaturation.**

In the first simulation involving the renaturation of renat-GC in the presence of PTO, the quinoline moiety immediately moved between two C bases and then the benzothiazole moiety associated with a G base, as seen at 2 ns in Figure 4.67B. This interaction continued for another 2 ns. The final structure has 6 base pairs formed at one end and 2 at the other end, along with 2 unpaired bases and π-stacking (rather than base pairing) between the 5'-A and 3'-T bases, as shown in Figure 4.67C.

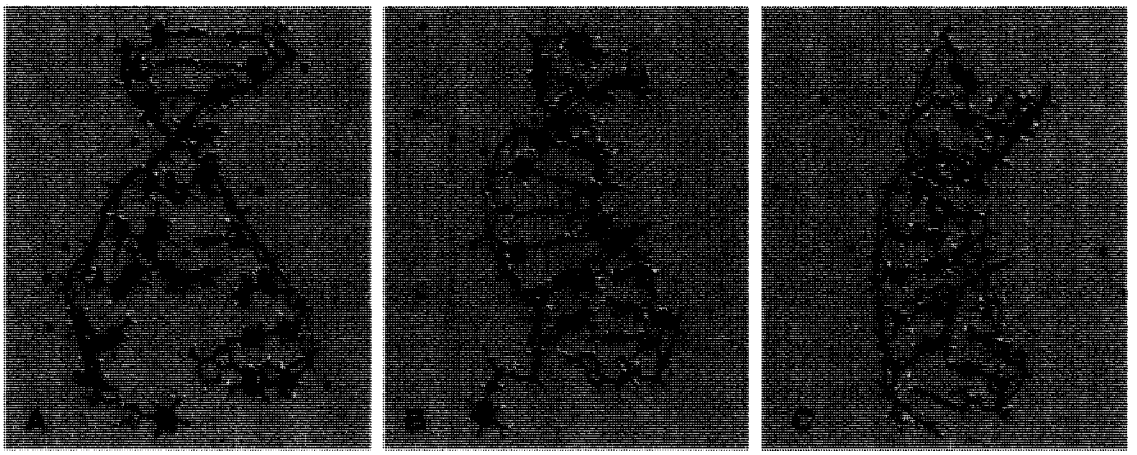

**Figure 4.67: Initial (A) conformation of PTO/renat-GC, and after 2 ns (B), showing the quinoline moiety between two C bases and the benzothiazole moiety interacting with a G base, and after 4 ns (C), showing the dye affecting renaturation.**

In another simulation of the renaturation of renat-GC in the presence of PTO, the benzothiazole moiety moved between two C bases and remained in that position for the first few hundred picoseconds. Subsequently, the quinoline moiety interacted with a G base, the benzothiazole moiety associated with the G base below it, and the pyridinium moiety showed an affinity for the 5'-A base, as seen after 2 ns in Figure 4.68B. There was very little change during the next 2 ns and the strands remained incompletely paired and twisted (Figure 4.68C).

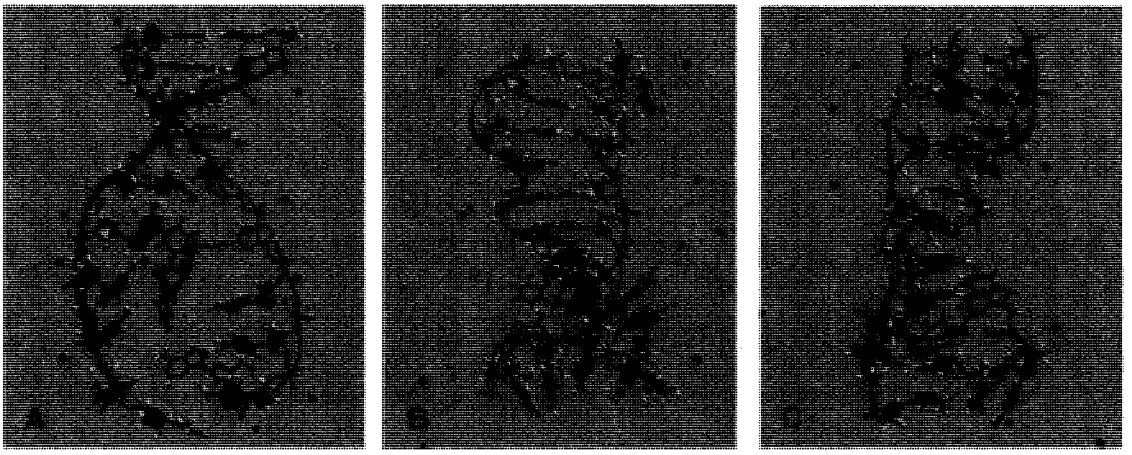

**Figure 4.68: Initial (A) conformation of PTO/renat-GC, and after 2 ns (B), showing all three moieties interacting with various bases, and after 4 ns (C), showing the dye hindering renaturation.**

In the third simulation where PTO was placed between the strands of renat-GC, the quinoline moiety moved between two C bases. The two strands got closer together and the quinoline moiety switched to having an interaction with a G base, as seen in Figure 4.69B. During the next 2 ns of the simulation, the quinoline moiety maintained its association with the G base and the unpaired bases remained far apart, as shown in Figure 4.69C.

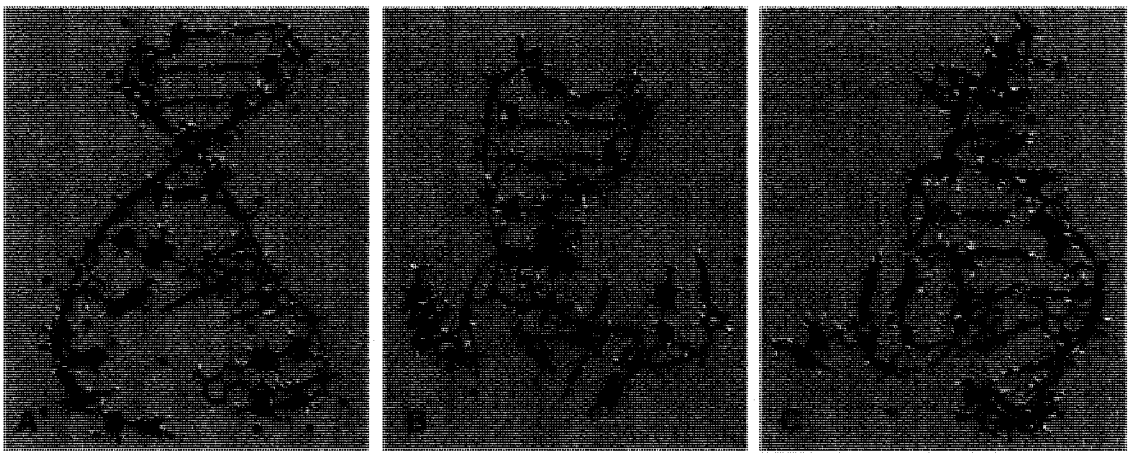

**Figure 4.69: Initial (A) conformation of PTO/renat-GC, and after 2 ns (B), showing the quinoline moiety interacting with a G base, and after 4 ns (C), showing the dye inhibiting renaturation.**

In the last simulation involving PTO and renat-GC, during the first 2 ns the quinoline moiety showed a π-association with one of the G bases, which resulted in twisting of the strands, as shown in Figure 4.70B. During the next 2 ns of the simulation, the quinoline moiety continued its interaction with the G base, and the benzothiazole moiety associated with a different G base. The ends of the DNA strands were far apart and twisted (Figure 4.70C), thus the dye prevented renaturation.

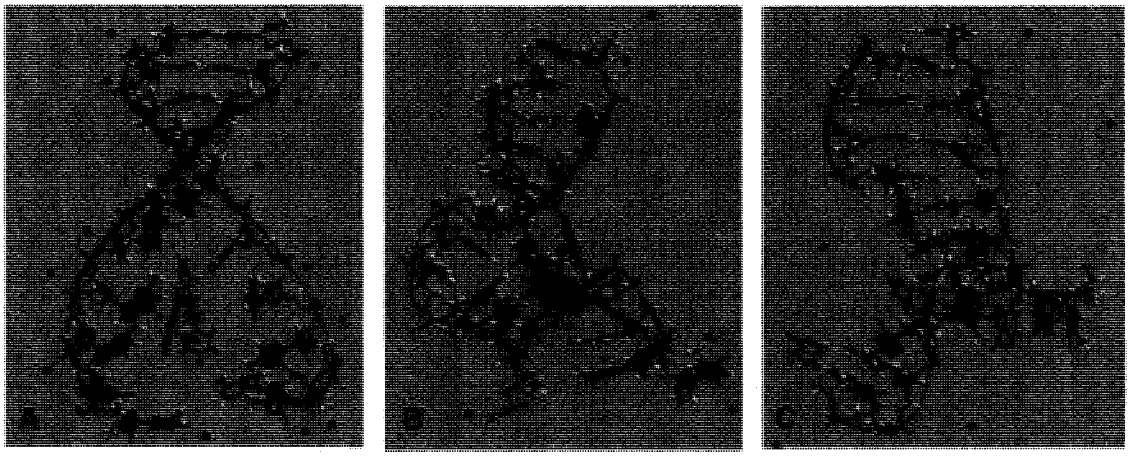

**Figure 4.70: Initial (A) conformation of PTO/renat-GC, and after 2 ns (B), showing the quinoline moiety interacting with a G base, and after 4 ns (C), showing the dye preventing renaturation.**

In summary, the presence of the dye (PTO or TO) inhibited renaturation in every case examined. In some cases the effect was significant and the DNA strands became twisted and/or moved far apart. In the other cases, the bases did not pair up properly, or did not pair up in the vicinity of the dye. In the simulations involving PTO, the majority of the time either the PTO benzothiazole or quinoline moiety (or both) interacted with the bases, rather than the pyridinium moiety.

## 4.3. Discussion

### 4.3.1. Experimental Studies

When the dyes (PTO, TO and PG) were added to either ss or ds CT DNA, both the monomer and aggregate absorption bands red-shifted, indicative of intercalation.[24] Another sign of intercalation is a decrease in extinction coefficient, which only occurred for PG. However, at the concentrations studied, PTO and TO were always present in both monomeric and aggregate forms thus the observed decrease in the aggregate absorption band and increase in the monomer absorption band reflects the suppression of dye aggregation and the resulting increase in monomeric dye, as well as dye intercalation. One notable difference between the two dyes is that, if the extinction coefficients of monomeric and aggregate dye are similar in both ss and ds CT DNA, then there is a higher TO monomer:aggregate ratio in dsDNA compared to ssDNA, while PTO and CT DNA show very little difference between the monomer:aggregate ratios in ss- and dsDNA. This is consistent with the LD results, which show extremely weak LD for TO and ssDNA compared to PTO and ssDNA. The molecular dynamics simulations indicated some potential heterogeneity in how the dyes were bound within a given intercalation site, but this should not affect the intensity of the LD bands compared to an intercalator that has a single preferred orientation. The LD intensity depends on the average orientation between the transition moment and the orientation axis, thus the experimentally measured LD is simply reporting on this average orientation.

It has been proposed that TO binds to ds CT DNA in its monomeric form[14] and inhibits dye aggregation,[25] but our LD results show that both monomeric and dimeric forms of TO intercalate in ds CT DNA. The smaller LD intensity for the dye/ssDNA complexes compared to ssDNA alone indicate that TO and PG bend ssDNA. On the other hand, increased LD for the PTO/DNA complexes support DNA stiffening. The LD of PTO in CT DNA demonstrated monomeric and dimeric intercalation in both ds- and ssDNA, although in the case of ssDNA some dimers

were free in solution rather than intercalated, as shown by the comparison of the normalized absorbance and the normalized LD. Comparison of the normalized absorbance and the normalized LD of PG with dsDNA indicated that all of the PG molecules (mostly monomeric, a considerably smaller fraction of dimer) were bound to the dsDNA. One reviewer suggested that the dimer intercalation mode is relatively minor compared with monointercalation. Curve fitting the absorbance and linear dichroism spectra of a variety of TO/dsDNA solutions to two distributions (one for monomeric TO and one for dimeric TO) demonstrated that all of the TO that is present in the absorbance spectrum is also present to exactly the same extent in the linear dichroism spectrum (data not shown). The curve fitting also indicated that 5 μM TO with 50 μM CT DNA and 18 μM TO with 180 μM CT DNA both contain approximately 42% monomer and 58% dimer, thus dimer intercalation is a significant association mode.

It seems highly unlikely that a dimer would be able to position itself within one intercalation site, but a possible explanation for our experimental observations is that a nucleotide (or both nucleotides comprising a base pair) was forced out of the helix to accommodate the intercalating dimer and maintain the rest of the helical structure. This possibility describes a phenomenon known as "nucleotide flipping", which is generally employed by DNA proofreading enzymes following DNA duplication during normal cell division.[53,54] This phenomenon has also been caused by the small molecule ligand naphthyridine-azaquinolone, as evidenced by NMR studies reported by Nakatani *et al.*[55] However, in both cases of nucleotide flipping there is a stabilization mechanism. In the former, the modified base is flipped out of the DNA helix into the active site of the enzyme and an amino acid residue, for example leucine in uracil-DNA glycosylase, occupies the space vacated by the flipped out base.[56,57] In the latter, the ligand forms hydrogen bonds with the opposing bases and undergoes $\pi$-stacking interactions with the adjacent bases.[55]

PTO shows a negative ICD signal whose shape is essentially identical in both ss- and dsDNA, but which does not correspond to any of the ICD signals observed for PTO with ss homopolymers. The ICD troughs are very similar to the

absorption maxima. These characteristics were also found for PG and CT DNA, where it has been shown that monomeric intercalation occurs,[29] supporting monomeric intercalation of PTO in CT DNA. Comparison of the ICD spectra of TO and CT DNA with TO and single-stranded homopolymers (see Chapter 3) suggests that association of TO with A bases in both ss- and dsDNA contribute to the observed ICD, and there may also be a contribution from TO binding to G bases. However, the spectra of TO/ssDNA and TO/dsDNA are unique, indicating that TO binds somewhat differently to each one. When all three cyanine dye/dsDNA complexes were subjected to thermal cycling, their ICD indicated that they either did not renature upon cooling to room temperature, presumably due to the presence of the dyes, or partial renaturation occurred but the dye region remained largely denatured.

When each of the three dyes are added to DNA, there is a peak in the excitation spectrum that corresponds to the absorption peak of monomeric dye. In dsDNA and ssDNA the dyes emitted at specific wavelengths, independent of the excitation wavelength, signifying that all excited species lead to monomer fluorescence. However, there is a very slight shoulder in the emission spectra of PTO and TO with DNA, which could be a (minor) contribution from the *cis* isomer or a vibrational band (from the *trans* monomer). The aggregates that contribute to fluorescence must either transfer their energy to the monomer through FRET and the monomer fluoresces, or dissociate into monomers and then fluoresce. The areas under the fluorescence curves were 1.9 to 5.1 times larger for the dyes with dsDNA than with ssDNA, consistent with the dye being more rotationally restricted in dsDNA compared to ssDNA.

In both ss- and dsDNA, PTO fluorescence decays biexponentially, suggesting that PTO binds to CT DNA in more than one intercalation site or in more than one position. These findings differ from those of PG with ds CT DNA, where PG decays monoexponentially with a 4.26 ns lifetime,[29] highlighting the importance of the substituents and/or the charge on the fluorescence decay. When the dye/base pair ratio was 0.10 or lower in dsDNA, the PTO fluorescence decays

contained components with mean values of 3.11 ± 0.1 ns and 1.29 ± 0.09 ns. Interestingly, for the 0.10 PTO/ssDNA complex, one fluorescence decay component closely resembles that of PTO in poly(dA), suggesting that PTO binds to A bases in ss CT DNA. The average lifetime of TO in dsDNA was significantly shorter than that of PTO in dsDNA. In contrast, the average lifetimes of TO and PTO in ssDNA were remarkably similar (for the same dye:DNA base concentration). They both had lifetime components with mean values of 0.48 ± 0.4 ns (71 ± 2%) and 1.80 ± 0.10 ns (28 ± 1%), although an extra component was needed to obtain an adequate fit for TO/ssDNA. These findings suggest that TO and PTO bind similarly to ss CT DNA, but differently to ds CT DNA. For all three dyes, the average fluorescence lifetime is longer in dsDNA compared to ssDNA, and in dsDNA it decreases in the order PG > PTO > TO. However, PG is the only dye for which the fluorescence decay in dsDNA is monoexponential.[45]

Westerlund *et al.* showed that anionic surfactants play an active role in dissociating cationic intercalators from DNA,[23] and our work, where SDS removed both PTO and PG from CT DNA and poly(dA)•poly(dT), supports this finding. It was not possible to measure dye dissociation rates using our equipment as the initial drop in fluorescence occurred too quickly (< 2 s). However, the final fluorescence tells us what percentage of dye remained intercalated. The lack of PTO ICD in the presence of SDS indicates that SDS removes the dye from the DNA, rather than just quenching its fluorescence. The blue shift and increase in absorbance also support a loss of intercalated dye upon addition of SDS. At SDS concentrations below the CMC, PTO was extracted from ds CT DNA to a greater extent and more rapidly than PG. At SDS concentrations above the CMC, all intercalated PTO and PG were extracted from ds CT DNA. As part of a collaboration, Dr. C. C. Trevithick-Sutton measured the following dye dissociation rates using a stopped-flow apparatus: 32-44 $s^{-1}$ (or lifetimes of 23-32 ms) and 2.0-3.7 $s^{-1}$ (or lifetimes of 272-513 ms) for PTO and PG, respectively, in CT DNA with 1-50 mM SDS.

We have found that the presence of PG or PTO during hybridization of poly(dA) and poly(dT) results in the formation of a new (and more stable) type of

complex, which cannot be obtained by addition of the dye to poly(dA)•poly(dT). This information could be useful when considering the effects of drugs on double-stranded DNA formation. The experimental evidence consists of unique CD and ICD, and an increased steady-state fluorescence intensity and a higher DNA affinity (measured using SDS to extract the dye) relative to the complex formed by adding the dye to hybridized poly(dA)•poly(dT). There are additional hydrogen bonds in oligo(dA)•oligo(dT) tracts: these diagonal non-Watson-Crick hydrogen bonds occur between the H on the N6 atom of adenine and the O4 atom of thymine, resulting in a zig-zag system of bifurcated hydrogen bonds along the major groove.[58,59] One reviewer suggested that these additional hydrogen bonds might play a role in the stability of our new dye/DNA complex. However, this does not explain why the "new" complex (where the dye was added before strand hybridization) is more stable than the "regular" complex (where the dye was added after strand hybridization), as we would expect there to be more chance of preserving the bifurcated hydrogen bonds in the latter complex. Alternatively, the explanation may be related to the hydration of the complexes. Experimentally determined enthalpies of intercalation and molar volume changes suggest that entropy is the driving force in the intercalation of ethidium bromide and propidium iodide into poly(dA)•poly(dT), and that poly(dA)•poly(dT) is more hydrated than poly[d(A-T)]$_2$.[60] Measurements of relative changes in ultrasonic velocity provided direct estimates of the extent of hydration of various oligo- and polynucleotides, and it was suggested that oligo(dA)•oligo(dT) tracts have unusually high levels of hydration.[61] It is conceivable that the "new" complex might exclude more water molecules than the "regular" complex, making the former complex the more thermodynamically stable one. Another possible explanation is that the "new" complex involves the association of the dye with both poly(dT)•poly(dA)•poly(dT) and poly(dA). Although poly(dA)•poly(dT) is stable for months in the presence of coralyne (a small crescent-shaped molecule) at 4°C, upon heating to 35°C or above, the duplex disproportionates into poly(dT)•poly(dA)•poly(dT) and self-

complexed poly(dA).[62] The authors suggested that the disproportionation is due to a higher binding affinity of coralyne for both the triplex and the poly(dA) self-structure.

The above-mentioned hybridization effect was not observed for TO at all, nor for PG and PTO with poly(dG)•poly(dC); the absence of the effect in the latter cases may be due to the stronger base-pairing or to the tendency of single-stranded poly(dG) and poly(dC) to form self-complexed structures. Upon thermal cycling of the complexes where the dye (TO or PTO) was added to poly(dG)•poly(dC) before and after hybridization, a unique ICD was obtained which did not resemble that of the dye/poly(dG) or dye/poly(dC) or either dye/poly(dG)•poly(dC) complex before thermal cycling. This suggests that heating the dye/poly(dG)•poly(dC) complexes places the dye molecules in thermodynamically favourable orientations, which are similar to those of the dyes with single-stranded poly(dA) except the spectra are red-shifted by a few nanometres.

### 4.3.2. Computational Studies

The results of all of the molecular dynamics simulations involving the duplex DNA oligomers and the most stable structures of PTO and TO are summarized in Table 4.2.

**Table 4.2: Summary of computational results involving duplex DNA oligomers and PTO and TO.**

| Initial intercalated moiety | $(dG)_{10}$•$(dC)_{10}$ |
|---|---|
| PTO benzothiazole (Figure 4.33) | In both cases, the dye remained intercalated (in 1 case the benzothiazole moiety was between the G bases, and in the other case it was between the C bases). |
| PTO quinoline (Figure 4.39) | In 1 case, the dye remained intercalated and the quinoline moiety moved between the G bases.<br>In 1 case, both moieties became intercalated with the quinoline moiety between the G bases and the benzothiazole moiety between the C bases. |
| PTO pyridinium (Figure 4.48) | In 1 case, the dye dissociated.<br>In 1 case, the dye remained intercalated and the pyridinium moiety moved between the C bases. |
| TO benzothiazole (Figure 4.36) | In 2 cases, the dye dissociated.<br>In 1 case, the dye remained intercalated and the benzothiazole moiety moved between the G bases.<br>In 1 case, both moieties became intercalated with the benzothiazole moiety between the C bases and the quinoline moiety between the G bases. |
| TO quinoline (Figure 4.42) | In 3 cases, both moieties became intercalated (in 2 cases the quinoline moiety was between the C bases and the benzothiazole moiety was between the G bases, and in the other case it was reversed).<br>In 1 case, the dye remained intercalated and the quinoline moiety moved between the G bases. |
| TO benzothiazole and quinoline (Figure 4.45) | In all 4 cases, both moieties remained intercalated (in 2 cases the benzothiazole moiety was between the G bases and the quinoline moiety was between the C bases, and in the other 2 cases it was reversed). |

| **Initial intercalated moiety** | **$(dA)_{10}$•$(dT)_{10}$** |
|---|---|
| PTO benzothiazole (Figure 4.34) | In 1 case, the dye dissociated.<br>In 1 case, the dye remained intercalated and the benzothiazole moiety moved between the T bases. |
| PTO quinoline (Figure 4.40) | In 1 case, the dye remained intercalated and the quinoline moiety moved between the T bases.<br>In 1 case, both moieties became intercalated with the quinoline moiety between the A bases and the benzothiazole moiety between the T bases. |
| PTO pyridinium (Figure 4.49) | In the 2 cases, the dye dissociated. |
| TO benzothiazole (Figure 4.37) | In 1 case, the dye dissociated.<br>In 1 case, the dye remained intercalated but there was a shift that placed the quinoline moiety between the A bases.<br>In 2 cases, both moieties became intercalated with the benzothiazole moiety between the A bases and the quinoline moiety between the T bases. |
| TO quinoline (Figure 4.43) | In 3 cases, both moieties became intercalated (in 2 cases the quinoline moiety was between the T bases and the benzothiazole moiety was between the A bases, and in the other case it was reversed).<br>In 1 case, the dye remained intercalated and the quinoline moiety moved between the A bases. |
| TO benzothiazole and quinoline (Figure 4.46) | In all 4 cases, dye remained close to the starting orientation (in 2 cases the benzothiazole moiety was between the A bases and the quinoline moiety was between the T bases, and in the other 2 cases it was reversed). |
| | **duplex 2G** |
| PTO benzothiazole (Figure 4.51) | Dye remained intercalated with the benzothiazole moiety between the C bases. |
| PTO quinoline (Figure 4.51) | Dye remained intercalated with the quinoline moiety between the C bases and the benzothiazole moiety between the G bases. |
| PTO pyridinium (Figure 4.51) | Dye dissociated. |
| TO benzothiazole (Figure 4.54) | Dye remained intercalated with the benzothiazole moiety between the C bases and the quinoline moiety between the G bases. |

| Initial intercalated moiety | duplex 2G (continued) |
|---|---|
| TO quinoline (Figure 4.54) | Dye remained intercalated with the quinoline moiety between the C bases and the benzothiazole moiety between the G bases. |
| TO benzothiazole and quinoline (Figure 4.56) | Dye remained close to the starting orientation (the benzothiazole moiety was between the C bases and the quinoline moiety was between the G bases). |
| | **duplex 2A** |
| PTO benzothiazole (Figure 4.52) | Dye remained intercalated with the benzothiazole moiety between the A bases. |
| PTO quinoline (Figure 4.52) | Dye remained intercalated with the quinoline moiety between the A bases. |
| PTO pyridinium (Figure 4.52) | Dye dissociated. |
| TO benzothiazole (Figure 4.55) | Dye remained intercalated with the benzothiazole moiety between the T bases and the quinoline moiety between the A bases. |
| TO quinoline (Figure 4.55) | Dye remained intercalated with the quinoline moiety between the T bases and the benzothiazole moiety between the A bases. |
| TO benzothiazole and quinoline (Figure 4.56) | Dye remained close to the starting orientation (the benzothiazole moiety was between the T bases and the quinoline moiety was between the A bases). |

In almost all of the cases studied, the two dyes remained intercalated in $(dG)_{10}$•$(dC)_{10}$ and $(dA)_{10}$•$(dT)_{10}$: this occurred in 7 of the 8 PTO cases and in 21 of the 24 TO cases. In Chapter 3 it was suggested that intercalation of the PTO quinoline moiety is preferred in $(dA)_{10}$ and $(dG)_{10}$, but this base specificity was not apparent for PTO and the duplex oligomers. In 5 of the 8 cases involving PTO and $(dG)_{10}$•$(dC)_{10}$ or $(dA)_{10}$•$(dT)_{10}$, whichever moiety (either the benzothiazole or the quinoline) was initially placed between the base pairs remained intercalated throughout the simulation. In 2 of the remaining cases both PTO moieties became intercalated, and in one case the dye dissociated. In Chapter 3 there was no preference for intercalation of a specific TO moiety in $(dA)_{10}$ and $(dG)_{10}$, and the same was true of TO in $(dA)_{10}$•$(dT)_{10}$ or $(dG)_{10}$•$(dC)_{10}$.

The PTO pyridinium moiety consists of only one aromatic ring and has significant flexibility, thus it seems unlikely that this moiety would become intercalated. In Chapter 3 it was found that intercalation of the pyridinium moiety in single-stranded DNA oligomers led to dissociation or partial dissociation in 15 of the 16 cases studied. This also occurred in 3 of the 4 simulations involving intercalation of the PTO pyridinium moiety in $(dA)_{10}$•$(dT)_{10}$ or $(dG)_{10}$•$(dC)_{10}$. When studying the intercalation of the PTO pyridinium moiety in double-stranded DNA oligomers containing mixed base pairs, both cases led to dye dissociation.

In Chapter 3 a strong association between the dyes (PTO and TO) and the single-stranded homopolymers poly(dA) and poly(dG) was found, both experimentally and computationally. Such a binding preference was not observed in the simulations involving the dyes and double-stranded DNA containing mixed base pairs. All 4 cases involving intercalation of the TO benzothiazole or quinoline moiety in duplex 2G or duplex 2A ended up with both moieties between the bases, and whichever moiety was initially placed between the 4 bases ended up between the 2 pyrimidine bases. Of the 4 cases involving intercalation of the PTO benzothiazole or quinoline moiety in duplex 2G or duplex 2A, only 1 resulted in intercalation of both moieties and, like with TO, the moiety that was initially intercalated became positioned between the pyrimidine bases. Of the 3 remaining cases, in one the intercalated moiety remained intercalated but shifted so that it was between the pyrimidine bases. In the other 2 cases, which both involved duplex 2A, the intercalated moiety shifted so that it was between two A bases. With the exception of these 2 cases, it would appear that intercalation of either the benzothiazole or the quinoline moiety of PTO or TO in these duplexes results in a shift that places the moiety that was initially intercalated between the pyrimidine bases.

In Chapter 3 it was mentioned how Spielmann *et al.* used NOE-derived distance restraints in restrained molecular dynamics calculations and found that TOTO bis-intercalates in the CTAG•CTAG site of d(5'-CGCTAGCG-3')$_2$ with the benzothiazole moiety between the pyrimidines and the quinoline moiety between

the purines.[63] When the initially intercalated dye moiety remained intercalated during the simulation, the benzothiazole moiety did not show an affinity for being between pyrimidines nor did the quinoline moiety prefer the purines. When one moiety was initially intercalated and the other moiety became intercalated during the simulation, neither moiety showed an affinity for a specific type of base.

In the renaturation simulations, the starting orientation for the DNA oligomers consisted of the two strands being far apart with the exception of 3 base pairs at one end, which represents the nucleation event being complete and the zippering event about to commence. Many trials were run and there was never a case where all 10 base pairs formed thus starting orientations from the simulations where 9 and 8 base pairs formed in renat-AT and renat-GC, respectively, were used in the simulations involving PTO and TO. In every case, the presence of the dye inhibited renaturation. In some cases the effect was significant and the DNA strands became twisted and/or moved far apart. The majority of the time either the PTO benzothiazole or quinoline moiety (or both) interacted with the bases, rather than the pyridinium moiety.

## 4.4. Conclusions

The results of the molecular dynamics simulations involving the dyes and double-stranded DNA show a strong association between the dyes and the duplexes, as do the experimental results. The dyes associate with both natural and synthetic dsDNA, evidenced by the change in their absorption spectra, the appearance of induced circular dichroism and linear dichroism, and the strong fluorescence enhancement (relative to the dye in buffer). Evidence supporting dye intercalation in DNA consists of a red-shift in the dye absorption bands and the similarity in the reduced linear dichroism amplitudes in the DNA and dye regions. However, the LD results indicate that both the monomeric and dimeric forms of the dyes intercalate in both ss- and dsDNA, although a portion of the dimeric form is free in solution rather than intercalated. In the case of PG, the majority of the dye is present as the monomeric form in both buffer and DNA.

There is no conclusive experimental evidence supporting or contesting sequence specificity of the binding of cyanine dyes to DNA. It is difficult to draw any conclusions about binding specificity from our experimental findings as there are 10 different intercalation sites in CT DNA.[27] Even in the synthetic duplexes where there is one unique intercalation site the dye can bind in 3 different ways, for example, in poly(dA)•poly(dT) it can intercalate between two A bases, two T bases, or between two AT base pairs. The usefulness of the molecular dynamics simulations in providing insight into the interactions between the dyes and the DNA is apparent. In our computational studies we did not observe a preference for intercalation of a specific moiety of the dye in the duplex oligomers, nor did we see any affinities between the moieties and specific bases or types of bases. This supports PTO and TO binding to DNA without sequence specificity.

It was interesting to discover that a new type of stable dye/DNA complex is formed when single-strands of poly(dA) and poly(dT) are hybridized in the presence of PG or PTO, which cannot be obtained by the addition of the dye to poly(dA)•poly(dT). It was also found for all three dyes that complete DNA

renaturation did not occur during thermal cycling of dye/ds CT DNA complexes. The exact structure of the new dye/DNA complexes is unknown, although the results of the molecular dynamics simulations indicate that in some cases the DNA strands are far apart and twisted, while in others the base pairs have formed except in the area near the dye, and the base pairing does not always follow the Watson-Crick model.

While the exact structure of these new complexes, the possibilities for their formation in biological systems, and their effects on such systems are unknown, it is clear that these intercalating dyes interfere with DNA hybridization to double-stranded DNA. This information could contribute to the design of more effective chemotherapeutic agents and antibiotics. The results also reveal that, in DNA hybridization experiments, one cannot use fluorescence enhancement of intercalators as a means of studying DNA structure, as the information it provides is ambiguous.

## 4.5. Materials and Methods

### 4.5.1. Materials

The Tris buffer solutions were prepared in 18 MΩ water (Millipore Corporation) with Trizma Pre-Set Crystals (reagent grade, pH 7.4) from Sigma-Aldrich, $Na_2EDTA$ (Sigma Grade) from Sigma-Aldrich, and NaCl (optical grade) from Alfa Aesar. The N-propyl pyridinium derivative of thiazole orange is commercially available from Dr. Todor Deligeorgiev at the University of Sofia, Bulgaria. Thiazole orange tosylate (for fluorescence, ≥98.0% by HPLC) and sodium dodecyl sulfate (MicroSelect for molecular biology) were purchased from Fluka, PicoGreen dsDNA quantitation reagent was from Invitrogen, DMSO (HPLC grade) was obtained from OmniSolv, and calf thymus DNA (Type I, highly polymerized, sodium salt) was bought from Sigma-Aldrich. Poly(dA), poly(dT), and poly(dC) were obtained from Midland Certified Reagent Company, and poly(dG) was purchased from BioCorp. For poly(dA) most of the material had between 125 and 350 bases; poly(dT) was longer, with most of the material between 900 and 1200 bases. The size of poly(dC) was not available, and poly(dG) was 40 bases in length. Quartz Suprasil cuvettes (Hellma or Luzchem Research Inc.) with a 10 mm optical path were employed for absorbance, induced circular dichroism and fluorescence measurements, although on occasion a 5 mm optical path was used instead for recording induced circular dichroism. A 1 mm optical path was used to monitor the circular dichroism in the DNA region, and a 6 mm optical path was used to measure linear dichroism.

### 4.5.2. Solution Preparation

A stock buffer solution of pH 7.4 was prepared containing 0.01 M Tris, 0.001 M EDTA, and 0.1 M NaCl. All DNA concentrations were determined by absorption spectroscopy using the following 260 nm extinction coefficients: 6 600 $M^{-1}cm^{-1}$ per base for calf thymus DNA, 15 100 $M^{-1}cm^{-1}$ for poly(dA), 11 700 $M^{-1}cm^{-1}$ for poly(dG), 8 700 $M^{-1}cm^{-1}$ for poly(dT) and 7 400 $M^{-1}cm^{-1}$ for

poly(dC). The concentrations of the dye stock solutions were determined by measuring the absorption of a diluted dye solution (a concentration where no aggregation occurs) and using the extinction coefficient of 73 900 $M^{-1}cm^{-1}$ for PTO (510.5 nm),[64] and 63 000 $M^{-1}cm^{-1}$ for TO (500 nm).[14] The PG concentration was estimated using the reported extinction coefficient of 70 000 $M^{-1}cm^{-1}$.[6] The PTO, SDS and DNA stock solutions were prepared in buffer and subsequently diluted in buffer when the dye:DNA solutions were prepared. The DNA stock solutions were shaken for 1 h (to ensure dissolution of the DNA) and stored at -4°C, or at -20°C for long-term storage. The dyes, as received from the suppliers, were kept at -20°C. A stock solution of TO was made by dissolving the dye in DMSO and then adding buffer to produce a 1:30 DMSO:buffer solution which was subsequently diluted in buffer when the dye:DNA solutions were prepared. The dye:DNA base or dye:DNA base pair ratio (d/b) is defined as the number of chromophores per base or base pair, respectively. A 1:10 d/b ratio was used to ensure that the dominant binding mode would be that of intercalation. Dye/CT DNA concentrations in the final mixtures were (20/200) μM when monitoring absorbance, steady-state fluorescence, and circular dichroism and induced circular dichroism. A dye/CT DNA concentration of (10/100) μM was used to measure linear dichroism as well as the ICD of the heated solutions. Time-resolved fluorescence decays were recorded using various d/b ratios, specifically (9/90), (20/1000), (20/200) and (20/22.2), as mentioned in Table 4.1. For each experiment, freshly prepared solutions using the stocks were made. In between measurements, the samples were covered in aluminum foil to prevent unnecessary exposure to light, i.e. degradation of the dye. Experiments were carried out at room temperature, except for the CD work where the temperature was kept fixed at 20°C.

### 4.5.3. Thermal Cycling and Shock Cooling

Thermal cycling refers to the following procedure: heating the solution at 90 or 95°C for 10 minutes (to denature the DNA) and then allowing it to return to room temperature (to allow renaturation). To generate single-stranded DNA, double-

stranded DNA was heated at 95°C for 10 minutes (to denature the DNA) and then shock cooled in an ice bath (to prevent renaturation).

### 4.5.4. SDS Experiments

The dye (PG or PTO) was added to the CT DNA the day before the SDS experiment was performed. When studying dye extraction from hybridized poly(dA)•poly(dT), the dye (PG or PTO) was incubated with the DNA for 4 hours and the strands were allowed to hybridize for 17 hours while stored at room temperature and protected from light exposure. The only exception was the 0 mM SDS solution, where the dye and DNA were mixed at the beginning of the fluorescence measurement. The dye/DNA solution was placed in a cuvette (with a stir bar) in the fluorimeter sample holder and then an equal volume of SDS solution was injected (from a syringe) into the cuvette via a hole in the top of the sample chamber. A homemade cardboard guide was used to direct the needle into the cuvette. Dye/DNA concentrations in the final mixtures were (3.5/35) μM, except for PTO and poly(dA)•poly(dT) where it was (5/50) μM.

### 4.5.5. Hybridization Experiments

The dye was incubated with the DNA for 4 hours and the strands were allowed to hybridize for 17 hours while stored at room temperature and protected from light exposure. Dye/DNA concentrations in the final mixtures were either (3.5/35) or (7/70) μM, except for PG and poly(dG)•poly(dC) where the extremely weak signal required the use of (20/200) μM solutions.

### 4.5.6. Instrumentation

Absorption spectra were recorded using a Varian Cary-50 with a scan rate of 600 nm/min. Steady-state fluorescence spectroscopy was carried out using a Photon Technology International luminescence spectrometer. Fluorescence emission spectra were recorded upon 355 nm excitation, or an excitation wavelength corresponding to the dye monomer or dimer/aggregate absorption maximum, using a 1 s integration time and 1 nm integration step. The excitation

slits were 1 nm while the emission slits were 4 nm. Fluorescence excitation spectra were recorded while monitoring the fluorescence at the emission maximum of the dye monomer.

Time-resolved studies were made with the third harmonic of a Continuum PY-61 Nd:YAG laser ($\lambda$= 355 nm, fwhm = 35 ps, pulse energy $\leq$ 4 mJ), using a Hamamatsu C4334 streak camera and Hamamatsu Photoluminescence Measurement Software U4790 version 2.2 for luminescence detection.

Circular dichroism experiments were performed on a Jasco J-810 spectrometer with a 150 W Xenon lamp. The instrumental parameters were a 1 nm data pitch, continuous scanning mode, 50 nm/min scan speed, 2 s response, and 1 nm bandwidth. The buffer solution spectrum was used as a blank, which was subtracted from the CD signals. Linear dichroism experiments were also performed on this instrument with the same instrumental parameters, using a rotating Couette cell to orient the sample. The blank was obtained by monitoring the linear dichroism signal of the non-rotating sample, i.e. 0 rpm, and subtracting it from the signal that was obtained when the sample was rotating at an rpm that produced laminar flow (approximately 80-90 rpm). A complete description of the linear dichroism apparatus is given in Chapter 2.

### 4.5.7. Computational Details

The computational details were discussed in detail in Section 3.5.4 of this thesis. The only things done differently in this chapter were that the canonical structures of the dsDNA fragments were composed of 10 base pairs (rather than 10 bases for ssDNA), and 18 $Na^+$ counterions (rather than 9 for ssDNA) were added in the proximity of the $PO_4^-$ groups of the dsDNA to maintain the neutrality of the system.

As mentioned in the Results section, the starting orientations for the DNA renaturation simulations were obtained by running a minimization *in vacuo* with a nonbonded cutoff of 999 Å, which pushed the two strands apart due to the large repulsive charge on the two chains. To aid in the strand separation, the temperature was increased from 0-300K and 0-900K for renat-AT and renat-GC,

respectively. Three base pairs at one end of the duplex were constrained using 100 and 150 kcal $mol^{-1}$ restraint forces for renat-GC and renat-AT, respectively, during the minimization. To get the two strands apart (but not too far apart), a total of 5500 and 5700 molecular dynamics steps with a time step of 1 fs per step were run for renat-GC and renat-AT, respectively.

## 4.6. References


1. Hurley, L. H., DNA and associated targets for drug design. *J. Med. Chem.* **1989,** 32, (9), 2027-2033.

2. Dougherty, G.; Pilbrow, J. R., Physico-chemical probes of intercalation. *Int. J. Biochem.* **1984,** 16, (12), 1179-1192.

3. Becker, M. M.; Dervan, P. B., Molecular recognition of nucleic acid by small molecules. Binding affinity and structural specificity of bis(methidium)spermine. *J. Am. Chem. Soc.* **1979,** 101, (13), 3664-3666.

4. Graves, D. E.; Velea, L. M., Intercalative binding of small molecules to nucleic acids. *Curr. Org. Chem.* **2000,** 4, (9), 915-929.

5. Rye, H. S.; Yue, S.; Wemmer, D. E.; Quesada, M. A.; Haugland, R. P.; Mathies, R. A.; Glazer, A. N., Stable fluorescent complexes of double-stranded DNA with bis-intercalating asymmetric cyanine dyes: properties and applications. *Nucleic Acids Res.* **1992,** 20, (11), 2803-2812.

6. Singer, V. L.; Jones, L. J.; Yue, S. T.; Haugland, R. P., Characterization of PicoGreen reagent and development of a fluorescence-based solution assay for double-stranded DNA quantitation. *Anal. Biochem.* **1997,** 249, (2), 228-238.

7. Lee, L. G.; Chen, C.-H.; Chiu, L. A., Thiazole orange: a new dye for reticulocyte analysis. *Cytometry* **1986,** 7, 508-517.

8. Boger, D. L.; Fink, B. E.; Brunette, S. R.; Tse, W. C.; Hedrick, M. P., A simple, high-resolution method for establishing DNA binding affinity and sequence selectivity. *J. Am. Chem. Soc.* **2001,** 123, (25), 5878-5891.

9. Rye, H. S.; Quesada, M. A.; Peck, K.; Mathies, R. A.; Glazer, A. N., High-sensitivity two-color detection of double-stranded DNA with a confocal fluorescence gel scanner using ethidium homodimer and thiazole orange. *Nucleic Acids Res.* **1991,** 19, (2), 327-333.

10. Glazer, A. N.; Rye, H. S., Stable dye-DNA intercalation complexes as reagents for high-sensitivity fluorescence detection. *Nature* **1992,** 359, 859-861.

11. Glazer, A. N.; Peck, K.; Mathies, R. A., A stable double-stranded DNA-ethidium homodimer complex: application to picogram fluorescence detection of DNA in agarose gels. *Proc. Natl. Acad. Sci. U.S.A.* **1990,** 87, 3851-3855.

12. Zhu, H.; Clark, S. M.; Benson, S. C.; Rye, H. S.; Glazer, A. N.; Mathies, R. A., High-sensitivity capillary electrophoresis of double-stranded DNA fragments using monomeric and dimeric fluorescent intercalating dyes. *Anal. Chem.* **1994,** 66, (13), 1941-1948.

13. Netzel, T. L.; Nafisi, K.; Zhao, M.; Lenhard, J. R.; Johnson, I., Base-content dependence of emission enhancements, quantum yields, and lifetimes for cyanine dyes bound to double-strand DNA: photophysical properties of monomeric and bichromophoric DNA stains. *J. Phys. Chem.* **1995,** 99, (51), 17936-17947.

14. Nygren, J.; Svanvik, N.; Kubista, M., The interactions between the fluorescent dye thiazole orange and DNA. *Biopolymers* **1998,** 46, 39-51.

15. Petty, J. T.; Bordelon, J. A.; Robertson, M. E., Thermodynamic characterization of the association of cyanine dyes with DNA. *J. Phys. Chem. B.* **2000,** 104, (30), 7221-7227.

16. Müller, W.; Crothers, D. M., Studies of the binding of actinomycin and related compounds to DNA. *J. Mol. Biol.* **1968,** 35, 251-290.

17. Wilson, D. W.; Grier, D.; Reimer, R.; Bauman, J. D.; Preston, J. F.; Gabbay, E. J., Structure-activity relationship of daunorubicin and its peptide derivatives. *J. Med. Chem.* **1976,** 19, (3), 381-384.

18. Gabbay, E. J.; Grier, D.; Fingerle, R. E.; Reimer, R.; Levy, R.; Pearce, S. W.; Wilson, W. D., Interaction specificity of the anthracyclines with deoxyribonucleic acid. *Biochemistry* **1976,** 15, (10), 2062-2070.

19. White, R. J.; Phillips, D. R., Drug-DNA dissociation kinetics: *in vitro* transcription and sodium dodecyl sulphate sequestration. *Biochem. Pharmacol.* **1989,** 38, (2), 331-334.

20. Fox, K. R.; Brassett, C.; Waring, M. J., Kinetics of dissociation from DNA: comparison with other anthracycline antibiotics. *Biochim. Biophys. Acta* **1985,** 840, 383-392.

21. Phillips, D. R.; Greif, P. C.; Boston, R. C., Daunomycin-DNA dissociation kinetics. *Mol. Pharmacol.* **1988,** 33, 225-230.

22. Wakelin, L. P. G.; Atwell, G. J.; Rewcastle, G. W.; Denny, W. A., Relationships between DNA-binding kinetics and biological activity for the 9-aminoacridine-4-carboxamide class of antitumor agents. *J. Med. Chem.* **1987,** 30, (5), 855-861.

23. Westerlund, F.; Wilhelmsson, L. M.; Nord*n, B.; Lincoln, P., Micelle-sequestered dissociation of cationic DNA-intercalated drugs: unexpected surfactant-induced rate enhancement. *J. Am. Chem. Soc.* **2003,** 125, (13), 3773-3779.

24. Bloomfield, V. A.; Crothers, D. M.; Tinoco, I., Jr., Interaction and Reaction with Drugs. In *Nucleic Acids: Structures, Properties, and Functions*, University Science Books: Sausalito, 2000; pp 535-596.

25. Ogul'chansky, T. Y.; Losytskyy, M. Y.; Kovalska, V. B.; Yashchuk, V. M.; Yarmoluk, S. M., Interactions of cyanine dyes with nucleic acids. XXIV. Aggregation of monomethine cyanine dyes in presence of DNA and its manifestation in absorption and fluorescence spectra. *Spectrochim. Acta A* **2001,** 57, 1525-1532.

26. Cosa, G.; Focsaneanu, K.-S.; McLean, J. R. N.; McNamee, J. P.; Scaiano, J. C., Photophysical properties of fluorescent DNA-dyes bound to single- and double-stranded DNA in aqueous buffered solution. *Photochem. Photobiol.* **2001,** 73, (6), 585-599.

27. Ardhammar, M.; Nordén, B.; Kurucsev, T., DNA-Drug Interactions. In *Circular Dichroism: Principles and Applications*, 2nd ed.; Berova, N.; Nakanishi, K.; Woody, R. W., Eds. Wiley-VCH: New York, 2000; pp 741-768.

28. Gray, D. M.; Ratliff, R. L.; Vaughan, M. R., Circular dichroism spectroscopy of DNA. *Methods Enzymol.* **1992,** 211, 389-406.

29. Schweitzer, C.; Scaiano, J. C., Selective binding and local photophysics of the fluorescent cyanine dye PicoGreen in double-stranded and single-stranded DNA. *Phys. Chem. Chem. Phys.* **2003,** 5, 4911-4917.

30. Rodger, A., Linear dichroism. *Methods Enzymol.* **1993,** 226, 232-258.

31. Vogt, H.; Hänisch, G.; Hochstrasser, R. A., A simple inexpensive Couette cell for flow-oriented linear dichroism. *Rev. Sci. Instrum.* **1995,** 66, (8), 4385-4386.

32. Marrington, R.; Dafforn, T. R.; Halsall, D. J.; Rodger, A., Micro-volume Couette flow sample orientation for absorbance and fluorescence linear dichroism. *Biophys. J.* **2004,** 87, (3), 2002-2012.

33. Nordén, B.; Seth, S., Structure of strand-separated DNA in different environments studied by linear dichroism. *Biopolymers* **1979,** 18, (9), 2323-2339.

34. Wada, A., Chain regularity and flow dichroism of deoxyribonucleic acids in solution. *Biopolymers* **1964,** 2, (4), 361-380.

35. Larsson, A.; Carlsson, C.; Jonsson, M.; Albinsson, B., Characterization of the binding of the fluorescent dyes YO and YOYO to DNA by polarized light spectroscopy. *J. Am. Chem. Soc.* **1994,** 116, (19), 8459-8465.

36. Larsson, A.; Carlsson, C.; Jonsson, M., Characterization of the binding of YO to $[poly(dA\text{-}dT)]_2$ and $[poly(dG\text{-}dC)]_2$, and of the fluorescent properties of YO and YOYO complexed with the polynucleotides and double-stranded DNA. *Biopolymers* **1995,** 36, (2), 153-167.

37. Nordén, B.; Tjerneld, F., Structure of methylene blue-DNA complexes studied by linear and circular dichroism spectroscopy. *Biopolymers* **1982,** 21, (9), 1713-1734.

38. Simonson, T.; Kubista, M., DNA orientation in shear flow. *Biopolymers* **1993,** 33, (8), 1225-1235.

39. Nordén, B.; Kubista, M.; Kurucsev, T., Linear dichroism spectroscopy of nucleic acids. *Quart. Rev. Biophys.* **1992,** 25, (1), 51-170.

40. Lerman, L. S., The structure of the DNA-acridine complex. *Proc. Natl. Acad. Sci. U.S.A.* **1963,** 49, (1), 94-102.

41. Rodger, A.; Latham, H. C.; Wormell, P.; Parkinson, A.; Ismail, M.; Sanders, K. J., DNA-drug systems: how circular dichroism data is complemented by other spectroscopic techniques. *Enantiomer* **1998,** 3, 395-408.

42. Eriksson, M.; Nordén, B.; Eriksson, S., Anthracycline-DNA interactions studied with linear dichroism and fluorescence spectroscopy. *Biochemistry* **1988,** 27, (21), 8144-8151.

43. Bailly, C.; Hénichart, J.-P.; Colson, P.; Houssier, C., Drug-DNA sequence-dependent interactions analysed by electric linear dichroism. *J. Mol. Recognit.* **1992,** 5, 155-171.

44. Tuite, E.; Nordén, B., Sequence-specific interactions of methylene blue with polynucleotides and DNA: a spectroscopic study. *J. Am. Chem. Soc.* **1994,** 116, (17), 7548-7556.

45. Cosa, G.; Focsaneanu, K.-S.; McLean, J. R. N.; Scaiano, J. C., Direct determination of single-to-double stranded DNA ratio in solution applying time-resolved fluorescence measurements of dye-DNA complexes. *Chem. Commun.* **2000,** 8, 689-690.

46. Wilhelmsson, L. M.; Westerlund, F.; Lincoln, P.; Nordén, B., DNA-binding of semirigid binuclear ruthenium complex $\Delta,\Delta$-[μ-(11,11'-bidppz)(phen)$_4$Ru$_2$]$^{4+}$: extremely slow intercalation kinetics. *J. Am. Chem. Soc.* **2002,** 124, (41), 12092-12093.

47. Rosen, M. J., *Surfactants and Interfacial Phenomena*. 2nd ed.; John Wiley & Sons: New York, 1989; p 122-123.

48. Johnson, W. C., Jr., Determination of the conformation of nucleic acids by electronic CD. In *Circular Dichroism and the Conformational Analysis of Biomolecules*, Fasman, G. D., Ed. Plenum Press: New York, 1996; pp 433-468.

49. Gray, D. M.; Bollum, F. J., A circular dichroism study of poly dG, poly dC, and poly dG:dC. *Biopolymers* **1974,** 13, (10), 2087-2102.

50. Jacobsen, J. P.; Pedersen, J. B.; Hansen, L. F.; Wemmer, D. E., Site selective bis-intercalation of a homodimeric thiazole orange dye in DNA oligonucleotides. *Nucleic Acids Res.* **1995,** 23, (5), 753-760.

51. Barton, D., Sir; Nakanishi, K.; Meth-Cohn, C., *Comprehensive natural products chemistry.* Elsevier: Amsterdam; New York, 1999; Vol. 7, p 417-476.

52. Wetmur, J. G.; Davidson, N., Kinetics of renaturation of DNA. *J. Mol. Biol.* **1968,** 31, (3), 349-370.

53. Huffman, J. L.; Sundheim, O.; Tainer, J. A., DNA base damage recognition and removal: New twists and grooves. *Mutat. Res.* **2005,** 577, 55-76.

54. Lloyd, R. S., Investigations of pyrimidine dimer glycosylases - a paradigm for DNA base excision repair enzymology. *Mutat. Res.* **2005,** 577, 77-91.

55. Nakatani, K.; Hagihara, S.; Goto, Y.; Kobori, A.; Hagihara, M.; Hayashi, G.; Kyo, M.; Nomura, M.; Mishima, M.; Kojima, C., Small-molecule ligand induces nucleotide flipping in $(CAG)_n$ trinucleotide repeats. *Nat. Chem. Biol.* **2005,** 1, (1), 39-43.

56. Slupphaug, G.; Mol, C. D.; Kavli, B.; Arvai, A. S.; Krokan, H. E.; Tainer, J. A., A nucleotide-flipping mechanism from the structure of human uracil-DNA glycosylase bound to DNA. *Nature* **1996,** 384, (7), 87-92.

57. Wong, I.; Lundquist, A. J.; Bernards, A. S.; Mosbaugh, D. W., Presteady-state analysis of a single catalytic turnover by *Escherichia coli* uracil-DNA glycosylase reveals a "pinch-*pull*-push" mechanism. *J. Biol. Chem.* **2002,** 277, (22), 19424-19432.

58. Nelson, H. C. M.; Finch, J. T.; Luisi, B. F.; Klug, A., The structure of an oligo(dA)•oligo(dT) tract and its biological implications. *Nature* **1987,** 330, (19), 221-226.

59. Coll, M.; Frederick, C. A.; Wang, A. H.-J.; Rich, A., A bifurcated hydrogen-bonded conformation in the d(A•T) base pairs of the DNA dodecamer d(CGCAAATTTGCG) and its complex with distamycin. *Proc. Natl. Acad. Sci. U.S.A.* **1987,** 84, (23), 8385-8389.

60. Marky, L. A.; Macgregor, R. B., Jr., Hydration of dA•dT polymers: role of water in the thermodynamics of ethidium and propidium intercalation. *Biochemistry* **1990,** 29, (20), 4805-4811.

61. Buckin, V. A.; Kankiya, B. I.; Bulichov, N. V.; Lebedev, A. V.; Gukovsky, I. Y.; Chuprina, V. P.; Sarvazyan, A. P.; Williams, A. R., Measurement of anomalously high hydration of $(dA)_n$•$(dT)_n$ double helices in dilute solution. *Nature* **1989,** 340, 321-322.

62. Polak, M.; Hud, N. V., Complete disproportionation of duplex poly(dT)•poly(dA) into triplex poly(dT)•poly(dA)•poly(dT) and poly(dA) by coralyne. *Nucleic Acids Res.* **2002,** 30, (4), 983-992.

63. Spielmann, H. P.; Wemmer, D. E.; Jacobsen, J. P., Solution structure of a DNA complex with the fluorescent bis-intercalator TOTO determined by NMR spectroscopy. *Biochemistry* **1995,** 34, (27), 8542-8553.

64. Timtcheva, I.; Maximova, V.; Deligeorgiev, T.; Zaneva, D.; Ivanov, I., New asymmetric monomethine cyanine dyes for nucleic-acid labelling: absorption and fluorescence spectral characteristics. *J. Photochem. Photobiol. A: Chem.* **2000,** 130, (1), 7-11.

# 5. Thiazole Orange as a Reporter of UVC-Induced DNA Damage

## 5.1. Introduction

Damage to DNA is of intense interest because of its importance in biological systems. Even the modification of a single nucleotide in the three billion nucleotide human genome can have a drastic effect on a person's health.[1] DNA damage can be caused by reactive oxygen species, by exposure to gamma radiation, or simple exposure to sunlight. In addition to studying DNA damage in humans, it is also of interest to study it in foods and biomaterials. Several foodstuffs in Canada and elsewhere, such as mangoes, seafood, poultry, beef, potatoes, onions, and spices, are exposed to ionizing radiation in order to disinfect them and to increase their shelf life.[2-6] In addition to the many medical applications, the regulatory application to determine food authenticity (following irradiation of food), could benefit from rapid screening methods for detecting DNA damage. Our analytical technique is geared towards food authenticity applications (following treatment with ionizing radiation). We do not characterize specific DNA lesions caused by food sterilization techniques or ultraviolet exposure, rather our aim is to easily indicate the presence of DNA damage from the loss of intercalation sites, independently of the identity of the products.

Fluorescence-based techniques are good candidates for rapid screening of DNA damage due to their high sensitivity. Previous work in our laboratory has shown that the fluorescence lifetimes of intercalated dyes, particularly PicoGreen®, can be used to distinguish single- from double-stranded DNA, and ultimately to monitor DNA damage.[7,8] When PicoGreen is free in solution and it is irradiated, it decays almost exclusively by radiationless transitions involving the rotation around its central methine bridge. When the dye is intercalated between two bases (or base pairs) its rotational freedom is restricted, forcing it to dissipate its energy predominantly via fluorescence emission. The more restrictive environment in double-stranded DNA (dsDNA) results in a longer excited dye lifetime than of that in single-stranded DNA (ssDNA). Current limitations of this technique relate to the high cost of the instrumentation and the high level of operator expertise required.

An alternative to time-resolved fluorescence is steady-state fluorescence in which results can be obtained within minutes. Previous work in our laboratory has shown that quantification of ss:dsDNA ratios is possible through a simple method involving simultaneous measurements of steady-state fluorescence from PicoGreen and ethidium bromide.[9] Quantitative determinations can be made on very small amounts of DNA as long as the DNA concentration is accurately known. When monomethine cyanine dyes are used in steady-state experiments the same principle can be applied where free dye is virtually non-fluorescent whilst the intercalated dye is strongly fluorescent. Steady-state fluorescence techniques are an attractive option, given their high sensitivity, relatively low cost, and the low level of operator training required for steady-state measurements.

The cyanine dye that we chose for these experiments is thiazole orange (TO), which is shown in Scheme 5.1. TO was first introduced as an RNA stain in reticulocyte analysis using flow cytometry.[10] Its fluorescence quantum yield increases ~3,000 times upon binding to nucleic acids[10] due to the change in rotational flexibility going from water, where energy dissipating rotations occur readily, to intercalation in DNA, where forced planarity (dsDNA) or restricted rotation (ssDNA) result in enhanced dye fluorescence. TO has also been used for fluorescence-detected capillary electrophoresis separations,[11] as the intercalator in a fluorescent intercalator displacement assay[12] and as a DNA stain in agarose gels.[13]

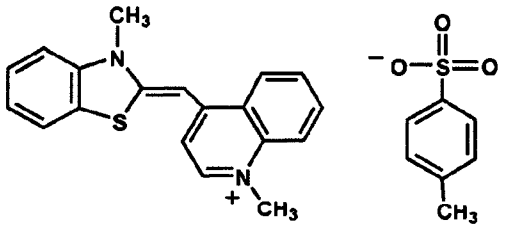


**Scheme 5.1: The structure of thiazole orange (TO) as a tosylate salt.**

DNA damage can be identified by agarose gel electrophoresis, circular dichroism spectroscopy, and even absorbance spectroscopy. Fluorescence spectroscopy is more sensitive than any of these techniques, and we have found that adding an intercalating fluorescent molecule to DNA allows one to measure DNA damage by studying its effect on post-exposure intercalation. In this case, the fluorescent molecule is reporting damage to the DNA because of its reduced ability to intercalate, thereby leading to a decrease in fluorescence emission intensity. This novel technique provides a fast screening method to identify damage to DNA, which is geared towards high levels of damage, such as those that may result during radiation treatment of food products.

With respect to verifying food authenticity, irradiation of foodstuffs ranges from 0.5 kGy to 10 kGy (i.e., over one hundred times the lethal dose for humans), and microbes are killed by fragmentation of DNA.[6] In our laboratory setup we have employed UVC radiation to cause extensive DNA damage, comparable to that produced by ionizing radiation in food sterilization technologies. In this work we explore the ability of TO to report DNA damage; ultraviolet-C light is simply a convenient tool to cause such damage. Molecular modeling was employed to gain further insight into the interaction of TO with damaged DNA.

This project was a collaboration with a postdoctoral fellow in our laboratory, Dr. C.C. Trevithick-Sutton. V. Filippenko, who worked, under our supervision, in our laboratory as part of her honours project during her undergraduate studies at the University of Ottawa, performed some of the measurements presented in this chapter. I am grateful for her help. The molecular dynamics simulations were done in collaboration with a postdoctoral fellow in our laboratory, Dr. C. Carra.

## 5.2. Results

### 5.2.1. Irradiation

Ultraviolet-C (UVC) light (200-280 nm, predominantly 254 nm in our case) was employed to irradiate the DNA samples because photochemical reactions in DNA are most efficient with this radiation source[14-34] since the purines and pyrimidines absorb UVC light strongly. UVC damages DNA via the formation of cyclobutadipyrimidine and other pyrimidine photoadducts (major products)[16,20] and oxidizes guanine (minor product)[30] and results in base transversions (minor product).[26,35] Although UVC radiation does not reach the Earth, in the laboratory it forms the DNA photoproducts that also result from atmosphere-penetrating ultraviolet-B (UVB) radiation. Cyclobutadipyrimidines (CPDs) (thymine dimers are most frequent, but uracil dimers in RNA can also occur and cytosine can engage in dimerization of the [2+2] variety, too) and pyrimidine (6-4) pyrimidones (6-4PPs) are the major DNA photoproducts upon exposure to UVB light.[14]

The yields of 8-oxo-2'-deoxyguanosine (8-oxo-dG) are reduced when DNA is irradiated with UVC light under nitrogen.[30] Our assay is directed towards food sterilization technologies, performed mostly in the presence of air; this assay has not been evaluated for DNA damage under anaerobic conditions.

In this work we attempt to quantify interference of dye intercalation due to all types of DNA lesions caused by UVC light. Large UVC doses are employed in order to obtain damage levels comparable to those employed in food sterilization technologies.

### 5.2.2. Absorbance Spectroscopy

Irradiation of the DNA samples with UVC light results in a significant decrease in the absorbance at 260 nm and a comparatively smaller increase at 310 nm (Figure 5.1A and Figure 5.2A,C). It is not surprising that such a significant decrease at 260 nm occurs since this band results from intense $\pi \rightarrow \pi^*$ transitions that are eliminated in the pyrimidines upon the [2+2] reaction that forms the

pyrimidine dimers and the reactions forming the other photoadducts. A new transition, likely n→π*, appears as a shoulder around 310 nm in the spectrum, presumably due to the carbonyl group in the newly formed minor product 8-oxo-dG. Since 8-oxo-dG absorbs around 295 nm[17,23,36] the asymmetric peak at 310 nm is probably a shoulder of a 295 nm maximal absorbance partially masked by the 260 nm absorbance.

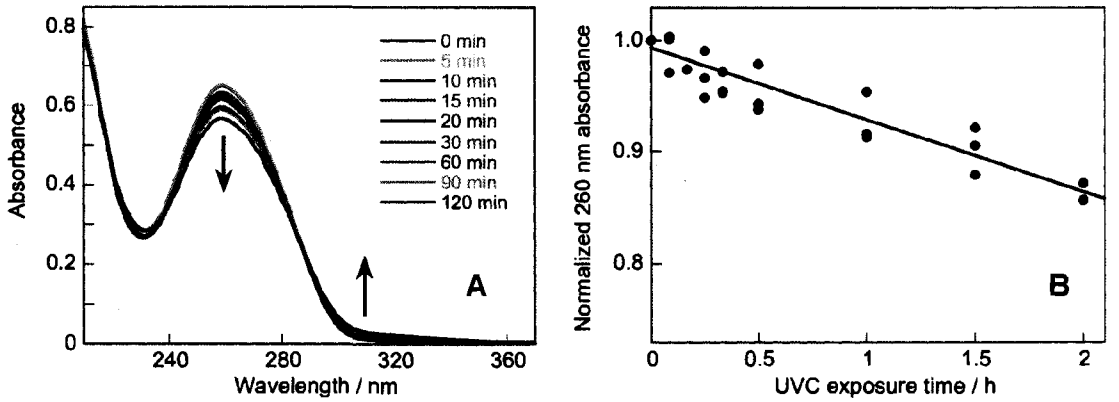


**Figure 5.1: (A) Absorption spectra of 50 μM CT DNA solutions in water after UVC irradiation from 0 to 120 minutes, recorded at room temperature with a 10 mm pathlength. (B) The linear relationship between the (normalized) 260 nm absorbance and the UVC exposure time. The maximum energy flux (at 120 min) was 270 kJ/m$^2$.**

The absorbance of DNA at 260 nm decreases linearly by 6.5% per 135 kJ/m$^2$ (or per hour) of UVC exposure (up to 2 hours) to 100 μM base pairs CT DNA, as seen in Figure 5.1B. The linear fit is used just for convenience, but seems adequate for the relatively small (< 20%) change. When UVC exposure is continued up to 12 hours, the rate slows to 5.3% per 135 kJ/m$^2$ (or per hour), as shown in Figure 5.2B. Surprisingly, a linear fit works well even after 12 h of UVC exposure. The absorbance around 310 nm is very low (due to the forbidden nature of the n→π* transition) and it is masked by π→π* transitions, making absorption spectroscopy of DNA less than ideal as a technique for measuring DNA damage.

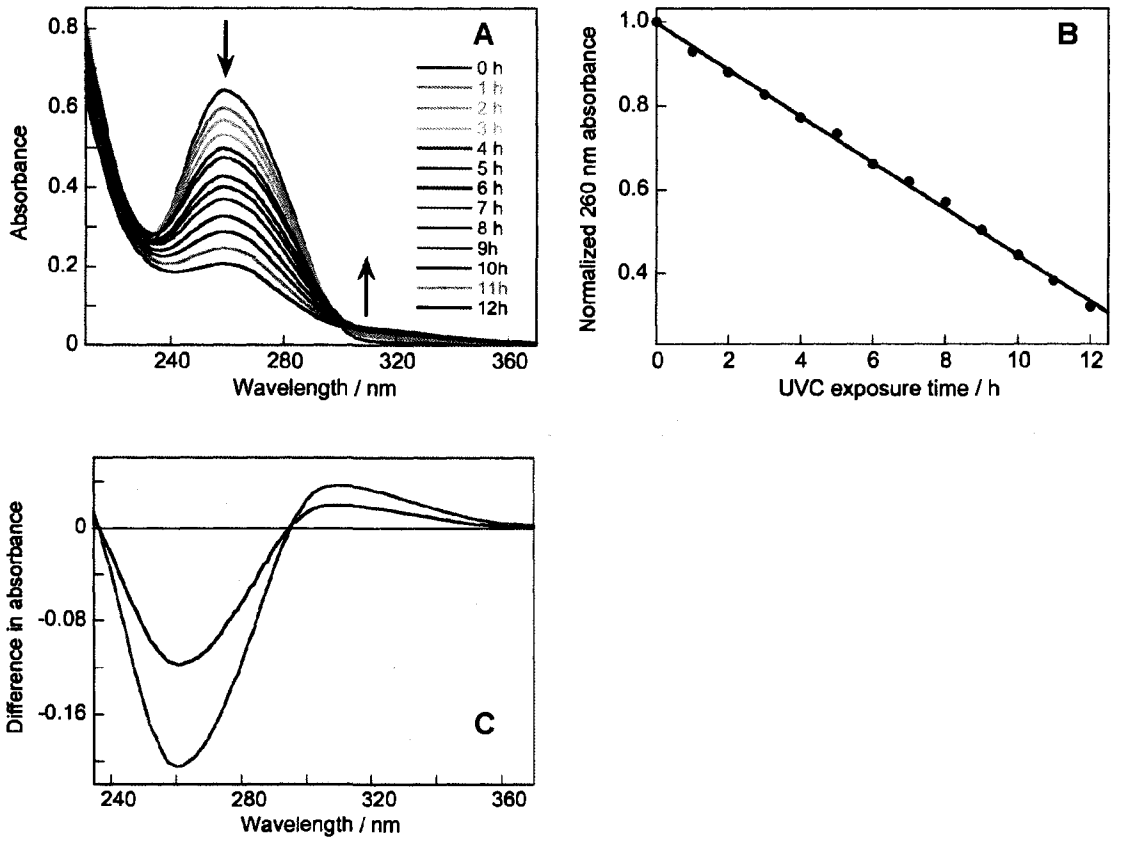


**Figure 5.2: (A) Absorption spectra of 50 μM CT DNA solutions in water after UVC irradiation from 0 to 12 hours, recorded at room temperature with a 10 mm pathlength. (B) The linear relationship between the (normalized) 260 nm absorbance and the UVC exposure time. (C) Difference spectra of 50 μM CT DNA solutions after 1 (blue) and 3 (red) hours (135 and 405 kJ/m$^2$, respectively) of UVC-irradiation recorded at room temperature with a 10 mm optical pathlength. In (A) and (B) the maximum energy flux (at 12 h) was 1620 kJ/m$^2$, while in (C) it was 405 kJ/m$^2$ (at 3 h).**

An alternative to examining DNA damage directly by looking at the absorption of the DNA bases is the strategy of using a reporter molecule, in our case the intercalating dye thiazole orange (TO), and its absorbance. TO has limited solubility in aqueous solutions, forming dimers and aggregates.[37] When TO is

added to DNA, both the monomer and the dimer are always present. The monomeric form intercalates in DNA, showing a peak around 503 nm, the dimeric form shows a peak around 480 nm and the aggregated form absorbs around 450 nm. TO was *not* present during the irradiations, but was added afterwards. The ratio between the monomer and dimer absorbance of TO shifts with increasing UVC exposure time, as shown in Figure 5.3A. The relative change of this ratio can be conveniently fit to an exponential decay with a half-life of 23.9 ± 5.2 kJ/m$^2$ (10.6 ± 2.2 minutes) of UVC exposure to 100 μM base pairs CT DNA in water (see Figure 5.3B). The change in the TO absorbance ratio is likely due to DNA damage preventing TO intercalation, hence the dye aggregates; this hypothesis is supported by the other techniques used here (*vide infra*). The fact that the area under the absorbance spectrum changes upon aggregation suggests that not only the extinction coefficient, but also the oscillator strength, is affected by aggregation.

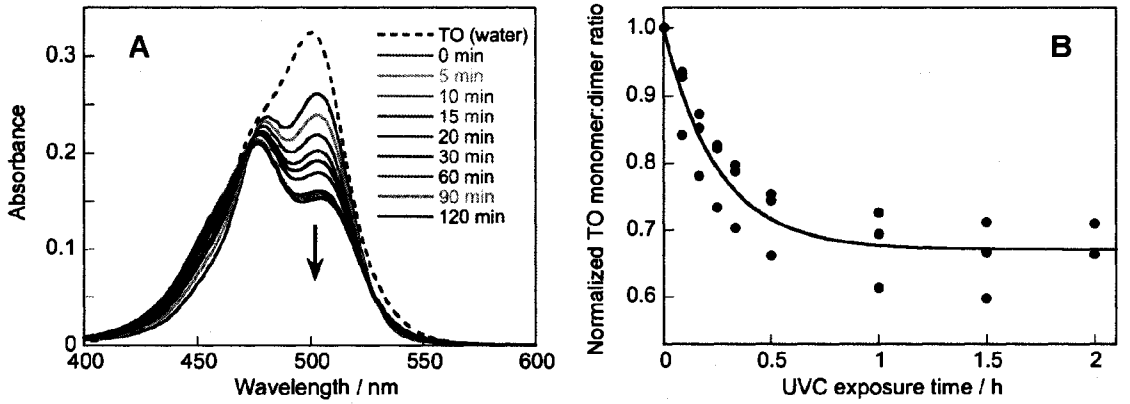


**Figure 5.3: (A) Absorption spectra of 5 μM TO in water (no DNA, dashed blue line) and of 5 μM TO (added after irradiation) with 50 μM CT DNA solutions in water after UVC irradiation from 0 to 120 minutes, recorded at room temperature with a 10 mm path length. (B) Dye monomer ($A_{503}$):dimer ($A_{480}$) ratio (normalized to control) against time, fitted for convenience with an exponential function. The maximum energy flux (at 120 min) was 270 kJ/m$^2$.**

### 5.2.3. Circular Dichroism Spectroscopy

Examining the circular dichroism (CD) spectra in the DNA region (Figure 5.4A) of irradiated solutions, one can see that although the signal intensities decrease, the shape remains the same. If single-stranded DNA was formed, one would expect a slight shift of the maxima towards longer wavelengths.[38] In addition, a 3-4 nm shift of the long-wavelength crossover to the red is an indication of denaturation.[39] As neither of these criteria is met, it appears that no significant amount of single-stranded DNA is formed. Irradiating the DNA for less than 90 minutes (less than 203 $kJ/m^2$) destroys some of its secondary structure but does not produce significant yields of single-stranded DNA.

The decrease of the CD signal around 278 nm was fitted for convenience with a monoexponential decay, providing a half-life of $46.8 \pm 8.3$ $kJ/m^2$ ($20.8 \pm 3.7$ minutes) of UVC exposure (up to 2 hours) to 100 μM base pairs CT DNA in water (see Figure 5.4B). Consequently circular dichroism spectroscopy is more sensitive to UVC-induced DNA damage than absorbance spectroscopy.

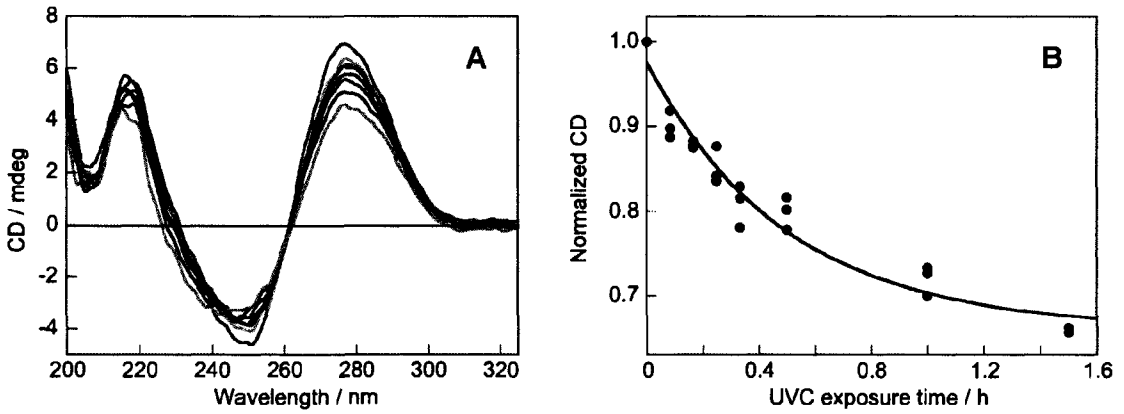


**Figure 5.4: (A) CD spectra of 50 μM CT DNA solutions after irradiation with UVC recorded at 20°C with a 10 mm path length. With decreasing intensity at 278 nm are DNA exposed for 0, 5, 10, 15, 20, 30, 60 and 90 minutes of UVC-irradiation. (B) The CD (normalized) at the long-wavelength maximum against time, fitted for convenience with an exponential function. The maximum energy flux (at 90 min) was 203 kJ/m$^2$.**

Long irradiation times lead to a loss of secondary structure, as seen in Figure 5.5. After 12 hours of UVC irradiation the CD spectrum is almost a flat line, indicating a complete loss of secondary structure. This is not a surprising result considering the extremely large dose of radiation.

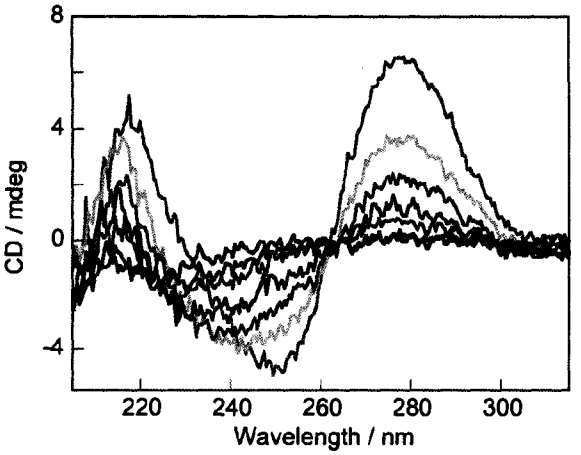


**Figure 5.5: CD spectra of 50 μM CT DNA solutions after irradiation with UVC recorded at 20°C with a 10 mm path length. With decreasing intensity at 278 nm are DNA exposed for 0, 2, 4, 6, 8, 10 and 12 hours of UVC irradiation. The maximum energy flux (at 12 h) was 1620 kJ/m$^2$.**

Achiral TO does not exhibit a CD signal, but intercalation in DNA imparts chirality, allowing an induced CD (ICD) signal to be observed. The ICD of TO is sensitive to UVC exposure of DNA (see Figure 5.6A), presumably because the dye cannot intercalate to the same extent in damaged DNA as in intact DNA. The decrease in ICD upon UVC exposure indicates that the DNA damage (in the literature: CPDs, 6-4PP, 8-oxo-dG, etc.) interferes with TO intercalation. This may be caused by steric or electronic effects, since there is evidence that cyanine dyes may be stabilized by π-stacking in DNA.[40]

The ICD signal with UVC flux was fitted for convenience with an exponential function yielding a half-life of 41.0 ± 8.3 kJ/m$^2$ (18.2 ± 3.7 minutes) of UVC exposure to 100 μM base pairs CT DNA in water (see Figure 5.6B), which is somewhat shorter than that found for the DNA alone.

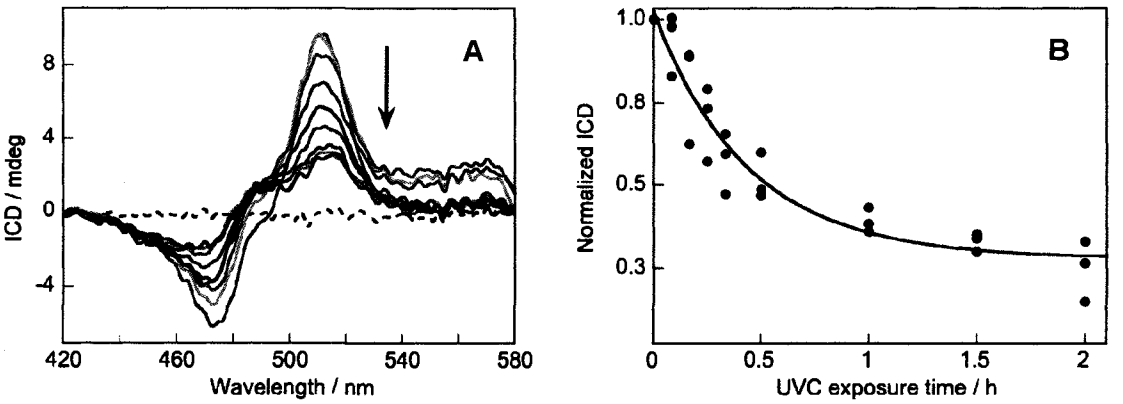


**Figure 5.6: (A) ICD spectra of 5 μM TO (added after irradiation) and 50 μM CT DNA solutions after irradiation with UVC recorded at 20°C with a 10 mm path length. With decreasing intensity at 511 nm are TO with DNA exposed for 0, 5, 10, 15, 20, 30, 60, 90 and 120 minutes to UVC-irradiation, and TO in water (no DNA). (B) The ICD (normalized) at the maximum can be fitted with an exponential function for the 2 hour UVC exposure time. The maximum energy flux (at 120 min) was 270 kJ/m$^2$.**

### 5.2.4. Fluorescence Spectroscopy

Even with only 5 minutes of UVC irradiation, a large drop in TO fluorescence is recorded, as shown in Figure 5.7A. Our results suggest that TO binds more weakly to UVC-irradiated DNA than to non-irradiated DNA. We have also observed that when the dye:DNA base pair ratio (d/b) is increased beyond 1 dye to 10 base pairs in native DNA, the ability of the dye to intercalate is compromised and the TO fluorescence decreases (results not shown). It has been shown that at d/b > 0.4, YO binds externally to DNA,[41] and external binding may explain the decrease in TO fluorescence at d/b beyond 0.1. We believe that as DNA is damaged by UVC radiation the number of sites available for intercalation decreases and manifests itself as a decrease in the fluorescence intensity. An alternative explanation is that electron transfer between excited TO and 8-oxo-dG may account for the fluorescence reduction. While we favor the simple explanation above, we cannot rule out some contribution from charge transfer.

The absorption of the fluorescent probe at the excitation wavelength (480 nm) decreases upon UVC exposure because of the change in its ability to intercalate. The emission spectra are not corrected for this decrease because the ability to intercalate is the indicator of damage.

The 535 nm fluorescence of TO in UVC-irradiated CT DNA was fitted for convenience with a monoexponential function, giving a half-life of 14.2 ± 0.7 kJ/m$^2$ (6.3 ± 0.3 minutes) for UVC exposure of 100 μM base pairs CT DNA (see Figure 5.7B).

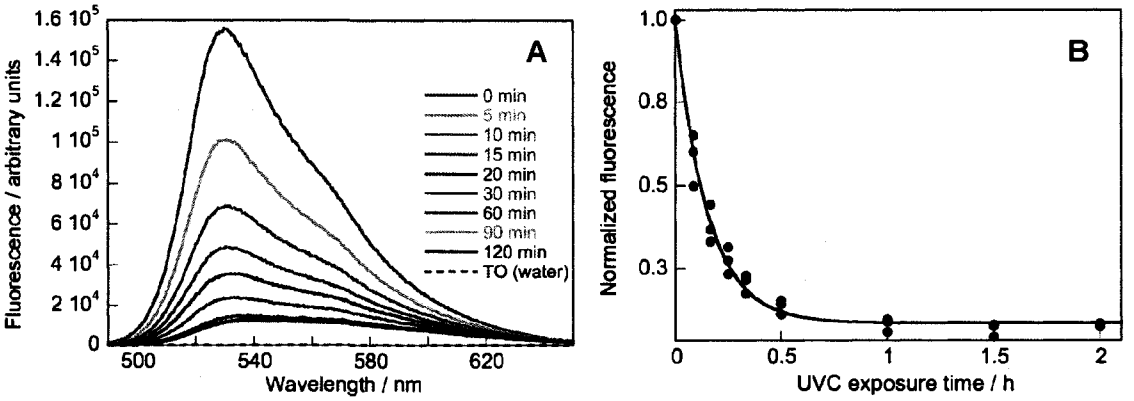


**Figure 5.7: Fluorescence spectra of 5 μM TO in water (no DNA, dashed blue line that blends with the baseline) and of 5 μM TO (added after irradiation) with 50 μM CT DNA solutions after (0 to 120 minutes) irradiation with UVC light, recorded at room temperature with a 10 mm path length. (B) Fluorescence (normalized) change with the UVC exposure time, fitted for convenience to an exponential function. The maximum energy flux (at 120 min) was 270 kJ/m$^2$.**

### 5.2.5. Agarose Gel Electrophoresis

The intensity of the dark band in the control lane decreases with increasing UVC flux, as seen in Figure 5.8. Exposure times of 60 minutes and greater eliminate this band. The intensity of the smear below this band remains constant, suggesting that the amount of shorter segments of DNA remains constant.

However, our spectral results (*vide infra*) indicate that as the UVC exposure time increases, the ability of TO to intercalate decreases. The phenomenon of dye intercalation being susceptible to DNA damage was also observed for ethidium bromide (EB) in solution. The damage seen in the gels during the first 15 minutes of UVC exposure appears to be due to the loss of EB fluorescence from decreased intercalation, not strand breaks (see Figure 5.9). Thus the responses observed for irradiation times of 20 minutes and longer are a combination of both DNA strand breaks and compromised EB intercalation. The (normalized) EB fluorescence in DNA solutions reaches a minimal value after 60 minutes of UVC exposure, indicating that the decay seen in the gel for irradiation times of 60 minutes and longer is due solely to DNA strand breaks.

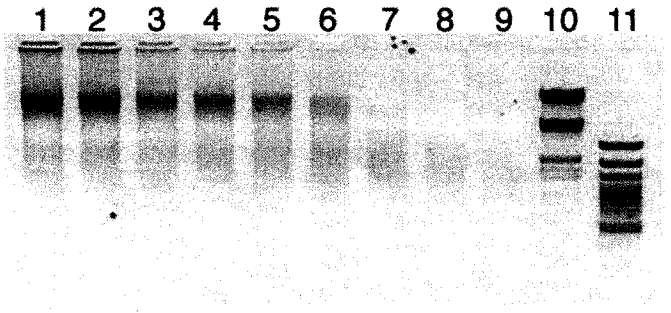


**Figure 5.8: Agarose gel electrophoresis of 6 µg DNA following UVC irradiation visualized by ethidium bromide staining. Lane 1: control DNA; lane 2: 5 min UVC-irradiated DNA; lane 3: 10 min UVC-irradiated DNA; lane 4: 15 min UVC-irradiated DNA; lane 5: 20 min UVC-irradiated DNA; lane 6: 30 min UVC-irradiated DNA; lane 7: 60 min UVC-irradiated DNA; lane 8: 90 min UVC-irradiated DNA; lane 9: 120 min UVC-irradiated DNA; lane 10: HindIII+EcoRI Ladder has 21, 5, 3.5, 2, 1.5, 1.4 kbp bands; lane 11: O'GeneRuler has 3, 2, 1.5, 1.2, 1, 0.9, 0.8, 0.7, 0.6, 0.5, 0.4, 0.3, 0.2, 0.1 kbp bands. The maximum energy flux (at 120 min) was 270 kJ/m$^2$.**

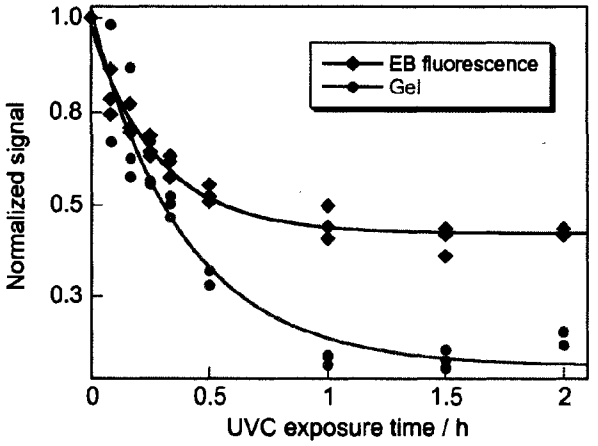


**Figure 5.9: Comparison between the decays of EB fluorescence in DNA solutions (black diamonds) and in agarose gels following electrophoresis of 6 μg of DNA (red circles), irradiated with UVC light. Both techniques exhibit similar decays during the first 15 minutes of UVC exposure. The maximum energy flux (at 2 h) was 270 kJ/m$^2$.**

The fact that the intensities of the bands in the agarose gel can depend on two processes (DNA damage and the ability of EB to intercalate) while the TO fluorescence always depends on only one process (the ability of TO to intercalate) highlights the advantage of using TO fluorescence over agarose gel electrophoresis for detecting UVC-induced DNA damage. Consequently, one cannot conclude from the agarose gels that the genomic DNA has been completely eliminated or that the amount of shorter segments of DNA remains constant.

After 120 minutes (270 kJ/m$^2$) of UVC exposure there is an extremely small fraction of short double-stranded DNA remaining detectable by gel electrophoresis (see lane 9 in Figure 5.8 and lane 3 in Figure 5.10), and irradiation times of 3 hours (405 kJ/m$^2$) or longer completely eliminate this double-stranded DNA (see Figure 5.10). However, the CD spectrum of the 2 hour-irradiated DNA sample still shows the characteristic spectrum of double-stranded DNA with a signal at 278 nm that is approximately half that of the non-irradiated sample, and an extremely weak CD spectrum can still be observed after 8 hours (1080 kJ/m$^2$) of UVC exposure (see

Figure 5.5), demonstrating that the disappearance of the band representing genomic DNA in the agarose gel is predominantly due to the reduced ability of EB to intercalate in UVC-exposed DNA.

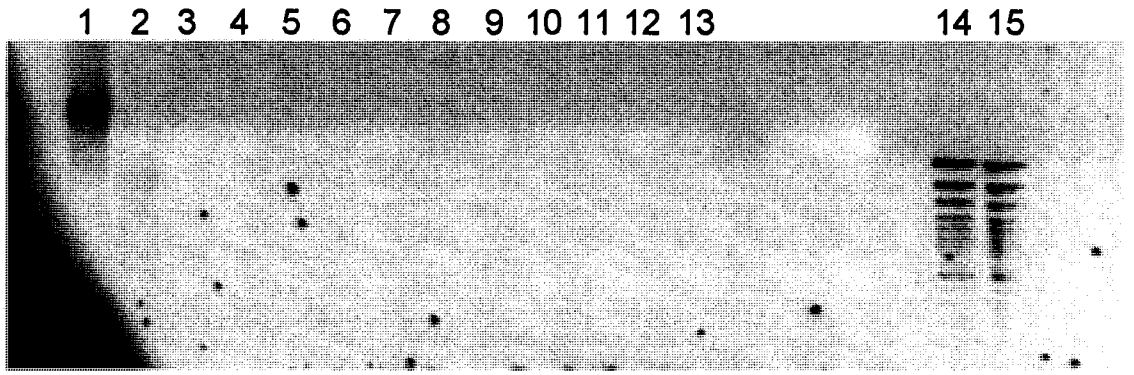


**Figure 5.10: Agarose gel electrophoresis of 6 µg DNA following UVC irradiation visualized by ethidium bromide staining. Lane 1: control DNA; lane 2: 1 h UVC-irradiated DNA; lane 3: 2 h UVC-irradiated DNA; lane 4: 3 h UVC-irradiated DNA; lane 5: 4 h UVC-irradiated DNA; lane 6: 5 h UVC-irradiated DNA; lane 7: 6 h UVC-irradiated DNA; lane 8: 7 h UVC-irradiated DNA; lane 9: 8 h UVC-irradiated DNA; lane 10: 9 h UVC-irradiated DNA; lane 11: 10 h UVC-irradiated DNA; lane 12: 11 h UVC-irradiated DNA; lane 13: 12 h UVC-irradiated DNA; lanes 14 and 15: O'GeneRuler has 3, 2, 1.5, 1.2, 1, 0.9, 0.8, 0.7, 0.6, 0.5, 0.4, 0.3, 0.2, 0.1 kbp bands. The maximum energy flux (at 12 h) was 1620 kJ/m$^2$.**

Densitometric measurements of the dark band in the control lane representing genomic calf thymus DNA provided a quantification of the DNA staining by ethidium bromide fluorescence. These data were fitted for convenience with a monoexponential function, providing a half-life of 36.5 ± 5.2 kJ/m$^2$ (16.2 ± 2.3 minutes) of UVC exposure, see Figure 5.11. In comparing signal changes by fluorescence spectroscopy and gel electrophoresis (Figure 5.11), the respective half-lives associated with their exponential fits are 6.3 ± 0.3 minutes and 16.2 ± 2.3 minutes of UVC exposure to 100 µM base pairs CT DNA, respectively, showing

the enhanced sensitivity of TO fluorescence over gel electrophoresis. When comparing all of the methods to characterize DNA damage, fluorescence detection using an intercalating dye is by far the most sensitive and the most rapid.

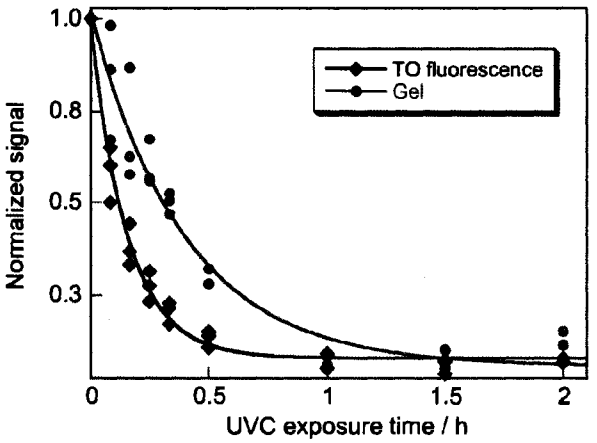


**Figure 5.11: Comparison between the decays of TO fluorescence in DNA solutions (black diamonds) and agarose gel electrophoresis with EB staining (red circles), following UVC irradiation. TO fluorescence exhibits a faster decrease than the EB fluorescence staining in agarose gel electrophoresis. The maximum energy flux (at 2 h) was 270 kJ/m$^2$.**

### 5.2.6. Computational Studies

The experimental studies demonstrate that UVC light induces changes in DNA that interfere with TO intercalation. To investigate the cause of this phenomenon, we studied TO and duplex DNA oligomers containing a DNA lesion computationally. The DNA lesions that were incorporated in the duplex DNA oligomers were the *cis-syn* cyclobutane thymine dimer (the dominant diastereoisomer that results from UVC exposure[20]) and 8-oxo-2'-deoxyguanosine (8-oxo-dG), whose structures are illustrated in Figure 5.12.

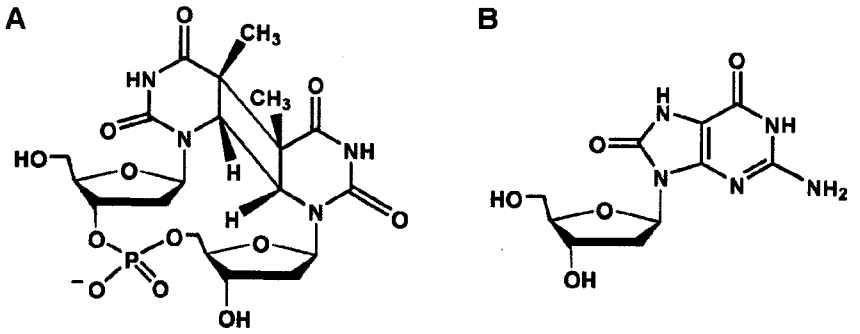


**Figure 5.12: Structures of two UVC-induced DNA photoproducts.**
**(A) *cis-syn* cyclobutane thymine dimer.[20] (B) 8-oxo-2'-deoxyguanosine.[14]**

As was discussed in Chapter 3, the isomers and conformers of TO were fully optimized (*in vacuo*) by B3LYP/6-31G* and the lowest energy structure (shown in Figure 5.13) was chosen for the simulations. Based upon the identical cross peak patterns in the NOESY spectra of TOTO/dsDNA and free TOTO, Jacobsen *et al.* concluded that the conformation of the dye does not change upon intercalation.[42] As TOTO is simply a covalently linked dimer of TO, we have assumed that the most stable TO structure in solution will also be the most stable in DNA for the purposes of our calculations.

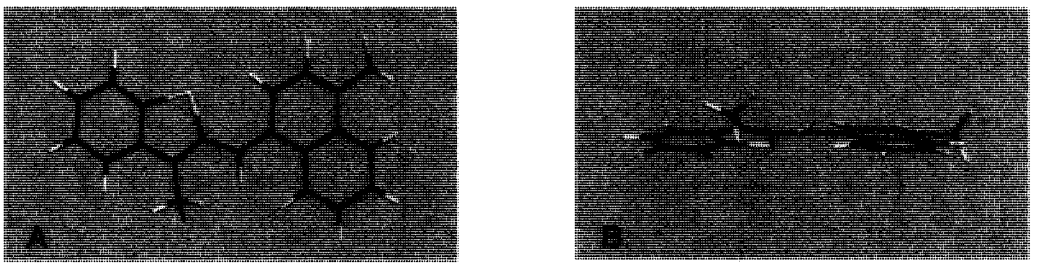

**Figure 5.13: (A) Optimized structure of TO that is lowest in energy by 4.18 kcal mol$^{-1}$.**
**(B) Structure in (A) that was rotated 90°.**

The DNA oligomers consisted of 10 base pairs to coincide with the experimental conditions, where a 1:10 dye:base pair ratio was employed. The cyclobutane thymine dimer was created on the 4$^{th}$ and 5$^{th}$ thymine bases in the

$(dA)_{10}$•$(dT)_{10}$ duplex, which will be referred to as the T-dimer duplex (see Scheme 5.2). For the modeling, we inserted TO between the cyclobutane thymine dimer and the two adjacent adenine bases in the T-dimer duplex. The 8-oxo-dG lesion was created on the 5$^{th}$ guanine base in the $(dG)_{10}$•$(dC)_{10}$ duplex, which will be referred to as the 8-oxo-dG duplex (see Scheme 5.2). For the modeling, we inserted TO between 8-oxo-dG, the 6$^{th}$ guanine base, and the two adjacent cytosine bases in the 8-oxo-dG duplex. As such, each 2 ns simulation required 10 days of CPU time, thus it was not feasible to place the dye in the proximity of the DNA and monitor its intercalation as this would require extremely long simulations. In order to provide a complete description of the system, several orientations between TO and the DNA oligomers were considered. These consisted of placing the benzothiazole moiety between the bases, the quinoline moiety between the bases, or both the benzothiazole and the quinoline moieties between the bases (8-oxo-dG duplex only). It was not possible to insert both TO moieties between the bases of the T-dimer duplex (in the vicinity of the cyclobutane thymine dimer) as the steric bulk of the cyclobutane thymine dimer and the sugar-phosphate backbone would not allow it. Table 5.2 in the Discussion section (Section 5.3.2) summarizes the observations that follow.

5'-TTT (T-T)T TTT T-3' (T-dimer duplex)
3'-AAA AAA AAA A-5'

5'-GGG GG*G GGG G-3' (8-oxo-dG duplex)
3'-CCC CCC CCC C-5'

**Scheme 5.2: Nomenclature of the duplexes, where G* represents 8-oxo-2'-deoxyguanosine and (T-T) represents the *cis-syn* cyclobutane thymine dimer.**

### 5.2.6.1. Intercalation via the Benzothiazole Moiety in the T-dimer Duplex

When inserting the TO benzothiazole moiety between the cyclobutane thymine dimer and the two adjacent adenine bases in the T-dimer duplex, six orientations were considered, as illustrated in Figure 5.14.

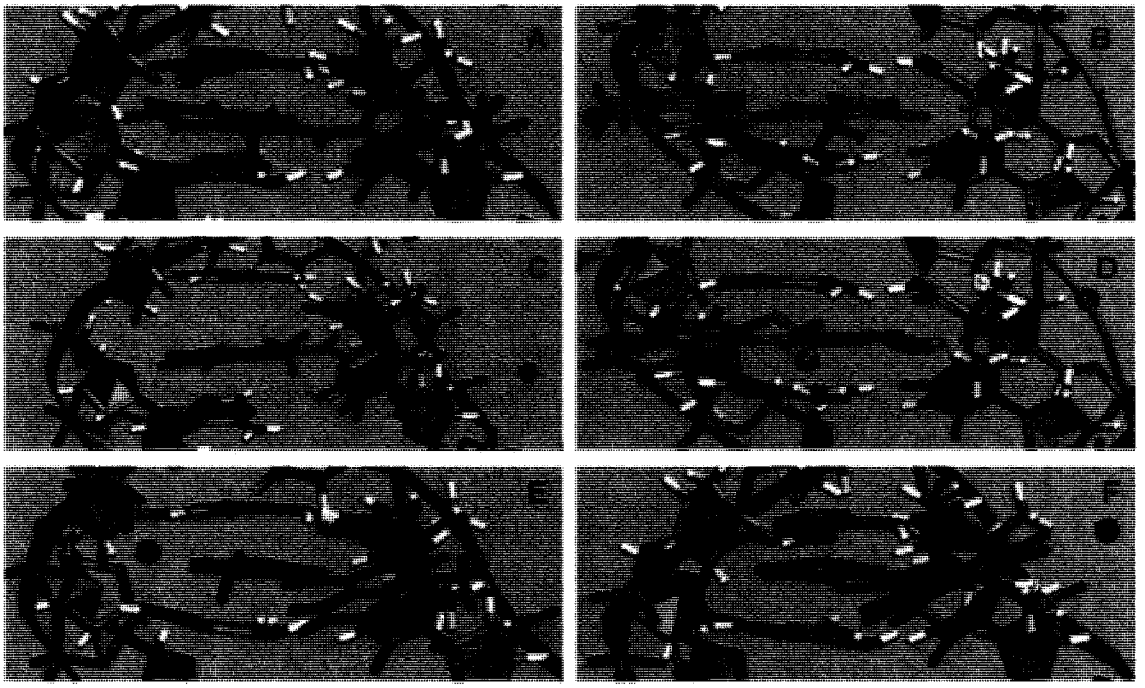

**Figure 5.14: Illustration of the modes of insertion of the TO benzothiazole moiety between the cyclobutane thymine dimer and the two adjacent adenine bases in the T-dimer duplex. (A,B) Benzothiazole $CH_3$ is perpendicular to the intercalation pocket (coming out of the plane of the paper); in (A) the quinoline moiety is near the thymine dimer while in (B) it is near the backbone of the A strand. (C,D) Benzothiazole $CH_3$ is perpendicular to the intercalation pocket (going into the plane of the paper); in (C) the quinoline moiety is near the thymine dimer while in (D) it is near the backbone of the A strand. (E) Benzothiazole $CH_3$ is between two A bases while the methine H is away from the thymine dimer. (F) Benzothiazole $CH_3$ is between the thymine dimer and the methine H is near the thymine dimer.**

In 3 of the 6 simulations where the TO benzothiazole moiety was intercalated in the T-dimer duplex, the dye dissociated (immediately in two cases and after approximately 100 ps in the other) but stayed in the proximity of the DNA duplex, presumably due to electrostatic interactions, as seen in Figure 5.15B. In one of the remaining simulations, the dye remained close to the starting orientation although there was a lengthening of the DNA duplex and disruption of its helicity (data not shown). In one of the other remaining simulations, there was an immediate shift that placed the quinoline moiety between the two A bases and the benzothiazole moiety between the phosphate backbones of the two strands, as shown in Figure 5.15D. In the last simulation, there was a shift that resulted in the benzothiazole moiety interacting with one A base and the quinoline moiety interacting with another A base in the intercalation site (data not shown).

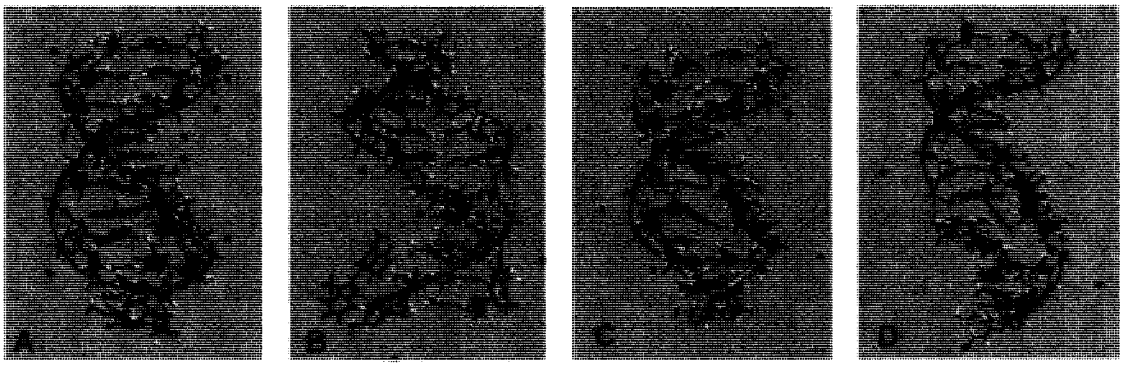

**Figure 5.15: Initial (A) conformation of TO/T-dimer duplex, and after 2 ns (B), showing the dye dissociated. Initial (C) conformation of TO/T-dimer duplex, and after 2 ns (D), showing the quinoline moiety between two A bases.**

### 5.2.6.2. Intercalation via the Quinoline Moiety in the T-dimer Duplex

When inserting the TO quinoline moiety between the cyclobutane thymine dimer and the two adjacent adenine bases in the T-dimer duplex, four orientations were considered, as illustrated in Figure 5.16.

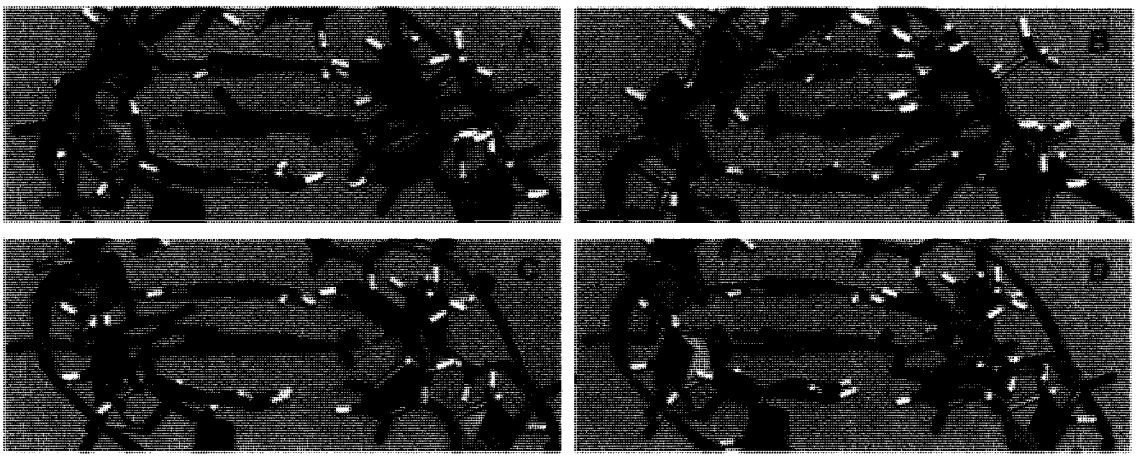


**Figure 5.16: Illustration of the modes of insertion of the TO quinoline moiety between the cyclobutane thymine dimer and the two adjacent adenine bases in the T-dimer duplex. (A,B) Quinoline $CH_3$ is perpendicular to the intercalation pocket (going into the plane of the paper); in (A) the benzothiazole S is near the thymine dimer while in (B) the benzothiazole $CH_3$ is near the thymine dimer. (C) Quinoline $CH_3$ is between the thymine dimer while the benzothiazole $CH_3$ is near the backbone of the A strand. (D) Quinoline $CH_3$ is between two A bases while the benzothiazole $CH_3$ is near the thymine dimer.**

In 2 of the 4 cases where the TO quinoline moiety was intercalated in the T-dimer duplex, the dye dissociated immediately but stayed in the proximity of the DNA duplex, presumably due to electrostatic interactions, as shown in Figure 5.17B. In the remaining two cases, near the very beginning of the simulation, one of the A bases flipped out of the DNA helix. Subsequently the benzothiazole moiety interacted with the flipped out base, and the quinoline moiety associated with two nearby A bases (Figure 5.17D). It appears that without the A

base flipping out of the DNA helix, there would not be enough room for the dye in the intercalation pocket due to the presence of the cyclobutane thymine dimer. Consequently, it seems doubtful that TO would intercalate (in these two orientations) if it were placed in the proximity of the DNA strand, due to the steric crowding in the intercalation site.

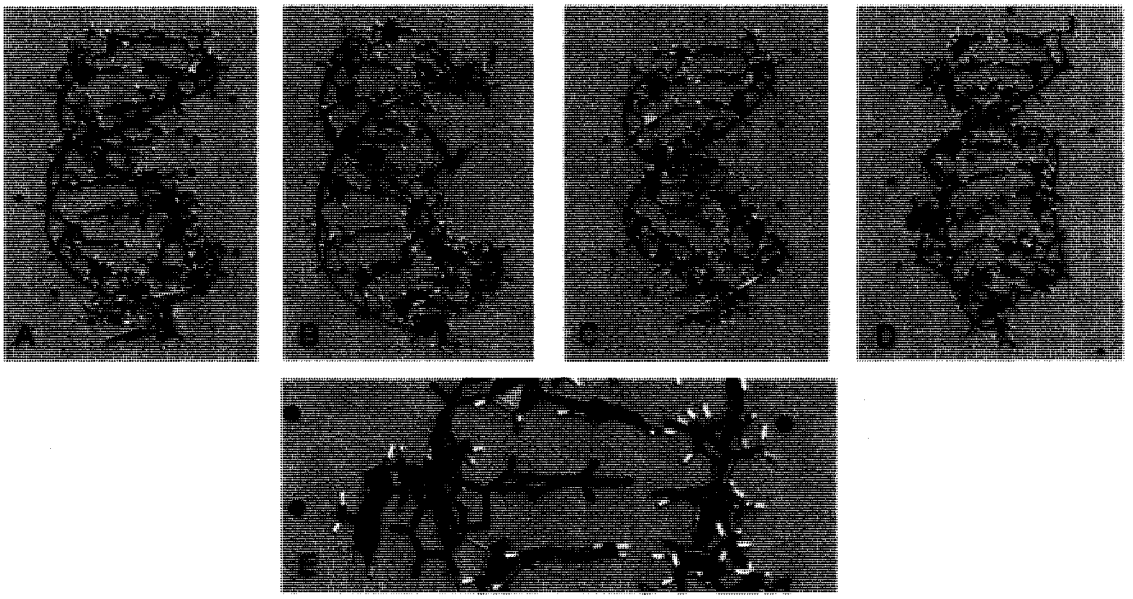


**Figure 5.17: Initial (A) conformation of TO/T-dimer duplex, and after 2 ns (B), showing the dye dissociated. Initial (C) conformation of TO/T-dimer duplex, and after 2 ns (D), showing both moieties interacting with A bases, and one A base flipped out from the DNA helix. (E) Close-up of the structure in (D).**

### 5.2.6.3. Intercalation via the Benzothiazole Moiety in the 8-oxo-dG Duplex

When inserting the TO benzothiazole moiety between 8-oxo-dG, the 6$^{th}$ guanine base and the two adjacent cytosine bases in the 8-oxo-dG duplex, four orientations were considered, as illustrated in Figure 5.18.

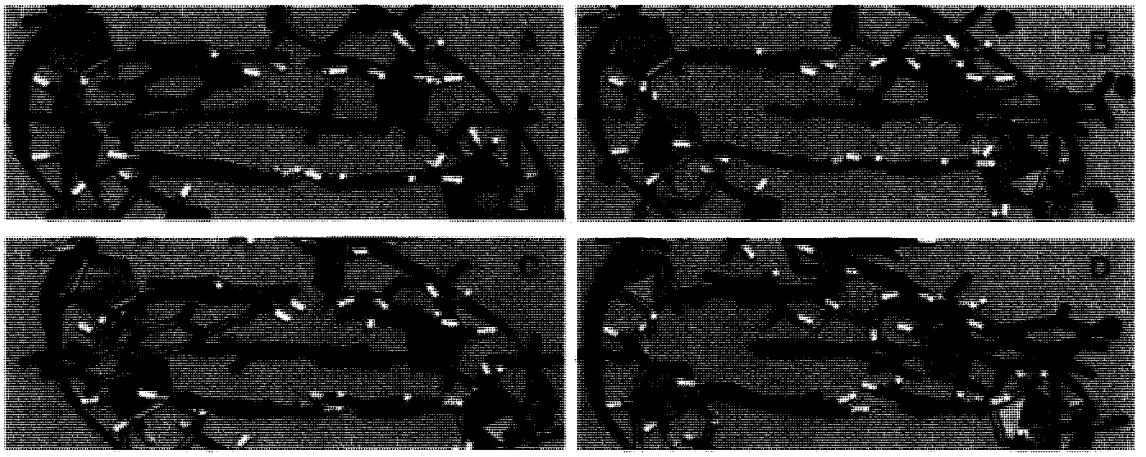

**Figure 5.18: Illustration of the modes of insertion of the TO benzothiazole moiety between 8-oxo-dG, the 6$^{th}$ guanine base and the two adjacent cytosine bases in the 8-oxo-dG duplex. (A,B) Benzothiazole $CH_3$ is perpendicular to the intercalation pocket and it is coming out of the plane of the paper; in (A) the quinoline moiety is near the backbone of the G strand while in (B) it is near the backbone of the C strand. (C,D) Benzothiazole $CH_3$ is perpendicular to the intercalation pocket and it is going into the plane of the paper; in (C) the quinoline moiety is near the backbone of the G strand while in (D) it is near the backbone of the C strand.**

In 2 of the 4 simulations where the TO benzothiazole moiety was intercalated in the 8-oxo-dG duplex, the dye remained close to the starting orientation and caused lengthening of the DNA duplex, as seen in Figure 5.19B. In the other two simulations, the dye immediately shifted to a position between the 8-oxo-dG and G bases, and remained in this position for the duration of the 2 ns simulation, as shown in Figure 5.19D.

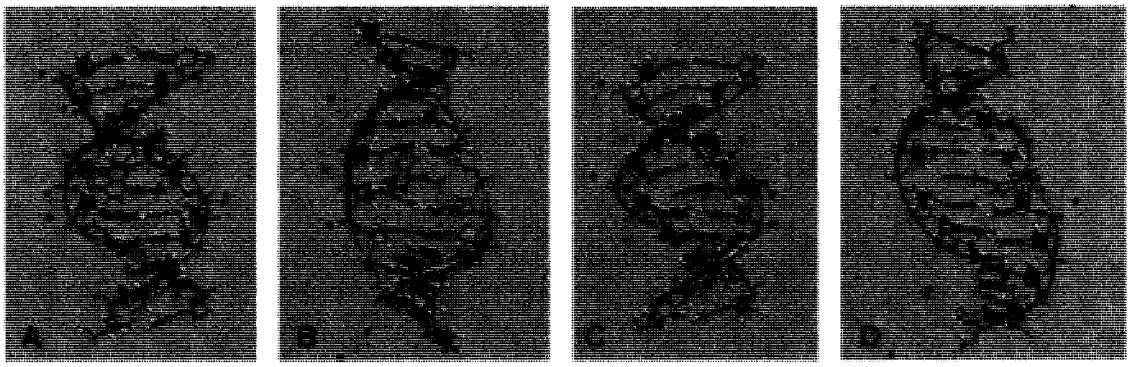


**Figure 5.19: Initial (A,C) conformations of TO/8-oxo-dG duplex, and after 2 ns (B,D), showing the benzothiazole moiety intercalated.**

### 5.2.6.4. Intercalation via the Quinoline Moiety in the 8-oxo-dG Duplex

When inserting the TO quinoline moiety between 8-oxo-dG, the 6$^{th}$ guanine base and the two adjacent cytosine bases in the 8-oxo-dG duplex, four orientations were considered, as illustrated in Figure 5.20.

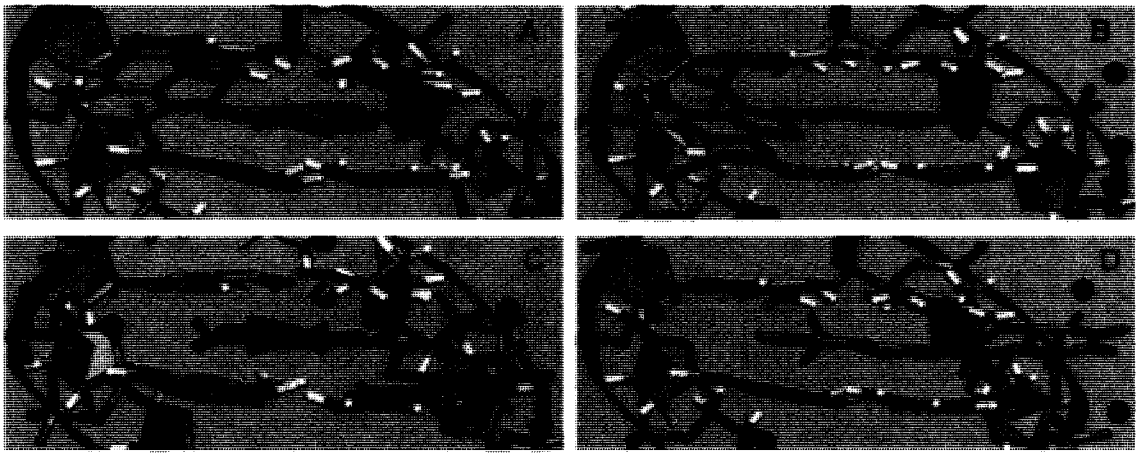

**Figure 5.20: Illustration of the modes of insertion of the TO quinoline moiety between 8-oxo-dG, the 6$^{th}$ guanine base and the two adjacent cytosine bases in the 8-oxo-dG duplex. (A,B) Quinoline $CH_3$ is between two C bases; in (A) the benzothiazole $CH_3$ is near the backbone of the G strand while in (B) it is not near the backbone of the G strand. (C) Quinoline $CH_3$ is between the G and 8-oxo-dG bases while the benzothiazole $CH_3$ is near the backbone of the C strand. (D) Quinoline $CH_3$ is partly between the G and 8-oxo-dG bases (not fully between them due to steric interactions between the benzothiazole moiety and the phosphate backbone) while the benzothiazole $CH_3$ is not near the backbone of the C strand.**

In the first simulation where the TO quinoline moiety was inserted in the 8-oxo-dG duplex, the dye immediately moved between the two C bases. After several hundred picoseconds, the dye dissociated but stayed in the proximity of the DNA, presumably due to electrostatic interactions (Figure 5.21B). In the second simulation, the dye remained close to the starting orientation during the 2 ns simulation and lengthened the DNA helix (data not shown). In the last two simulations, the quinoline moiety immediately moved between the 8-oxo-dG and G bases, and remained in this position for the duration of the 2 ns simulation, as seen in Figure 5.22D.

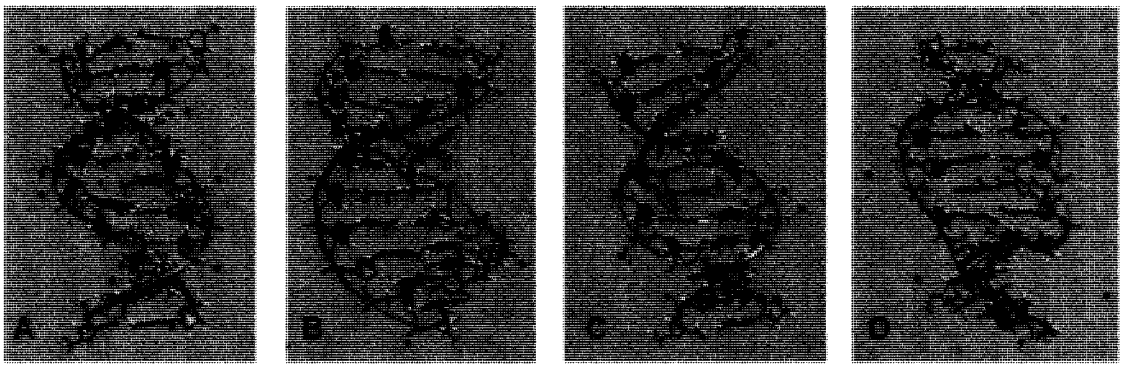


**Figure 5.21: Initial (A) conformation of TO/8-oxo-dG duplex, and after 2 ns (B), showing the dye dissociated. Initial (C) conformation of TO/8-oxo-dG duplex, and after 2 ns (D), showing the quinoline moiety intercalated.**

### 5.2.6.5. Intercalation via Both TO Moieties in the 8-oxo-dG Duplex

When inserting both the benzothiazole and the quinoline moieties between 8-oxo-dG, the 6$^{th}$ guanine base and the two adjacent cytosine bases in the 8-oxo-dG duplex, four orientations were considered, as illustrated in Figure 5.22.

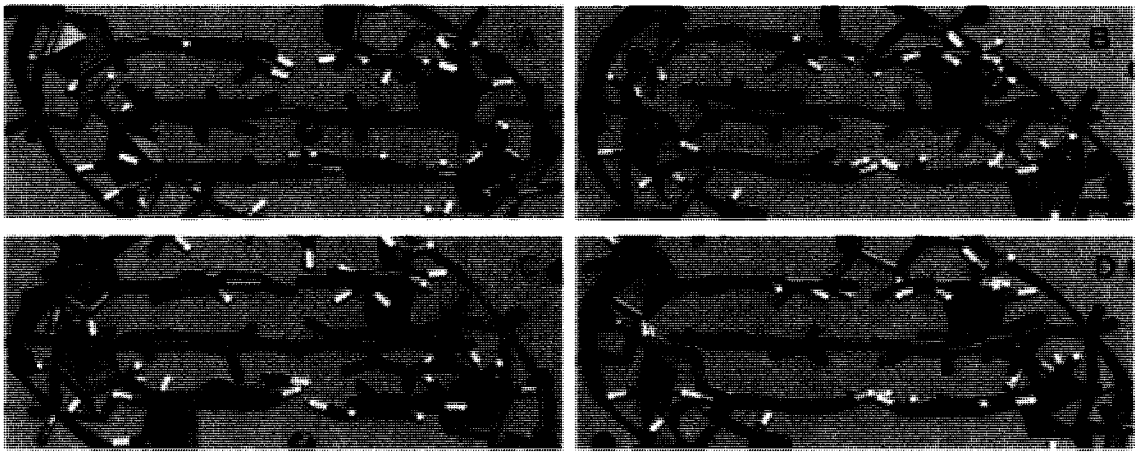

**Figure 5.22: Illustration of the modes of insertion of both the benzothiazole and the quinoline moieties between 8-oxo-dG, the 6$^{th}$ guanine base and the two adjacent cytosine bases in the 8-oxo-dG duplex. (A,B) Quinoline moiety is between the G and 8-oxo-dG bases while the benzothiazole moiety is between the two C bases. In (A) the benzothiazole $CH_3$ is going into the plane of the paper while in (B) it is coming out of the plane of the paper. (C,D) Benzothiazole moiety is between the G and 8-oxo-dG bases while the quinoline moiety is between the two C bases. In (C) the benzothiazole $CH_3$ is coming out of the plane of the paper while in (D) it is going into the plane of the paper.**

In 3 of the 4 simulations where both TO moieties were intercalated in the 8-oxo-dG duplex, the dye remained close to the starting orientation and extended the DNA duplex, as seen in Figure 5.23B. In the remaining simulation, the quinoline moiety moved away from the bases and then the benzothiazole moved from its position between the 8-oxo-dG and G bases to a position between all 4 bases in the intercalation site, as shown in Figure 5.23D.

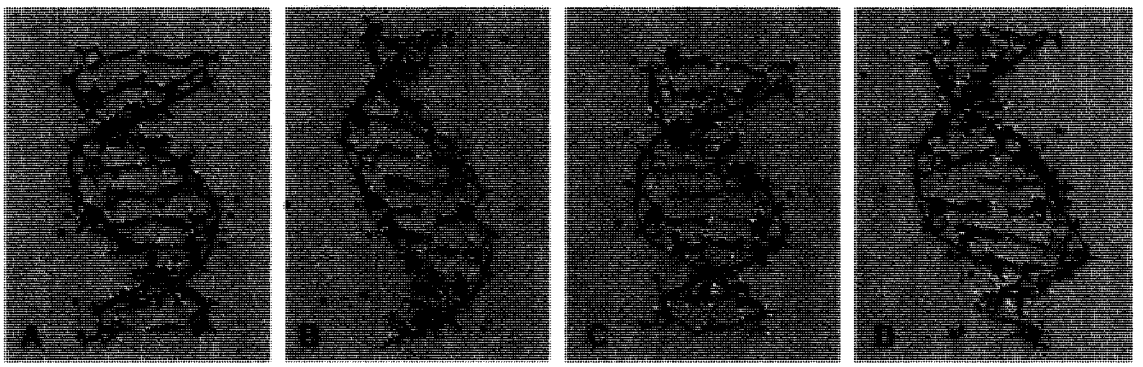

**Figure 5.23: Initial (A) conformation of TO/8-oxo-dG duplex, and after 2 ns (B), showing the dye close to the starting orientation. Initial (C) conformation of TO/8-oxo-dG duplex, and after 2 ns (D), showing the benzothiazole moiety intercalated.**

## 5.3. Discussion

### 5.3.1. Experimental Studies

An important observation was made during the course of the experiments. When performing the UVC irradiations, the amount of DNA damage, and hence its detection via the various methodologies, depended on the DNA concentration. Our irradiations were typically done with 100 μM base pairs DNA, but when the concentration was increased (200-1000 μM base pairs DNA) the amount of damage appeared to be considerably lower. This may reflect the complete or partial depletion of dissolved oxygen (~0.3 mM at room temperature[43]) in the aqueous solutions.

The abilities of the various methodologies to detect UVC-induced DNA damage are compared in Table 5.1.

**Table 5.1: Comparison of methodologies for determining DNA damage.**

| Methodology | DNA Damage Detection Rate | Energy Dose |
|---|---|---|
| TO Fluorescence | $t_{1/2}$ is 6.3 ± 0.3 minutes with monoexponential decay | $t_{1/2}$ at 14.2 ± 0.7 kJ/m$^2$ with monoexponential decay |
| TO Absorbance Ratio $A_{500}/A_{480}$ | $t_{1/2}$ is 10.6 ± 2.2 minutes with monoexponential decay | $t_{1/2}$ at 23.9 ± 5.2 kJ/m$^2$ with monoexponential decay |
| Agarose Gel Electrophoresis with EB Staining | $t_{1/2}$ is 16.2 ± 2.3 minutes with monoexponential decay | $t_{1/2}$ at 36.5 ± 5.2 kJ/m$^2$ with monoexponential decay |
| TO ICD | $t_{1/2}$ is 18.2 ± 3.7 minutes with monoexponential decay | $t_{1/2}$ at 41.0 ± 8.3 kJ/m$^2$ with monoexponential decay |
| DNA CD | $t_{1/2}$ is 20.8 ± 3.7 minutes with monoexponential decay | $t_{1/2}$ at 46.8 ± 8.3 kJ/m$^2$ with monoexponential decay |
| DNA Absorbance | Linear with 6.5% loss per hour of $A_{260}$ up to 2 h | Linear with 6.5% loss per 135 kJ/m$^2$ |

In summary, the absorbance of CT DNA at 260 nm decreases almost linearly (0-120 minutes) at 6.5% per 135 kJ/m$^2$ (per hour) for UVC exposure of 100 μM CT base pairs DNA, while the other methodologies are more sensitive and can be fitted (for convenience) with monoexponential functions. Among the various techniques employed, TO fluorescence is the most sensitive.

As the level of UVC exposure increased, the TO monomer:dimer ratio decreased. The H-dimer (or aggregate) that assembles on DNA will be non-fluorescent.[44,45] 8-oxo-dG is more easily oxidized that dG: the oxidation potential of guanine is 1.49 V vs. NHE,[46] and 8-oxo-guanine has an oxidation potential that is approximately 0.4 V lower than that of guanine.[47] Any 8-oxo-dG formed during the irradiations could quench the fluorescence of thiazole orange via electron transfer. One reviewer suggested that both of these possibilities would contribute to the observed fluorescence quenching without necessarily implying that the DNA has been destroyed, with the risk of "false negative" readings. Although the creation of DNA lesions (CPDs, 6-4PPs, 8-oxo-dG, etc.) does not directly lead to strand breaks, i.e. destroyed DNA, these base modifications will lead to strand scissions if the DNA is subjected to heat, alkali, or enzymatic treatment.[16] Base modification is an indicator of DNA damage, thus any decrease in TO fluorescence, whether it be from reduced TO intercalation (resulting in free, non-fluorescent TO), assembly of non-fluorescent H-dimers (or aggregates) on DNA, or quenching of TO fluorescence by 8-oxo-dG, signals DNA damage and does not contribute to a "false negative" reading. Thus it appears to us as though all conceivable mechanisms of fluorescence quenching are related to DNA damage, but we cannot rule out the possibility of some contribution from quenching unrelated to DNA damage. In the context of food authenticity, "false negative" readings are unimportant as one wants to know the *minimum* amount of DNA damage that an irradiated foodstuff has undergone.

The efficacy of our assay for detecting UVC-induced DNA damage has been demonstrated. UVC-induced photoproducts in DNA have been well studied and characterized by many other research groups.[14-34] It is clear that these

photoproducts interfere with TO intercalation in DNA. Other cyanine dyes prefer guanine intercalation sites, in both single- and double-stranded DNA.[40,48] It is likely that TO behaves in a similar manner. Any DNA damage that interferes with TO intercalation will affect its fluorescence, where changes in rotational flexibility can lead to substantial changes in quantum yield.

Although the irradiation doses in this assay were comparable to those used in the irradiation of food (0.5 kGy to 10 kGy), the fluorescence of thiazole orange was extremely sensitive to UVC-induced DNA damage thus it could potentially be used to detect lower levels of DNA damage, such as those found in health applications. For example, an average chest X-ray delivers a dose of approximately 0.001 Gy while radiotherapy treatments involve doses around 2 Gy. The fluorescence of TO in UVC-irradiated CT DNA was fit, for convenience, to a monoexponential function (Figure 5.7B). However, within the first 22.5 $kJ/m^2$ (or 10 minutes) of UVC exposure, the fluorescence decreased sharply, suggesting that TO fluorescence could also be used with lower doses of radiation, as seen in Figure 5.24. It would be necessary to determine whether TO fluorescence decays linearly or monoexponentially with lower doses of radiation, but it appears as though fluorescence spectroscopy using TO could also be used to report lower levels of DNA damage, such as those found in health applications.

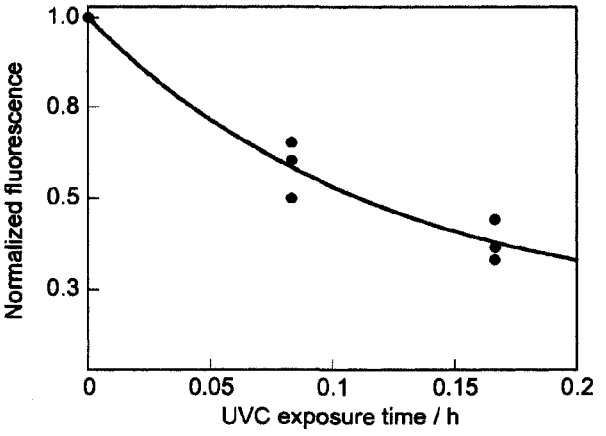


**Figure 5.24: Close-up of the fluorescence (normalized) change with the UVC exposure time (from Figure 5.7B), fitted for convenience to an exponential function.**

### 5.3.2. Computational Studies

The results of all of the molecular dynamics simulations involving TO and the two duplexes containing DNA lesions are summarized in Table 5.2.

**Table 5.2: Summary of computational results involving duplex DNA oligomers and TO.**

| **Initial intercalated moiety** | **T-dimer duplex** |
|---|---|
| Benzothiazole (Figure 5.15) | In 3 cases, the dye dissociated.<br>In 1 case, the dye remained intercalated but there was a shift that placed the quinoline moiety between the A bases.<br>In 1 case, both moieties interacted with A bases.<br>In 1 case, the dye remained close to the starting orientation. |
| Quinoline (Figure 5.17) | In 2 cases, the dye dissociated.<br>In 2 cases, the benzothiazole moiety interacted with an A base that was flipped out from the helix while the quinoline moiety interacted with 2 other A bases. |
| **Initial intercalated moiety** | **8-oxo-dG duplex** |
| Benzothiazole (Figure 5.19) | In 2 cases, the dye remained close to the starting orientation, i.e. the benzothiazole moiety stayed between all four bases in the intercalation site.<br>In 2 cases, the dye remained intercalated and the benzothiazole moiety moved between the 8-oxo-dG and G bases. |
| Quinoline (Figure 5.21) | In 1 case, the dye dissociated.<br>In 1 case, the dye remained close to the starting orientation.<br>In 2 cases, the dye remained intercalated and the quinoline moiety moved between the 8-oxo-dG and G bases. |
| Benzothiazole and quinoline (Figure 5.23) | In 3 cases, the dye remained close to the starting orientation.<br>In 1 case, the quinoline moiety moved away from the bases and then the benzothiazole moved between all four bases in the intercalation site. |

In 5 of the 10 simulations involving the intercalation of TO in the T-dimer duplex, the dye dissociated (immediately or within the first 100 ps) but remained in

the vicinity of the DNA duplex, presumably due to electrostatic interactions. These results suggest that the dye would not intercalate (in these orientations) in sites containing a cyclobutane thymine dimer. In 2 of the remaining cases, at the very beginning of the simulation one of the A bases flipped out of the DNA helix and then the benzothiazole moiety interacted with this base while the quinoline moiety associated with two nearby A bases. It appears that without the A base flipping out of the DNA helix, there would not be enough room for the dye (in its current orientation) in the intercalation pocket due to the presence of the cyclobutane thymine dimer. Consequently, it seems doubtful that TO would intercalate if it were placed in the proximity of the DNA strand, due to the steric crowding in the intercalation site. In the last 3 cases, the dye remained intercalated with either one or both moieties between the two A bases in the intercalation site. All of the simulations indicate that there is no affinity of the dye to the cyclobutane thymine dimer, and in half of the cases TO dissociated when placed in the proximity of the cyclobutane thymine dimer. The experimental studies demonstrate that UVC light induces changes in DNA that interfere with TO intercalation, which is consistent with the computational studies of TO and the T-dimer duplex.

TO dissociated from the 8-oxo-dG duplex in only 1 of the 12 simulations, suggesting that the experimentally observed tendency of TO to intercalate less readily into UVC-damaged DNA is not a consequence of the presence of 8-oxo-dG. In fact, in 4 of the 11 cases the dye showed a preference for intercalation between the 8-oxo-dG and dG bases over intercalation between all four bases.

In Chapters 3 and 4, TO did not show a preference for intercalation of a specific TO moiety in the modeling of its interaction with single- and double-stranded DNA oligomers, and the same was true of TO and both the T-dimer and the 8-oxo-dG duplexes.

## 5.4. Conclusions

Photodamage of DNA by UVC light is well established. Various methods can be used to characterize this damage, the most well known being gel electrophoresis. Absorption spectroscopy, circular dichroism spectroscopy, fluorescence spectroscopy, and gel electrophoresis can all report DNA damage. In our experiments, the UV-visible absorbance shows a slow approximately linear decrease in DNA absorbance at 260 nm upon UVC exposure (of comparable doses as those employed for radiation-induced sterilization of food), while changes in the CD and fluorescence spectra and agarose gel electrophoresis can be adequately fit with exponential functions with different rates of detection of UVC-induced DNA damage. All of the spectroscopic techniques involving thiazole orange (dye absorbance, induced circular dichroism and fluorescence) indicate that thiazole orange intercalation is susceptible to UVC-induced DNA damage. The computational studies suggest that the presence of cyclobutadipyrimidines, and not 8-oxo-2'-deoxyguanosine, is a factor in the experimentally observed reduction in dye intercalation.

The fluorescence of thiazole orange showed the damage to DNA with considerably less energy flux than the gel electrophoresis and CD methodologies. We suggest here that fluorescence by intercalated thiazole orange is even more sensitive than gel electrophoresis with ethidium bromide staining and can be performed easily and rapidly. Fluorescence spectroscopy is reliable even with small changes thus it should be able to detect very small amounts of DNA damage. We anticipate that a technique of this type will constitute a convenient tool for the detection of DNA damage in relation to regulatory compliance in the use of irradiation technologies in food treatment.

## 5.5. Materials and Methods

### 5.5.1. Materials

All results presented here were obtained in solutions of 18 MΩ water (Millipore Corporation). Calf thymus DNA (Type I, highly polymerized, sodium salt) was obtained from Sigma-Aldrich Co., thiazole orange tosylate (for fluorescence, ≥98.0% by HPLC) was purchased from Fluka and DMSO (HPLC grade) was obtained from OmniSolv. Certified electrophoresis agarose and 50X TAE pH 8.0 buffer were purchased from Bio-Rad. The gel loading solution (0.05% (w/v) bromphenol blue, 40% (w/v) sucrose, 0.1 M EDTA and 0.5% (w/v) sodium lauryl sulfate) was purchased from Sigma-Aldrich Co. The DNA markers, Lambda DNA HindIII+EcoRI Ladder and O'GeneRuler 100 bp DNA Ladder Plus, were obtained from Fermentas. HindIII+EcoRI Ladder has 21, 5, 3.5, 2, 1.5 and 1.4 kbp bands. O'GeneRuler has 3, 2, 1.5, 1.2, 1, 0.9, 0.8, 0.7, 0.6, 0.5, 0.4, 0.3, 0.2 and 0.1 kbp bands. All concentrations were determined by absorption spectroscopy using the extinction coefficient of 6600 $M^{-1}cm^{-1}$ per DNA base at 260 nm, and $6.3 \times 10^4\ M^{-1}cm^{-1}$ at 500.6 nm for TO.[49] Thiazole orange, as received from the supplier, was kept at -20°C. A stock solution of TO was made in DMSO and subsequently diluted in water when the dye:DNA solutions were prepared. The calf thymus DNA stock solution was shaken for 1 h (to ensure dissolution of the DNA in the water) and allowed to fully dissolve overnight before use while stored at -4°C. The stock solution of CT DNA was diluted in water when the dye:DNA solutions were prepared. The dye:DNA base pair ratio (d/b) is defined as the number of chromophores per base pair. Dye/DNA base pair concentrations in the final mixtures were (5/50) μM. A 1:10 d/b ratio was used to ensure that the dominant binding mode would be that of intercalation. Quartz Suprasil cuvettes (Luzchem Research Inc.) with a 10 mm optical path were employed in all the experiments. Experiments were carried out at room temperature, except for the CD work where the temperature was kept fixed at 20°C.

### 5.5.2. Irradiation

A Luzchem photoreactor containing four LZC-UVC lamps (energy flux of 37.5 W/m$^2$) was used to irradiate the DNA solutions (100 μM base pairs in water). The shorter irradiation times were 0 (control), 5, 10, 15, 20, 30 minutes and then every 30 minutes until 90 or 120 minutes and correspond to 0, 11.3, 22.5, 33.8, 45, 67.5, 135, 203 and 270 kJ/m$^2$; longer irradiations were monitored hourly for 12 hours corresponding to a total energy flux of up to 1620 kJ/m$^2$ (at 12 hours). When performing spectroscopic measurements, the dye TO was added to the solutions *after* the irradiation was complete.

### 5.5.3. Instrumentation

Absorption spectra were recorded using a Varian Cary-50 with a scan rate of 600 nm/min. Each difference spectrum is the absolute difference of the UVC-irradiated DNA spectrum minus the non-irradiated control DNA spectrum, a procedure utilized in the literature.[50]

Circular dichroism experiments were performed on a Jasco J-810 spectrometer with a 150 W Xenon lamp. The instrumental parameters were a 0.5 nm data pitch, continuous scanning mode, 20 nm/min scan speed, 2 s response, and 1 nm bandwidth. The water spectrum was used as a blank, which was subtracted from the CD spectra.

Fluorescence spectra were recorded using a Photon Technology International luminescence spectrometer operated in the CW mode. Fluorescence emission spectra were recorded upon 480 nm excitation with a 0.5 s integration time and 0.5 nm integration step. The fluorescence spectra were not corrected for changes in the absorbance at the excitation wavelength.

### 5.5.4. Agarose Gel Electrophoresis

The samples were analyzed by agarose gel electrophoresis. Agarose gels (1.25% w/v) were prepared in 1X TAE buffer. Approximately 6 μg of sample DNA was loaded per well. DNA markers used were Lambda DNA HindIII+EcoRI Ladder and O'GeneRuler 100 bp DNA Ladder Plus. The samples were run at 130 Volts in

1X TAE buffer, and the DNA was visualized under UV light in a Bio-Rad Gel-doc trans-illuminator by ethidium bromide staining. The intensity of ethidium bromide staining was quantified using ImageJ software (http://rsb.info.nih.gov/ij/). The dark stain in the control lane of the TIFF file was outlined with a rectangle, the density of the rectangular area was measured, and across the gel each lane was measured in the same area. The percentage of loss was determined from the control lane (0% loss).

### 5.5.5. Fitting the Data

Regarding the insets in the figures, results from 3 separate trials are shown (with the exception of the 0-12 hour irradiation, where only 1 trial was performed) and the fits were generated by Kaleidagraph software. The errors reported are one standard deviation based on the applicable Kaleidagraph fit.

### 5.5.6. Computational Details

The computational details were discussed in detail in Section 3.5.4 of this thesis. The things done differently in this chapter were that the canonical structures of the dsDNA fragments were composed of 10 base pairs (rather than 10 bases for ssDNA), 18 $Na^+$ counterions (rather than 9 for ssDNA) were added in the proximity of the $PO_4^-$ groups of the dsDNA to maintain the neutrality of the system, and each dsDNA fragment contained one DNA lesion.

Associate Professor M.L. Dodson kindly provided the library file for the cyclobutane thymine dimer, which was generated as follows. The fractional coordinates from the crystal structure of the *cis-syn* photodimer of thymidylyl (3'-5') thymidine cyanoethyl ester were taken from the published work of Cadet *et al.*[51] and converted first to Cartesian coordinates and then to PDB format. A phosphate group was manually docked at the 5' end and the cyanoethyl group was removed by editing the PDB file. The geometry of the dinucleotide (including the two phosphates) was optimized at 6-31G* with the Gaussian 94[52] series of the program. Electrostatic potential data was also generated with Gaussian 94 using the optimized geometry. The AMBER prep file was generated from the Gaussian

geometry optimized output and the partial atomic charges were added in a text editor. The names of the atoms were changed to follow nucleic acid conventions, and the topology descriptors and the atom types were added, following descriptions on the AMBER web site (http://amber.scripps.edu). Since LEaP works better with mononucleotide residues, the prep file was copied and one copy was made for the TT5 residue (the 5'-moiety of the cyclobutane thymine dimer) by editing out the atoms from the 3'-moiety, and the other became TT3 (by editing out the atoms for the 5'-moiety). The charges were the same as in the dinucleotide. The C5-C5 and C6-C6 bonds were added with LEaP when the topology for the whole DNA molecule was generated. The force field parameters were assigned by analogy to other, similar bond lengths, angles and torsions already in the AMBER ff94 force field.[53]

Associate Professor C. Simmerling kindly provided the library file for 8-oxo-2'-deoxyguanosine (8-oxo-dG), which was generated using published parameters for 8-oxo-dG from Miller *et al.*[54] As described by Cheng *et al.*[55], the starting structure for DNA containing 8-oxo-dG was obtained from canonical B-form DNA by replacing the hydrogen at C8 with oxygen and adding hydrogen to N7.

## 5.6. References


1. Stivers, J. T.; Kuchta, R. D., Introduction: DNA damage and repair. *Chem. Rev.* **2006,** 106, (2), 213-214.

2. Ashley, B. C.; Birchfield, P. T.; Chamberlain, B. V.; Kotwal, R. S.; McClellan, S. F.; Moynihan, S.; Patni, S. B.; Salmon, S. A.; Au, W. W., Health concerns regarding consumption of irradiated food. *Int. J. Hyg. Environ. Health* **2004,** 207, (6), 493-504.

3. Farkas, J., Irradiation as a method for decontaminating food. A review. *Int. J. Food Microbiol.* **1998,** 44, (3), 189-204.

4. Mikelsons, L.; Scaiano, J. C., Will my strawberries glow in the dark? *Canadian Chemical News, October issue* **2004**, 18-19.

5. Parnes, R. B.; Lichtenstein, A. H., Food irradiation: a safe and useful technology. *Nutr. Clin. Care* **2004,** 7, (4), 149-155.

6. Shea, K. M., Technical report: irradiation of food. Committee on Environmental Health. *Pediatrics* **2000,** 106, (6), 1505-1510.

7. Cosa, G.; Vinette, A. L.; McLean, J. R. N.; Scaiano, J. C., Novel DNA damage detection technique applying time-resolved fluorescence measurements. *Anal. Chem.* **2002,** 74, (24), 6163-6169.

8. Cosa, G.; Focsaneanu, K.-S.; McLean, J. R. N.; Scaiano, J. C., Direct determination of single-to-double stranded DNA ratio in solution applying time-resolved fluorescence measurements of dye-DNA complexes. *Chem. Commun.* **2000,** 8, 689-690.

9. Beach, L.; Schweitzer, C.; Scaiano, J. C., Direct determination of single-to-double stranded DNA ratio in solution using steady-state fluorescence measurements. *Org. Biomol. Chem.* **2003,** 1, (3), 450-451.

10. Lee, L. G.; Chen, C.-H.; Chiu, L. A., Thiazole orange: a new dye for reticulocyte analysis. *Cytometry* **1986,** 7, 508-517.

11. Schwartz, H. E.; Ulfelder, K. J., Capillary electrophoresis with laser-induced fluorescence detection of PCR fragments using thiazole orange. *Anal. Chem.* **1992,** 64, (15), 1737-1740.

12. Boger, D. L.; Tse, W. C., Thiazole orange as the fluorescent intercalator in a high resolution FID assay for determining DNA binding affinity and sequence selectivity of small molecules. *Bioorg. Med. Chem.* **2001,** 9, 2511-2518.

13. Rye, H. S.; Quesada, M. A.; Peck, K.; Mathies, R. A.; Glazer, A. N., High-sensitivity two-color detection of double-stranded DNA with a confocal fluorescence gel scanner using ethidium homodimer and thiazole orange. *Nucleic Acids Res.* **1991,** 19, (2), 327-333.

14. Ravanat, J.-L.; Douki, T.; Cadet, J., Direct and indirect effects of UV irradiation on DNA and its components. *J. Photochem. Photobiol. B.* **2001,** 63, 88-102.

15. Bogdanov, K. V.; Chukhlovin, A. B.; Zaritskey, A. Y.; Frolova, O. L.; Afanasiev, B. V., Ultraviolet irradiation induces multiple DNA double-strand breaks and apoptosis in normal granulocytes and chronic myeloid leukaemia blasts. *Br. J. Haematol.* **1997,** 98, (4), 869-872.

16. Burrows, C. J.; Muller, J. G., Oxidative nucleobase modifications leading to strand scission. *Chem. Rev.* **1998,** 98, (3), 1109-1151.

17. Cavalieri, L. F.; Bendich, A., The ultraviolet absorption spectra of pyrimidines and purines. *J. Am. Chem. Soc.* **1950,** 72, (6), 2587-2594.

18. Cheng, K. C.; Cahill, D. S.; Kasai, H.; Nishimura, S.; Loeb, L., 8-Hydroxyguanine, an abundant form of oxidative DNA damage, causes G to T and A to C substitutions. *J. Biol. Chem.* **1992,** 267, (1), 166-172.

19. Choy, C. K. M.; Benzie, I. F. F.; Cho, P., UV-mediated DNA strand breaks in corneal epithelial cells assessed using the comet assay procedure. *Photochem. Photobiol.* **2005,** 81, (3), 493-497.

20. Douki, T.; Court, M.; Sauvaigo, S.; Odin, F.; Cadet, J., Formation of the main UV-induced thymine dimeric lesions within isolated and cellular DNA as measured by high performance liquid chromatography-tandem mass spectrometry. *J. Biol. Chem.* **2000,** 275, (16), 11678-11685.

21. Douki, T.; Perdiz, D.; Gróf, P.; Kuluncsics, Z.; Moustacchi, E.; Cadet, J.; Sage, E., Oxidation of guanine in cellular DNA by solar UV radiation: biological role. *Photochem. Photobiol.* **1999,** 70, (2), 184-190.

22. Hall, A.; Ballantyne, J., Characterization of UVC-induced DNA damage in bloodstains: forensic implications. *Anal. Bioanal. Chem.* **2004,** 380, 72-83.

23. Johnson, N. A.; McKenzie, R.; McLean, L.; Sowers, L. C.; Fletcher, H. M., 8-Oxo-7,8-dihydroguanine is removed by a nucleotide excision repair-like mechanism in *Porphyromonas gingivalis* W83. *J. Bacteriol.* **2004,** 186, (22), 7697-7703.

24. Mφller, P.; Wallin, H.; Dybdahl, M.; Frentz, G.; Nexφ, B., Psoriasis patients with basal cell carcinoma have more repair-mediated DNA strand breaks after UVC damage in lymphocytes than psoriasis patients without basal cell carcinoma. *Cancer Lett.* **2000,** 151, (2), 187-192.

25. Madigan, J. P.; Chotkowski, H. L.; Glaser, R. L., DNA double-strand break-induced phosphorylation of *Drosophila* histone variant H2Av helps prevent radiation-induced apoptosis. *Nucleic Acids Res.* **2002,** 30, (17), 3698-3705.

26. Miller, J. H., Mutagenic specificity of ultraviolet light. *J. Mol. Biol.* **1985,** 182, (1), 45-68.

27. Munch-Petersen, B., Thymidine in the micromolar range promotes rejoining of UVC-induced DNA strand breaks and prevents azidothymidine from inhibiting the rejoining in quiescent human lymphocytes. *Mutat. Res.* **1997,** 383, (2), 143-153.

28. Peak, J. G.; Peak, M. J., Ultraviolet light induces double-strand breaks in DNA of cultured human P3 cells as measured by neutral filter elution. *Photochem. Photobiol.* **1990,** 52, (2), 387-392.

29. Smith, C. A.; Taylor, J.-S., Preparation and characterization of a set of deoxyoligonucleotide 49-mers containing site-specific cis-syn, trans-syn-I, (6-4), and Dewar photoproducts of thymidylyl(3'-5') thymidine. *J. Biol. Chem.* **1993,** 268, (15), 11143-11151.

30. Wei, H.; Cai, Q.; Rahn, R.; Zhang, X., Singlet oxygen involvement in ultraviolet (254 nm) radiation-induced formation of 8-hydroxy-deoxyguanosine in DNA. *Free Rad. Biol. Med.* **1997,** 23, (1), 148-154.

31. Wei, Z.; Lifen, J.; Jiliang, H.; Jianlin, L.; Baohong, W.; Hongping, D., Detecting DNA repair capacity of peripheral lymphocytes from cancer patients with UVC challenge test and bleomycin challenge test. *Mutagenesis* **2005,** 20, (4), 271-277.

32. Zhang, X.; Rosenstein, B. S.; Wang, Y.; Lebwohl, M.; Wei, H., Identification of possible reactive oxygen species involved in ultraviolet radiation-induced oxidative DNA damage. *Free Radic. Biol. Med.* **1997,** 23, (7), 980-985.

33. Zhang, X. S.; Rosenstein, B. S.; Wang, Y.; Lebwohl, M.; Mitchell, D. M.; Wei, H. C., Induction of 8-oxo-7,8-dihydro-2'-deoxyguanosine by ultraviolet radiation in calf thymus DNA and HeLa cells. *Photochem. Photobiol.* **1997,** 65, (1), 119-124.

34. Zheng, W.; He, J. L.; Jin, L. F.; Lou, J. L.; Wang, B. H., Assessment of human DNA repair (NER) capacity with DNA repair rate (DRR) by comet assay. *Biomed. Environ. Sci.* **2005,** 18, (2), 117-123.

35. Wood, R. D.; Skoper, T. R.; Hutchinson, F., Changes in DNA base sequence induced by targeted mutagenesis of lambda phage by ultraviolet light. *J. Mol. Biol.* **1984,** 173, (3), 273-291.

36. Kawai, K.; Fujitsuka, M.; Majima, T., Selective guanine oxidation by UVB-irradiation in telomeric DNA. *Chem. Commun.* **2005,** 11, 1476-1477.

37. Ogul'chansky, T. Y.; Losytskyy, M. Y.; Kovalska, V. B.; Yashchuk, V. M.; Yarmoluk, S. M., Interactions of cyanine dyes with nucleic acids. XXIV. Aggregation of monomethine cyanine dyes in presence of DNA and its manifestation in absorption and fluorescence spectra. *Spectrochim. Acta A* **2001,** 57, 1525-1532.

38. Fasman, G. D., *Circular Dichroism and the Conformational Analysis of Biomolecules*. Plenum Press: New York, 1996; p 460.

39. Gray, D. M.; Ratliff, R. L.; Vaughan, M. R., Circular dichroism spectroscopy of DNA. *Methods Enzymol.* **1992,** 211, 389-406.

40. Mikelsons, L.; Carra, C.; Shaw, M.; Schweitzer, C.; Scaiano, J. C., Experimental and theoretical study of the interaction of single-stranded DNA homopolymers and a monomethine cyanine dye: nature of specific binding. *Photochem. Photobiol. Sci.* **2005,** 4, (10), 798-802.

41. Larsson, A.; Carlsson, C.; Jonsson, M.; Albinsson, B., Characterization of the binding of the fluorescent dyes YO and YOYO to DNA by polarized light spectroscopy. *J. Am. Chem. Soc.* **1994,** 116, (19), 8459-8465.

42. Jacobsen, J. P.; Pedersen, J. B.; Hansen, L. F.; Wemmer, D. E., Site selective bis-intercalation of a homodimeric thiazole orange dye in DNA oligonucleotides. *Nucleic Acids Res.* **1995,** 23, (5), 753-760.

43. Murov, S. L.; Carmichael, I.; Hug, G. L., *Handbook of Photochemistry.* 2nd ed.; Marcel Dekker: New York, 1993; p 293.

44. Seifert, J. L.; Connor, R. E.; Kushon, S. A.; Wang, M.; Armitage, B. A., Spontaneous assembly of helical cyanine dye aggregates on DNA nanotemplates. *J. Am. Chem. Soc.* **1999,** 121, (13), 2987-2995.

45. Chowdhury, A.; Wachsmann-Hogiu, S.; Bangal, P. R.; Raheem, I.; Peteanu, L. A., Characterization of chiral H and J aggregates of cyanine dyes formed by DNA templating using Stark and fluorescence spectroscopies. *J. Phys. Chem. B* **2001,** 105, (48), 12196-12201.

46. Seidel, C. A. M.; Schulz, A.; Sauer, M. H. M., Nucleobase-specific quenching of fluorescent dyes. 1. Nucleobase one-electron redox potentials and their correlation with static and dynamic quenching efficiencies. *J. Phys. Chem.* **1996,** 100, (13), 5541-5553.

47. Sheu, C.; Foote, C. S., Reactivity toward singlet oxygen of a 7,8-dihydro-8-oxoguanosine ("8-hydroxyguanosine") formed by photooxidation of a guanosine derivative. *J. Am. Chem. Soc.* **1995,** 117, (24), 6439-6442.

48. Schweitzer, C.; Scaiano, J. C., Selective binding and local photophysics of the fluorescent cyanine dye PicoGreen in double-stranded and single-stranded DNA. *Phys. Chem. Chem. Phys.* **2003,** 5, 4911-4917.

49. Nygren, J.; Svanvik, N.; Kubista, M., The interactions between the fluorescent dye thiazole orange and DNA. *Biopolymers* **1998,** 46, 39-51.

50. Trumbore, C. N.; Hyde, C. T.; Hudson, R. D.; Jurman, L. A.; Gehring, A. G.; Masselink, J. K., Ultraviolet difference spectral studies in the gamma radiolysis of DNA and model compounds. I. Aqueous solutions of DNA bases. *Int. J. Radiat. Biol.* **1989,** 56, (6), 923-941.

51. Cadet, J.; Voituriez, L.; Hruska, F. E.; Grand, A., Crystal structure of the *cis-syn* photodimer of thymidylyl (3'-5') thymidine cyanoethyl ester. *Biopolymers* **1985,** 24, (5), 897-903.

52. Frisch, M. J.; Trucks, G. W.; Schlegel, H. B.; Gill, P. M. W.; Johnson, B. G.; Robb, M. A.; Cheeseman, J. R.; Keith, T.; Petersson, G. A.; Montgomery, J. A.; Raghavachari, K.; Al-Laham, M. A.; Zakrzewski, V. G.; Ortiz, J. V.; Foresman, J. B.; Cioslowski, J.; Stefanov, B. B.; Nanayakkara, A.; Challacombe, M.; Peng, C. Y.; Ayala, P. Y.; Defrees, W.; Baker, J.; Stewart, J. P.; Head-Gordon, M.; Gonzalez, C.; Pople, J. A. *Gaussian 94*, Gaussian, Inc.: Pittsburgh, 1994.

53. Cornell, W. D.; Cieplak, P.; Bayly, C. I.; Gould, I. R.; Merz, K. M., Jr.; Ferguson, D. M.; Spellmeyer, D. C.; Fox, T.; Caldwell, J. W.; Kollman, P. A., A second generation force field for the simulation of proteins, nucleic acids, and organic molecules. *J. Am. Chem. Soc.* **1995,** 117, (19), 5179-5197.

54. Miller, J. H.; Fan-Chiang, C.-C. P.; Straatsma, T. P.; Kennedy, M. A., 8-Oxoguanine enhances bending of DNA that favors binding to glycosylases. *J. Am. Chem. Soc.* **2003,** 125, (20), 6331-6336.

55. Cheng, X.; Kelso, C.; Hornak, V.; de los Santos, C.; Grollman, A. P.; Simmerling, C. L., Dynamic behavior of DNA base pairs containing 8-oxoguanine. *J. Am. Chem. Soc.* **2005,** 127, (40), 13906-13918.

# 6. Final Comments and Future Directions

## 6.1. Final Comments

The work presented in this thesis has explored the associations of cyanine dyes with DNA, with the ultimate goal of using these dyes to detect DNA damage. The property that makes these dyes such good sensors is that, upon intercalation, their rotations are restricted, suppressing the nonradiative decay mechanism active in solution and forcing them to dissipate their energy radiatively via fluorescence emission. This results in extremely large increases in fluorescence quantum yield upon binding to DNA, with a low background of fluorescence for free dye. Although there have been numerous studies involving these dyes, the nature of the association process is not always clear.

Thiazole orange (TO) and its N-propyl pyridinium derivative (PTO) interact with single-stranded DNA homopolymers very similarly: monomeric association with poly(dA), at least two binding modes with poly(dG), and dimeric/aggregate association with poly(dC) and poly(dT). As these two dyes differ only in the substituent on the quinoline ring, our findings demonstrate the unimportance of the pyridinium moiety in the association process. In contrast, the structurally similar cyanine dye PicoGreen® (PG) binds strongly to poly(dG) and poly(dT) but not to poly(dA) and poly(dC), indicating that its substituents play a significant role in its binding specificity, which differs from that of TO and PTO which both bind strongly to poly(dA) and poly(dG) but weakly to poly(dC) and poly(dT). The results of the molecular dynamics simulations agreed remarkably well with the experimental spectral results, demonstrating how the combination of experimental and computational methods provides a unique understanding of the associations of cyanine dyes with DNA homopolymers. This information could contribute to the design of new dyes that are more effective in binding to a specific base or sequence of bases, and this research could play a role in the development of dye-based methodologies to detect/monitor DNA damage.

The experimental and computational results involving the dyes and both natural and synthetic double-stranded DNA show a strong association between the

dyes and the duplexes. While there is no conclusive experimental evidence regarding sequence-specific binding, the computational studies suggest that TO and PTO bind to double-stranded DNA without sequence specificity. Surprisingly, the LD results indicate that both the monomeric and dimeric forms of the dyes intercalate in both ss- and dsDNA, although a portion of the dimeric form is free in solution rather than intercalated. Interestingly, a new type of stable dye/DNA complex was formed when single-strands of poly(dA) and poly(dT) were hybridized in the presence of PG or PTO, which cannot be obtained by the addition of the dye to double-stranded poly(dA)•poly(dT). In addition, all three dyes prevented complete renaturation of calf thymus DNA during thermal cycling. Although the exact structure of these new complexes, the possibilities for their formation in biological systems, and their effects on such systems are unknown, it is clear that these intercalating dyes interfere with DNA hybridization to double-stranded DNA. This information could contribute to the design of more effective chemotherapeutic agents and antibiotics. The results also reveal that, in DNA hybridization experiments, one cannot use fluorescence enhancement of intercalators as a means of studying DNA structure, since the information it provides is ambiguous.

Various spectroscopic and biochemical methods were compared for their ability to detect ultraviolet-induced DNA damage. Of all the techniques examined, fluorescence spectroscopy using thiazole orange was found to be the most sensitive in our exposure range. All of the spectroscopic techniques involving TO indicated that TO intercalation is affected by UVC-induced DNA damage. The computational studies pointed to the presence of cyclobutadipyrimidines, and not 8-oxo-2'-deoxyguanosine, as the major factor responsible for the experimentally observed reduction in dye intercalation. Fluorescence spectroscopy can be performed easily and rapidly, and should be able to detect very small amounts of DNA damage. We anticipate that a technique of this type will constitute a convenient tool for the detection of DNA damage in relation to regulatory compliance in the use of irradiation technologies in food treatment.

In some of the molecular dynamics simulations, the dye (either PTO or TO) was significantly twisted. Such an orientation seems fairly unlikely for the ground state of the dye. Overall, it was found that the combination of experimental and computational methods provided the most insight in cases where the system under study was relatively simple, such as the binding of dyes to single-stranded DNA homopolymers where there is only one possible intercalation site (although more than one mode of association exists).

## 6.2. Future Directions

1. TO and PTO both show strong associations with poly(dA) and poly(dG), and PG binds strongly to poly(dG) and poly(dT), but these studies were done with homopolymers that only contained one of the four bases. Studying the associations of the dyes with custom sequence DNA oligomers containing all of the bases would provide a more in-depth understanding of their binding specificities.
2. It might be possible to further investigate the relationship between dye aggregates and DNA using dynamic light scattering.
3. A new type of stable dye/DNA complex was formed when single-strands of poly(dA) and poly(dT) were hybridized in the presence of PG or PTO, which cannot be obtained by the addition of the dye to double-stranded poly(dA)•poly(dT). To investigate whether this phenomenon is caused by a noncanonical structure of poly(dA)•poly(dT), some of the experiments could be repeated with the alternating copolymer $[poly(dA\text{-}dT)]_2$. To ensure that this phenomenon still occurs when G•C base pairs are present, the effects of the dyes on strand hybridization could be examined for custom sequence DNA oligomers containing both A•T and G•C base pairs. To examine whether there is a structural basis for the stability of the new dye/DNA complex, the resistance of the complexes to nuclease activity could be studied.
4. The phenomenon described in point 3 was not observed when using poly(dG) and poly(dC). To investigate whether the stronger base-pairing in poly(dG)•poly(dC) is a factor, one could examine the interactions of these dyes with poly(dI)•poly(dC), which should behave like poly(dA)•poly(dT).
5. There exisits the possibility that our "new" dye/DNA complex involves the association of the dye with both poly(dT)•poly(dA)•poly(dT) and poly(dA). This could be tested by recording the circular dichroism spectra of

poly(dT)•poly(dA)•poly(dT) with and without the dye, and the spectra of poly(dA) with and without the dye. The spectra where the dye was present could then be used to make a composite spectrum, which could be compared with that of the "new" complex.

6. Linear dichroism spectroscopy is an invaluable diagnostic tool for studying dye intercalation in DNA. As the linear dichroism accessory was purchased near the end of this thesis (and building/optimizing the Couette apparatus took significant time), only a few preliminary linear dichroism measurements were possible. It would be interesting to examine the linear dichroism of the dyes with both single-stranded and double-stranded DNA homopolymers, including the new type of complex that is formed when DNA strands are hybridized in the presence of a dye.
7. To ensure that the counterion does not play a role in the association process, the interaction of thiazole orange with DNA could be studied where the tosylate counterion has been replaced with another counterion, such as iodide.
8. Surprisingly, the linear dichroism of dye/calf thymus DNA complexes indicated that both the monomeric and dimeric forms of the dyes intercalate in both single-stranded and double-stranded DNA. Modeling is currently underway, as part of a collaboration with Dr. C. Beddie and Dr. C.C. Trevithick-Sutton, to examine how the dimeric dyes intercalate in double-stranded DNA oligomers.
9. A nucleotide flipping mechanism was proposed as a possible explanation for how the dimeric forms of the dyes intercalate in DNA. This could be investigated using NMR spectroscopy or by studying the interactions of these dyes with oligonucleotide duplexes containing mismatches or abasic sites. However, these duplexes may not be amenable to linear dichroism spectroscopy due to the difficulty in aligning short duplexes. Another alternative for studying dimer intercalation is LD spectroscopy of

a covalently linked dimer where a linker joins the two benzothiazole moieties and another linker joins the two quinoline moieties.

10. Testing other dyes, such as oxazole yellow analogues, for dimer intercalation might also be informative. These dyes would presumably be less inclined to dimerize due to the lower polarizability of the oxygen atom relative to a sulfur atom, thus there should be a reduction in dimer intercalation.
11. One reviewer suggested that the degree of unwinding in the molecular dynamics simulations appeared to be significantly greater than what is typically found experimentally (<30° per intercalator). Thus it could be informative to determine the unwinding angle at several points in the simulations to see how it evolves.
12. To ensure that thiazole orange fluorescence is in fact reporting on DNA damage levels and that the dye is not being quenched by mechanisms unrelated to DNA damage, the assay could be calibrated against actual DNA damage. We have had difficulties in extracting DNA from fruits, but we could use PCR to amplify a specific region of the DNA and monitor how the yield of that DNA changes with irradiation time. Variability in extraction efficiencies could be accounted for by spiking the samples with a known amount of a separate DNA before the extraction.
13. It would be extremely interesting to compare all of the different methodologies established in our laboratory for determining DNA damage (time-resolved fluorescence measurements using PG, steady-state fluorescence measurements in the two-dye method, TO steady-state fluorescence measurements) and ascertain which technique is the best for quantifying DNA damage, while taking into account the level of expertise required. All three techniques would be performed on identical samples, preferably DNA extracted from irradiated sources, for example irradiated foods, rather than commercially purchased DNA that was irradiated.

## 6.3. Claims to Original Research

1. Although cyanine dyes are commonly used as sensors for DNA and its structural changes, the nature of the association process is not always clear. This work demonstrates how, through the combination of experimental spectral and computational methods, one can get an in-depth understanding of the interactions between cyanine dyes and DNA.
2. The interactions between three structurally similar cyanine dyes and DNA were reported. The dyes show selective associations with single-stranded DNA homopolymers. Although conclusions cannot be drawn on the dye/double-stranded DNA complexes from the experimental findings, the computational studies suggest that the dyes bind without sequence specificity to double-stranded DNA.
3. Although there are examples in the literature of linear dichroism spectra showing both monomeric and dimeric forms of cyanine dyes bound to DNA, the intercalated (face-to-face) dimer has not been discussed nor investigated. Preliminary work on projects described in this thesis led to the identification of the intercalated dimer, and current work in our laboratory is focused on investigating this phenomenon.
4. It was demonstrated that a new type of stable dye/DNA complex is formed upon DNA strand hybridization in the presence of intercalating dyes, which both differs from and is more stable than that obtained when the dye is added to hybridized DNA.
5. A novel method of identifying DNA damage is presented, based on the compromised ability of thiazole orange to intercalate in damaged DNA, resulting in decreases in its fluorescence emission intensity.

## 6.4. Publications

### 6.4.1. Publications Resulting from Research Presented in this Thesis

1. Mikelsons, L.; Carra, C.; Shaw, M.; Schweitzer, C.; Scaiano, J.C, Experimental and theoretical study of the interaction of single-stranded DNA homopolymers and a monomethine cyanine dye: nature of specific binding, *Photochem. Photobiol. Sci.*, **2005**, 4, 798-802.
2. Scaiano, J.C.; Aliaga, C.; Chrétien, M.N.; Frenette, M.; Focsaneanu, K.S.; Mikelsons, L., Fluorescence sensor applications as detectors for DNA damage, free radical formation, and in microlithography, *Pure Appl. Chem.*, **2005**, 77, 1009–1018.
3. Trevithick-Sutton, C.; Mikelsons, L.; Filippenko, V.; Scaiano, J.C., Effect of UVC-induced damage to DNA on the intercalation of thiazole orange: a convenient reporter for DNA damage, *Photochem. Photobiol.*, **2007**, in press.
4. Mikelsons, L.; Schweitzer, C.; Antonic, M.; Carra, C.; Scaiano, J.C., Formation of a new type of stable molecule-DNA complex by hybridization of complementary single strands in the presence of an intercalator, in preparation.
5. Trevithick-Sutton, C.; Mikelsons, L.; Beddie, C.; Ghandi, N.; Scaiano, J.C., Linear dichroism studies of thiazole orange and DNA in water: the dimer intercalates!, in preparation.
6. Trevithick-Sutton, C.; Mikelsons, L.; Filippenko, V.; Ghandi, N.; Scaiano, J.C., DNA-intercalating fluorophores report DNA damage differently following UVA and UVB exposure to DNA in water, in preparation.

### 6.4.2. Dissemination of Knowledge Publications

7. Mikelsons, L.; Scaiano, J.C., Will my strawberries glow in the dark? *October issue of ACCN*, **2004**, 18-19.

### 6.4.3. Other Publications

8. Quintella, C.M.; Musse, A.P.S.; Castro, M.T.P.O.; Watanabe, Y.N.; Scaiano, J.C.; Mikelsons, L., Polymeric surfaces for heavy oil pipelines to inhibit wax deposition: PP, EVA28, and HDPE, *Energy & Fuels*, **2006**, 20, 620-624.
9. Bueno, C.; Mikelsons, L.; Scaiano, J.C.; Aspée, A., Photophysical properties of the pre-fluorescent nitroxide probes QT and C343T, in preparation.